

The German Central Graben (North Sea):
Tectonostratigraphic evolution and hydrocarbon systems

Von der Naturwissenschaftlichen Fakultät der
Gottfried Wilhelm Leibniz Universität Hannover

zur Erlangung des Grades
Doktor der Naturwissenschaften (Dr. rer. nat.)

genehmigte Dissertation

von

Simon Maximilian Müller, M.Sc. RWTH

2023

Referentin: Prof. Dr. rer. nat. Jutta Winsemann

Korreferent: Hon.-Prof. Dr. rer. nat. Christoph Gaedicke

Tag der Promotion: 12.12.2022

Table of contents

Summary	VI
Zusammenfassung	VII
List of abbreviations.....	VIII
Structure of thesis	IX
1. Introduction	1
1.1. Geological introduction	2
1.2. Previous studies	7
1.2.1. Shallow Gas southern North Sea.....	7
1.2.2. Seafloor methane seepage:	9
1.2.3. Mesozoic Hydrocarbon Systems of the southern North Sea	10
1.2.4. (Tectono-)stratigraphic evolution of the southern Central Graben.....	12
1.3. TUNB and 3DGEO-EU Project.....	14
1.4. Aims of the thesis.....	15
1.5. Publications and author contributions.....	18
References.....	19
2. Methodology.....	25
2.1. Introduction	26
2.2. Data availability and legislation	26
2.3. Data used.....	26
2.4. Well log interpretation	27
2.4.1. Well correlation.....	27
2.4.2. Well tie.....	29
2.5. Interpretation of reflection seismic data.....	30
2.5.1. Structural interpretation.....	30
2.5.2. Stratigraphic interpretation	31
2.5.3. Amplitude interpretation and direct hydrocarbon indicators	31
2.6. Petroleum system modelling	32
References.....	34
3. Shallow gas accumulations in the German North Sea.....	36
Abstract.....	37
3.1. Introduction	37

Table of contents

3.2.	Geological setting.....	38
3.2.1.	Sedimentary system	38
3.2.2.	Shallow gas in the Dutch North Sea	40
3.3.	Data and methodology	42
3.3.1.	Seismic data	42
3.3.2.	Direct hydrocarbon indicators	43
3.4.	Results	45
3.4.1.	Example 1.....	45
3.4.2.	Example 2.....	47
3.4.3.	Example 3.....	49
3.5.	Discussion	50
3.5.1.	Common characteristics of the shallow gas accumulations in the Dutch and German offshore areas.....	50
3.5.2.	Significance of shallow gas offshore Germany.....	54
3.6.	Conclusions	55
	Acknowledgments	57
	References.....	58
4.	Seafloor methane seepage related to salt diapirism in the northwestern part of the German North Sea	63
	Abstract.....	64
4.1.	Introduction	65
4.2.	Materials and methods	67
4.2.1.	Hydroacoustic data.....	68
4.2.2.	Electromagnetic data.....	68
4.2.3.	Water sampling	70
4.2.4.	Methane sensor deployment.....	71
4.3.	Results and discussion.....	72
4.3.1.	Gas flare occurrence in the “Entenschnabel”-area	72
4.3.2.	Dissolved methane in the water column and bottom waters	75
4.3.3.	Subsurface gas indications.....	79
4.3.3.1.	Sediment echosounder profiling	79
4.3.3.2.	Electromagnetic seabed mapping	81
4.3.4.	Gas distribution and the shallow gas system in the “Entenschnabel”-area	82
4.3.4.1.	Flare distribution in the study area	82
4.3.4.2.	Potential gas release related to abandoned wells	85
4.3.4.3.	Specific gas system at salt diapir Berta.....	86

Table of contents

4.4. Conclusion and outlook	87
Data availability statement	88
Funding	88
Acknowledgments	88
References.....	89
Supplementary material	95
5. Source rocks of the German Central Graben	114
Abstract.....	115
5.1. Introduction	115
5.2. Geology of the Central Graben	117
5.3. Potential source rocks	120
5.3.1. Major source rocks	120
5.3.2. Minor source rocks.....	123
5.4. Data and methodology.....	126
5.4.1. Mapping.....	126
5.4.2. Petroleum model.....	127
5.5. Results	128
5.5.1. Mapping of the Posidonia Shale Formation and the Clay Deep Member	128
5.5.2. Petroleum Model	129
5.6. Discussion	132
5.6.1. Potential as source rocks	132
5.6.2. Thermogenic contribution to shallow gas accumulations	135
5.6.3. Migration and accumulation.....	137
5.6.4. Influence of glaciations and deglaciations.....	138
5.7. Conclusions.....	139
Acknowledgments	140
References.....	141
6. Jurassic to Lower Cretaceous tectonostratigraphy of the German Central Graben, southern North Sea	148
Abstract.....	149
6.1. Introduction	149
6.2. Geological evolution.....	152
6.2.1. Tectonic and sedimentary evolution	152
6.2.2. Jurassic sequence- and tectonostratigraphy in the southern Central Graben	154

Table of contents

6.2.2.1.	Danish Central Graben.....	154
6.2.2.2.	Dutch Central Graben	156
6.3.	Data and methods.....	156
6.3.1.	Seismic interpretation	156
6.3.2.	Thickness and subsidence maps.....	158
6.3.3.	Well log correlation	158
6.4.	Results	159
6.4.1.	Seismic interpretation and gridding	159
6.4.1.1.	Pre-rift (Altena Group).....	162
6.4.1.2.	TMS-1.....	164
6.4.1.3.	TMS-2.....	165
6.4.1.4.	TMS-3.....	167
6.4.1.5.	TMS-4 and Holland Formation (Lower Cretaceous)	167
6.4.2.	Pillar maps.....	168
6.4.3.	Well log correlation	169
6.5.	Discussion	173
6.5.1.	Pre-rift (Altena Group).....	173
6.5.2.	TMS-1.....	174
6.5.3.	TMS-2.....	177
6.5.4.	TMS-3 and Lower Cretaceous	179
6.5.5.	Influence of supra-regional tectonics.....	181
6.6.	Conclusions.....	183
	Acknowledgements	184
	References.....	185
7.	Synthesis and conclusions	191
7.1.	Amplitude anomalies and their relation to shallow gas accumulations	192
7.2.	Impact of the tectonostratigraphic evolution on the petroleum systems of the Southern Central Graben	193
7.2.1.	Pre-rift (Altena Group).....	193
7.2.2.	TMS-1.....	193
7.2.3.	TMS-2.....	194
7.2.4.	TMS-3.....	195
7.2.5.	TMS-4 until the present.....	195
	References.....	197
8.	Outlook	200

Table of contents

References.....	202
Curriculum vitae	203
Danksagung	204
List of publications.....	206

Summary

The German Central Graben is part of the Central Graben in the southern North Sea, which is essentially a Mesozoic half-graben structure. The interaction of active rifting and salt tectonics formed its geology and deeply influenced sedimentation, which resulted in a differentiated basin architecture with various sub-basins.

The Central Graben is also a major hydrocarbon province for both The Netherlands and Denmark. Therefore, and due to a more liberal data publication policy in The Netherlands, most geoscientific studies concentrate on the Danish and Dutch part of the graben. One aim of this thesis is hence to advance research in this rather neglected part of the Central Graben regarding its hydrocarbon systems and geological evolution

The studies that are included in this thesis were mostly realized within the projects “Subsurface potentials for storage and economic use in the North German Basin (TUNB)” and “Establishing the European geological surveys research area to deliver a geological service for Europe (GeoERA)”. These projects provided the opportunity to interpret reflection seismic data (3D and 2D) and well log data in regard of shallow and conventional hydrocarbon systems as well as the tectonostratigraphic evolution of the German Central Graben.

Amplitude anomalies, which are indicative for gas accumulations, were mapped on reflection seismic data within the northwestern German North Sea, including the German Central Graben. These anomalies occur mainly within unconsolidated Cenozoic sediments above Zechstein salt domes. Three exemplary seismic profiles with anomaly clusters, including bright spots, seismic attenuation, and velocity pull-downs, are discussed and compared to the seismic image of currently producing Dutch shallow gas fields.

Seafloor methane seep sites were mapped in the northwestern German North Sea, above the German Central Graben, using a ship-based multibeam echosounder. Most detected seep sites occur above salt structures that feature amplitude anomalies in their overburden on reflection seismic data. Abandoned offshore wells show no correlation with seep sites. Analysis of bottom and surface waters at the seep sites revealed increased methane concentrations and indicated a contribution to the atmospheric greenhouse gas inventory.

The potential for generating hydrocarbons of six Uppermost Triassic to Lowermost Cretaceous formations was investigated. These formations include important source rocks of the southern Central Graben, like the Lower Jurassic Posidonia Shale Formation and Upper Jurassic to Lower Cretaceous “Hot Shales”, which were both mapped anew on reflection seismic data. Additionally, other marine or terrestrial formations with mudstones or coal layers were investigated in a petroleum system model. The results reveal that some of these not-in-the-spotlight formations are likely to have generated hydrocarbons and are the most likely sources of the potentially in part thermogenic shallow gas accumulations in the area.

The tectonostratigraphic evolution of the German Central Graben was reconstructed. Therefore, nine laterally traceable horizons from the Lower Jurassic to the Lower Cretaceous were mapped on reflection seismic data, including the base horizons of tectonostratigraphic mega-sequences (TMS) of the tectonostratigraphic concept from offshore The Netherlands. The results reflect the evolution of the basin from rift to salt dominated, to thermally induced subsidence. The findings were integrated in the Dutch and Danish tectono- and sequence stratigraphic concepts and discussed regarding the influence of tectonics on (litho-)stratigraphy.

Zusammenfassung

Der Deutsche Zentralgraben ist Teil des Zentralgrabens in der südlichen Nordsee, welcher im Wesentlichen eine Mesozoische Halbgraben-Struktur darstellt. Aktive Grabenbildung in Verbindung mit Salztektonik beeinflussten dessen Struktur und Stratigraphie, so dass eine differenzierte Becken-Architektur mit mehreren untergeordneten Becken entstand.

Der südliche Zentralgraben beherbergt auch bedeutende Kohlenwasserstoffvorkommen der Niederlande und Dänemarks. Deshalb und wegen einer freizügigeren Gesetzeslage zur Veröffentlichung von Daten, konzentrieren sich die meisten geowissenschaftlichen Studien der Gegend auf den dänischen und niederländischen Teil des Grabens. Das Ziel dieser Arbeit ist es, die Forschung zu Kohlenwasserstoffsystemen und der geologischen Entwicklung dieses im Vergleich wenig erforschten Teils des Zentralgrabens voranzubringen. Diese Arbeit fand größtenteils im Rahmen der Projekte „Tieferer Untergrund Norddeutsches Becken (TUNB)“ und „Establishing the European geological surveys research area to deliver a geological service for Europe (GeoERA)“ statt. In diesem Rahmen konnten 2D und 3D reflexionsseismische und bohrlochgeophysikalische Daten ausgewertet werden.

Amplitudenanomalien, die Hinweise auf Gasvorkommen liefern können, wurden in reflexionsseismischen Daten kartiert, welche die nordwestliche deutsche Nordsee, einschließlich des deutschen Zentralgrabens, umfassen. Diese Anomalien kommen vornehmlich in unkonsolidierten känozoischen Sedimenten oberhalb von Zechstein-Salzdiapiren vor. Als Beispiele werden drei seismische Profile mit Häufungen dieser Anomalien, einschließlich deutlich erhöhter Amplituden („bright spots“), Abschwächungen des seismischen Signals („seismic attenuation“) und verlängerter Laufzeiten des seismischen Signals („velocity pull-down“) diskutiert und mit dem seismischen Abbild von derzeit produzierenden niederländischen Flachgas-Feldern verglichen.

Austrittsstellen von Methan im Meeresboden der nordwestlichen deutschen Nordsee, oberhalb des deutschen Zentralgrabens, wurden mit Hilfe eines schiffbasierten Mehrfachstrahl-Echolots kartiert. Die meisten dieser Austrittsstellen traten oberhalb von Salzstrukturen auf, welche in reflexionsseismischen Daten Amplitudenanomalien in ihrem Deckgebirge aufweisen. Aufgegebene Offshore-Bohrlöcher zeigen dagegen keine Beziehung zu den Austrittsstellen. Die Analyse von sowohl boden- als auch oberflächennahen Wasserproben an den Austrittsstellen zeigte erhöhte Methankonzentrationen und weist auf einen Beitrag zum atmosphärischen Treibhausgashaushalt hin.

Das Potential zur Kohlenwasserstoffgenerierung von sechs Formationen der Obersten Trias bis zur Untersten Kreide wurde untersucht. Diese Formationen beinhalten bedeutende Kohlenwasserstoff-Muttergesteine des südlichen Zentralgrabens, wie den unterjurassischen Posidonienschiefer und die oberjurassischen bis unterkretazischen „Hot Shales“, welche beide mit Hilfe reflexionsseismischer Daten neu kartiert wurden. Zusätzlich wurden andere marine oder terrestrische Formationen untersucht, welche Tonsteine oder Kohleschichten enthalten. Die Ergebnisse zeigen, dass Formationen, welche ansonsten nicht im Fokus stehen, wahrscheinlich Kohlenwasserstoffe gebildet haben und die wahrscheinlichsten Quellen für mögliches thermisch gebildetes Gas innerhalb der Flachgasvorkommen im Untersuchungsgebiet sind.

Die tektonostratigraphische Entwicklung des deutschen Zentralgrabens wurde rekonstruiert. Dafür wurden neun lateral verfolgbare Horizonte des Unteren Juras bis zur Unteren Kreide mit Hilfe reflexionsseismischer Daten kartiert, einschließlich der Basishorizonte von tektonostratigraphischen Megasequenzen. Die Ergebnisse stellen die Entwicklung des Beckens von rift- zu salzdominierter, zu thermisch induzierter Subsidenz dar. Sie werden in die tektono- und sequenzstratigraphischen Konzepte der Niederlande und Dänemarks eingeordnet und hinsichtlich des tektonischen Einflusses auf die (Litho-)stratigraphie diskutiert.

List of abbreviations

2D = 2 dimensional	Ma = million years
3D = 3 dimensional	max. = maximum
4WDC = four way dip closure	MBES = multibeam echosounder
AHRS = Attitude-Heading-Reference- System	MBF = main bounding fault
BGR = Bundesanstalt für Geowissenschaften und Rohstoffe	mbsf = meters below sea floor
CCS = carbon capture and storage	MCGTZ = Mid Central Graben Transfer Zone
CSF = Coffee Soil Fault	METS = methane sensor
CTD = conductivity temperature depth probe	ml = milliliter
DHI = direct hydrocarbon indicator	MMU = Mid Miocene Unconformity
DT = sonic (delta transit time)	mol/L = mol per Liter
EBN = Energie Beheer Nederland	m/s = meter per second
EEZ = Exclusive Economic Zone	nM = nanomolar
e.g. = for example (exempli gratia)	ppb = parts per billion
EM = electromagnetic	ppm = parts per million
FDC = fault-dip closure	R/V = research vessel
Fig. = figure	SF = Schillgrund Fault
GeoERA = “Establishing the European Geological Surveys Research Area to deliver a Geological Service for Europe” - project	SPB = Southern Permian Basin
GR = gamma ray	SU = seismic unit
i.e. = that is (id est)	Tab. = table
kH = kilohertz	TMS = tectonostratigraphic mega-sequence
km = kilometer	TTZ = Teisseyre-Tomquist-Zone
kn = knots	TUNB =“ Tieferer Untergrund Norddeutsches Becken“ - project
kPa = kilopascal	TWT = two-way time
kt year⁻¹ = 1000 tons per year	v. = version
L/min = liter per minute	
LOD = last occurrence datum	
m = meter	

Structure of thesis

The presented dissertation entitled “The German Central Graben (North Sea): Tectonostratigraphic evolution and hydrocarbon systems” is organized in eight chapters.

Chapter 1 provides a brief introduction to the scientific topic, a recapitulation of previous studies, an overview of the projects linked to this thesis, and major aims of this thesis.

Chapter 2 gives a brief description of the methods used in this thesis.

The main results of this thesis appear in the **chapters 3 to 6**, which are individual papers published or submitted to a peer-reviewed scientific journal:

Chapter 3 investigates amplitude anomalies in reflection seismic data that indicate shallow gas accumulations in unconsolidated Cenozoic sediments in the northwestern German North Sea (Entenschnabel). The most prominent anomaly clusters occur above salt domes in the German Central Graben area, which were compared to shallow gas accumulations in northern offshore The Netherlands. This chapter has previously been published as Müller, S., Reinhardt, L., Franke, D., Gaedicke, C., & Winsemann, J., 2018. Shallow gas accumulations in the German North Sea. *Marine and Petroleum Geology*, 91, 139-151.

Chapter 4 describes how evidence of seafloor methane seeps in the northwestern German North Sea (Entenschnabel) was provided by detecting gas flares using a ship-based multibeam echosounder and by measuring dissolved methane concentrations in bottom and surface waters. Most of the seeps and the highest methane concentrations occur above salt structures in the German Central Graben area. This chapter has previously been published as Römer M., Blumenberg M., Heeschen K., Schloemer S., Müller H., Müller S., Hilgenfeldt C., Barckhausen U., & Schwalenberg K., 2021. Seafloor Methane Seepage Related to Salt Diapirism in the Northwestern Part of the German North Sea. *Frontiers in Earth Science*.

In **chapter 5**, potential thermogenic sources for hydrocarbons in the German Central Graben in general, and for shallow gas accumulations in particular were investigated. Therefore, the potential for generating thermogenic hydrocarbons of Upper Triassic to Lower Cretaceous formations was assessed by mapping potential source rock horizons in reflection seismic data and implementing them into a modified petroleum system model of the northern German North Sea. This chapter has previously been published as Müller, S., Arfai, J., Jähne-Klingberg, F., Bense, F., & Weniger, P., 2020. Source rocks of the German Central Graben. *Marine and Petroleum Geology*, 113, 104-120.

In **chapter 6**, the tectonostratigraphic evolution of the German Central Graben is reconstructed. Therefore, base horizons of four tectonostratigraphic mega-sequences (TMS) and several subdivisions were mapped on reflection seismic data. Local depocenters were identified by creating thickness and subsidence maps, the relative influence of rifting and salt tectonics was distinguished, and the results were integrated into Dutch and Danish tectono- and sequence stratigraphic concepts of the southern Central Graben. This chapter has been submitted to a peer-reviewed journal (*Netherlands Journal of Geosciences*) on 24th July 2022 as “Jurassic to Lower Cretaceous tectonostratigraphy of the German Central Graben, southern North Sea”.

Chapter 7 synthesizes the findings of this thesis and discusses the petroleum systems of the southern Central Graben in a tectonostratigraphic context.

Chapter 8 concludes the thesis with some recommendations for future studies.

1. Introduction

1.1. Geological introduction

The Southern Permian Basin (SPB), which includes the later German Central Graben, was affected by a major transgression at the beginning of the Upper Permian Zechstein that turned the once continental environment into an intracratonic sea (Glennie et al., 2003). During the Zechstein, several cycles of evaporites were deposited, including Zechstein salt with a depositional thickness of up to 900 m in the northern Dutch and German Central Graben (ten Veen et al., 2012; Fig. 2). At the transition from the Permian to the Triassic, the supercontinent Pangaea began to break up and a triple junction developed in today's North Sea (Ziegler 1990; 1992). The German Central Graben is part of the Central Graben (Fig. 1), which is the southern arm of the triple junction with the Viking Graben and the Moray Firth Basin as its northern arms (Ziegler 1990). In the Early Triassic, a terrestrial environment led to the deposition of clastics of the Buntsandstein (Geluk 2007; Fig. 2). Terrestrial conditions were replaced by marine conditions in the Middle Triassic by an ingression of the Tethys Ocean from the south. At that time, shallow marine carbonates and clastics of the Muschelkalk were deposited in the southern Central Graben area (Geluk 2007).

During the Late Triassic (Keuper), sedimentation was predominantly terrestrial with flood-plain playa and occasional evaporitic deposits. A transgression in the Rhaetian re-established marine conditions that led to the deposition of marine mudstones of the Sleen Formation (Bachmann et al., 2010). The Sleen Formation is believed to have contributed to hydrocarbon accumulations in the northern Dutch Central Graben (de Jager & Geluk, 2007). The Zechstein salt began to form salt pillows in the Late Triassic, which led to the development of depocenters away from the new salt structures (van Winden et al., 2018). During the Early Jurassic, the sedimentation of marine mud of the later Altena Group offshore The Netherlands or of the Fjerritslev Formation offshore Denmark was still relatively uniform (Wong, 2007; Fig. 2). In the Toarcian, basin circulation became restricted and the bituminous Posidonia Shale Formation was deposited, which is preserved in deep parts of the graben and is a prolific source rock of the northern Dutch Central Graben (de Jager & Geluk, 2007; Lott et al., 2010). In the Middle Jurassic, the volcanic Mid North Sea Dome, developed at the center of the triple junction, causing a thermal uplift of the area that resulted in a regional unconformity due to widespread erosion and truncation of the older strata (Underhill & Partington 1993; Fig. 2). Main rifting of the Central Graben started in the Late Callovian to Oxfordian (Ziegler, 1992). The eastern boundary of the German Central Graben is formed by a major NE-SW trending listric fault system, the Schillgrund Fault. The fault is the prolongation of the NW-SE trending Coffee Soil Fault that forms the eastern boundary of the Danish Central Graben. Its western boundary is formed by the transition to the Step Graben System, an array of structural highs and grabens (Arfai et al., 2014; Fig. 1).

1. Introduction

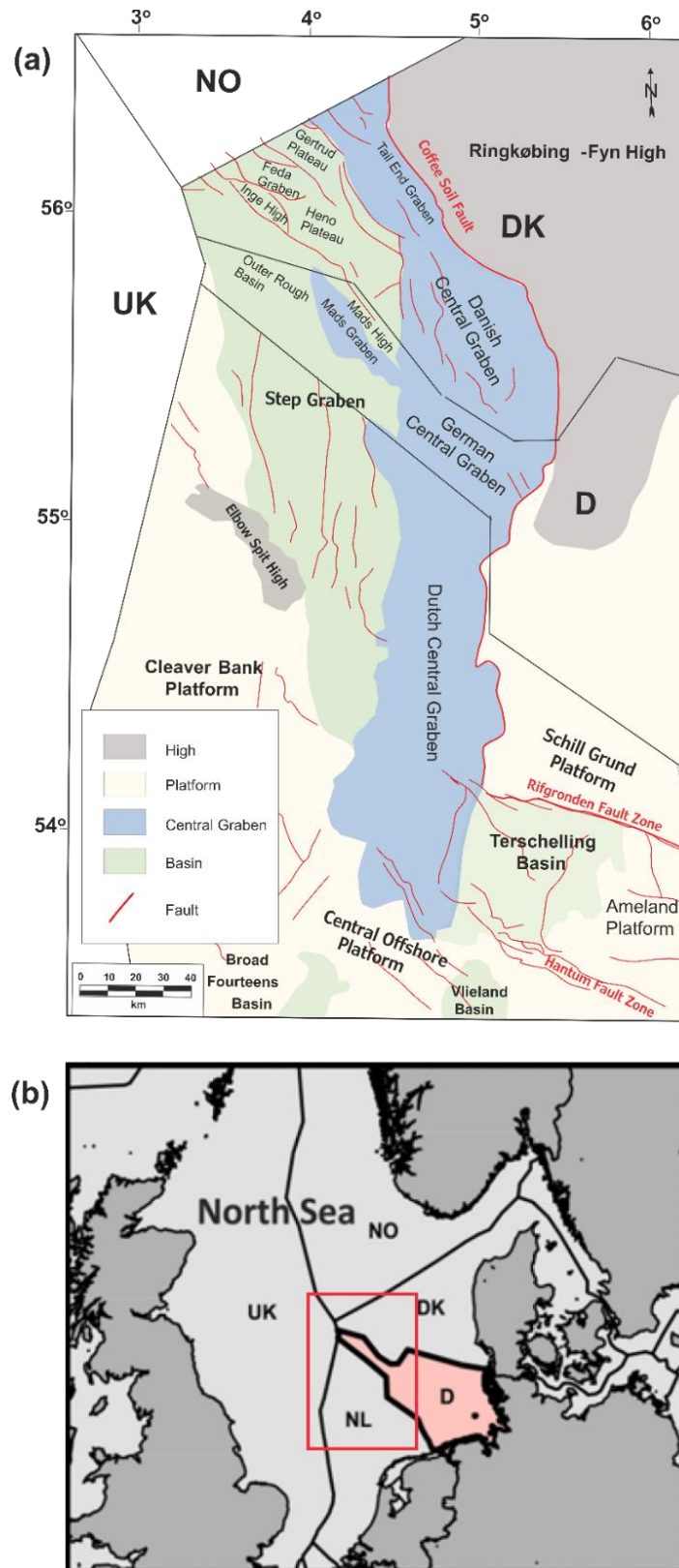


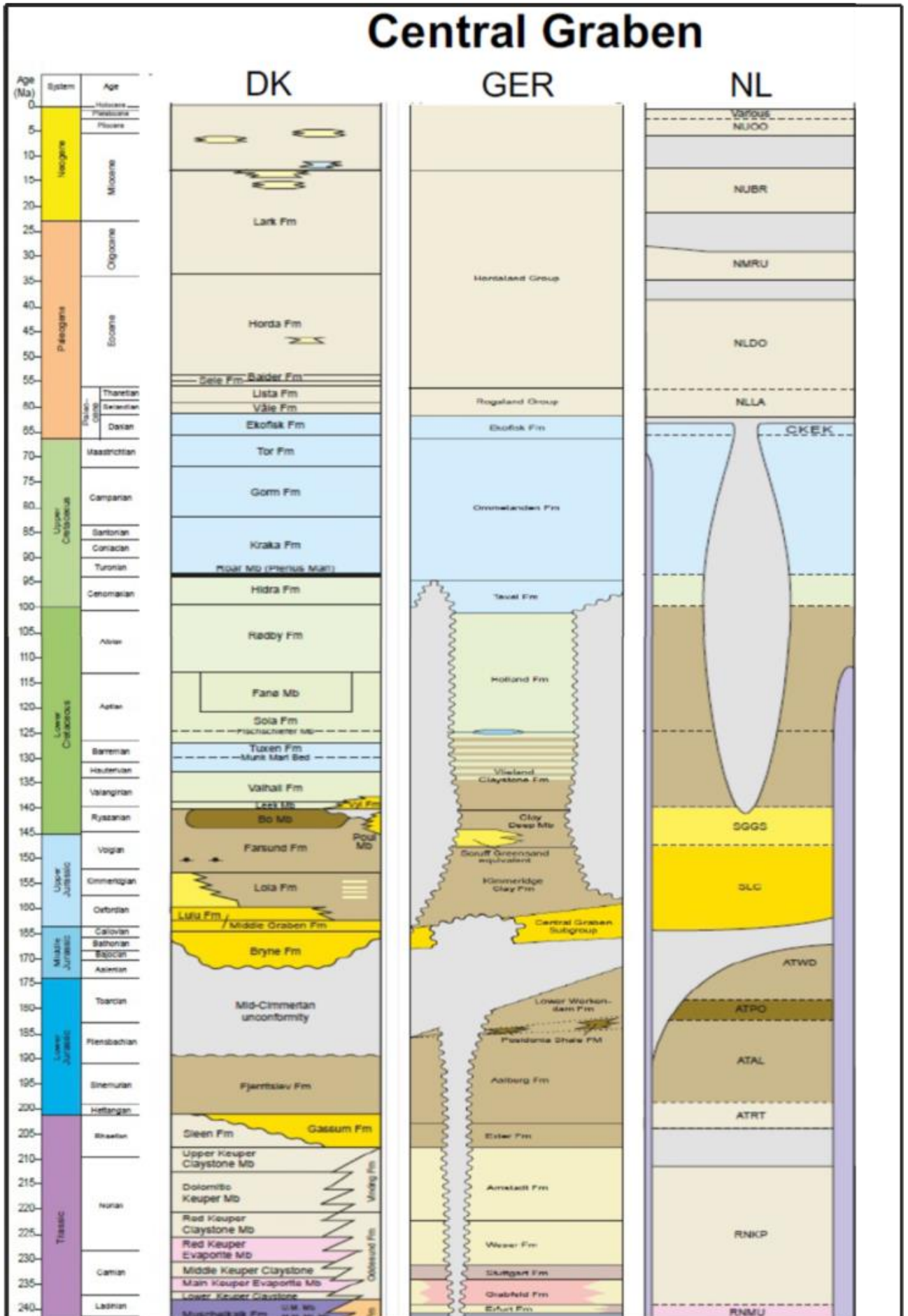
Fig. 1 (a) Map of the Danish, German, and Dutch parts of the Central Graben and adjacent structural elements as platforms and basins (from Jakobsen et al., 2020a). The Central Graben is a half-graben system with eastern main bounding faults (MBF), the Coffee Soil Fault system (CSF) for the Danish part and the Schillgrund Fault system (SF) for the German and Dutch part of the graben. The western boundary, where it transitions into the Step Graben system, is less distinctly defined. (b) Map of the location of (a) in the southern North Sea.

The German Central Graben itself is highly differentiated into various sub-basins, which for the most part evolved during the Late Jurassic (Arfai et al., 2014). Additionally, there are several salt structures that are located within the boundaries of the German Central Graben (Arfai et al., 2014). Resuming subsidence after the collapse of the Mid North Sea Dome resulted in the deposition of continental and deltaic sediments of the Central Graben Subgroup in the Dutch Central Graben and their Danish equivalents, the Bryne, Lulu, and Middle Graben Formation (Michelsen et al., 2003; Wong, 2007; Fig. 2). A southward progressing transgression reestablished marine conditions in the Late Jurassic, resulting in the deposition of marine mud of the Kimmeridge Clay Formation and shallow-marine sands of the Scruff Greensand Formation offshore The Netherlands and the equivalent marine mud of the Lola and Farsund Formation offshore Denmark (Lott et al., 2010).

Salt tectonics peaked in the Late Jurassic due to a regional extension and continued until the Early Cretaceous, accompanied with distinct diapirism and the formation of salt rim synclines (Remmelts, 1995; de Jager, 2007; van Winden et al., 2018). Bituminous “Hot Shales” were deposited in the southern Central Graben when basin circulation stagnated again at the transition from the Late Jurassic to the Early Cretaceous. They form as part of the Bo Member (Farsund Formation) the most prolific source rock of the Danish Central Graben (Ineson et al., 2003). During the Early Cretaceous, rifting ceased, and thermal subsidence affected the southern North Sea area, resulting in a long-term transgression and the deposition of open-marine clays and marls (Herngreen & Wong, 2007). Further thermal contraction in combination with an eustatic sea level rise and reduced influx of erosional detritus led to the deposition of Upper Cretaceous to Lower Paleogene (Danian) chalk sediments, which form important reservoir rocks of major oil fields in the southern Danish Central Graben and of the Hanze field in the northern Dutch Central Graben (Surlyk et al., 2003; de Jager & Geluk, 2007; Fig. 2).

The regional stress regime changed from extensional to compressional in the Santonian to Campanian resulting in the reactivation of pre-existing normal faults as reverse faults and the inversion of Jurassic basins due to the initiation of the Alpine Orogeny (Herngreen & Wong, 2007; Vejbaek et al., 2010). The Paleogene is characterized by a regional transgression that resulted in clay-dominated sedimentation and further major inversion pulses (Ziegler 1990; 1992; Vejbaek & Andersen, 2002). During the Cenozoic, the North Sea developed to an intracratonic sag basin, centered at the Central Trough, which is situated above the older Mesozoic rift-structures (Huuse & Clausen, 2001; Arfai et al., 2018). Above the Mid-Miocene Unconformity (MMU), a prominent sequence boundary that is visible on reflection seismic data, shelf-prism clinofolds prograded westwards into the southern North Sea from the Late Miocene to the Pleistocene, forming the so-called Eridanos Delta (Overeem et al., 2001; Thöle et al., 2014). The delta ceased due to the development of the Fennoscandian ice sheet, and its sediments were superimposed by alternating glacial and interglacial sediments (Zagwijn, 1989; Kuhlmann & Wong, 2008). Shallow gas reservoirs offshore The Netherlands are located in these unconsolidated to moderately consolidated deltaic and glacial sediments of Plio-Pleistocene age (ten Veen et al., 2011).

1. Introduction



1.2. Previous studies

This chapter summarizes the results of relevant studies that have been previously conducted in the southern North Sea on topics related to this thesis. The geographic frame of these studies is mainly the southern North Sea. The topics are shallow gas occurrences, seafloor methane seepage, Mesozoic hydrocarbon systems, and the (tectono-)stratigraphic evolution of the southern Central Graben.

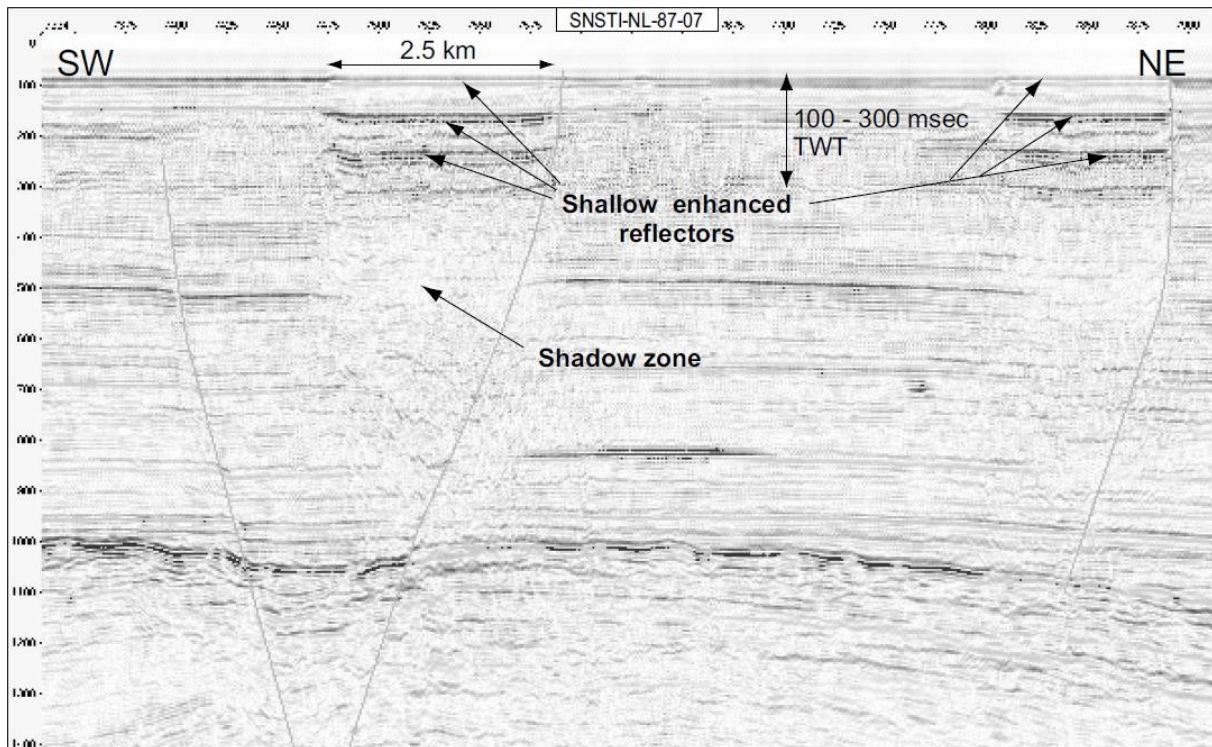


Fig. 3 Bright spots on reflection seismic data offshore The Netherlands (from Schroot & Schüttenhelm, 2003a)

1.2.1. Shallow Gas southern North Sea

Shallow gas is commonly defined as gas that occurs between the seabed and a depth of 1000 m below sea level (MSL) (e.g., Schroot & Schüttenhelm, 2003a; Fig. 3). The presence of gas in shallow, unconsolidated sediments is known to geophysicists since shortly after the Second World War due to geophysical exploration of the seafloor (Davis, 1992). High amplitude anomalies on reflection seismic data were first observed and connected to shallow gas accumulations by Shell geophysicists in the Gulf of Mexico at the end of the 1960s, which they called “bright spots” (Forrest, 2002). The hydrocarbon industry was interested in shallow gas either as potential hazards for drilling and the construction of oil platforms, or as indicators for deeper conventional reservoirs.

In the 1980s and 1990s several studies regarding shallow gas and gas seepages in the North Sea, mainly from the Norwegian sector, were published (e.g., Hovland & Sommerville, 1985; Davis, 1992; Floodgate & Judd, 1992; Judd & Hovland, 1992; Heggland, 1997). At the beginning of the 2000s, an increased interest in natural seepages of hydrocarbons contributing to the global climate change, natural analogues to potential leakage of CO₂ from future locations for carbon capture and storage (CCS), as well as the economic exploitation of shallow gas fields came up. Hence, shallow gas anomalies in northern offshore The Netherlands were increasingly investigated (e.g., Schroot & Schüttenhelm, 2003a; Schroot & Schüttenhelm, 2003b; Schroot et al., 2005).

Schroot and Schüttenhelm (2003a) described amplitude anomalies in reflection seismic data, which they attributed to shallow gas accumulations and gas migration in shallow sediments. The authors observed surface expressions indicative for shallow gas such as pockmarks (topographic lows at the seabed due to the leakage of gas), sub-surface expressions for shallow gas accumulations such as bright spots, flat spots and velocity push-downs, as well as expressions for gas migration in shallow sediments such as gas chimneys (Fig. 3; see chapter 3 for a more detailed definition of the terms). They also noted the connection of shallow gas accumulations with Zechstein salt domes and associated normal faults. Thus, they ascribed the origin of the gas to a deeper thermogenic source with microbial contributions.

Research to the topic continued in the 2010s. Stuart and Huuse (2012) located the shallow gas accumulations in the northern Dutch North Sea in Plio-Pleistocene deltaic and interglacial sediments, building upon a seismo-stratigraphic framework of Kuhlmann and Wong (2008). A major step in understanding the shallow gas in the southern North Sea was conducted by ten Veen et al. (2013). In this TNO report, the authors investigated systematically the shallow gas system offshore The Netherlands with the objective to predict the location and quality of shallow gas reservoirs and seals. They - inter alia - evaluated well logs petrophysically, interpreted reflection seismic data, and conducted sequence stratigraphy to analyze the reservoir architecture and bright spot distribution. As a result, they developed scenarios regarding the generation, migration, charging, and leakage of shallow gas accumulations. They could not resolve the question of the origin of the shallow gas. Though most gases showed typical characteristics of a microbial origin, there were also geochemical indications for a thermogenic source.

Trampe et al. (2014) mapped amplitude anomalies on reflection seismic data in the German North Sea, including bright spots, velocity push-downs, and gas chimneys and conducted AVO-analysis (amplitude variation with offset) on selected examples. They concluded that almost the complete German North Sea is covered with bright spots. Verweij et al. (2018) investigated the generation, migration, entrapment, and leakage of shallow gas accumulations in the northern Dutch North Sea, which they assigned a microbial origin. They concluded that the organic matter in Plio-Pleistocene sediments is of terrigenous origin and that microbial gas generation started in the Early Pleistocene. They concluded that the typical stacked reservoir architecture of the shallow gas accumulations is ascribed to seal leakage and that the microbial gas system is still active.

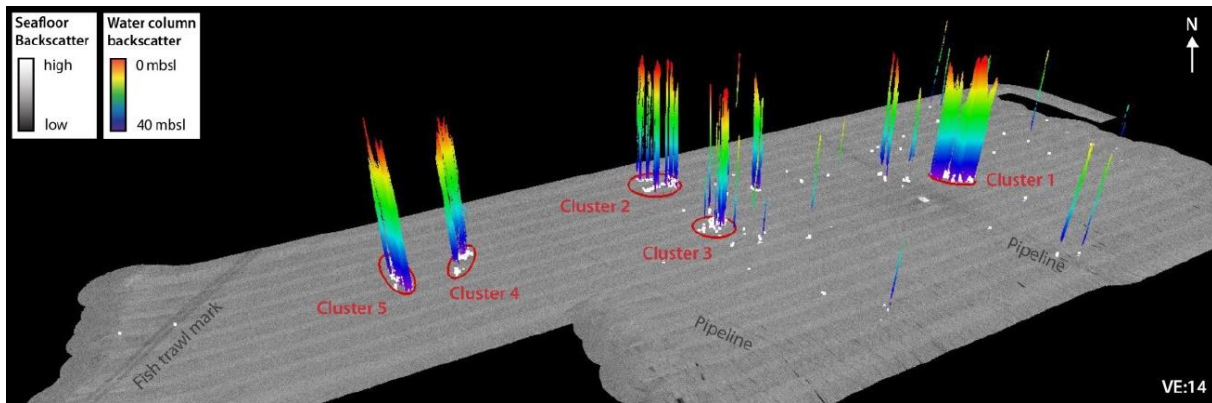


Fig. 4 3D depiction of gas flares above shallow gas accumulations offshore The Netherlands, indicating seafloor methane seepage (from Römer et al., 2017).

1.2.2. Seafloor methane seepage:

Seafloor methane seepage is common on continental shelf margins (e.g., Hovland, 1993; Judd et al., 1994; Wever et al., 1998; Schroot et al., 2005; Krämer et al., 2017). Vielstädte et al. (2015) investigated the leakage of natural gas out of abandoned hydrocarbon exploration and production wells in the Norwegian sector of the North Sea. Therefore, they took samples of seafloor sediments and of free gas from the bubble stream, which were analyzed in a gas chromatograph onshore. Additionally, they quantified the gas emissions via video analysis and measured the gas flow at well locations. The results show that the gas is of microbial origin and probably comes from shallow gas pockets that were penetrated by the wells. These shallow gas pockets are visible on reflection seismic data as high amplitude anomalies (bright spots). They concluded that the path of abandoned wells serves as conduits for natural gas to the seafloor, but that most of the gas is dissolved in the water column and that the contribution to the greenhouse gas budget of the atmosphere is negligible.

Römer et al., (2017) investigated gas seepage from the seafloor located above a shallow gas field in the Dutch North Sea sector B13 close to the northwestern German North Sea sector (Fig. 4). They used a ship-based subbottom echosounder to locate gas pockets in shallow sediments and to map gas flares in the water column. Additionally, they measured the atmospheric methane concentrations above the flares. They found elevated methane concentrations in the atmosphere and concluded that the leaking shallow gas reaches the atmosphere. They suggest that the methane transport to the atmosphere is dependent of the flux rates of the gas flares.

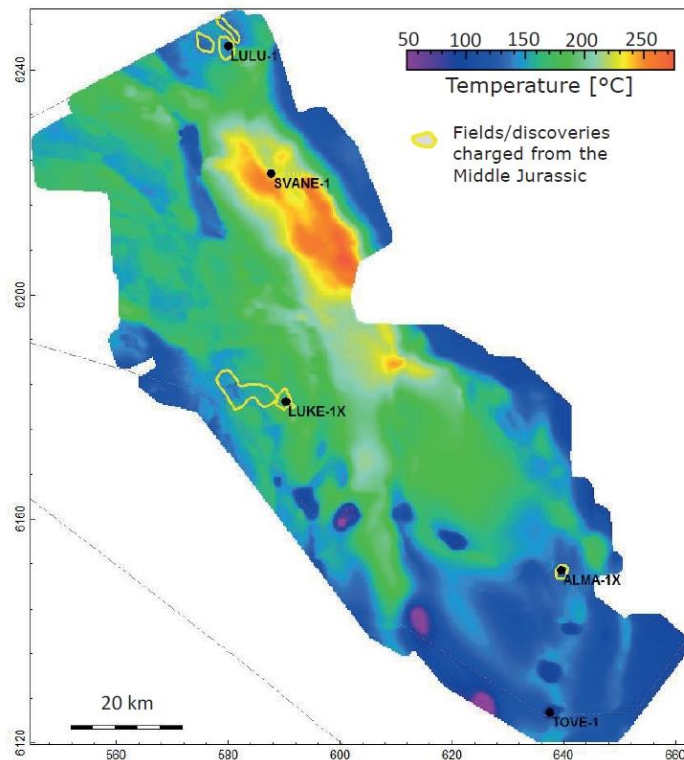


Fig. 5 Modelled present day temperature of the Middle Jurassic coal-bearing horizon, which is believed to be an underestimated source rock in the Danish part of the Central Graben (from Petersen & Hertle, 2018).

1.2.3. Mesozoic Hydrocarbon Systems of the southern North Sea

There are several publications that attend to the petroleum systems of the North Sea due to its significance for its neighboring countries as a major hydrocarbon province. Some books offer a summary of the petroleum systems of the entire North Sea area (e.g., Glennie et al., 2009). Other publications give overviews of different parts of the North Sea. The Millennium Atlas of Evans et al. (2003) concentrates on the petroleum geology of the central and northern North Sea, including Norway, the UK, and Denmark. Pletsch et al. (2010) discuss the petroleum systems of the Southern Permian Basin, including offshore The Netherlands, Germany, and Denmark, and de Jager & Geluk (2007) the petroleum geology of The Netherlands.

Besides these overviews, there are several studies that focus on different aspects of the petroleum geology of the southern North Sea. Ineson et al. (2003) discuss the stratigraphy, facies, and geochemistry of Denmark's most prolific source rock for oil, the Upper Jurassic to Lowermost Cretaceous Bo Member of the Farsund Formation.

Verweij et al. (2009) looked at the petroleum systems of the southern Dutch Central Graben and the neighboring Terschelling Basin offshore The Netherlands. Therefore, they mapped the structural framework and stratigraphic key horizons of the basins on reflection seismic data. They integrated the horizons in 1D, 2D, and 3D petroleum system models, in which they reconstructed the burial and temperature history, source rock maturity and timing of hydrocarbon

generation of the investigated basins. The modelled source rocks include the Lower Jurassic Posidonia Shale Formation.

Fattah et al. (2012) used 3D petroleum system modelling to investigate similar questions regarding the burial and temperature history, source rock maturity and hydrocarbon generation in the northwestern Dutch offshore. In contrast to Verweij et al. (2009), they completely concentrated on pre-Mesozoic source rocks like Westphalian coal seams and Namurian shales. Petersen et al. (2013), Petersen et al. (2017), as well as Ponsaing et al. (2018) investigated the source rock potential of the Upper Jurassic to lowermost Cretaceous Farsund Formation in the Danish Central Graben, which includes the organic-rich Bo Member at its top. Geochemical analysis confirms that the high quality of the Bo Member as an oil source rock but also indicates that lower intervals of the Farsund Formation have the potential to generate hydrocarbons and probably contributed to hydrocarbon accumulations in the Danish Central Graben.

Arfai and Lutz (2017) investigated the hydrocarbon potential of the northwestern German North Sea, which includes the German Central Graben. Therefore, they built a petroleum system model and reconstructed the thermal history, maturity, and petroleum generation of Namurian to Visean coals, of the Lower Jurassic Posidonia Shale Formation and of the Upper Jurassic to lowermost Cretaceous Hot Shale. The depth and the distribution of Posidonia Shale Formation and the Hot Shale were derived from the base of the Lower Jurassic and the base of the Upper Jurassic, respectively, from Arfai et al. (2014). The results show that the Posidonia Shale Formation entered the oil window in the Late Jurassic and is now a mature source rock. The Hot Shale currently early mature with low transformation ratios of organic matter to hydrocarbons.

Petersen and Hertle (2018) examined the potential of Middle Jurassic coals of the Danish Central Graben to generate hydrocarbons (Fig. 5). Therefore, they reviewed published geochemical data to assess the source rock quality of coals and coaly shales of the Middle Jurassic Bryne and Lulu Formations and built a 3D petroleum system model of the Danish Central Graben to reconstruct the temperature and maturity history and timing of hydrocarbon generation and expulsion from the Middle Jurassic coals. They concluded from the results that the petroleum system of the Middle Jurassic constitutes an additional exploration goal to the main source rocks of the Upper Jurassic.

1. Introduction

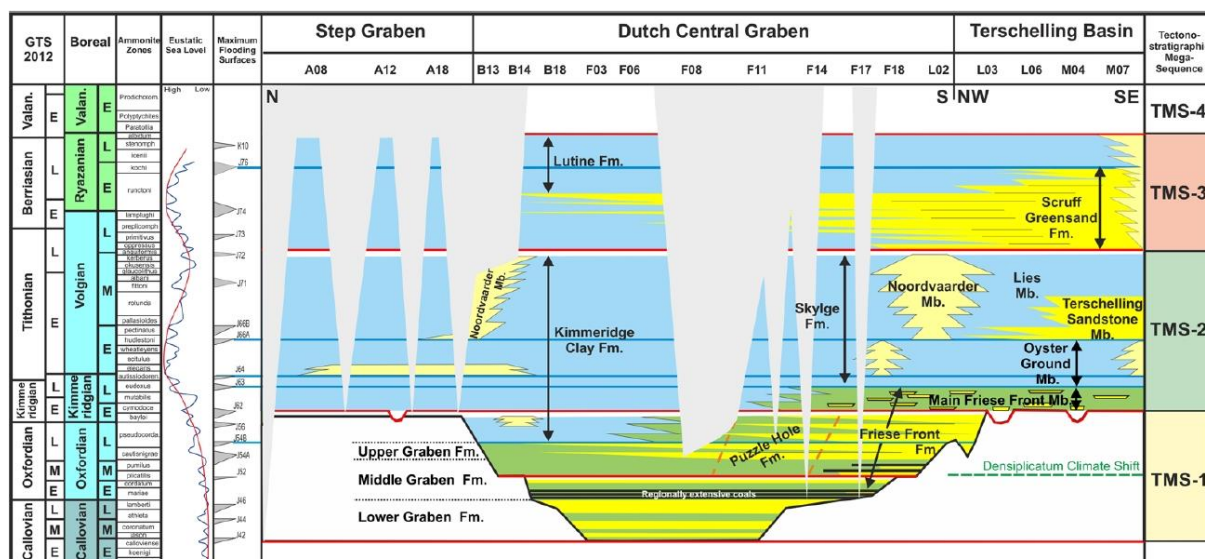


Fig. 6 Tectonostratigraphic subdivision of the Dutch Central Graben and adjacent areas offshore The Netherlands (from Bouroullec et al., 2018).

1.2.4. (Tectono-)stratigraphic evolution of the southern Central Graben

There are several publications that focus on the sedimentary and / or tectonic history of the individual Danish, German, and Dutch Central Graben or of the southern Central Graben as a whole. Andsbjerg and Dybkjaer (2003) developed a sequence stratigraphic framework for the Jurassic of the Danish Central Graben based on petrophysical log data, core sedimentology, and biostratigraphic data. They subdivided the Jurassic rocks into 20 sequences and constructed isochore maps for the individual sequences. Additionally, they subdivided the basin history of the Danish Central Graben into seven phases from a pre-rift phase to the onset of the post-rift stage.

Møller and Rasmussen (2003) divided the tectonic evolution of the Danish central Graben into three tectonic pulses. Therefore, they interpreted 2D and 3D reflection seismic data and additional well log information. The first pulse was active from the Callovian to the Early Oxfordian and is characterized by N-S striking faults, the second was active during the latest Late Kimmeridgian and Early Volgian and is characterized by NNW-SSE-trending faults. The third and last tectonic pulse occurred in the mid-Ryazanian and is characterized by rotated fault blocks.

Duffy et al. (2013) investigated the dependency of the basin evolution, especially in the Danish Salt Dome Province, from the initial salt thickness. Therefore, they interpreted a 3D reflection seismic survey and built structure and thickness maps. They concluded that the thickness of the pre-rift stratigraphy significantly influenced the structural styles, basin geometries and the tectono-stratigraphic evolution in the Jurassic rift phase of the Danish Central Graben.

Arfai et al. (2014) investigated the geological evolution of the northwestern German offshore from the Late Palaeozoic to the Early Cenozoic. They mapped 13 chronostratigraphic horizons from the Late Permian to the Palaeogene on 2D and 3D reflection seismic data and created

thickness and depth maps. With these maps they were able to reconstruct the geological evolution of the northwestern German North Sea.

Abbink et al. (2006) investigated the stratigraphic evolution of the Dutch Central Graben and the adjacent Terschelling Basin. They used biostratigraphic, sedimentological, and lithologic data of 150 wells to divide the Jurassic rocks of the Dutch Central Graben into three stratigraphic sequences. The first sequence from the Callovian to the earliest Kimmeridgian is characterized by the initiation of the Dutch Central Graben, the second sequence from the early Kimmeridgian to the early Portlandian by the initiation of the Terschelling Basin, and the third sequence by the by a regional transgression during the late Portlandian to the Ryazanian.

Bouroullec et al. (2018) and Verreussel et al. (2018) built upon the results of Abbink et al. (2006) and developed a tectonostratigraphic framework of the southern Central Graben (Fig. 6). Bouroullec et al. (2018) used core descriptions, palynological and geochemical analyses, and seismic and well log interpretation. They were able to define three tectonostratigraphic mega-sequences within the Middle Jurassic to the Lower Cretaceous of the Dutch Central Graben. Verreussel et al. (2018) presented a tectonostratigraphic basin evolution model of the Middle Jurassic to the Lower Cretaceous of the Dutch to the Danish Central Graben. They correlated palynological data from Dutch and Danish wells and they defined a series of four tectonostratigraphic mega-sequences and several sequences for the southern Central Graben that reflect the stepwise evolution of the southern Central Graben.

Stollhofen et al. (2008) attend to the bigger picture and described the basin evolution of the Central European Basin System, that includes the Northern and Southern Permian Basin, from the Upper Rotliegend to the Early Cretaceous. Inter alia, they summarized the stratigraphic framework, the basin evolution, the paleogeography and depositional environments, and geodynamics during the Jurassic and Early Cretaceous.

1.3.TUNB and 3DGEO-EU Project

The studies, which are presented in chapters 3 “Shallow gas accumulations in the German North Sea”, chapter 4 “Seafloor Methane Seepage Related to Salt Diapirism in the Northwestern Part of the German North Sea”, chapter 5 “Source rocks of the German Central Graben”, and chapter 6 “Jurassic to Lower Cretaceous tectonostratigraphy of the German Central Graben, southern North Sea” were realized within the project “Subsurface potentials for storage and economic use in the North German Basin (TUNB)”. TUNB is a joint project of the state geological survey organizations of the north German federal states (Schleswig-Holstein, Mecklenburg-Vorpommern, Brandenburg, Sachsen-Anhalt, Niedersachsen) that is coordinated by the federal geological survey of Germany (Federal Institute for Geosciences and Resources (BGR)). The aim of the project was to develop a structural 3D model of the North German Basin. This thesis aims to investigate subsurface potentials of the basin and forms parts of other modules of the project.

Parts of the study, on which chapter 6 “Jurassic to Lower Cretaceous tectonostratigraphy of the German Central Graben, southern North Sea” is based, were also realized within the project “3D geomodelling for Europe (3DGEO-EU)”. 3DGEO-EU is part of the superordinated European project “Establishing the European Geological Surveys Research Area to deliver a Geological Service for Europe (GeoERA)”, in which 45 national and regional geological surveys from 32 European countries collaborated in 15 research projects regarding the subsurface. As one of those projects, 3DGEO-EU aimed to demonstrate the implementation of cross-border harmonization of national geological interpretations on pilot areas around Germany.

1.4. Aims of the thesis

The Central Graben, a Mesozoic half-graben system, is an extraordinary interesting and prolific area of investigation for a geoscientist. Its geological history witnessed the interaction of tectonics and halokinesis, erosion and deposition, extension and inversion, and formed shallow and deep petroleum systems. The German Central Graben in particular is of interest, because it connects the roughly NW-SE trending Danish Central Graben in the north and the roughly N-S trending Dutch Central Graben in the south (Fig. 1). The hydrocarbon reservoirs in the Salt Domes Province of the Danish Central Graben are mostly charged by Upper Jurassic to lowermost Cretaceous source rocks, while the reservoirs in the Dutch Central Graben are mostly sourced by Lower Jurassic source rocks. Additionally, there are shallow gas fields in Cenozoic sediments above the Dutch Central Graben and its prolongation, the Dutch Step Graben. In contrast to its sibling graben parts, which are objects of comparably intensive research due to the presence of these prolific hydrocarbon occurrences and due to a different legislation regarding the rights of geophysical data, the German Central Graben is far less investigated.

The aim of this thesis is to reduce the research gap between the graben parts and to advance the understanding of the relation between (salt-)tectonics and stratigraphy, and their influence on petroleum systems of the German Central Graben. In the following section, the specific aims of individual studies are elucidated that function as steppingstones to the overall aim and as chapters of this dissertation

Topic 1

Knowledge about shallow gas accumulations is important in various aspects. They are a natural hazard for offshore drilling and may compromise the stability of the underground in the offshore construction of, for example, drilling platforms or offshore wind farms. Also, they can be exploited as a natural energy resource and may indicate active thermogenic source rocks at depths and undiscovered hydrocarbon accumulations. Previous compilations of the distribution of bright spots in the German North Sea from Pletsch et al. (2010) and Trampe et al. (2014) show that high amplitude anomalies expand over large areas offshore Germany but they do not allow to distinguish between pore fluids or lithology as the origin of the anomalies.

One aim of this thesis is to assess the existence and distribution of high amplitude anomalies that are with high probability caused by hydrocarbon pore fluids and not by other lithological reasons and to present a theory of their formation. Therefore, bright spots were systematically mapped on reflection seismic data that occur in combination with other amplitude anomalies indicative for hydrocarbons like seismic attenuation, velocity pull-downs, flat spots, and gas chimneys and that feature typical attributes of Dutch shallow gas fields like a stockwork architecture and a combined occurrence with salt structures. The results are presented within chapter 3.

Topic 2:

Besides the strong indications for shallow gas accumulations from reflection seismic data seen in chapter 3, hard evidence for natural gas being the origin of the amplitude anomalies is still missing. Seafloor methane seepage is common on continental shelf margins like the North Sea. Vielstädte et al. (2015) investigated the leakage of natural gas out of abandoned hydrocarbon exploration and production wells in the Norwegian North Sea and Römer et al. (2017) described gas seepage out of the seafloor above a shallow gas field in the Dutch North Sea. However, proof for methane seepage is lacking within the area of presumed shallow gas accumulations in the German North Sea besides its possible significance for the regional greenhouse gas budget.

A specific aim of this thesis is therefore to detect methane seepage within the northwestern German North Sea and to inquire if its occurrence is connected to the presumed shallow gas accumulations above salt structures or abandoned hydrocarbon exploration wells. Hydroacoustic, electromagnetic, and geochemical data were acquired during a cruise with a research vessel in the northwestern German North Sea to presumed shallow gas accumulations. The results are presented in chapter 4.

Topic 3:

Shallow gas accumulations may have a microbial origin, a thermogenic origin, or may be a mixture of both. The limited occurrence of German shallow gas accumulations within the Mesozoic graben structure of the German Central Graben may be indicative for a contribution of thermogenic natural gas sourced by Upper Triassic to Lower Cretaceous sedimentary rocks that were eroded or not deposited elsewhere offshore Germany.

Arfai and Lutz (2017) built a petroleum system model of the northwestern German North Sea. However, they did not map the two most important Mesozoic source rocks of the southern North Sea, the Lower Jurassic Posidonia Shale Formation and the Upper Jurassic to lowermost Cretaceous Hot Shales (Bo Member offshore Denmark and Clay Deep Member offshore The Netherlands) but derived their distribution and depth from other existing horizons. Also, they did not investigate the petroleum potential of other possible source rocks, like Middle Jurassic coals or Upper Triassic Rhaetian marine shales.

Consequently, another aim of this thesis is to create accurate maps of the distribution of the Posidonia Shale Formation and the Hot Shales within the German Central Graben and to assess the petroleum potential of these formations and other previously neglected potential Mesozoic source rocks. The Posidonia Shale Formation and the Hot Shales were mapped on reflection seismic data and the petroleum system model of Arfai and Lutz (2017) was modified regarding the new mapping results and the other potential source rocks. The results are presented in chapter 5.

Topic 4:

The shallow gas accumulations and deeper petroleum systems are closely linked to the Mesozoic rift system of the Central Graben. Either due to salt structures that created migration pathways and structural traps, or due to the occurrence of Upper Triassic to lowermost Cretaceous sedimentary rocks with sufficient organic matter at a sufficient depth to generate hydrocarbons. The relationship between sedimentation, rifting, and salt tectonics – the tectonostratigraphy – was described for the Dutch Central Graben by Verreussel et al. (2018) and Bouroullec et al. (2018), for the Danish Central Graben by Andsbjerg and Dybkjaer (2003). A tectonostratigraphic study of the German Central Graben was still outstanding, though.

To fill this gap we investigated how rifting and salt tectonics influenced the sedimentation during the Jurassic and Lower Cretaceous. We adapted the tectonostratigraphic approach of Verreussel et al. (2018) and Bouroullec et al. (2018) for the German Central Graben and mapped base horizons of tectonostratigraphic mega-sequences (TMS) and additional horizons within the German Central Graben and adjacent areas and created subsidence and thickness maps. The results are presented in chapter 6.

1.5. Publications and author contributions

Chapter 3 was published as Müller, S. (SM), Reinhardt, L. (LR), Franke, D. (DF), Gaedicke, C. (CG), & Winsemann, J. (JW), 2018. Shallow gas accumulations in the German North Sea. *Marine and Petroleum Geology*, 91, 139-151. SM developed the concept of the paper, designed the methodology, analyzed the data and executed the seismic interpretation, interpreted and discussed the results, and took the lead in writing the manuscript, especially the original draft and after reviews. LR, DF, CG, and JW critically reviewed the paper in the pre-publication stage.

Chapter 4 was published as Römer M. (MR), Blumenberg M. (MB), Heeschen K. (KH), Schloemer S. (SS), Müller H. (HM), Müller S. (SM), Hilgenfeldt C. (CH), Barckhausen U. (UB), & Schwalenberg K. (KS), 2021. Seafloor Methane Seepage Related to Salt Diapirism in the Northwestern Part of the German North Sea. *Frontiers in Earth Science*. KS provided funding acquisition as well as cruise preparation and management for R/V Heincke cruise HE537. MR, SM, and UB carried out on board hydroacoustic data collection. MR took care about the hydroacoustic data processing, curation, and archiving. MB, SS, and KH acquired sediment and water sampling. MB and SS conducted gas analysis. KH collected, processed, and archived the hydrological data. KH, MB, HM, and MR interpreted the METS data. HM, CH, and KS conducted, processed, and interpreted electromagnetic measurements. MR, MB, HM, KH, SS, and KS contributed to the interpretation of the results. MR took the lead in writing the manuscript. All authors helped shape the research, analysis, and manuscript.

Chapter 5 was published as Müller, S. (SM), Arfai, J. (JA), Jähne-Klingberg, F. (FJK), Bense, F. (FB), & Weniger, P. (PW), 2020. Source rocks of the German Central Graben. *Marine and Petroleum Geology*, 113, 104-120. SM developed the concept of the paper, designed the methodology, analyzed the data and executed the seismic interpretation, interpreted and discussed the results, and took the lead in writing the manuscript, especially the original draft and after reviews. SM and JA performed the petroleum system modeling. PW conducted the geochemical analyses. FJK and FB critically reviewed the paper in the pre-publication stage.

Chapter 6 was submitted for publication as Müller, S. (SM), Jähne-Klingberg, F. (FJK), Thöle, H. (HT), Jakobsen, F. (FJ), Bense, F. (FB), Winsemann, J. (JW), Gaedicke, C. (CG), 2022. Jurassic to Lower Cretaceous tectonostratigraphy of the German Central Graben, southern North Sea [manuscript submitted for publication]. SM developed the concept of the paper, designed the methodology, analyzed the data and executed the seismic interpretation, interpreted and discussed the results, and took the lead in writing the manuscript, especially the original draft and after reviews. FJK contributed to fabricating the results, especially the thickness, subsidence and pillar maps, and critically reviewed and edited the paper in the pre-publication stage. HT performed the well log correlation. FJ contributed the pre-modification structural map, lithostratigraphy, and time-stratigraphic panel. FB contributed to fabricating the results, especially the thickness maps. JW and CG critically reviewed and edited the paper in the pre-publication stage.

References

- Abbink, O. A., Mijnlief, H. F., Munsterman, D. K., & Verreussel, R. M. C. H., 2006. New stratigraphic insights in the 'Late Jurassic' of the southern Central North Sea Graben and Terschelling Basin (Dutch Offshore) and related exploration potential. *Netherlands Journal of Geosciences*, 85(3), 221-238.
- Andsbjerg, J. & Dybkjær, K., 2003. Sequence stratigraphy of the Jurassic of the Danish central graben. In: Surlyk, F., Ineson, J.R. (eds.), *The Jurassic of Denmark and Greenland*. Geological Survey of Denmark and Greenland Bulletin, vol. 1. pp. 265–300.
- Arfai, J. & Lutz, R., 2017. 3D basin and petroleum system modeling of the NW German North Sea (Entenschnabel). In: Bowman, M., Levell, B. (eds.), *Petroleum Geology of NW Europe: 50 Years of Learning – Proceedings of the 8th Petroleum Geology Conference*. Geological Society, London, pp. 8–35.
- Arfai, J., Jähne, F., Lutz, R., Franke, D., Gaedicke, C. & Kley, J., 2014. Late Palaeozoic to Early Cenozoic geological evolution of the northwestern German North Sea (Entenschnabel): New results and insights. *Netherlands Journal of Geosciences* 93(4): 147-174.
- Arfai, J., Franke, D., Lutz, R., Reinhardt, L., Kley, J., & Gaedicke, C., 2018. Rapid quaternary subsidence in the northwestern German North Sea. *Scientific reports*, 8(1), 1-12.
- Bachmann, G.H., Geluk, M.C., Warrington, G., Becker-Roman, A., Beutler, G., Hagdorn, H., Hounslow, M.W., Nitsch, E., Röhling, H.-G., Simon, T. & Szulc, A., 2010. Triassic. In: Doornenbal, J.C. & Stevensen, A.G. (eds.) *Petroleum Geological Atlas of the Southern Permian Basin Area*. European Association of Geoscientists and Engineers (EAGE), Houten, The Netherlands, 149–173.
- Bouroullec, R., Verreussel, R. M. C. H., Geel, C. R., De Bruin, G., Zijp, M. H. A. A., Körösi, D., Munsterman, D. K., Janssen, N. M. M. & Kerstholt-Boegehold, S. J., 2018. Tectonostratigraphy of a rift basin affected by salt tectonics: synrift Middle Jurassic–Lower Cretaceous Dutch Central Graben, Terschelling Basin and neighbouring platforms, Dutch offshore. *Geological Society, London, Special Publications*, 469(1), 269-303.
- Davis, A. M., 1992. Shallow gas: an overview. *Continental shelf research*, 12(10), 1077-1079.
- de Jager, J., 2007. Geological development. In: Wong, T.E., Batjes, D.A.J. & de Jager, J. (eds.) *Geology of the Netherlands*. Royal Netherlands Academy of Arts and Sciences, Amsterdam, 5–26.
- de Jager, J., & Geluk, M. C., 2007. Petroleum Geology. In: Wong, T.E., Batjes, D.A.J. & de Jager, J. (eds.) *Geology of the Netherlands*. Royal Netherlands Academy of Arts and Sciences, Amsterdam, 241–264.
- Duffy, O. B., Gawthorpe, R. L., Docherty, M. & Brocklehurst, S. H., 2013. Mobile evaporite controls on the structural style and evolution of rift basins: Danish Central Graben, North Sea. *Basin Research*, 25(3), 310-330.

Evans, D., Graham, C., Armour, A. & Bathurst, P. (eds.). 2003. The Millennium Atlas: petroleum geology of the central and northern North Sea. The Geological Society of London, London.

Fattah, R. A., Verweij, J. M., Witmans, N. & Ten Veen, J. H., 2012. Reconstruction of burial history, temperature, source rock maturity and hydrocarbon generation in the northwestern Dutch offshore. *Netherlands Journal of Geosciences*, 91(4), 535-554.

Floodgate, G. D. & Judd, A. G., 1992. The origins of shallow gas. *Continental Shelf Research*, 12(10), 1145-1156.

Forrest, M. C., 2002. Gulf of Mexico “Bright Spots” – Early Shell Discoveries. Search and Discovery Article #40054

Geluk, M.C., 2007. Triassic. In: Wong, T.E., Batjes, D.A.J., de Jager, J. (eds.), *Geology of the Netherlands*. Royal Netherlands Academy of Arts and Sciences, Amsterdam, pp. 85–106.

Glennie, K. W. (ed.), 2009. *Petroleum Geology of the North Sea: Basic concepts and recent advances*. Wiley-Blackwell. 656 pp.

Glennie, K.W., Higham, J. & Stemmerik, L., 2003. Permian. In: Evans, D., Graham, C., Armour, A. and Bathurst, P. (eds.): *The Millennium Atlas: Petroleum Geology of the Central and Northern North Sea*. The Geological Society (London): 91-103. 01608468033

Heggland, R., 1997. Detection of gas migration from a deep source by the use of exploration 3D seismic data. *Marine Geology*, 137(1-2), 41-47.

Herngreen, G.F.W. & Wong, T.E., 2007. Cretaceous. In: Wong, T.E., Batjes, D.A.J. & de Jager, J. (eds.): *Geology of the Netherlands*. Royal Netherlands Academy of Arts and Sciences (Amsterdam): 127-150.

Hovland, M., 1993. Submarine gas seepage in the North Sea and adjacent areas. In: Geological Society, London, *Petroleum Geology Conference series* (Vol. 4, No. 1, pp. 1333-1338). Geological Society of London.

Hovland, M. & Sommerville, J. H., 1985. Characteristics of two natural gas seepages in the North Sea. *Marine and Petroleum Geology*, 2(4), 319-326.

Huuse, M., & Clausen, O.R., 2001. Morphology and origin of major Cenozoic sequence boundaries in the eastern North Sea Basin: top Eocene, near-top Oligocene and the mid-Miocene unconformity. *Basin Research* 13(1): 17-41.

Ineson, J.R., Bojesen-Koefoed, J.A., Dybkjær, K. & Nielsen, L.H., 2003. Volgian–Ryazanian ‘hot shales’ of the Bo member (Farsund Formation) in the Danish Central Graben, North Sea: stratigraphy, facies and geochemistry. In: Surlyk, F., Ineson, J.R. (eds.), *The Jurassic of Denmark and Greenland*, vol. 1. Geological Survey of Denmark and Greenland Bulletin, pp. 403–436.

Judd, A. G. & Hovland, M., 1992. The evidence of shallow gas in marine sediments. *Continental Shelf Research*, 12(10), 1081-1095.

Jakobsen, F., Britze, P., Thöle, H., Jähne-Klingberg, F., Doornenbal, H., Bouroullec, R., Verreussel, R., 2020a. Lithostratigraphic / chronostratigraphic correlation profiles through the study area. 3D Geomodeling for Europe Report GeoE.171.005

Jakobsen, F., Britze, P., Thöle, H., Jähne-Klingberg, F., Doornenbal, H., Vis, G.-J., 2020b. Harmonized stratigraphic chart for the North Sea area NL-DE-DK. 3D Geomodeling for Europe Report GeoE.171.005

Krämer, K., Holler, P., Herbst, G., Bratek, A., Ahmerkamp, S., Neumann, A., Bartholomä, A., van Beusekom, Holtappels, M. & Winter, C., 2017. Abrupt emergence of a large pockmark field in the German Bight, southeastern North Sea. *Sci. Rep.* 7:5150

Kuhlmann, G. & Wong, T.E., 2008. Pliocene paleoenvironment evolution as interpreted from 3D-seismic data in the southern North Sea, Dutch offshore sector. *Mar. Petrol. Geol.* 25 (2), 173–189.

Lott, G. K., Wong, T. E., Duser, M., Andsbjerg, J., Mönnig, E., Feldman-Olszewska, A., & Verreussel, R. M. C. H., 2010. Jurassic. In: Doornenbal, J.C. & Stevenson, A.G. (eds.): Petroleum Geological Atlas of the Southern Permian Basin Area. EAGE Publications b.v. (Houten): 175-193.

Michelsen, O., Nielsen, L.H., Johannessen, P.N., Andsbjerg, J. & Surlyk, F., 2003. Jurassic lithostratigraphy and stratigraphic development onshore and offshore Denmark. In: Surlyk, F., Ineson, J.R. (eds.), *The Jurassic of Denmark and Greenland*. Geological Survey of Denmark and Greenland Bulletin, vol. 1. pp. 147–216.

Møller, J.J. & Rasmussen, E.S., 2003. Middle Jurassic – early Cretaceous rifting of the Danish central graben. In: Surlyk, F., Ineson, J.R. (eds.), *The Jurassic of Denmark and Greenland*. Geological Survey of Denmark and Greenland Bulletin, vol. 1. pp. 247–264.

Overeem, I., Weltje, G.J., Bishop-Kay, C. & Kroonenberg, S.B., 2001. The late Cenozoic Eridanos delta system in the southern North Sea Basin: a climate signal in sediment supply? *Basin Res.* 13 (3), 293–312.

Petersen, H.I. & Hertle, M., 2018. A review of the coaly source rocks and generated petroleums in the Danish North Sea: an underexplored Middle Jurassic petroleum system? *J. Pet. Geol.* 41 (2), 135–154.

Petersen, H.I., Holme, A. C., Andersen, C., Whitaker, M.F., Nytoft, H. P. & Thomsen, E., 2013. The source rock potential of the Upper Jurassic – lowermost Cretaceous in the Danish and southern Norwegian sectors of the Central Graben, North Sea. *First Break*, 31, 43-53.

Petersen, H.I., Hertle, M. & Sulsbrück, H., 2017. Upper Jurassic–lowermost Cretaceous marine shale source rocks (Farsund Formation), North Sea: kerogen composition and quality and the adverse effect of oil-based mud contamination on organic geochemical analyses. *Int. J. Coal Geol.* 173, 26–39.

Pletsch, T., Appel, J., Botor, D., Clayton, C.J., Duin, E.J.T., Faber, E., Górecki, W., Kombrink, H., Kosakowski, P., Kuper, G., Kus, J., Lutz, R., Mathiesen, A., Ostertag-Henning, C., Papiernek, B. & Van Bergen, F., 2010. Petroleum generation and migration. In: Doornenbal, J.C.

and Stevenson, A.G. (eds.): Petroleum Geological Atlas of the Southern Permian Basin Area. EAGE Publications b.v. (Houten): pp. 225-253.

Ponsaing, L., Bojesen-Koefoed, J. A., Thomsen, E. & Stemmerik, L., 2018. Temporal organic facies variations of Upper Jurassic-lowermost Cretaceous source rocks in the Danish Central Graben, North Sea. *International Journal of Coal Geology*, 195, 217-237.

Rommelts, G., 1995. Fault-related salt tectonics in the southern North Sea, the Netherlands. In: Jackson, M.P.A., Roberts, D.G., Snelson, S. (eds.), *Salt Tectonics: a Global Perspective*, AAPG Memoir. 65, pp. 261-272.

Römer, M., Wenau, S., Mau, S., Veloso, M., Greinert, J., Schlüter, M., & Bohrmann, G., 2017. Assessing marine gas emission activity and contribution to the atmospheric methane inventory: A multidisciplinary approach from the Dutch Dogger Bank seep area (North Sea). *Geochemistry, Geophysics, Geosystems*, 18(7), 2617-2633.

Schroot, B.M. & Schüttenhelm, R.T.E., 2003a. Expressions of shallow gas in The Netherlands North Sea. *Neth. J. Geosci.* 82 (1), 91–106.

Schroot, B. M. & Schüttenhelm, R. T., 2003b. Shallow gas and gas seepage: expressions on seismic and other acoustic data from the Netherlands North Sea. *Journal of Geochemical Exploration*, 78, 305-309.

Schroot, B.M., Klaver, G.T. & Schüttenhelm, R.T., 2005. Surface and subsurface expressions of gas seepage to the seabed—examples from the Southern North Sea. *Mar. Petrol. Geol.* 22 (4), 499–515.

Stollhofen, H., Bachmann, G. H., Barnasch, J., Bayer, U., Beutler, G., Franz, M., Kästner, M., Legler, B., Mutterlose, J. & Radies, D., 2008. Upper Rotliegend to early cretaceous basin development. In: Littke, R., Bayer, U., Gajewski, D. & Nelskamp, S. (eds.), *Dynamics of complex intracontinental basins: The Central European Basin System* (pp. 181–207). Berlin, Heidelberg, Germany: Springer-Verlag.

Stuart, J.Y. & Huuse, M., 2012. 3D seismic geomorphology of a large Plio-Pleistocene delta—‘Bright spots’ and contourites in the Southern North Sea. *Mar. Petrol. Geol.* 38 (1), 143–157.

Surlyk, F., Dons, T., Clausen, C.K. & Higham, J., 2003. Upper Cretaceous. In: Evans D, Graham C, Armour A, Bathurst P (eds.) *The Millennium Atlas: petroleum geology of the central and Northern North Sea*. Geological Society of London, London, pp 213–233

ten Veen, J.H., Geel, C.R., Kunakbayeva, G., Donders, T.H. & Verreussel, R.M.C.H., 2011. Property Prediction of Plio-pleistocene Sediments in the A15 Shallow Gas System. TNO Report TNO-060-UT-2011–20101184/C12. TNO Utrecht, The Netherlands.

ten Veen, J.H., van Gessel, S. & den Dulk, M., 2012. Thin-and thick-skinned salt tectonics – Examples from the Dutch North Sea. *Netherlands Journal of Geosciences* 91–4: 447-464.

ten Veen, J., Verweij, H., Donders, T., Geel, K., de Bruin, G., Munsterman, D., Verreussel, R., Daza Cajjal, V., Harding, R. & Cremer, H., 2013. Anatomy of the Cenozoic Eridanos Delta Hydrocarbon System. TNO Report TNO 2013 R10060. TNO Utrecht, The Netherlands.

Thöle, H., Gaedicke, C., Kuhlmann, G. & Reinhardt, L., 2014. Late Cenozoic sedimentary evolution of the German North Sea—A seismic stratigraphic approach. *Newslett. Stratigr.* 47 (3), 299–329.

Trampe, A.F., Lutz, R., Franke, D., Bücker, C., 2014. Oberflächennahes Erdgas in der deutschen Nordsee. *Erdöl Erdgas Kohle* 130, 8–10.

Underhill, J.R. & Partington, M.A., 1993. Jurassic thermal doming and deflation in the North Sea: Implications of the sequence stratigraphic evidence. In: Parker, J.R. (ed.): *Petroleum Geology of Northwest Europe: Proceedings of the 4th conference: The Geological Society (London)*. Petroleum Geology Conference series 4: 337-345.

van Winden, M., de Jager, J., Jaarsma, B., & Bouroullec, R., 2018. New insights into salt tectonics in the northern Dutch offshore: a framework for hydrocarbon exploration. *Geological Society, London, Special Publications*, 469(1), 99-117.

Vejbæk, O. V & Andersen, C, 2002. Post mid-Cretaceous inversion tectonics in the Danish Central Graben – regionally synchronous tectonic events. *Bulletin of the Geological Society Denmark* 49:129–144

Vejbæk, O.V., Andersen, C., Dusar, M., Herngreen, G.F.W., Krabbe, H., Leszczyński, K., Lott, G.K., Mutterlose, J. & Van der Molen, A.S., 2010. Cretaceous. In: Doornenbal, J.C. and Stevenson, A.G. (eds.): *Petroleum Geological Atlas of the Southern Permian Basin Area*. EAGE Publications b.v. (Houten): 195-209.

Verreussel, R. M. C. H., Bouroullec, R., Munsterman, D. K., Dybkjær, K., Geel, C. R., Houben, A. J. P., Johannessen, P. N. & Kerstholt-Boegehold, S. J., 2018. Stepwise basin evolution of the Middle Jurassic–Early Cretaceous rift phase in the Central Graben area of Denmark, Germany and The Netherlands. *Geological Society, London, Special Publications*, 469(1), 305-340.

Verweij, J. M., Souto Carneiro Echternach, M. & Witmans, N., 2009. Terschelling Basin and Southern Dutch Central Graben. Burial History, Temperature, Source Rock Maturity and Hydrocarbon Generation—Area 2A. Built Environment and Geosciences—National Geological Survey, Utrecht, Netherlands, TNO report TNO-034-UT-2009-02065/A.

Verweij, J.M., Nelskamp, S.N., ten Veen, J.H., de Bruin, G., Geel, K. & Donders, T.H., 2018. Generation, migration, entrapment and leakage of microbial gas in the Dutch part of the Southern North Sea Delta. *Mar. Pet. Geol.* 97, 493–516.

Vielstädte, L., Karstens, J., Haeckel, M., Schmidt, M., Linke, P., Reimann, S. & Wallmann, K., 2015. Quantification of methane emissions at abandoned gas wells in the Central North Sea. *Mar. Petrol. Geol.* 68, 848–860.

Wever, T. F., Abegg, F., Fiedler, H. M., Fechner, G., & Stender, I. H., 1998. Shallow gas in the muddy sediments of Eckernförde Bay, Germany. *Continental Shelf Research*, 18(14-15), 1715-1739.

Wong D. A., 2007. Jurassic. In: Wong, T.E., Batjes, D.A.J. & de Jager, J. (eds.): *Geology of the Netherlands*. Royal Netherlands Academy of Arts and Sciences (Amsterdam): 107-125.

Zagwijn, W.H., 1989. The Netherlands during the Tertiary and the Quaternary: a case history of coastal lowland evolution. In: Coastal Lowlands. Springer, Netherlands, pp. 107–120.

Ziegler, P.A., 1990. Geological Atlas of Western and Central Europe, 2nd edn. Shell Internationale Petroleum Maatschappij B.V.; Geological Society Publishing House (Bath): 239.

Ziegler, P.A., 1992. North Sea rift system. *Tectonophysics* 208(1-3): 55-75.

2. Methodology

2.1. Introduction

The purpose of this chapter is to introduce the main interpretation methods used. For comprehensive descriptions of interpretation techniques of geophysical exploration data, it is referred to, e.g., Bacon et al. (2003) and Brown (2011). Geophysical exploration data like well logs and 2D and 3D reflection seismic data were interpreted (chapters 3, 5, and 6). Horizons resulting from the seismic interpretation were gridded and subsequently converted from the time to the depth domain (chapter 5 and chapter 6). Gridded and depth converted horizons were used for petroleum system modelling (chapter 5). For reflection seismic data and well log interpretation Schlumberger's GeoFrame and Paradigm's StratEarth and SeisEarth software were used.

The data used in chapter 4 were derived during the R/V Heincke cruise HE537 in July 2019. During this cruise, hydroacoustic, electromagnetic, and hydro-geochemical were acquired to investigate gas seepage sites in the northwestern German North Sea. The materials and methods used to derive and interpret these data are described in detail in chapter 4.

2.2. Data availability and legislation

The legislation regarding the usage and publication of geological exploration data in Germany affected the studies of this thesis. In Germany, the legislation was rather restricted until June 2020. Until this date, the "Natural Resources Law (Lagerstättengesetz)" from 1934 was effective that gave the data owner the right to decline usage publication disregarding the data's age. It was sometimes difficult to find the holder of rights to the data, because exploration companies merged or ceased to exist, and the current holder of rights had no knowledge of the data and rights. Also, the companies were restrictive in conferring the right to publicate data, which they considered an asset. For this reason, well log and reflection seismic data in chapters 3 and 5 are either not depicted, were anonymized, or it was switched to free data of the northern Dutch Central Graben. In The Netherlands, geological exploration data like well logs or reflection seismic data are open to the public after a certain period. In June 2020, though, the new "Geological Data Law (Geologiedatengesetz)" came into effect and replaced the antiquated "Natural Resources Law". According to the new law, data of private companies, which were used to explore for natural resources, are available ten years after generation. For this reason, well log and reflection seismic data from the German North Sea sector could be used for chapter 6. Nevertheless, the measured depths of the German wells were anonymized.

2.3. Data used

The basis for the research conducted in chapters 3, 5, and 6 was 2D and 3D reflection seismic data and well logs, e.g., sonic (DT) and gamma-ray (GR) logs (Fig. 7). The logs were used to tie the seismic data to (litho-)stratigraphy and to correlate over large and often structurally complicated distances. The reflection seismic data was interpreted regarding amplitude anomalies

(chapter 3) and regarding the extent of specific horizons (chapters 5 and 6). The interpretation results of chapter 5 were then further used in petroleum system modeling, the results of chapter 6 further processed to thickness, subsidence, and pillar maps.

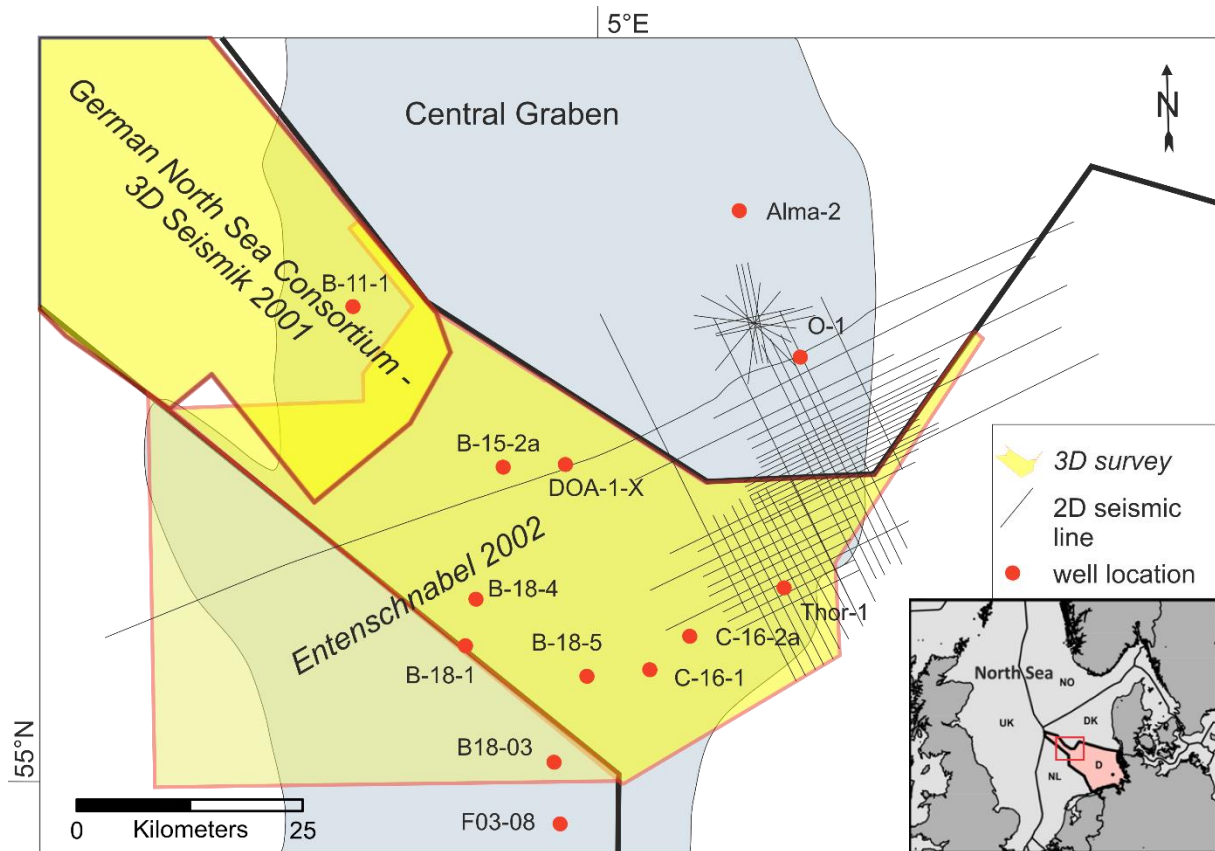


Fig. 7 Data used in the for the studies in chapter 3, 5, and 6. If possible, 3D reflection seismic surveys “German North Sea Consortium – 3D Seismik 2001” and “Entenschnabel 2002” were used for seismic interpretation. The 3D survey “Entenschnabel 2002” is divided in a Dutch and German survey. If it was not possible to use 3D data, 2D reflection seismic lines were interpreted. The depicted wells penetrate Jurassic strata and were used for, e.g., well ties and correlation.

2.4. Well log interpretation

2.4.1. Well correlation

Well logs were used to establish the relationship between seismic reflections on reflection seismic data and stratigraphy. The well logs used were equipped with checkshot data for transformation into the time domain, as well as with chronostratigraphic markers from base Zechstein to the Mid-Miocene Unconformity as described in Arfai et al. (2014) and lithostratigraphic markers with Dutch formation nomenclature for the wells offshore The Netherlands. The Dutch lithostratigraphic formation concept was interpolated to the German and Danish wells using gamma-ray (GR) and sonic (DT) logs (Fig. 8). The Dutch, German, and Danish wells were correlated by identifying patterns on the log curves. For an initial rough correlation, lithological alterations with high impedance contrasts on reflection seismic data like the transition from Upper Cretaceous and Danian chalk to Paleogene mudstones or Lower Jurassic mudstones to

2. Methodology

Middle Jurassic sandstones were identified. For a more detailed correlation the log patterns of marine mudstones were used, because of their low-energy depositional environment, which makes them rather laterally continuous and correlatable from well to well.

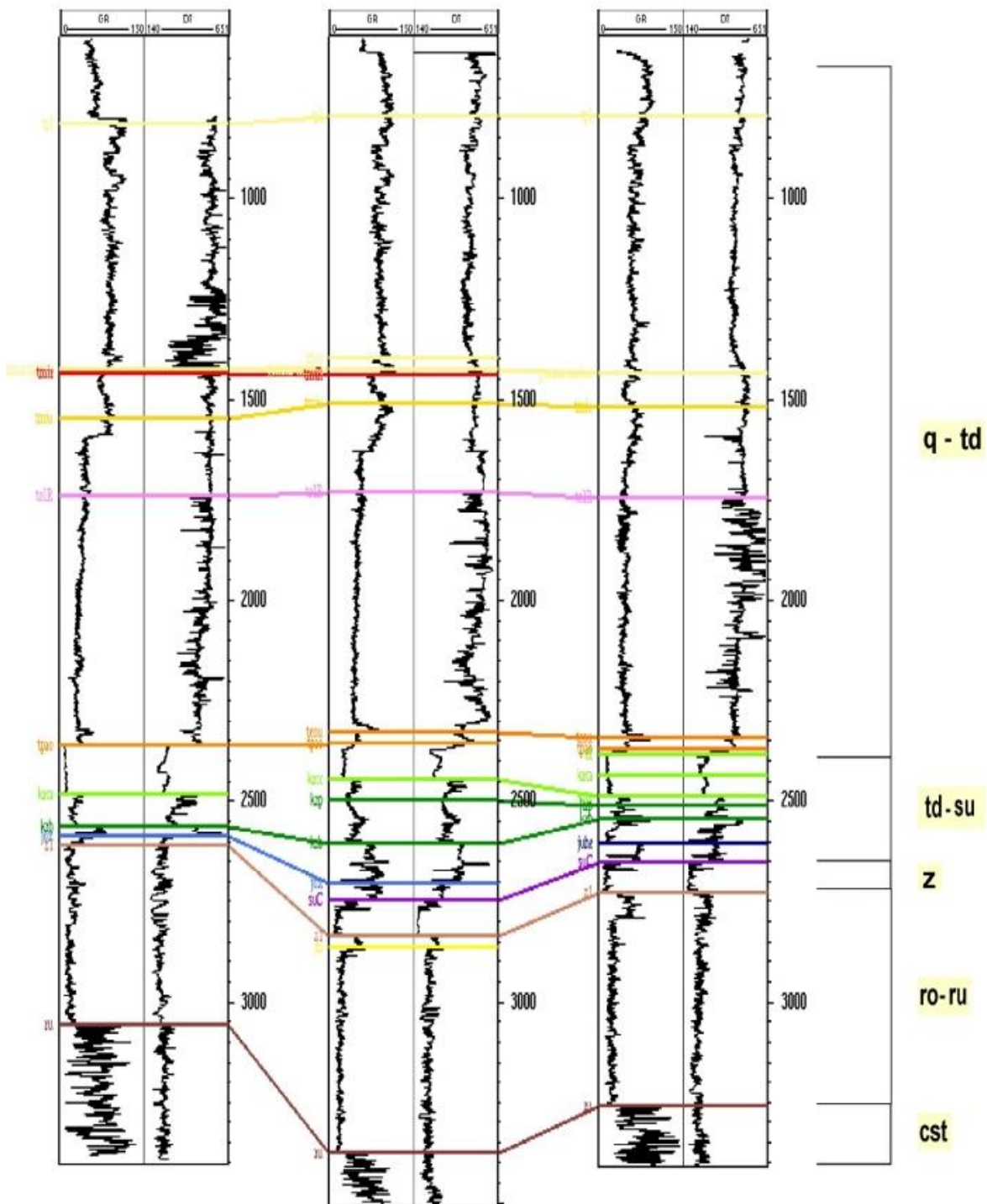


Fig. 8 Example of the correlation of three wells using sonic (DT) and gamma-ray (GR) log (from Arfai et al., 2011). The pattern of the logs is used to confirm, if necessary, change, and create new markers, which resemble geologic horizons of interest. These markers are then used to correlate the wells.

2.4.2. Well tie

Even though the wells are roughly tied to the reflection seismic data in the time domain by using checkshot data, there always is a miss-tie. To correct this mis-tie and to be able to connect stratigraphic information to the reflection seismic data, synthetic seismograms were used to tie well to seismic data more precisely (Fig. 9). Because the amplitude of a seismic reflection is dependent on the acoustic impedance contrast between two layers in the subsurface, and acoustic impedance being the product of the layer's density and the velocity of the transiting compressional wave, it is possible to construct a synthetic, one-dimensional seismic signal. Therefore, the sonic and bulk density logs are used to obtain an acoustic impedance log. The contrast of acoustic impedances above and below the interface of two layers gives the reflection coefficient of an interface. A synthetic wavelet is applied to the reflection coefficients to receive the synthetic one-dimensional seismogram. A zero-phase wavelet was used and the wavelet's amplitude spectrum was estimated from the reflection seismic data. Several copies of the one-dimensional synthetic seismogram placed closely side by side are superimposed on a reflection seismic section, which allows their correlation. If necessary, intervals of the synthetic seismogram were stretched or thinned for a more precise tie. Then, stratigraphic information from the markers could be transferred from the wells to the reflections seismic data.

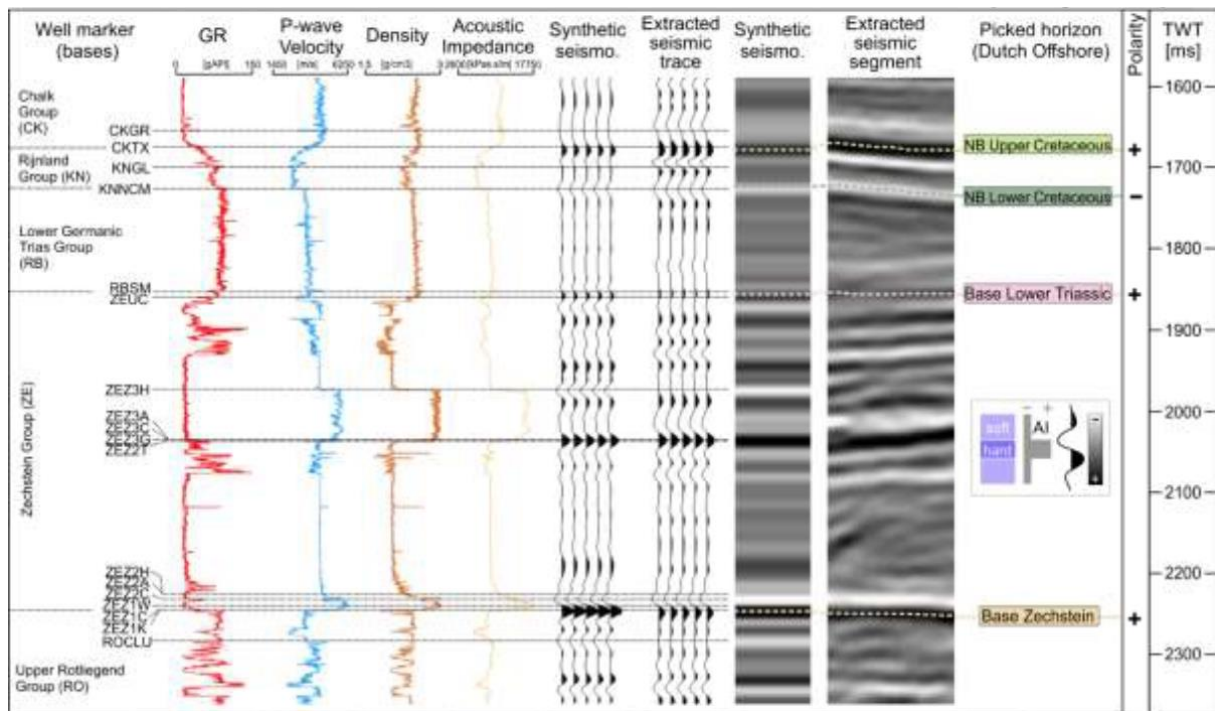


Fig. 9 Example of the creation of a synthetic seismogram that is used for a well tie (from Thöle et al., 2021). The acoustic impedances of an interval are created from the sonic log (here: p-wave velocity), the density log and a wavelet. The reflection coefficient (RC) is derived from the acoustic impedance, which is the base of the synthetic seismogram. The synthetic seismogram is compared with extracted seismic data from or near the well location and modified if necessary.

2.5. Interpretation of reflection seismic data

2.5.1. Structural interpretation

The interpretation of the reflection seismic data started with establishing a structural framework. Faults were mapped that created a visible offset on the reflection seismic data within the horizons in the relevant interval between the Zechstein salt and the seafloor (Fig. 10). On 3D seismic data, the strike direction of the faults was often identified using a data cube with the variance attribute. On a variance map, fault planes appear dark because their traces deviate strongly from their surroundings. A seismic attribute is a quantity derived from the original seismic data with the purpose of improved geological interpretation. The most common attribute is amplitude. Variance measures differences from a mean value of the seismic trace and displays the deviations. Then, the intersections of the faults with the seismic horizons were mapped perpendicular to or nearly perpendicular to the fault's strike direction. Salt structures were identified on reflection seismic data by their typical dome shape, their scattered and low amplitude reflection pattern, the abrupt ending of seismic horizons at their flanks, and anticlinal structures with radial faults at their top.

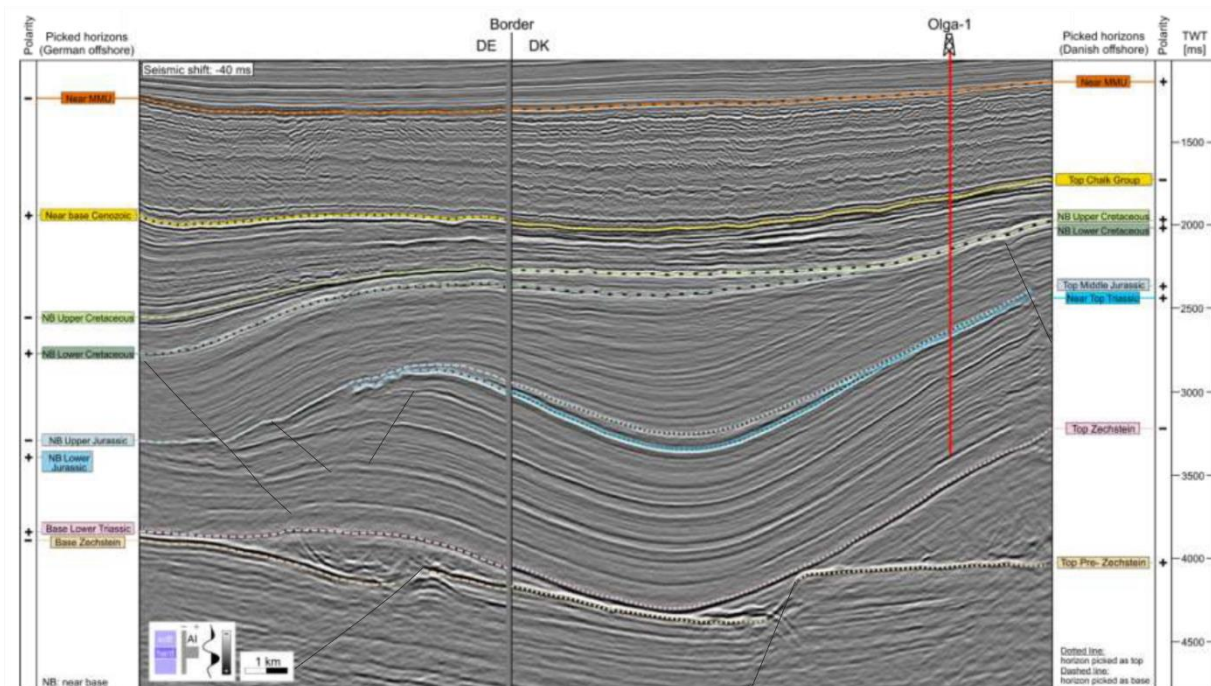


Fig. 10 Example of a reflection seismic section that is in part structurally and stratigraphically interpreted (Thöle et al., 2021). After the structural framework of the section was established by interpreting faults, the information from the wells is tied to the seismic data using a synthetic seismogram. The well information, e.g., markers and log patterns, are used to interpret the seismic section stratigraphically.

2.5.2. Stratigraphic interpretation

After tying the wells to the seismic data and establishing a structural framework, individual seismic horizons were picked and mapped (Fig. 10). The required stratigraphic horizons for seismic mapping, like top and base horizons of lithostratigraphic formations or of tectonostratigraphic mega-sequences, were selected and identified on the well logs (“markers”). Then, the reflections caused by the lithological interface at these markers were identified at well location on the well-tied reflection seismic data. Starting from the well locations, the seismic horizons were picked on the 3D reflection seismic data in a grid pattern of crosslines and inlines. The density of the grid depended on the complexity of the geologic situation and the character of the seismic reflection. 2D reflection seismic data was used for areas where no 3D reflection seismic data was available. The transition from 2D to 3D reflection seismic data was carried out at intersecting areas. For the most part, picking was carried out manually. Auto-tracker functions were only used on distinct reflections with high amplitudes and a consistent character limited to the visible part of a seismic sections and their results were controlled thoroughly. Subsequently to the picking, the horizons were gridded to continuous surfaces.

2.5.3. Amplitude interpretation and direct hydrocarbon indicators

The reflection seismic data was systematically scanned for seismic anomalies that are not the result of geological structures but of fluids within the sediments affecting the seismic signal, which are called direct hydrocarbon indicators (DHI). The most important DHI, because of their abundance, expressiveness, and recognizability, are the so-called “bright spots”. They are high amplitude anomalies that stand out of their lower amplitude environment on a seismic section (Fig. 11). They are caused by hydrocarbons within the pore volume of sand or sandstone, which increases the impedance contrast between the gas-filled sandstone and the overlying sealing shale and the underlying water-filled sandstone (Bacon et al., 2003). The effect decreases with depth due to the different compaction of clay and sand, with bright spots being replaced at first by a phase reversal, than by dim spots as hydrocarbon indicators (Fig. 11). Bright spots usually appear as two laterally confined, consecutive high amplitude anomalies (“peak-over-trough”) that conform to structure. They are, as well as any DHI, more pronounced for gas in the pore space, because the effect on acoustic properties of gas is significantly higher than for oil (Brown, 2011).

If the hydrocarbon column is high enough to be resolved on reflection seismic data, the second high amplitude anomaly is a horizontal reflection that intersects geological structure, e.g., reflections of an anticlinal structure. This so-called “flat spot” resembles a hydrocarbon-water contact at the base of the reservoir (Bacon et al., 2003; Fig. 11). If the flat spot or any reflection directly below bright spots are bent downwards in relation to the laterally adjacent reflections, presumably a so-called “velocity push-down” occurs due to the lower velocity of a seismic wave within gas-filled sediments in contrast to water-filled sediments (Brown, 2011).

Other amplitude anomalies that are connected to the presence of gas are the so-called “seismic attenuation” and “gas chimneys”. The attenuation of seismic reflections often occurs below bright spots because more of the seismic energy is reflected at the high-impedance-contrast interfaces that cause the high amplitude anomalies then from the surrounding reflectors with lower impedance contrasts (Anstey, 1977). Gas chimneys are more indicators for the migration of natural gas than for its accumulation. During its vertical migration in mostly unconsolidated sediments, some of the gas remains within the sediments. These isolated bubbles do not form linear reflectors and scatter the seismic signal resulting in a chaotic seismic reflection pattern (Cathles et al., 2010). For a more detailed description of amplitude anomalies acting as hydrocarbon indicators, see chapter 3.

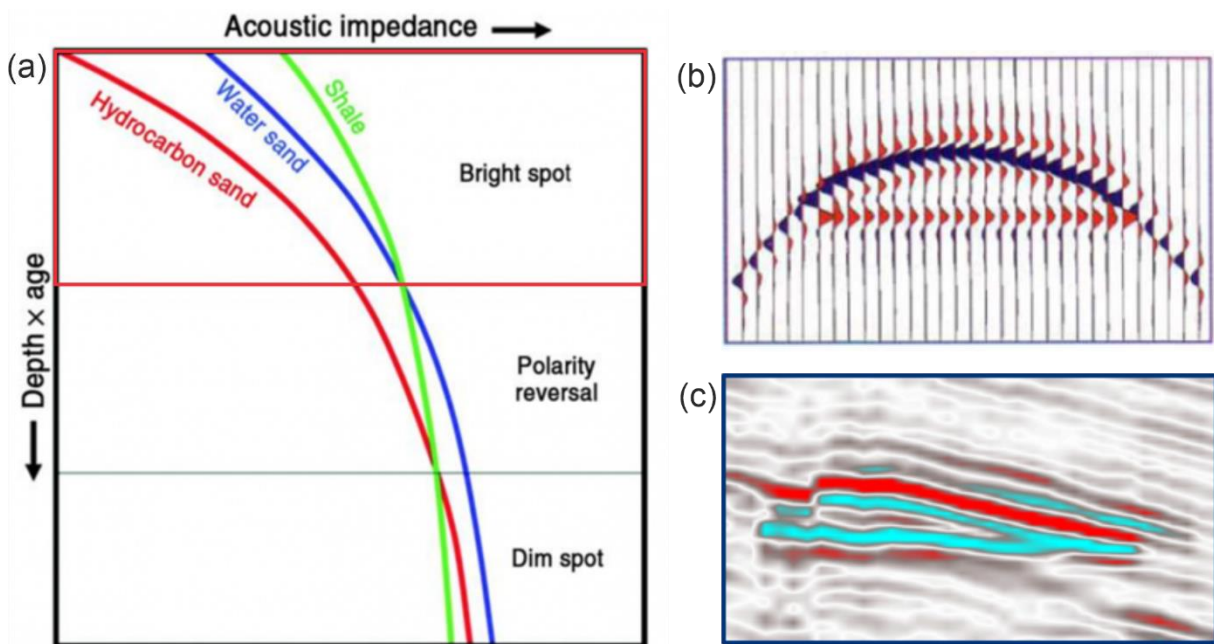


Fig. 11 (a) Graphical depiction of the development of the acoustic impedance of shale, water-filled and hydrocarbon-filled sand(-stone) with increasing depth and compaction (from Bacon et al., 2003). In relatively young and predominantly unconsolidated sediments, the acoustic impedance of shale is higher than the one of water-filled sand (red frame). If hydrocarbons, especially natural gas, are trapped in the pore space of the sand, the acoustic impedance is further decreased, hence increasing the impedance contrast between the shale and the sand. (b) Synthetic seismic section of gas trapped in an anticlinal structure (from Bacon et al., 2003). The higher impedance contrast effects higher amplitudes (bright spot) on the transition from the sealing shale to the gas-filled sand in relation to the water-filled sand. The gas-water contact at the bottom of the gas accumulation produces a flat spot that cuts the geological structure. (c) Real reflection seismic data example of a similar situation of (b) offshore The Netherlands. Gas is trapped in a combination of an anticlinal structure with a fault in unconsolidated sediments, resulting in a top and bottom bright spot, with the bottom bright spot also forming a flat spot.

2.6. Petroleum system modelling

Using the software PetroMod® V. 16 of Schlumberger, a 3D basin and petroleum system model of the German Central Graben was built. Therefore, an existing from Arfai and Lutz (2017) of the northwestern German offshore was modified. The database of the original model consists

of 27 stratigraphic layers from the Lower Cretaceous sedimentary basement to the Tortonian and Holocene (Arfai et al., 2014) and information of 29 wells of the northwestern German North Sea (Arfai and Lutz, 2017). The modifications of the original model integrate new mapping results of the Lower Jurassic Posidonia Shale Formation and the Upper Jurassic to Lowermost Cretaceous Hot Shale (Clay Deep Member offshore The Netherlands and Bo Member offshore Denmark), as well as more investigated layers. The modified model consists of 29 stratigraphic layers including six source rock layers of from the Upper Triassic Rhaetian to the lowermost Cretaceous for which the thermal history, maturity and petroleum generation was reconstructed. The software uses a forward modeling approach, in which the depositional evolution of the basin is reconstructed from the oldest to the youngest geological event (Hantschel and Kauer, 2009). For the calculations of the thermal history the EASY%Ro algorithm of Sweeney and Burnham (1990), for the hydrocarbon generation of marine source rocks the kinetic dataset TII North Sea of Vandenbroucke et al. (1999) and of terrestrial source rocks the kinetic dataset TIII of Burnham (1989) were applied. For more detailed information it is referred to chapter 5, Arfai et al. (2014), and Arfai and Lutz (2017).

References

- Anstey, N.A., 1977. *Seismic Interpretation: the Physical Aspects*. Springer Science & Business Media.
- Arfai, J. & Lutz, R., 2017. 3D basin and petroleum system modeling of the NW German North Sea (Entenschnabel). In: Bowman, M., Levell, B. (eds.), *Petroleum Geology of NW Europe: 50 Years of Learning – Proceedings of the 8th Petroleum Geology Conference*. Geological Society, London, pp. 8–35.
- Arfai, J., Jähne, F., Lutz, R., Reinhardt, L., Thöle, H., Wirth, H., 2011. *Datengrundlage, Arbeitskonzepte und erste vorläufige Ergebnisse zum Projekt Geopotenzial Deutsche Nordsee (2009-2010)*. Bundesanstalt für Geowissenschaften und Rohstoffe, Hannover, pp. 147
- Arfai, J., Jähne, F., Lutz, R., Franke, D., Gaedicke, C. & Kley, J., 2014. Late Palaeozoic to Early Cenozoic geological evolution of the northwestern German North Sea (Entenschnabel): New results and insights. *Netherlands Journal of Geosciences* 93(4): 147-174.
- Bacon, M., Simm, R. & Redshaw, T., 2003. *3-D seismic interpretation*. Cambridge University Press, Cambridge.
- Brown, A. R., 2011. *Interpretation of three-dimensional seismic data*. Society of Exploration Geophysicists and American Association of Petroleum Geologists, Tulsa.
- Burnham, A.K., 1989. *A Simple Kinetic Model of Petroleum Formation and Cracking*. Internal report of Lawrence Livermore National Laboratory, Report UCID 21665. Lawrence Livermore National Laboratory, Livermore, CA.
- Cathles, L.M., Su, Z., Chen, D., 2010. The physics of gas chimney and pockmark formation, with implications for assessment of seafloor hazards and gas sequestration. *Mar. Petrol. Geol.* 27 (1), 82–91.
- Hantschel, T. & Kauerauf, A.I. (eds.), 2009. *Fundamentals of Basin and Petroleum Systems Modeling*. Springer-Verlag, Berlin.
- Jackson, M. P., & Hudec, M. R. 2017. *Salt tectonics: Principles and practice*. Cambridge University Press.
- Judd, A. G., Long, D. & Sankey, M., 1994. Pockmark formation and activity, UK block 15/25, North Sea. *Bulletin of the Geological Society of Denmark*, 41(1), 34-49.
- Sweeney, J.J. & Burnham, A.K., 1990. Evaluation of a simple model of vitrinite reflectance based on chemical kinetics (1). *AAPG Bull.* 74 (10), 1559–1570.
- Thöle, H., Jähne-Klingberg, F., Doornenbal, H., den Dulk, M., Britze, P. & Jakobsen F., 2021. Deliverable 3.8 – Harmonized depth models and structural framework of the NL-GER-DK North Sea. Report, p.77; GEOERA 3DGEO-EU; 3D Geomodeling for Europe; project number GeoE.171.005.

Vandenbroucke, M., Behar, F. & Rudkiewicz, J.L., 1999. Kinetic modeling of petroleum formation and cracking: implications from the high pressure/high temperature Elgin Field (UK, North Sea). *Org. Geochem.* 30, 1105–1125.

3. Shallow gas accumulations in the German North Sea

This chapter has been published as Müller, S., Reinhardt, L., Franke, D., Gaedicke, C., & Winsemann, J., 2018. Shallow gas accumulations in the German North Sea. *Marine and Petroleum Geology*, 91, 139-151.

Abstract

Shallow gas, here defined as free gas that is trapped in unconsolidated, deltaic, and shallow marine siliciclastic sediments of Plio-Pleistocene age, is found within the topmost 1000m of sediment in the southern North Sea. Shallow amplitude anomalies in reflection seismic data are likely due to the presence of gas. The most prominent and easy-to-recognize indicators are high-amplitude anomalies, or “bright spots”, that are widespread within the southern North Sea. Gas from shallow reservoirs is currently produced offshore The Netherlands. In this study, we determine whether there are analogous shallow gas accumulations within the German North Sea. Therefore, we screened 2D and 3D multichannel seismic data for shallow amplitude anomalies. Several clusters of bright spots are identified above salt domes that closely resemble the economic deposits known in the Dutch sector in both size and their characteristic multilayered shape. Three of these potential gas accumulations, occurring in combination with additional hydrocarbon indicators such as seismic attenuation and velocity push-downs, are investigated in detail and compared to shallow gas fields from offshore The Netherlands. Amplitude anomalies indicate gas seepage on the seafloor that may contribute to the atmospheric methane budget and may have an impact on offshore infrastructure.

3.1. Introduction

As of 2015, about 21% of Germany's primary energy consumption derives from natural gas. However, less than ~10% of this natural gas is produced domestically, in Germany (BGR, 2016). Due to the ever-increasing depletion of producing fields, production and reserve volumes have decreased steadily. Germany's natural gas supply is highly dependent on exporting countries such as the Russian Federation, Norway, and The Netherlands, which together deliver 98% of Germany's natural gas imports (BGR, 2016). Therefore, to find and assess additional domestic sources of natural gas is important. During the previous two decades, the concept of shallow gas (in literature generally defined as gas accumulated at a depth below 1000 m) has changed. Whereas formerly seen as a drilling hazard, or at best as an indicator for deeper and more promising reservoirs, it is now increasingly regarded as a potential additional and profitable source of natural gas (e.g., Eriksen et al., 2011). Technical challenges in connection with shallow-gas production, such as low reservoir pressures, and substantial sand and water co-production from unconsolidated sediments, were addressed with the application of horizontal drilling, sand exclusion technology and gas compression to enable gas flow into production wells.

The first commercial shallow gas field A12-FA in the northern part of the Dutch North Sea was developed in 2007 (Kombrink et al., 2012; van den Boogaard and Hoetz, 2015). Since then, three more fields went into production (Fig. 12). Alongside the hydrocarbon industry, scientific research on shallow gas accumulations advanced in The Netherlands (e.g., Schroot et al., 2005; ten Veen et al., 2011; Stuart and Huuse, 2012; Verweij et al., 2012a, 2013; ten Veen et al., 2013; Alves and Elliott, 2014; ten Veen et al., 2014a; ten Veen et al., 2014b; Verweij and Nelskamp, 2014; Verweij et al., 2014; Williams and Gent, 2015). Beside its economic potential, shallow

gas may be important for a more accurate assessment of greenhouse gas emissions from marine sources (Bange et al., 1994; Krämer et al., 2017; Römer et al., 2017), and may have an impact on selecting suitable locations for offshore infrastructure (Trampe et al., 2014). In contrast to The Netherlands, studies on shallow gas in the adjacent German offshore sector are rare (e.g., Pletsch et al., 2010; Trampe et al., 2014; Krämer et al., 2017). This paper assesses the existence and distribution of comparable shallow gas accumulations in the German North Sea by mapping amplitude anomalies that are indicative for shallow gas and by integrating them into the seismo-stratigraphic context of Thöle et al. (2014).

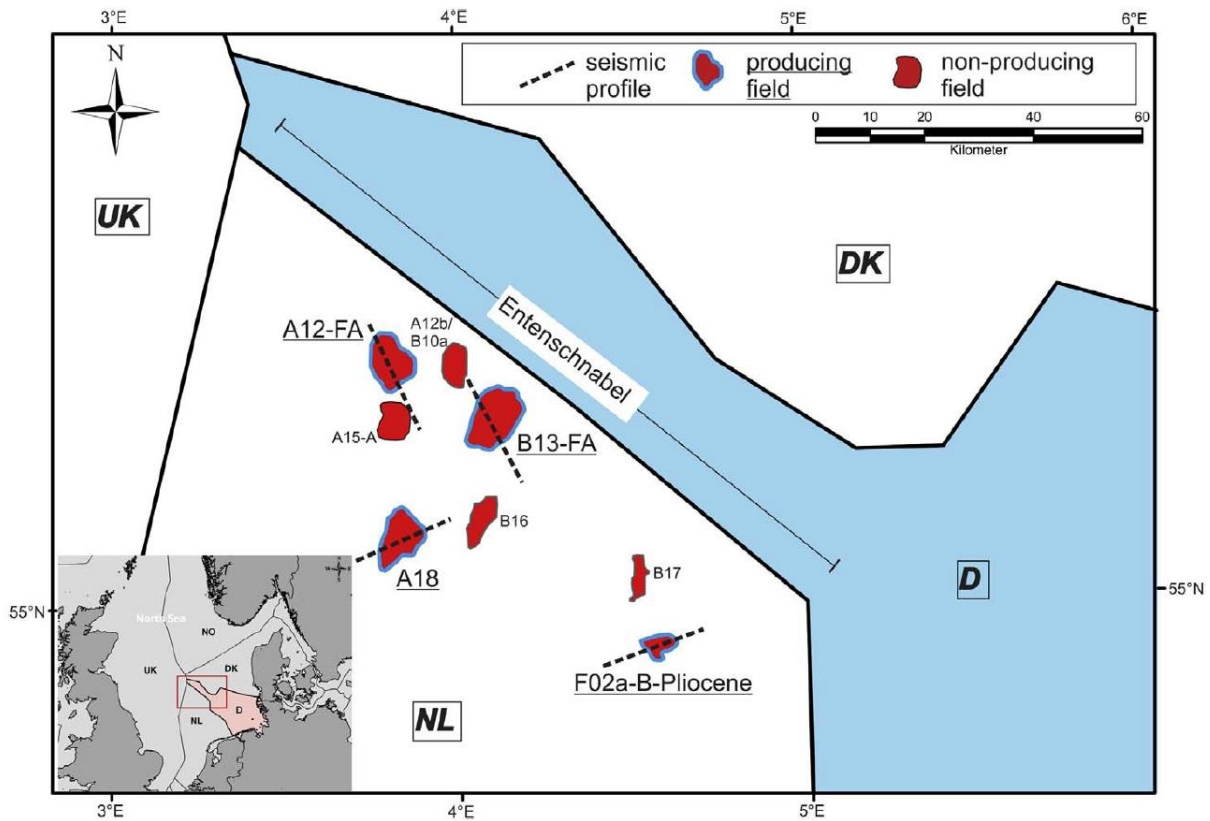


Fig. 12 Location and areal extent of bright spots that belong to producing and non-developed Dutch shallow gas fields in the vicinity of the study area, the northwestern German North Sea sector, called the Entenschnabel (Duck's Bill). Seismic profiles of the Dutch sector are shown in Fig. 21.

3.2. Geological setting

3.2.1. Sedimentary system

Subsequent to several Mesozoic rifting phases that affected the Southern Permian Basin, the North Sea entered a post-rift, thermal subsidence phase in the Cenozoic (Ziegler, 1992; Arfai et al., 2014). From the Late Miocene onwards, sedimentation in the northern sector of the German North Sea (locally referred to as “Entenschnabel” (Fig. 12), meaning “Duck's Bill”, because of the shape of its outline) is characterized by the Eridanos Delta system (Overeem et al.,

3. Shallow gas accumulations in the German North Sea

2001). From the Late Miocene until the Pliocene to Pleistocene transition, major sedimentary bodies resembling shelf-prism clinofolds prograded westwards over the surface of the distinct Mid-Miocene Unconformity (MMU) (e.g., Patruno et al., 2015). These sedimentary bodies were subdivided into seismic units by Thöle et al. (2014) within the German sector of the North Sea (Fig. 13), which helps to assign the seismic horizons chronologically. Progradation of the system into the present-day Dutch sector continued into the Pleistocene (Overeem et al., 2001; Kuhlmann et al., 2004), when the sediment influx from the Baltic River system ceased due to the development of the Fennoscandian ice sheet (Zagwijn, 1989). Continuous subsidence in the study area created accommodation for thick glacial and interglacial sediments (e.g., Lutz et al., 2009; Kuhlmann and Wong, 2008; Stewart and Lonergan, 2011).

Tab. 1 Summary of published reservoir properties of Dutch shallow gas fields (From: Knox et al. (2010); Schroot et al. (2005); Muntendam-Bos et al. (2009); van den Boogaard and Hoetz (2015); EBN (2012); van den Boogaard and Hoetz (2015); ten Veen et al. (2013).

	Producing fields			
	A12-FA	A18	F02a-B-Pliocene	In general
Permeability (mD)				high
Porosity (%)				20–40
Gas saturation (%)				55–60
Methane (%)	98–99	99		very dry
Nr. of Reservoir sands				
Reservoir thickness (m)				5–20 m
Trap type	4WDC		FDC	
Reservoir Pressure (bar)				50–80
Depth (m)	350–700			300–800
Recovery Factor (%)	65			60–75
Ultimate Recovery (BCM)	7.5			8.5, 18–62 (in total)
CH4 Isotopic Composition				
Reservoir age	Late Tertiary			Late Miocene to Pleistocene
	Non-producing fields			
	A15-A	A12b/B10a	B16	B17
Permeability (mD)	10			
Porosity (%)	29			
Gas saturation (%)	40			
Methane (%)	99	99	99	67–91
Nr. of Reservoir sands	7			
Reservoir thickness (m)	43 (net reservoir thickness)			
Trap type	4WDC			
Reservoir Pressure (bar)	800 (initial)			
Depth (m)	400–650		-600	
Recovery Factor (%)				
Ultimate Recovery (BCM)				
CH4 Isotopic Composition			-70.3‰	-34.8 to -24.8‰
Reservoir age	Quaternary		Plio-Pleistocene	

3.2.2. Shallow gas in the Dutch North Sea

The Netherlands played a pioneering role in the utilization of shallow gas in the North Sea. Eight shallow gas accumulations have recently been classified as proven fields in the Southern North Sea, with all of them located in the northern part of the Dutch North Sea, close to the German offshore sector (Muntendam-Bos et al., 2009). Four of these fields, A12-FA, B13-FA, A18 and F02a-B-Pliocene are currently being exploited (Fig. 13). Methane is by far the major constituent of the produced gas. Whether the gas is of biogenic or thermogenic origin has not yet been conclusively determined (e.g., Muntendam-Bos et al., 2009; ten Veen et al., 2013). The isotopic composition of shallow gas in the Dutch offshore indicates a microbial (B16-field) or a thermogenic (B17-field) origin (see Tab. 1). Furthermore, over another 150 leads for shallow gas were identified during gas exploration work in the Dutch offshore (Muntendam-Bos et al., 2009). Several of these leads are thought to have economic potential.

The reservoirs of the four producing fields are confined to structural traps either in low relief anticlines (4-way-dip closures (4WDC)) or in extensional normal-fault settings (fault-dip closure (FDC)). Both types of closures are associated with domes of Upper Permian Zechstein salt developed in deeper strata. Accumulations occur typically at depths between 300 and 800m in unconsolidated to moderately consolidated sediments of Late Miocene to Pleistocene age (Schroot and Schüttenhelm, 2003; van den Boogaard and Hoetz, 2015). The gas accumulations consist of multiple stacked gas-bearing levels. Layers of clay serving as seals alternate with coarser-grained sediments acting as reservoirs. On reflection seismic data, the gas-bearing horizons appear as patches with anomalously high amplitudes, the so-called bright spots. However, information of site-specific reservoir parameters of these shallow gas fields is scarce in the literature. Some information can be gathered from industry presentations and open reports (e. g., Muntendam-Bos et al., 2009; van den Boogaard and Hoetz, 2015; EBN, 2012; van den Boogaard and Hoetz, 2015). Table 1 gives a comprehensive overview of the published reservoir parameters for the Dutch shallow gas fields. The shallow gas is generally very dry (~99% methane), with exception of the B17-field, and occurs in relatively thin (5–20 m), stacked reservoir horizons of Late Miocene to Pleistocene ages (Tab. 1).

3. Shallow gas accumulations in the German North Sea

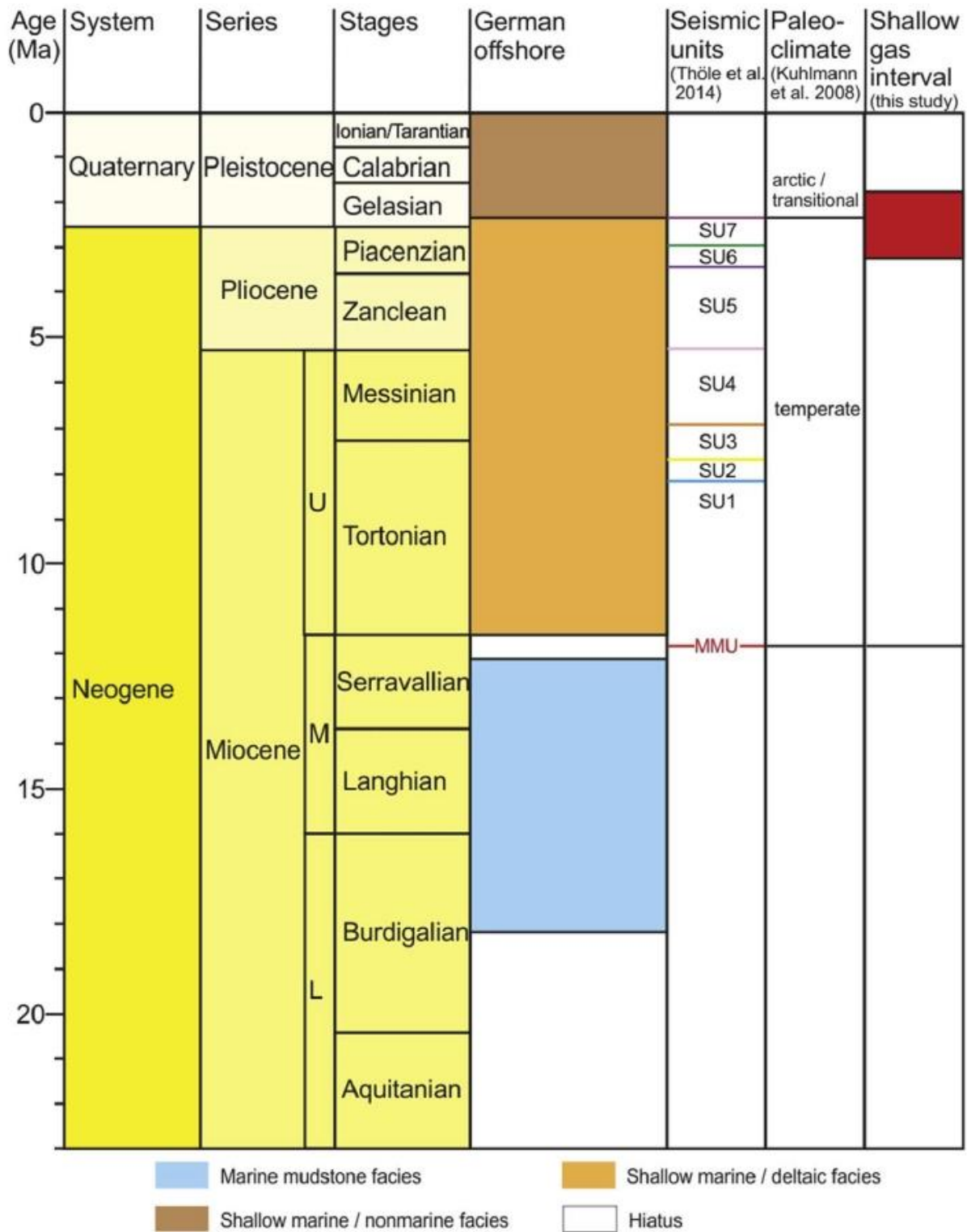


Fig. 13 Stratigraphic column of the Neogene and Quaternary sediments within the investigated area of the southern North Sea. The deltaic sedimentary bodies of the German North Sea were deposited during a temperate paleoclimate. They are subdivided into seismic units (SU1–SU7) by Thöle et al. (2014) which help to assign the seismic horizons chronologically. The shallow gas accumulations that are investigated in this study occur in sediments of a temperate as well as of an arctic climate.

3.3. Data and methodology

3.3.1. Seismic data

The data employed in this study comprises a single 3D seismic survey covering nearly a third of the Entenschnabel-area, and 28 surveys (approximately 30.000 line kilometers) of 2D multichannel seismic lines, distributed over the entire German North Sea sector (Fig. 14). Based on analysis of the available surveys, the 3D survey “German North Sea Consortium (GNSC)”, and a line from the 2D survey “Maersk g93 DOK” were selected for detailed study of the structures investigated in this paper (Fig. 14). All seismic data are post-stack time migrated; pre-stack data were not available at the time of the study. Our study displays reflection-seismic data in two-way travel time. However, previous investigations (e.g., Clausen and Huuse, 1999) have shown that at depths shallower than 1000 m, the relation between the two-waytime and depth is approximately 1:1 for Upper Cenozoic sediments of the North Sea. The vertical resolution of both, the 2D and 3D seismic data, is approximately 10–12m in the investigated interval (< 1000 ms TWT). The polarity of the seismic data is recorded as zero-phase SEG reverse polarity (also known as negative standard polarity or European polarity), which is commonly used in the North Sea area by the European hydrocarbon industry. It displays a positive impedance contrast (“hard” event) between two layers as a trough in blue and a peak in red.

The interpreted seismic data were integrated with well data to generate the working dataset for the study. Three wells were primarily used and penetrate horizons that are associated with high-amplitude anomalies. The time-depth relation of the seismic data and the wells was established using checkshot data. The well data include descriptions of lithology intervals derived from cuttings, as well as geophysical and mechanical well logs. Gamma ray logs (GR) were used to identify clay and sand intervals. Using available sonic and density logs, synthetic seismograms were calculated to correlate high amplitude anomalies to the gamma ray curves in selected wells and to identify potential seal and reservoir horizons. Where 3D seismic data were available, the areal extent of gas containing layers was determined through the outline of high-amplitude anomalies on horizon slices. If only 2D seismic data were available, the sections of a bright spot layer that are cut by one or more seismic lines were displayed on a map. These lines were then extended to an ellipsoidal form, due to the anticlinal structure of the trap, which corresponds to the probable areal extent of the gas-containing layer.

The detailed seismic stratigraphic framework established by Thöle et al. (2014) was adopted for the interpretation, where post-MMU reflectors are subdivided on the basis of major depositional or erosional boundaries. These sequences are arranged in seven seismic units (SU1–SU7) representing different phases of the prograding delta and have been biostratigraphically correlated to absolute ages (Fig. 12).

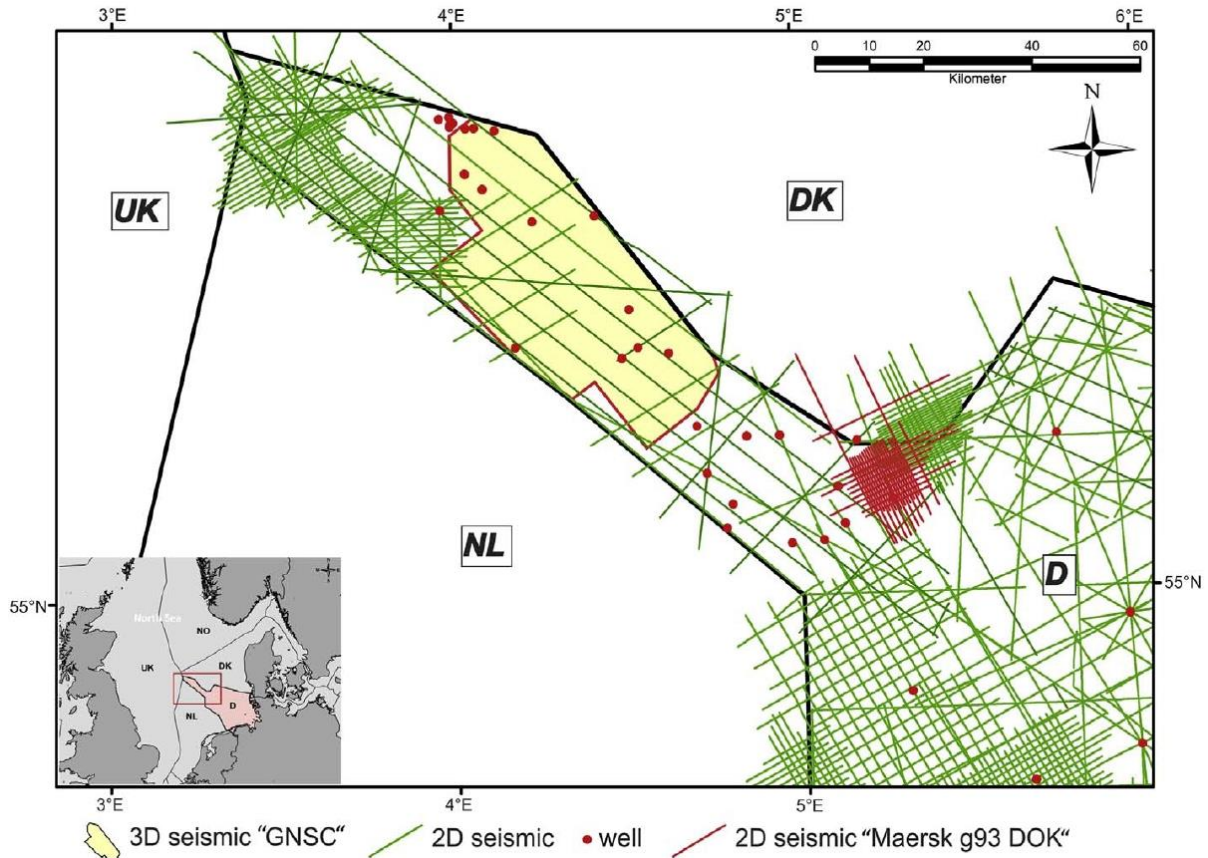


Fig. 14 Aerial extent of available data utilized in this study. Seismic data used in our detailed investigation is highlighted in red.

3.3.2. Direct hydrocarbon indicators

We conducted a systematic mapping of amplitude anomalies in the interpreted seismic data set, i.e., of seismic features that can be considered as direct hydrocarbon indicators (DHIs). We identified four different types of DHI: bright spots, seismic attenuation, velocity pushdown, and gas chimneys. In reflection seismic data, a bright spot resembles a localized high-amplitude anomaly that can indicate the presence of hydrocarbons in the formation (Sheriff, 1991). The presence of gas in a reservoir strongly affects the impedance contrast, and even a small gas content is able to produce a high-amplitude anomaly (Domenico, 1974; van den Boogaard et al., 2013). van den Boogaard and Hoetz (2015) conducted synthetic seismic modeling which affirmed the strong effect of a small single-digit content of gas on amplitude. While the increase in amplitude from 0% to 2% gas saturation was enormous, the difference in amplitude from 2% to 70% gas saturation proved to be insignificant. Characteristic for a gas-induced bright spot in seismic with zero-phase SEG reverse polarity is the so-called “peak-over-trough” pattern, in which a high-amplitude trough follows a high-amplitude peak (see Fig. 16b). The pattern is useful to distinguish between gas-induced bright spots and bright spots that are caused by changes in lithology, such as e.g., hard low-porosity sands, which feature a reverse reflection pattern. However, other lithologies like e.g., peat or coal may also induce a “peak-over-trough” response. Due to an increased energy loss of a seismic wave, the presence of gas in a layer

causes anomalous amplitude dimming of the underlying reflections, in what is called seismic attenuation (Anstey, 1977). It can also be caused by high-impedance rocks such as basalts (Simm et al., 2014). When dimming of reflectors occurs above and below a bright spot, it is likely to be caused by poor seismic processing rather than fluid effects (Anstey, 1977; Ebrom, 2004). A velocity push-down is an apparent depression in time domain seismic data that does not correspond to an actual structural low. The push-down is the direct result of a decrease in velocity of a compressional wave within a gas accumulation in seismic data. Other low-velocity anomalies, such as incised valleys, can also give rise to a velocity push-down (Marfurt and Alves, 2014).

A gas chimney is less an indicator for the presence of gas, but for its vertical migration. It can be recognized in seismic data by its chaotic reflection pattern with a columnar shape. The reflections within this column are discontinuous and generally feature lower amplitudes in relation to their adjacent horizon. These seismic signal characteristics are the result of irregularly distributed and discontinuous free gas of low concentration in the sediment column which resembles the upwards movement of gas due to density-driven buoyancy forces (Cathles et al., 2010). Flat spots are horizontal reflections that cut the reflections of dipping horizons on seismic data and represent a fluid contact (in a shallow gas scenario a gas-water contact). They have not been identified for the shallow gas accumulations in the German offshore.

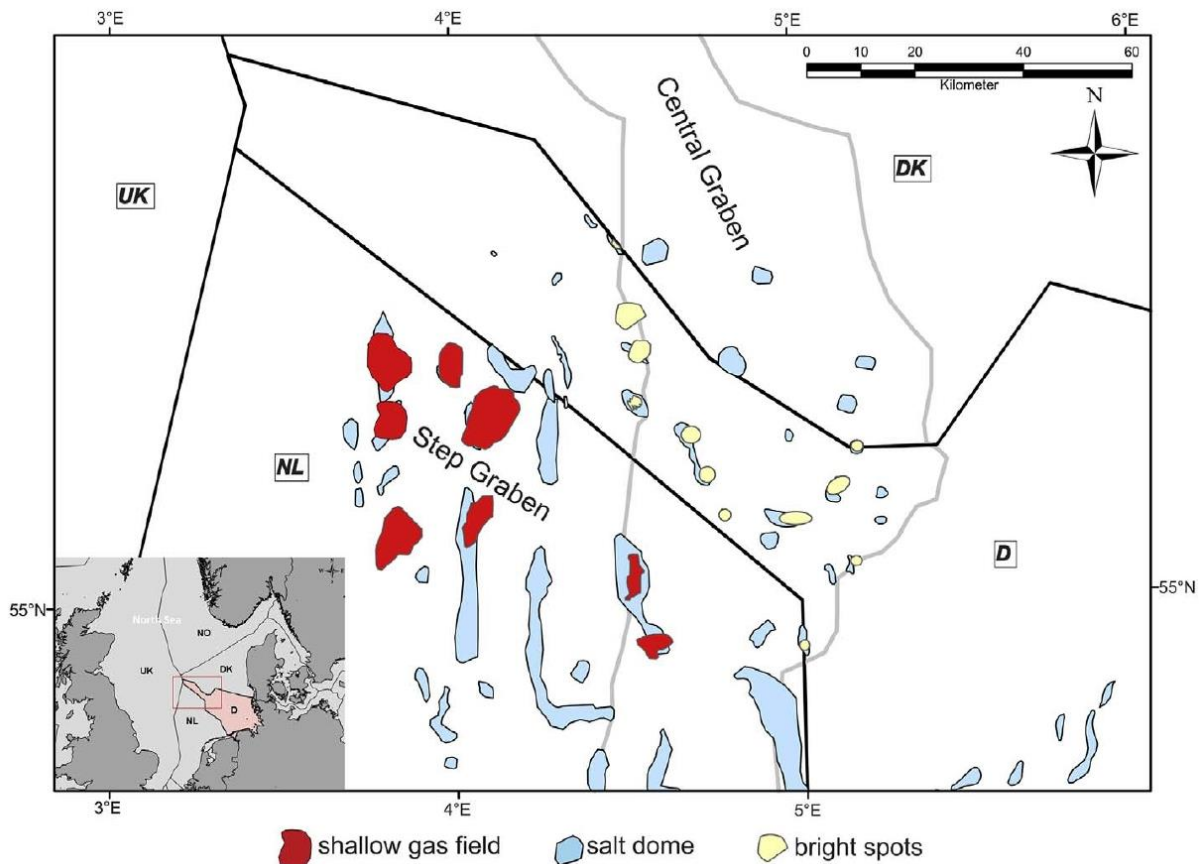


Fig. 15 Salt domes with the outlines of associated bright spots within the German and the Dutch North Sea sector (salt dome map modified from Reinhold et al. (2008)).

3.4. Results

The character of multiple stacked bright spot layers has been identified in association to eleven of the nineteen Zechstein salt domes present in the southern part of the “Entenschnabel”, in the area of the Central Graben (Fig. 15). The bright spots occur in Late Pliocene to early Pleistocene sediments in depths of ~350–900 ms TWT. Most reveal additional hydrocarbon indicators as, e.g., seismic attenuation and velocity- pull down. Three potential gas accumulations were further investigated regarding the age and depositional environment of their seal and reservoir layers, gas migration, and seepage to the seafloor. The three examples were selected because they represent different trapping types (4WDC for example 1, a mixture of 4WDC and FDC for example 2, and FDC for example 3) and because they are found in geographically dispersed positions to investigate the influence of the east-west prograding coastline on the interval with bright spots (examples 1 and 2 are located in the west and example 3 in the east of the investigation area). The exact location of the seismic profiles shown in Fig. 16 – Fig. 19 is confidential.

3.4.1. Example 1

The first example is located in the western part of the German Central Graben and is observed on 3D reflection seismic data. Six stacked horizons with distinct and parallel high-amplitude reflections are distinguished. The bright spots occur within parallel post-MMU topset sediments that form a low-relief anticline above a salt dome (Fig. 16a). The bright spot horizons exhibit a “peak-over-trough” pattern, typical for a gas-sand (Fig. 16b). They differ in their size, with generally a decreasing trend towards the seafloor. The areal extent of these bright spots varies between ~1.5 and 18 km².

The amplitudes of potential gas-containing horizons are strongly attenuated if they are located beneath other bright spots. They are only “bright” at the outer rim of the overlying bright spot where the gas content is presumably smaller. Pushed-down reflections in the center of the stacked bright spots is further evidence for the presence of free gas (Fig. 16c). The discontinuous reflection pattern with columnar shape below the bright spots is interpreted as a gas chimney that represents the path of vertically migrating gas into the shallow reservoir sediments. Another possible gas chimney leads from the uppermost bright spot towards the seafloor (Fig. 16d). The amplitudes at its flank and the uppermost reflections are increased compared to the surrounding reflections, indicating free gas within the sediments. In the interval below the MMU reflections exhibit generally lower amplitudes and are discontinuous. This reflection pattern can be attributed to a polygonal fault system within Lower Miocene and Paleogene claystones that is distributed over large areas of the North Sea (Cartwright, 1994). Due to overpressure in the pre-MMU formations, these faults are potentially conductive and pose possible migration pathways for upwards migrating gas from a deeper source (Verweij et al., 2012b; Mulrooney et al., 2017). The bright spots occur in the depth range of ~400–740 ms (TWT). This depth range corresponds to sediments of Gelasian age, starting at the top of SU7 (Thöle et al.,

2014). The boundary marks the transition from a temperate climate to a climate that is dominated by an alternation of warm and cold periods (Fig. 12). This change in climate is indicated by the onset of iceberg scour marks (Fig. 16a). No bright spots are found in Tortonian – Piacencian sediments (SU6 and older). These layers represent fine-grained, low-permeability toe-set sediments, in which gas could not be trapped.

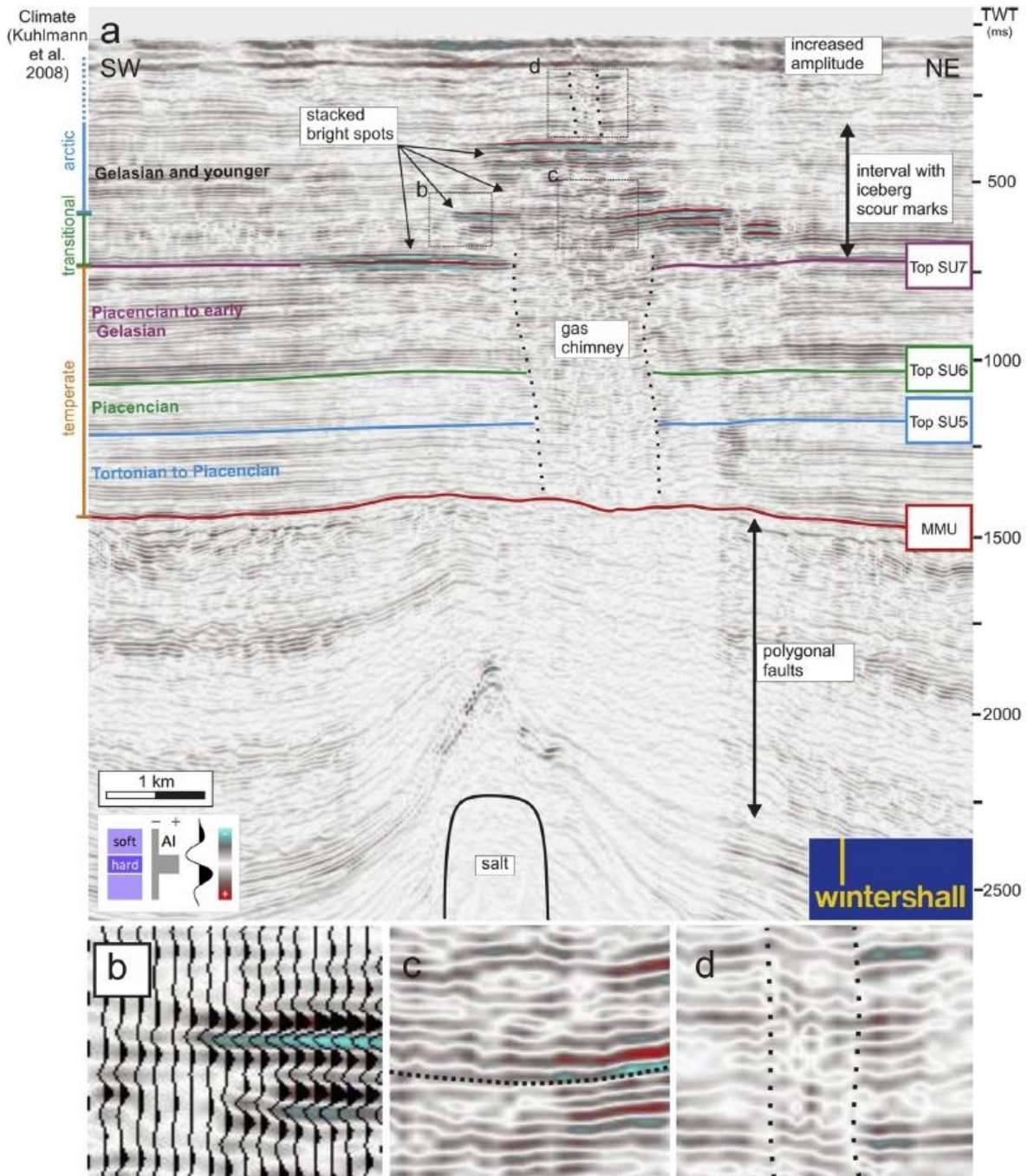


Fig. 16 Example 1 (a) seismic reflection profile with high-amplitude anomalies above a salt dome. The stratigraphic framework is adopted from Thöle et al. (2014). (b) Typical “peak-over-trough” pattern of gas-induced bright spots. (c) Alleged topographic low that is caused by velocity push-down (dotted line). The left side of the reflection is attenuated due to gas in the overlying strata. (d) Discontinuous seismic pattern above the bright spot cluster, indicating vertical gas migration along a chimney towards the seafloor. Seismic data courtesy of Wintershall Holding GmbH.

3.4.2. Example 2

The second example is also located in the western part of the German Central Graben and recorded on 3D reflection seismic data. The horizons above a salt dome are intersected by a NW-SE striking normal fault. Stacked bright spots are concentrated on both sides of the fault, forming a north-eastern and a south-western section. Four different layers, characterized by high-amplitudes with peak-over-trough patterns are distinguished in the southwest, and eight bright spot layers occur in the northeast of the fault (Fig. 17a). The center of the northeastern bright spots is distinctly attenuated, and its reflections are pushed down, which are both indications for free gas (Fig. 17b). On a horizontal section, the high-amplitude reflections on both sides of the fault exhibit an ellipsoidal form, conforming to the anticlinal structure, and featuring a tail in the northeast (Fig. 18). The bright spot-tail terminates at a NNW-SSE trending iceberg scour mark which acts as a lateral seal similar to shallow gas accumulations in the Central North Sea (Haavik and Landrø, 2014). Discontinuous low amplitude reflections from the top of the salt dome to the center of the bright spots may indicate a gas chimney (Fig. 17d). The southwestern and lowermost northeastern bright spots terminate onto the fault, indicating a fault-dip- closure. The closure of the uppermost northeastern bright spots, though, is controlled by dip only. Thus, the potential gas accumulations above the salt dome are a combination of fault-dip and 4-way-dip closures. Increased amplitudes at the flank of the fault and at uppermost reflections above the fault indicate further gas migration from the fault towards the seafloor (Fig. 17c). The stacked bright spots are predominately located above seismic unit SU7 in horizons of Gelasian age. These horizons were deposited in alternating warm and cold periods at the transition from a temperate to an arctic climate. Iceberg scour marks within the layers corroborate these climatic conditions. Further bright spots are located within Piacencian sediments (SU7) that were deposited in a temperate climate.

3. Shallow gas accumulations in the German North Sea

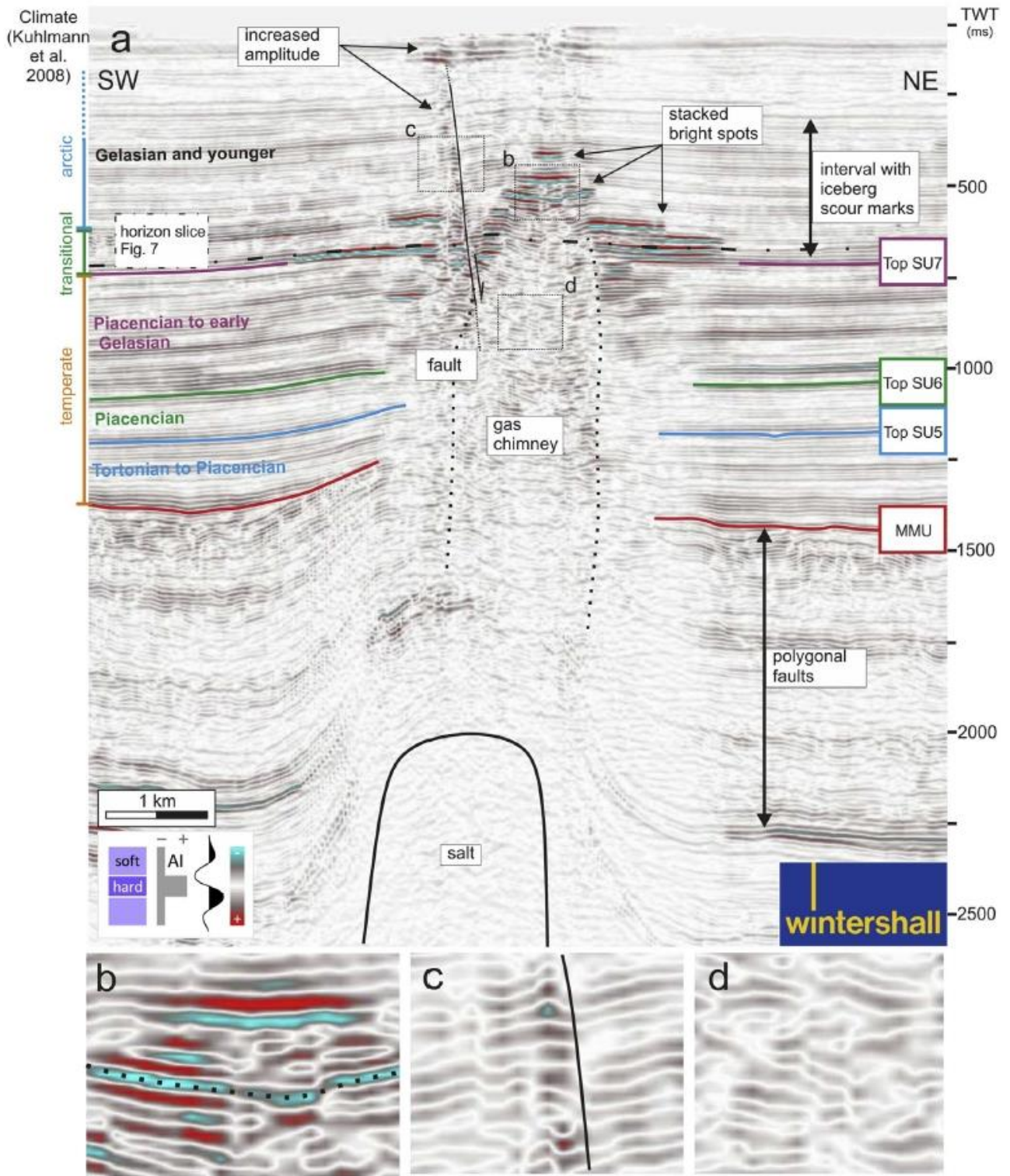


Fig. 17 Example 2 (a) seismic reflection profile with high-amplitude anomalies above a salt dome. Seismic stratigraphy is adopted from Thöle et al. (2014). (b) Alleged topographic low that is caused by velocity push-down (dotted line). (c) Increased amplitudes along a fault which indicate gas migration towards the seafloor and lead to increased amplitudes at the top of the seismic section. (d) Internal discontinuous seismic pattern subjacent of the bright spot cluster indicating a gas chimney. Seismic data courtesy of Wintershall Holding GmbH.

3.4.3. Example 3

The third example is located in the eastern part of the German Central Graben and is recorded in 2D reflection seismic data. Fig. 19a shows an example where salt movements generated an anticlinal structure in the overlying sediments, which are cut by several normal faults. These faults are connected with laterally confined peak-over-trough bright spots, indicating that potential gas accumulations are fault-dip confined (FDC) in this zone. Bright spots are predominantly found in three seismic reflections. The gas filled horizon that are affected by overlying bright spots show seismic attenuation and velocity push-down (Fig. 19b/c). The bright spots decrease towards the seafloor in their lateral extent. The reflection pattern below the bright spot cluster is discontinuous and of low amplitude, which may indicate migration in a gas chimney. The areal extent ranges from 1 km for the uppermost bright spot to 1.7 km² for the middle horizon to 6 km² for the lowermost bright spot. The bright spots are predominately found in shallow marine/deltaic sediments of Piacencian age, in which the climate was temperate. The lowermost bright spot horizon exhibits several internal onlapping structures (Fig. 19d). Upper and lower onlapping structures are bright, indicating that both structures contain gas. Therefore, the contact between the structures is permeable for gas and the trap is not stratigraphically (pinch-out trap) but structurally controlled. Similar structures are found offshore The Netherlands near the German North Sea Sector. Amplitude analysis of a horizon featuring an onlapping bright spot (Fig. 20a) reveals that the onlapping structures are elongated and perpendicular to the direction of propagation of the delta (Fig. 20b). Therefore, the structures are interpreted as contouritic bodies of relatively coarse-grained sediments that were sorted and aligned by bottom currents (Rebesco et al., 2014). A bright spot at the top of the seismic unit SU6 indicates efficient trapping of gas. The top of SU6 is interpreted by Thöle et al. (2014) as a maximum flooding surface. As a result of a rising sea level, finer grained sediments were deposited and may act as a seal.

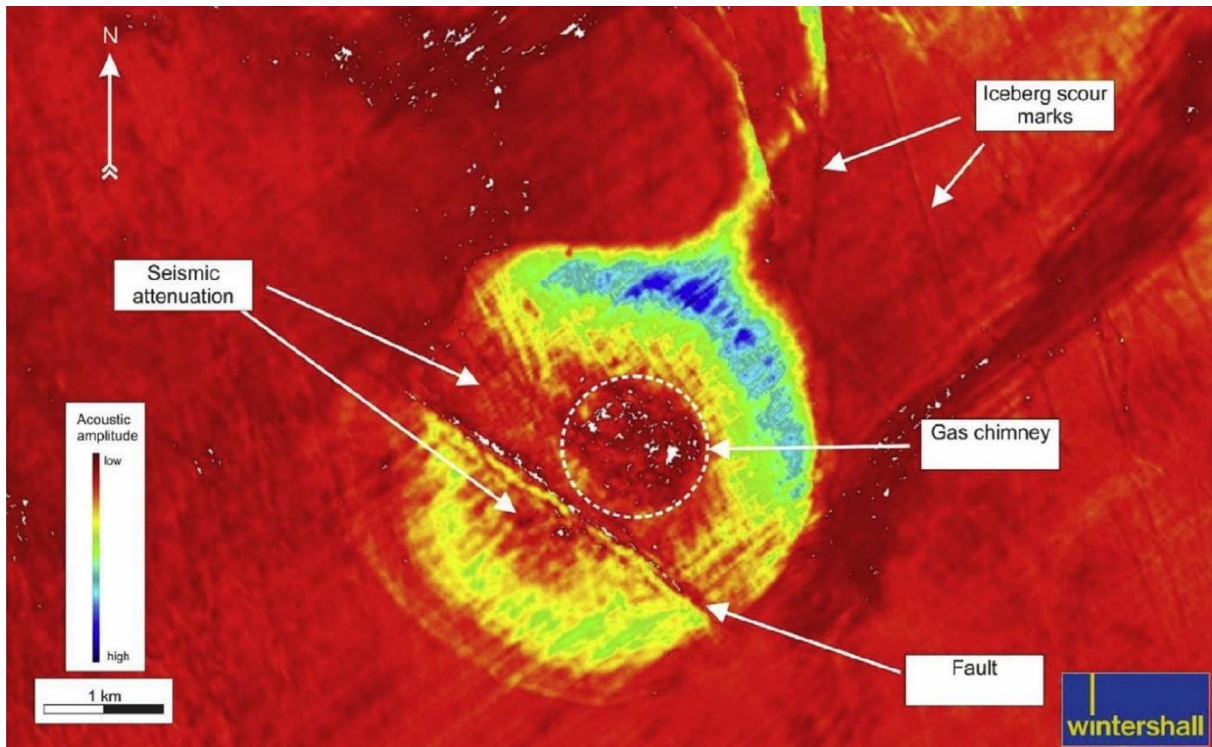


Fig. 18 Horizontal amplitude grid along a bright spot horizon of example 2 (Fig. 17). The slice is located at ~ 700 ms (TWT). High-amplitude bright spots stand out of the low-amplitude background. The semicircle shape of the bright spots is due to the separating NW-SE trending fault and the structure of the anticline. The seismic signal is attenuated by overlying bright spots in places. Iceberg scour marks indicate an arctic paleo-climate during sedimentation. The white dots are a product of the discontinuity of the reflections within the gas chimney. The automatic seismic area picking tool was not able to produce a grid at those locations. Seismic data courtesy of Wintershall Holding GmbH.

3.5. Discussion

3.5.1. Common characteristics of the shallow gas accumulations in the Dutch and German offshore areas

On seismic data, the investigated structures share the same indicators for gas as the Dutch fields: stacked bright spots with peak-over-trough pattern, seismic attenuation, velocity push-down and gas chimneys (Fig. 21).

Offshore Germany, the stacked bright spots occur in sediments that developed in two different climatic environments. The bright spot horizons of example 1 and example 2 are predominately located in an interval that consists of Gelasian sediments that were deposited during alternations of warm and cold periods. Within this interval, the grainsize of the deposited sediments varies considerably in response to a changing paleo-climate. During cold periods, fine-grained sediments chiefly reached the basin due to glaciation, constituting potential seals. In contrast, during warm periods the coarser-grained sediments that form potential reservoirs were transported due to glacial melting (Kuhlmann et al., 2004; ten Veen et al., 2013).

3. Shallow gas accumulations in the German North Sea

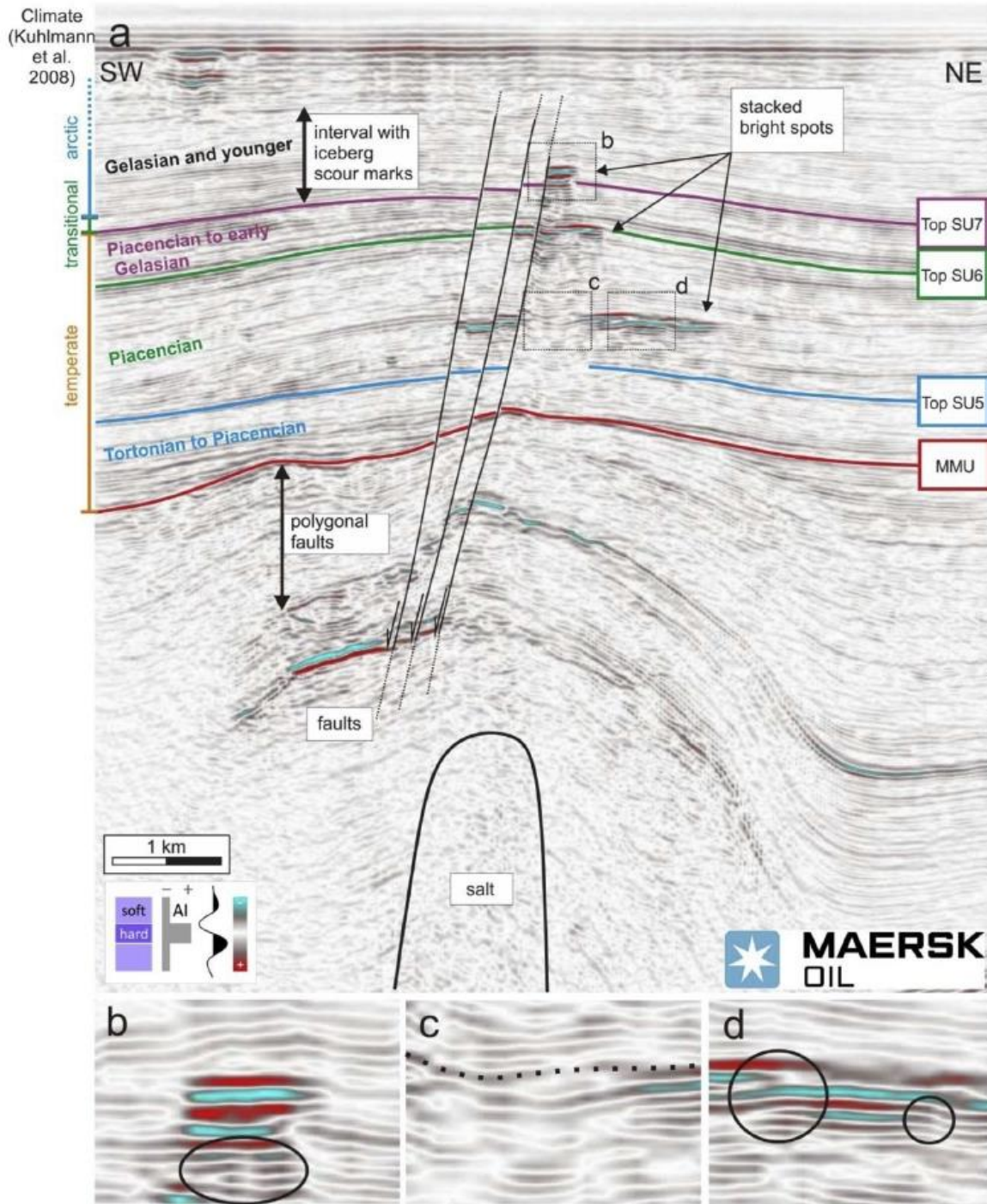


Fig. 19 (a) Reflection seismic example 3 showing high-amplitude anomalies above a third salt dome. Seismic stratigraphic framework according to Thöle et al. (2014) (b) Seismic attenuation below bright spots with typical “peak-over-trough” pattern of gas-induced bright spots. (c) Seismic attenuation of the underlying horizons. (d) Onlapping of the bright spots in the lowermost horizon. Seismic data courtesy of Maersk Oil.

The reservoir and seal intervals of example 1 and 2 correspond to the ones of the shallow gas fields in the Dutch offshore. The coupling of seal and reservoir layers reflects the alternation of warm and cold periods (Verweij et al., 2012a,b; ten Veen et al., 2013). The Dutch shallow gas fields within the Step Graben area (A12-FA, A18, and B13-FA) occur in Gelasian topset sedi-

ments, which consist predominately of silt and very fine sand (ten Veen et al., 2013). The reservoir horizons of the F02a-Pliocene field within the Dutch Central Graben consist of silty delta foreset sediments of early Gelasian age (ten Veen et al., 2013).

The reservoir and seal layers of example 3 were predominately deposited in a shallow marine setting, in a temperate climate. In contrast to examples 1 and 2, and the Dutch shallow gas fields, the grain sizes are mainly governed by the proximity within the shelf prism clinofolds (foreset, slope, topset) and not by climatic variations. The reservoir layers are thus found in the relatively coarse-grained topset sediments as well as in sediments sorted by bottom currents. Similar to the latter are gas containing sand wave deposits in the Dutch offshore (Fig. 21b). In contrast to the contouritic deposits of example 3, the gas charge of the Dutch sand waves is believed to have taken place before the formation of the structural trap. The gas content is believed to be only residual (ten Veen et al., 2013).

Vertical gas migration is indicated for the Dutch shallow gas fields as well as the German potential shallow gas accumulations by the distinct gas chimneys that are located between the bright spots and the salt domes. Similar chimneys and fluid pipes indicating fluid flow within Triassic to Cretaceous strata were also observed in seismic data offshore The Netherlands (Alves and Elliott, 2014). The formations underlying the MMU are overpressured, while the younger sediments of the Eridanos Delta have normal to close-to-normal pore pressures (Verweij et al., 2012a, 2012b; ten Veen et al., 2014a,b). A decrease in pore pressure towards salt domes in Upper Jurassic sediments of the northern Dutch Central Graben indicates dewatering and pressure dissipation towards the salt domes (Verweij et al., 2012b). Hence, fluid migration takes place along a pressure gradient in the overpressured pre-MMU sediments where the overpressure is able to dissipate through the weakened sediment texture above the salt domes. The overpressure also reduces the effective stress that acts on the polygonal faults in the Paleocene and Lower Miocene mudstones, hence increasing their permeability and potentially opening them for fluid migration. Within the post-MMU sediments, vertical gas migration is driven by buoyancy (Verweij et al., 2012a; ten Veen et al., 2014a,b). The gas is either dissolved in water and comes out of solution when the pressure declines or migrates as free gas using faults or fractures beyond seismic resolution as migration pathways (Heggland, 2005; Williams and Gent, 2015).

Bright spots within the Dutch and the German offshore sectors often occur vertically stacked. This is considered to be related to the shallow sediments being unconsolidated and thus often providing only limited seals. Buoyancy driven gas accumulates in layers with a higher horizontal permeability (Cartwright and Santamarina, 2015), e.g., silt, until the pressure that is applied by the gas column exceeds the capillary entry pressure of the sealing clay. After a breach of the seal, the gas migrates to the next potential reservoir layer (Fig. 22). The capillary entry pressure decreases towards the seafloor, resulting in a simultaneous decrease in gas saturation, height of the gas column, and areal extent of the bright spots. However, shallower than ~400 m, the capillary entry pressure of the unconsolidated sediments is too low to allow the successful trapping of gas (ten Veen et al., 2013). The lower boundary (~900 ms TWT) of the occurrence of bright spots in the Dutch and German offshore is set by Paleogene claystones and Neogene deep marine clays due to their low horizontal permeability.

Whether the shallow gas is of a microbial and/or thermogenic origin is not yet resolved. The available isotopic and molecular composition of the Dutch shallow gases are heterogeneous and point to a microbial (almost exclusively methane, light isotopic composition) as well as a thermogenic origin (higher portion of ethane and propane, heavier isotopic composition) in different shallow gas fields (Tab. 1; ten Veen et al., 2013). Geochemical data are not available for the shallow gas offshore Germany.

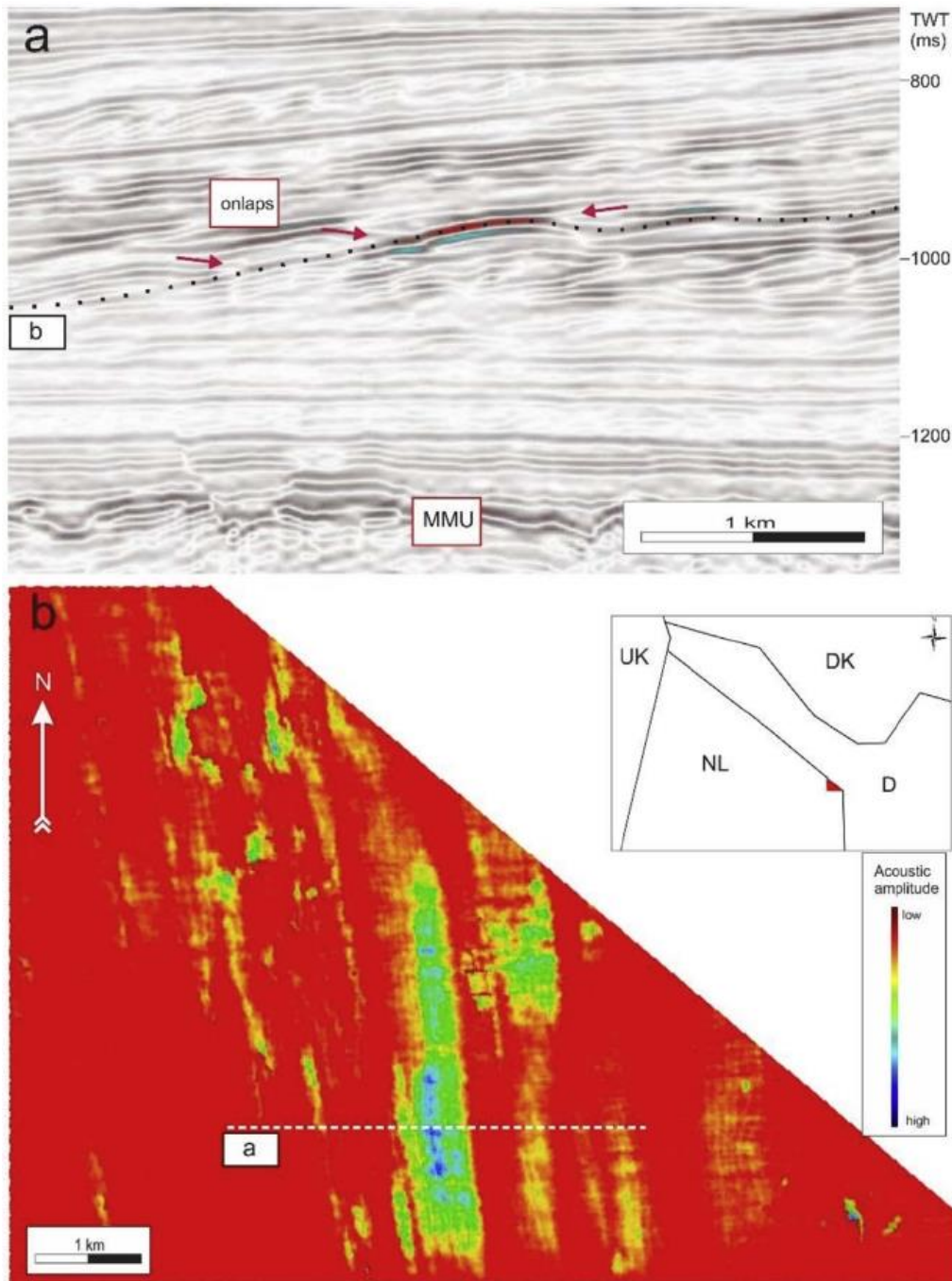


Fig. 20 (a) Seismic reflection profile showing onlapping sedimentary structures of partially anomalous high amplitude located offshore The Netherlands. The structures are presumably formed by bottom currents and are comparable to the lowermost bright spots of example 3. (b) Horizontal amplitude grid along a bright spot-containing horizon showing the elongated and parallel composition of the onlapping structures. The high amplitudes of some of the sedimentary bodies may be the result of gas charge or of a lithology change.

3.5.2. Significance of shallow gas offshore Germany

An assessment of the resources of the shallow gas accumulations within the German offshore is not yet feasible due to the lack of data concerning reservoir properties, and the great uncertainty concerning gas saturation and composition. However, the areal extent of the Dutch bright spots is greater than the extent of the German ones. The bright spots of example 1 have an expanse between ~ 1.5 and 18 km^2 , of example 2 between ~ 1 and 13 km^2 , and of example 3 between ~ 1 and 8 km^2 . The expanse of the lowermost and most extensive bright spots of the A12-FA and A18 fields is $\sim 60 \text{ km}^2$, of the field B13-FA even $\sim 80 \text{ km}^2$. The expanse of the main bright spot of the F02a-B-Pliocene field is, with $\sim 18 \text{ km}^2$, akin to example 1. The F02a-B-Pliocene bright spot features a distinct flat spot, however, that suggests a high gas column (Fig. 21d). Such a flat spot is absent for the German examples. To assess the full potential of the shallow gas accumulations within the German North Sea more research is needed regarding reservoir properties, content, origin, and composition of the gas that causes the amplitude anomalies.

Gas emissions from marine sources play only a minor role in the global methane budget (Cicerone and Oremland, 1988; Bange et al., 1994; Nisbet et al., 2016), but its accurate assessment is important for distinguishing the natural and anthropogenic sources of greenhouse gases and their effect on global warming. Methane emissions related to shallow gas accumulations within the North Sea are increasingly a subject of recent research, including emissions from abandoned wells that penetrated shallow gas accumulations (Vielstädte et al., 2015), abrupt eruptions of gas (Krämer et al., 2017), and seeps from Dutch shallow gas fields (Römer et al., 2017). Gas migration to the seafloor is indicated for the investigated examples by a possible gas chimney and high amplitudes alongside a fault. As in the Dutch offshore (Tab. 1), methane is assumed to be the main gas that causes the investigated amplitude anomalies in the German offshore. Methane is a potent greenhouse gas and even if the methane is partly metabolized by microbes within the water column, the greenhouse gas may partly still reach the atmosphere (Lelieveld et al., 1993). This is indicated by elevated atmospheric methane concentrations above the Dutch shallow gas field B 13-FA (Römer et al., 2017). Measurements of atmospheric methane concentrations above the investigated amplitude anomalies would clarify the degree to which methane is leaking naturally from these sites.

The high amplitudes of the uppermost reflections directly above the investigated shallow gas accumulations of example 1 and 2 may indicate gas within the sediments that could affect the properties of the subsoil and pose a risk for offshore infrastructure (Wheeler, 1988; Sultan and Garziglia, 2014). Possible offshore infrastructure includes drilling platforms as well as wind farms relating to the transition to an increasing use of renewable energy in Germany (Quitow et al., 2016).

3. Shallow gas accumulations in the German North Sea

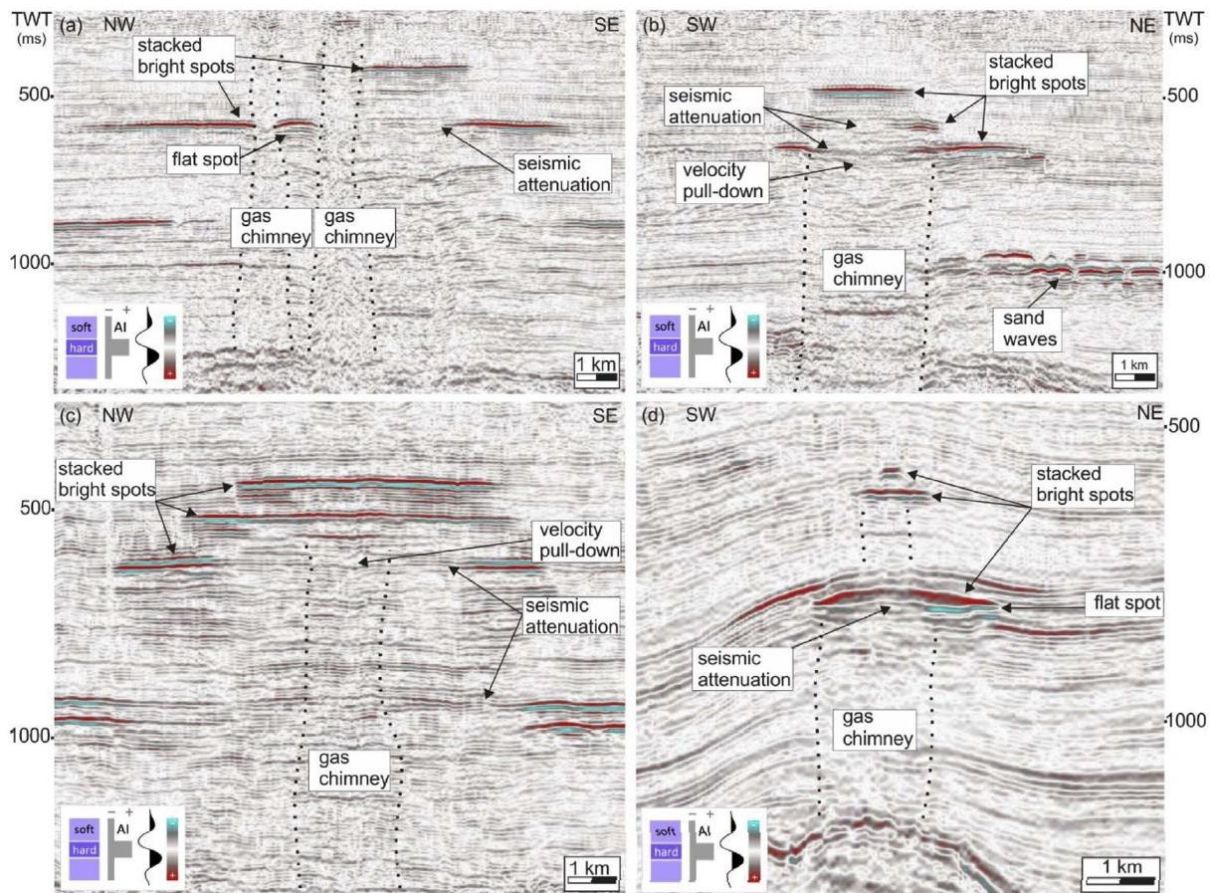


Fig. 21 Seismic profiles of the four currently producing Dutch shallow gas fields with direct hydrocarbon indicators: bright spot with peak-over-trough pattern, seismic attenuation, velocity push-down, and gas chimney. (a) B13-FA (b) A18 (c) A12-FA (d) F02a-B-Pliocene. For the location of the profiles see Fig. 13.

3.6. Conclusions

Gas accumulations in analogue settings to the producing shallow gas fields in the northern part of the Dutch offshore are identified in the Entenschnabel region of the German North Sea based on reflection seismic data. This similarity is expressed by several characteristics:

a) On seismic data, the gas-filled horizons feature anomalously high amplitudes (bright spots). The gas accumulations on both sides of the Dutch-German offshore border consist of multiple stacked layers.

b) The assumption that gas causes the high amplitudes is affirmed by the presence of other amplitude anomalies as velocity push-downs, seismic attenuation and gas chimneys indicative of the presence of gas.

c) Both in the Dutch and in the German North Sea these shallow gas accumulations are located above Zechstein salt domes. These formed structural traps within the up-domed overburden and sealing faults as well as possible pathways for gas migration along open faults and deformed sediment packages.

d) The reservoir sediments are either deltaic sands or silts of late Pliocene age, including possible contourite deposits, or early Pleistocene shallow marine sediments which are strongly influenced by glacial and inter-glacial cycles. The economic potential of the shallow gas accumulations within the German offshore has a high uncertainty due to the lack of reservoir data. The potential gas volume is probably less than that of the producing Dutch shallow gas fields due to either a smaller reservoir area or smaller gas column. Seismic anomalies indicate gas seepage from some of the shallow gas accumulations to the seafloor. Whether methane is emitted into the atmosphere and resembles an important source in the overall greenhouse gas budget, or whether it remains in major portion in the water column, has still to be studied. Furthermore, gas near the seabed may affect its properties and mapping of venting shallow gas accumulations can help mitigate against offshore construction and planning risks.

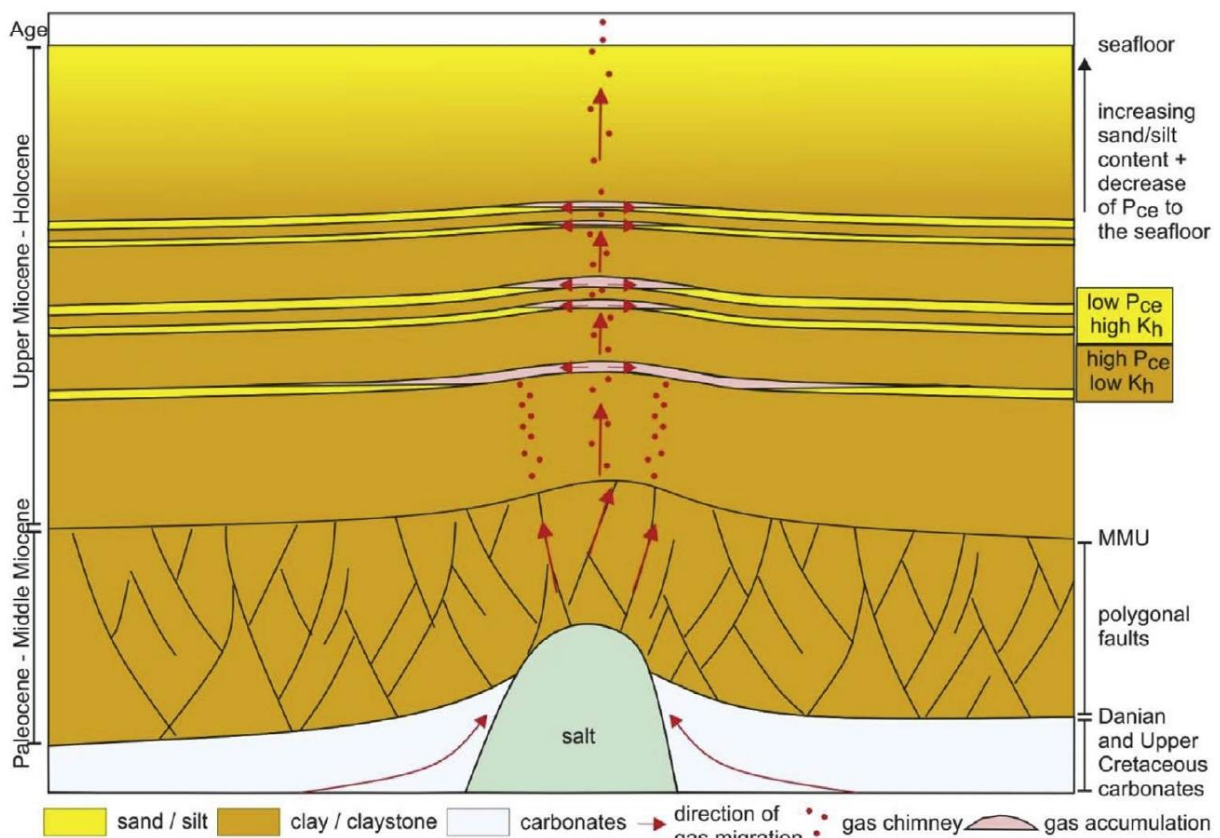


Fig. 22 Sketch of the formation of multiple stacked bright spots above a salt dome in the southern North Sea. Gas accumulations are controlled by the horizontal permeability (K_h) and the capillary entry pressure (P_{ce}) of the seal and reservoir layers. Gas migration takes place by buoyancy forces in the normally pressured sediments above the MMU and additionally along pressure gradients in the underlying overpressured formations.

Acknowledgments

We thank the companies Wintershall Holding GmbH and BEB Erdgas und Erdöl GmbH & Co. KG, organized in the industrial association BVEG (Bundesverband Erdgas, Erdöl und Geoenergie e.V.) and the company Maersk Oil for the permission to use their data sets for scientific research within this study. We also thank our colleagues Rüdiger Lutz, Jashar Arfai, Frithjof Bense, Fabian Jähne-Klingberg, Andreas Bahr, and Stefan Ladage who provided expertise that greatly assisted the research. We also thank the associate editor Tiago Alves, and the reviewers Dallas Dunlap, Johan ten Veen, Miles Leggett, and an anonymous reviewer for their helpful and detailed comments, which helped to improve this article.

References

- Alves, T.M. & Elliott, C., 2014. Fluid flow during early compartmentalisation of rafts: a North Sea analogue for divergent continental margins. *Tectonophysics* 634, 91–96.
- Anstey, N.A., 1977. *Seismic Interpretation: the Physical Aspects*. Springer Science & Business Media.
- Arfai, J., Jähne, F., Lutz, R., Franke, D., Gaedicke, C. & Kley, J., 2014. Late paleozoic to early cenozoic geological evolution of the northwestern German North Sea (Entenschnabel): new results and insights. *Neth. J. Geosci.* 93, 147–174.
- Bange, H.W., Bartell, U.H., Rapsomanikis, S. & Andreae, M.O., 1994. Methane in the Baltic and North Seas and a reassessment of the marine emissions of methane. *Global Biogeochem. Cycles* 8 (4), 465–480. BGR, 2016. *Energy Study 2016. Reserves, Resources and Availability of Energy Resources* 20. pp. 180 (Hannover).
- Cartwright, J.A., 1994. Episodic basin-wide hydrofracturing of overpressured early Cenozoic mudrock sequences in the North Sea Basin. *Mar. Petrol. Geol.* 11 (5), 587–607.
- Cartwright, J. & Santamarina, C., 2015. Seismic characteristics of fluid escape pipes in sedimentary basins: implications for pipe genesis. *Mar. Petrol. Geol.* 65, 126–140.
- Cathles, L.M., Su, Z. & Chen, D., 2010. The physics of gas chimney and pockmark formation, with implications for assessment of seafloor hazards and gas sequestration. *Mar. Petrol. Geol.* 27 (1), 82–91.
- Cicerone, R.J. & Oremland, R.S., 1988. Biogeochemical aspects of atmospheric methane. *Global Biogeochem. Cycles* 2 (4), 299–327.
- Clausen, O.R. & Huuse, M., 1999. Topography of the top chalk surface on- and offshore Denmark. *Mar. Petrol. Geol.* 16 (7), 677–691.
- Domenico, S., 1974. Effect of water saturation on seismic reflectivity of sand reservoirs encased in shale. *Geophysics* 39 (6), 759–769.
- EBN, 2012. *Focus on Dutch Oil and Gas 2012*. https://www.ebn.nl/wp-content/uploads/2014/11/ebn_focus_on_dutch_gas_2012.pdf, Accessed date: 5 December 2016.
- Ebrom, D., 2004. The low-frequency gas shadow on seismic sections. *Lead. Edge* 23 (8) 772–772.
- Eriksen, O.K., Berndt, C., Buenz, S., Eriksen, F.N. & Planke, S., 2011, May. Styles of shallow gas migration and accumulation on the Norwegian Continental Margin. In: *73rd EAGE Conference and Exhibition*, 23–26 May 2011, Vienna, Austria, (Extended abstract).
- Haavik, K.E. & Landrø, M., 2014. Iceberg ploughmarks illuminated by shallow gas in the central North Sea. *Quat. Sci. Rev.* 103, 34–50.

- Heggland, R., 2005. Using gas chimneys in seal integrity analysis: a discussion based on case histories. In: Boulton, P., Kaldi, J. (eds.), *Evaluating Fault and Cap Rock Seals*, vol. 2. AAPG Hedberg Series, pp. 237–245.
- Knox, R.W.O.B., Bosch, J.H.A., Rasmussen, E.S., Heilmann-Clausen, C., Hiss, M., De Lugt, I.R., Kasiński, J., King, C., Kothe, A., Słodkowska, B., Standke, G. & Vandenberghe, N., 2010. Cenozoic. In: Doornenbal, J.C., Stevenson, A.G. (eds.), *Petroleum Geological Atlas of the Southern Permian Basin Area*. EAGE Publications b.v, Houten, pp. 211–223.
- Kombrink, H., ten Veen, J.H. & Geluk, M.C., 2012. Exploration in The Netherlands, 1987-2012. *Neth. J. Geosci.* 91 (04), 403–418.
- Krämer, K., Holler, P., Herbst, G., Bratek, A., Ahmerkamp, S., Neumann, A., Bartholomä, A., van Beusekom, Holtappels, M. & Winter, C., 2017. Abrupt emergence of a large pockmark field in the German Bight, southeastern North Sea. *Sci. Rep.* 7.
- Kuhlmann, G. & Wong, T.E., 2008. Pliocene paleoenvironment evolution as interpreted from 3D-seismic data in the southern North Sea, Dutch offshore sector. *Mar. Petrol. Geol.* 25 (2), 173–189.
- Kuhlmann, G., de Boer, P.L., Pedersen, R.B. & Wong, T.E., 2004. Provenance of Pliocene sediments and paleoenvironmental changes in the southern North Sea region using Samarium–Neodymium (Sm/Nd) provenance ages and clay mineralogy. *Sediment. Geol.* 171 (1), 205–226.
- Lelieveld, J., Crutzen, P.J. & Brühl, C., 1993. Climate effects of atmospheric methane. *Chemosphere* 26 (1–4), 739–768.
- Lutz, R., Kalka, S., Gaedicke, C., Reinhardt, L. & Winsemann, J., 2009. Pleistocene tunnel valleys in the German North Sea: spatial distribution and morphology. *Z. Dtsch. Ges. Geowiss.* 160 (3), 225–235.
- Marfurt, K.J. & Alves, T.M., 2014. Pitfalls and limitations in seismic attribute interpretation of tectonic features. *Interpretation* 3 (1), SB5–SB15.
- Mulrooney, M.J., Leutscher, J. & Braathen, A., 2017. A 3D structural analysis of the Goliath field, Barents Sea, Norway. *Mar. Petrol. Geol.* 86, 192–212.
- Muntendam-Bos, A.G., Wassing, B.B.T., ter Heege, J.H., van Bergen, F., Schavemaker, Y.A., van Gessel, S.F., de Jong, M.L., Nelskamp, S., van Thienen-Visser, K., Guasti, E., van den Belt, F.J.G. & Marges, V.C., 2009. Inventory Non-conventional Gas. TNO report TNO-034-UT-2009–20000774/B. TNO Utrecht, The Netherlands.
- Nisbet, E.G., Dlugokencky, E.J., Manning, M.R., Lowry, D., Fisher, R.E., France, J.L., Michel, S.E., Miller, J.B., White, J.W.C., Vaughn, B., Bousquet, P., Pyle, J.A., Warwick, N.J., Cain, M., Brownlow, R., Zazzeri, G., Lanoisellé, M., Manning, A.C., Gloor, E., Worthy, D.E.J., Brunke, E.G., Labuschagne, C., Wolff, E.W. & Ganesan, A.L., 2016. Rising atmospheric methane: 2007-2014 growth and isotopic shift. *Global Biogeochem. Cycles* 30, 1356–1370.

- Overeem, I., Weltje, G.J., Bishop-Kay, C. & Kroonenberg, S.B., 2001. The late Cenozoic Eridanos delta system in the southern North Sea Basin: a climate signal in sediment supply? *Basin Res.* 13 (3), 293–312.
- Patrino, S., Hampson, G.J. & Jackson, C.A., 2015. Quantitative characterisation of deltaic and subaqueous clinoforms. *Earth Sci. Rev.* 142, 79–119.
- Pletsch, T., Appel, J., Botor, D., Clayton, C.J., Duin, E.J.T., Faber, E., Górecki, W., Kombrink, H., Kosakowski, P., Kuper, G., Kus, J., Lutz, R., Mathiesen, A., Ostertag-Henning, C., Papiernek, B. & Van Bergen, F., 2010. Petroleum generation and migration. In: Doornenbal, J.C., Stevenson, A.G. (eds.), *Petroleum Geological Atlas of the Southern Permian Basin Area*. EAGE Publications b.v, Houten, pp. 225–253.
- Quitow, L., Canzler, W., Grundmann, P., Leibenath, M., Moss, T. & Rave, T., 2016. The German Energiewende—What's happening? Introducing the special issue. *Util. Pol.* 41, 163–171.
- Rebesco, M., Hernández-Molina, F.J., Van Rooij, D. & Wåhlin, A., 2014. Contourites and associated sediments controlled by deep-water circulation processes: state-of-the-art and future considerations. *Mar. Geol.* 352, 111–154.
- Reinhold, K., Krull, P. & Kockel, F., 2008. *Karte der Salzstrukturen Norddeutschlands (BGR)*.
- Römer, M., Wenau, S., Mau, S., Veloso, M., Greinert, J., Schlüter, M. & Bohrmann, G., 2017. Assessing marine gas emission activity and contribution to the atmospheric methane inventory: a multidisciplinary approach from the Dutch Dogger Bank seep area (North Sea). *G-cubed* 18.
- Schroot, B.M. & Schüttenhelm, R.T.E., 2003. Expressions of shallow gas in The Netherlands North Sea. *Neth. J. Geosci.* 82 (1), 91–106.
- Schroot, B.M., Klaver, G.T. & Schüttenhelm, R.T., 2005. Surface and subsurface expressions of gas seepage to the seabed—examples from the Southern North Sea. *Mar. Petrol. Geol.* 22 (4), 499–515.
- Sheriff, R.E., 1991. *Encyclopaedic Dictionary of Exploration Geophysics*, vol. 1. SEG Geophysical References Series, Tulsa, USA, pp. 384.
- Simm, R. & Bacon, M., 2014. *Seismic Amplitude: an Interpreter's Handbook*. Cambridge University Press.
- Stewart, M.A. & Lonergan, L., 2011. Seven glacial cycles in the middle-late Pleistocene of northwest Europe: geomorphic evidence from buried tunnel valleys. *Geology* 39 (3), 283–286.
- Stuart, J.Y. & Huuse, M., 2012. 3D seismic geomorphology of a large Plio-Pleistocene delta—‘Bright spots’ and contourites in the Southern North Sea. *Mar. Petrol. Geol.* 38 (1), 143–157.
- Sultan, N. & Garziglia, S., 2014. Mechanical behaviour of gas-charged fine sediments: model formulation and calibration. *Geotechnique* 64 (11), 851–864.

- ten Veen, J.H., Geel, C.R., Kunakbayeva, G., Donders, T.H. & Verreussel, R.M.C.H., 2011. Property Prediction of Plio-pleistocene Sediments in the A15 Shallow Gas System. TNO Report TNO-060-UT-2011–20101184/C12. TNO Utrecht, The Netherlands.
- ten Veen, J., Verweij, H., Donders, T., Geel, K., de Bruin, G., Munsterman, D., Verreussel, R., Daza Cajigal, V., Harding, R. & Cremer, H., 2013. Anatomy of the Cenozoic Eridanos Delta Hydrocarbon System. TNO Report TNO 2013 R10060. TNO Utrecht, The Netherlands.
- Thöle, H., Gaedicke, C., Kuhlmann, G. & Reinhardt, L., 2014. Late Cenozoic sedimentary evolution of the German North Sea—A seismic stratigraphic approach. *Newslett. Stratigr.* 47 (3), 299–329.
- Trampe, A.F., Lutz, R., Franke, D. & Bücker, C., 2014. Oberflächennahes Erdgas in der deutschen Nordsee. *Erdöl Erdgas Kohle* 130, 8–10.
- van den Boogaard & M., Hoetz, G., 2015. Seismic characterisation of shallow gas in The Netherlands. In: Abstract FORCE Seminar Stavanger, 8–9 April 2015, Stavanger, Norway, (Extended abstract).
- van den Boogaard, M., Gras, R. & Hoetz, G., 2013. Shallow play in The Netherlands -derisked by seismic characterisation. In: 75th EAGE Conference & Exhibition Incorporating SPE EUROPEC 2013, 10–13 June 2013, London, UK, (Extended abstract).
- ten Veen, J.H., Verweij, J.M., de Bruin, G. & Donders, T., 2014a. First steps toward maturing the shallow gas play - results of an integrated exploration workflow. In: IPTC 2014: International Petroleum Technology Conference, 20–22 January 2014, Doha, Qatar, (Extended abstract).
- ten Veen, J.H., de Bruin, G., Verweij, J.M. & Donders, T., 2014b. Towards a better understanding of shallow seismic anomalies in the Dutch offshore. In: EAGE Shallow Anomalies Workshop, 23–26 November 2014, Malta, (Extended abstract).
- Verweij, J.M. & Nelskamp, S., 2014. Focus on shallow gas systems. In: First EAGE Basin & Petroleum Systems Modeling Workshop, 19–22 October 2014, Dubai, UAE, (Extended abstract).
- Verweij, J.M., ten Veen, J.H., De Bruin, G., Nelskamp, S.N., Donders, T., Kunakbayeva, G. & Geel, K., 2012a. Shallow gas migration and trapping in the Cenozoic Eridanos delta deposits, Dutch offshore. In: 74th EAGE Conference and Exhibition Incorporating EUROPEC 2012, 4–7 June 2012, Copenhagen, Denmark, (Extended abstract).
- Verweij, J.M., Simmelink, H.J., Unterschultz, J. & Witmans, N., 2012b. Pressure and fluid dynamic characterisation of the Dutch subsurface. *Neth. J. Geosci.* 91 (4), 465–490.
- Verweij, J.M., Cajigal, V.D., De Bruin, G. & Geel, K., 2014. Capillary seal capacity of Cenozoic mudstone caprocks of shallow gas occurrences, Dutch offshore. In: Fourth EAGE Shale Workshop, 6–9 April 2014, Porto, Portugal, (Extended abstract).

Verweij, J.M., Nelskamp, S. & Sarmiento, M.G., 2013. Timing and distribution of biogenic gas generation in the shallow gas play in the Dutch offshore. In: 75th EAGE Conference & Exhibition Incorporating SPE EUROPEC 2013, 10–13 June 2013, London, UK, (Extended abstract).

Vielstädte, L., Karstens, J., Haeckel, M., Schmidt, M., Linke, P., Reimann, S. & Wallmann, K., 2015. Quantification of methane emissions at abandoned gas wells in the Central North Sea. *Mar. Petrol. Geol.* 68, 848–860.

Wheeler, S.J., 1988. A conceptual model for soils containing large gas bubbles. *Geotechnique* 38 (3), 389–397.

Williams, J. & Gent, C., 2015. Shallow Gas Offshore Netherlands - the role of faulting and implications for CO₂ storage. In: 4th International Conference on Fault and Top Seals, 20–24 September 2015, Almería, Spain, (Extended abstract).

Zagwijn, W.H., 1989. The Netherlands during the Tertiary and the Quaternary: a case history of coastal lowland evolution. In: *Coastal Lowlands*. Springer, Netherlands, pp. 107–120.

Ziegler, P.A., 1992. North Sea rift system. *Tectonophysics* 208 (1), 55–75.

4. Seafloor methane seepage related to salt diapirism in the northwestern part of the German North Sea

This chapter has been published as Römer M., Blumenberg M., Heeschen K., Schloemer S., Müller H., Müller S., Hilgenfeldt C., Barckhausen U., & Schwalenberg K., 2021. Seafloor Methane Seepage Related to Salt Diapirism in the Northwestern Part of the German North Sea. *Frontiers in Earth Science*, 9, 556329.

Abstract

This study focuses on seafloor methane seep sites and their distribution in the northwestern part of the German North Sea. Methane seepage is a common phenomenon along marine shelves and known to occur in the North Sea, but proof of their existence was lacking in the study area. Using a ship-based multibeam echosounder we detected a minimum of 166 flares that are indicative for free gas releases from the seafloor in the German “Entenschnabel” area, which are not related to morphologic expressions at the seafloor. However, a group of small depressions was detected lacking water column anomalies but with indications of dissolved fluid release. Spatial analysis revealed that flares were not randomly distributed but show a relation to locations of subsurface salt diapirs. More than 60% of all flares were found in the vicinity of the salt diapir “Berta”. Dissolved methane concentrations of 100 nM in bottom waters were ten times the background value in the “Entenschnabel” area ($\text{CH}_4 < 10 \text{ nM}$), supporting the finding of enhanced seepage activity in this part of our study area. Furthermore, locations of flares were often related to acoustic blanking and high amplitude reflections in sediment profiler echograms, most prominently observed at location Berta. These hydroacoustic signatures are interpreted to result from increased free gas concentrations in the sediments. Electromagnetic seabed mapping depicts local sediment conductivity anomalies below a flare cluster at Berta, which can be explained by small amounts of free gas in the sediment. In our area of interest, ten abandoned well sites were included in our mapping campaign, but flare observations were spatially not related to these wells. Naturally seeping methane is presumably transported to the seafloor along sub-vertical faults, which have formed concurrently to the updoming salt. Due to the shallow water depths of 30 to 50 m in the study area, flares were observed to reach close to the sea surface and a slight oversaturation of surface waters with methane in the flare-rich northeastern part of the working area indicates that part of the released methane through seepage may contribute to the atmospheric inventory.

4. Seafloor methane seepage related to salt diapirism in the northwestern part of the German North Sea

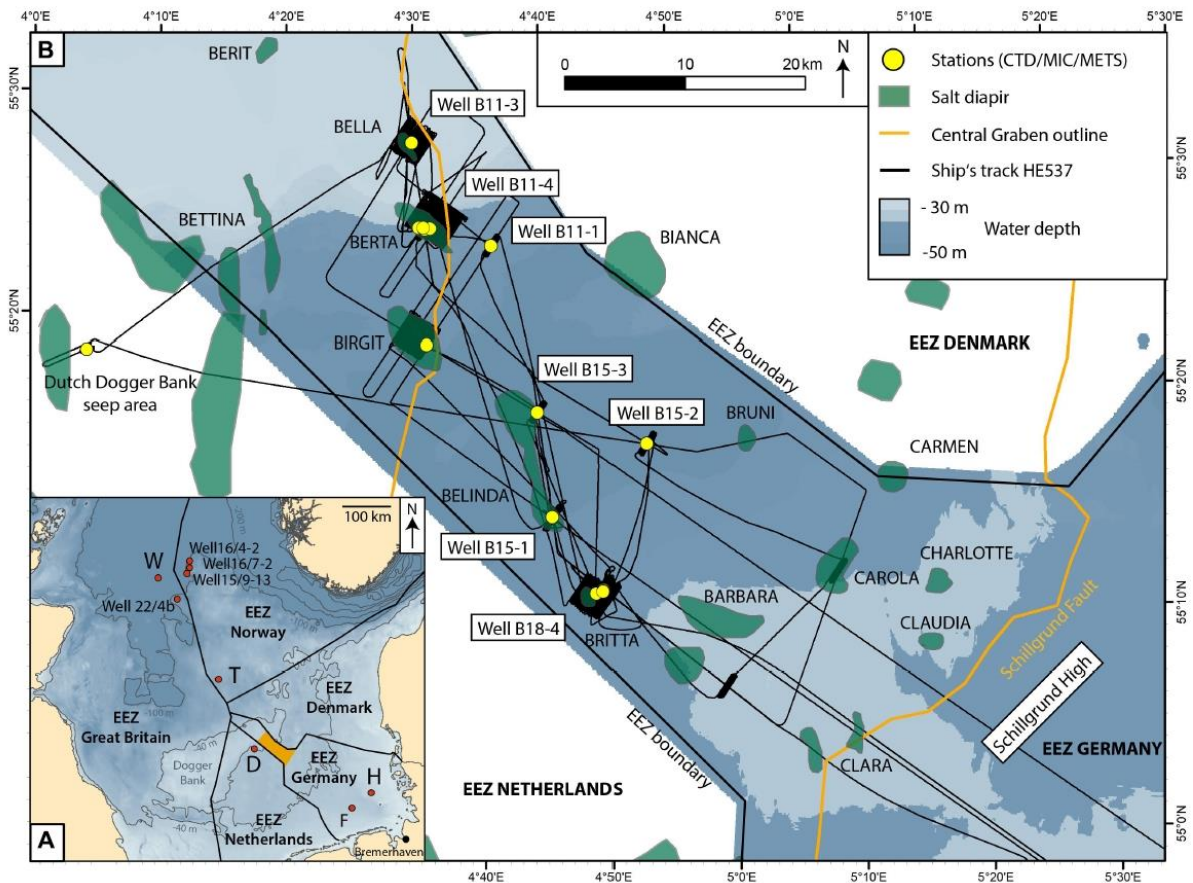


Fig. 23 (A) Overview of the study area in the German Exclusive Economic Zone [EEZ, Flanders Marine and Institute (2019)] of the North Sea (orange area). Known seep sites are marked as red dots. D: Dutch Dogger Bank seep area (Schroot et al., 2005), F: Figgemaar (Thatje et al., 1999), H: Helgoland Reef pockmark field (Krämer et al., 2017), T: Tommeliten seep area (Hovland, 1993), and W: Witch Ground Basin (Judd et al., 1994). Bathymetry downloaded from www.gebco.net. (B) Overview of the study area in the “Entenschnabel,” the northwestern part of the German EEZ. Major structural features depicted from Arfai et al. (2014) are the Central Graben (outlined in orange) and salt diapirs in the subsurface (green areas). Yellow dots point to sampling and measurement stations during R/V Heincke cruise HE537 conducted at seven abandoned well sites, a reference site at salt diapir Birgit, and the Dutch Dogger Bank seep area for comparison. Bathymetry downloaded from www.gpdm.de.

4.1. Introduction

Seafloor methane (CH₄) seepage is widely known to occur along almost all continental margins. This includes the diffusion or advection of dissolved methane from the sediment into the bottom water or the expulsion of free methane gas bubbles. Known natural seep areas in the North Sea, a shelf sea with an average water depth of 95 m, include: (1) Tommeliten seep area in the Norwegian Exclusive Economic Zone (EEZ; Hovland, 1993; Niemann et al., 2005), (2) Dutch Dogger Bank seep area in Netherlands EEZ (Schroot et al., 2005; Römer et al., 2017), (3) pockmarks in the Witch Ground Basin in the EEZ of United Kingdom (Judd et al., 1994; Böttner et al., 2019), and (4) the German Helgoland Reef pockmark field (Krämer et al., 2017; locations see Fig. 23A). The North Sea comprises large areas where shallow gas is being trapped in Cenozoic deltaic and marine sediments and has been detected as “bright spots” in

4. Seafloor methane seepage related to salt diapirism in the northwestern part of the German North Sea

seismic data (Müller et al., 2018). The observed bright spots are characterized by high amplitude seismic reflections, which can indicate a change in pore space filling (White, 1975). Hydrocarbon migration and accumulation are often related to salt diapirism, associated faulting and gas-charged sandfilled ice-scours and channels (Woodbury et al., 1980; Schroot and Schüttenhelm, 2003). Since the Pleistocene, the area has been effected by climate and sea level variations, leading to deposits of glacial-interglacial sediments that are characterized by abundant subglacial tunnel valleys related to melt water flows (Lutz et al., 2009). In our study area, several clusters of bright spots were identified above known salt diapirs, suggesting that salt diapirism lead to fracturing of the overburden strata and formation of migration pathways as well as anticlinal structures for hydrocarbon accumulation (Müller et al., 2018).

Indications of elevated methane concentrations in the North Sea have been deduced from continuous surface water measurements (Rehder et al., 1998) and atmospheric measurements (Judd, 2015), both conducted while crossing our study area in the “Entenschnabel” (local term of that area, meaning “Duck’s Bill,” because of the shape of its outline, Fig. 23A). Methane sources were thought to be related to natural seafloor seepage or alternatively to an anthropogenic well (Judd, 2015). Abandoned wells have been suggested to act as focused migration pathways for hydrocarbons after decommissioning and several recent studies on onshore boreholes have proven the release of hydrocarbons from former gas and oil wells (Kang et al., 2014; Boothroyd et al., 2016; Townsend-Small et al., 2016; Schout et al., 2019). The relative importance of this phenomenon is a matter of discussion [e.g., Schout et al. (2019) found 1 of 29 onshore wells to leak methane]. In a marine setting Vielstädte et al. (2015) studied three well sites in the North Sea and found gas bubbles emitting methane in varying amounts (1–19 tons of CH₄ per year per well). The authors demonstrated by stable carbon isotope analyses that the methane originates from shallow, microbial sources rather than the gas reservoirs. They concluded that mechanic disruption by drilling operations is responsible for methane leakages from shallow, methane-loaded sediments, and that such processes may hold for one third of wells in the North Sea. By extrapolating their observations to the roughly 11,000 abandoned well sites in the North Sea, Vielstädte et al. (2017) estimated that 3– 17 kt year⁻¹ methane potentially escape from the seafloor, which highly exceeds naturally released methane in this area. A recent study by Böttner et al. (2020) suggests that gas release from 1792 investigated decommissioned hydrocarbon wells in the United Kingdom sector of the North Sea is with 0.9–3.7 kt year⁻¹ a major source of methane in the North Sea. Even larger amounts of methane are emitted through well site 22/4b that experienced a man-made blowout in 1990 (Leifer and Judd, 2015 and references therein; Rehder et al., 1998). Leifer (2015) calculated an emission of 25 kt year⁻¹ of methane through gas bubbles even 22 years after the blowout.

Shallow seas such as the German sector of the North Sea may potentially be prone to natural and anthropogenic methane leakages into the sea-air boundary layer, because bubbles may reach shallow water layers and the sea surface. Gas exchange leads to fast dissolution of methane out of the bubbles during their ascent in the water column, but shallow seep sites are expected to transport some fraction of the methane up to the sea surface and contribute to the atmospheric methane inventory (Leifer and Patro, 2002). It has been shown for the nearby Dutch Dogger Bank seep area, located in 40 m water depth, that released bubbles reached the sea surface and elevated methane concentration could be detected in the air above the most

4. Seafloor methane seepage related to salt diapirism in the northwestern part of the German North Sea

intense flare areas (Römer et al., 2017). The vertical transport of dissolved methane is highly restricted by the density stratification in the water column and strong summer thermoclines can also limit the vertical gaseous transport (Schmale et al., 2010; Mau et al., 2015). For example, at the 70m deep Tommeliten area in the Norwegian sector of the North Sea, a summer thermocline constrained methane transport to the atmosphere, and numerical modeling showed that during the summer season less than 4% of the gas initially released as bubbles at the seafloor reaches the mixed layer (Schneider Von Deimling et al., 2011). An even smaller fraction of only 3% of the total water column inventory of dissolved methane was located in the mixed surface layer above the crater of the blowout well 22/4b, revealing that methane transfer across the thermocline was strongly impeded (Sommer et al., 2015).

The area of our investigation is located in the northwestern part of the German North Sea Sector. The geology there is characterized by a prominent Mesozoic rift-structure, the so-called Central Graben. The Central Graben is genetically a halfgraben, whose eastern flank is formed by a major fault array, the Schillgrund Fault, and whose western flank is dominated by a series of horst and graben structures (Arfai et al., 2014). During several Mesozoic rifting phases, organic-rich marine mudstones were deposited that are important source rocks of the southern North Sea area and pose a possible source for thermogenic gas (Wong, 2007). The Central Graben is therefore a major hydrocarbon province in the North Sea (Littke et al., 2008; Pletsch et al., 2010) and was the target area of extended oil and gas exploration and drilling activities, which resulted in more than 49 exploration drill sites in the “Entenschnabel” since 1976 (see Lower Saxony’s borehole database: www.lbeg.niedersachsen.de).

This study reports on the first detection of methane seepage in the “Entenschnabel” located in the North Sea with water depths between 30 and 50 m. An extensive hydroacoustic mapping campaign including water column recording and sediment profiling has been conducted to determine the presence and distribution of flares indicative for gas bubble releases, as knowledge on the integrity of respective deep wells and the occurrence of natural seep sites is so far limited. Continuous and discrete measurements of dissolved methane concentrations in the water column were retrieved to support identification of seepage from the seafloor. A major focus was the investigation of gas emission in relation to subsurface salt diapir locations, seismically identified gas accumulations and abandoned well sites. Our interdisciplinary approach enabled a first characterization of the seepage detected in the work area in the North Sea.

4.2. Materials and methods

The data for this study were acquired during R/V Heincke cruise HE537 in July 2019. The track line shown in Fig. 23B shows the hydroacoustic mapping strategy in the study area and illustrates the surveys focusing at six dedicated salt diapirs and seven abandoned well sites. Sediment and water samples were taken at five different salt diapir structures and two further abandoned well sites (yellow dots in Fig. 23B). A detailed electromagnetic (EM) survey of the shallow seafloor has been analyzed at salt diapir Berta. Finally, methane sensor (METS) deployments were conducted at salt diapirs Bella, Berta, Belinda and Britta as well as the two other

abandoned well sites. An example of the survey and sampling strategy is shown in the Supplementary Figure 1.

4.2.1. Hydroacoustic data

The Kongsberg EM710 is a shallow to mid-water specific multibeam echosounder (MBES) operating between 70 and 100 kHz and an optimal depth range from 10 to 1,200 m. With a transducer configuration of 1 by 2 degrees, this system has 200 beams, with 400 soundings in high density mode, measuring both bathymetry and backscatter. The system was operated with a swath angle of 130° (65° to both sides). Vessel speed was at maximum (during transit times) 8–10 knots, however, was reduced for hydroacoustic mapping in the work area to 3–5 knots. Between the surveys, CTD profiles were carried out and used to calculate sound velocity profiles that were inserted in the acquisition software Seafloor Information System. The open source software package MB-System (Caress and Chayes, 2017) has been utilized to post-process the bathymetric and backscatter data. The investigation of active gas emission sites on the seafloor where gas bubbles can be detected hydroacoustically in the water column (flares) was enabled by analyzing the water column data generated by the EM710. Post-cruise analyses with the FM Midwater module of QPS Fledermaus allowed for manual flare identification and geopicking of flare sources.

Geographical visualization and statistical analysis were performed using ESRI ArcMap 10.4. The spatial analyst tool “near” was used to obtain distances of all flare positions to outlines of salt diapirs, bright spots and abandoned well sites. All results were further normalized using the ships track (distances of 10-m points to the same features) to account for the different coverages and survey focus during cruise HE537. Maps included in this study were spatially projected in UTM zone 32N (WGS84).

During the second half of cruise HE537, the hullmounted SES-2000 medium (Innomar Technologies) sediment echosounder system was used to image shallow sedimentary structures and gas indications. The SES-2000 employs the parametric effect to achieve a small signal opening angle of about 2° at relatively low frequencies between 4 and 15 kHz. The data used in this study were recorded at 6 kHz and penetration depths down to ~25 m below seafloor were achieved. The raw data were converted to SEG-Y-format using the custom PS32SGY software (Hanno Keil, University of Bremen). The data were loaded into the commercial software package Kingdom Software (IHS) for display and interpretation (i.e., mean amplitude grid calculation and horizon mapping of gas indications). Conversions from two-way-traveltime to depth have been calculated using a sound velocity of 1,500 m/s.

4.2.2. Electromagnetic data

Sediment-physical properties of the seabed were mapped with MARUM’s benthic EM profiler NERIDIS III, dedicated for EM seafloor classification. The bottom-towed sled has dimensions of 5.2 x 1.2 x 0.8 m, and a weight of approx. 250 kg in water. It is equipped with a horizontal

4. Seafloor methane seepage related to salt diapirism in the northwestern part of the German North Sea

EM induction-loop sensor (1 m diameter), an Attitude-Heading-Reference- System (AHRS), and conductivity-temperature-depth probe (CTD) with turbidity sensor (Müller et al., 2011). The profiler was towed in contact with the seabed at speeds of 2–4 kn (1–2 m/s). The position of the EM-sensor was determined from triangulation using the ship’s differential GPS coordinates, tow cable length and water depths. EM data were measured at salt diapir Berta along 11 parallel profile lines with 50 m line spacing, covering an area of 2,300 600 m. Comparison of the CTD depth-profile of the bottom-towed sled with echosounder bathymetry allows to assess the position accuracy of EM soundings. Error propagation of DGPS-, layback-, and AHRS-uncertainty results in sensor positioning with about 5 m accuracy.

The central loop EM method coevally quantifies electric and magnetic properties in the topmost 1–2 m of the sediment by measuring the EM response at seven frequencies (range: 75–10 kHz) with stable sensor elevation of 25 cm (pitch varies between $\sim 0.5^\circ$ and 1°). A half-space inversion method (Müller et al., 2012) was used to convert calibrated raw-data into appropriate SI units of apparent electric conductivity and magnetic susceptibility (the term apparent is used to specify that this value is derived from EM data modeling and no vertical layering is considered). The apparent conductivity of the highest (10 kHz) frequency was despiked to remove local high-amplitude anomalies of metallic objects in the subsurface and median filtered (25 samples per second raw data, 2 s median). Data were interpolated on a regular grid of 10 m cell size using inverse distance gridding (100 m search radius). A directional cosine and a 100 m low pass filter were applied to remove small line-to-line errors and noise.

Gas saturation is often calculated from EM conductivities using Archie’s empirical porosity-resistivity relation (Archie, 1942) for a three-phase porous system of sediment grains, pore-fluid and resistive hydrocarbons such as gas or gas-hydrate (e.g., Schwalenberg et al., 2020):

$$\sigma_g = a \sigma_w \phi^m (1 - S_g)^n, \quad (1)$$

where σ_g is the electric bulk conductivity of the sediment section derived by inversion from EM data, σ_w the conductivity of the pore fluid (usually close to bottom water conductivity measured by the CTD probe), ϕ the sediment porosity and S_g the gas saturation of the pore space. Equation (1) contains empirical constants that are usually determined from physical properties measured in boreholes and on sediment samples, where a describes the tortuosity, m the cementation factor and n the saturation exponent. The latter varies from 1.8 to 4.0 but is often found close to 2.0 (e.g., Schwalenberg et al., 2017). Assuming that the lithology does not change between gas-charged and gas-free sediment sections, Eq. (1) simplifies to:

$$S_g = 1 - \left[\sigma_g / \sigma_0 \right]^{\frac{1}{n}}, \quad (2)$$

where σ_0 is the background conductivity of the pore water saturated sediment and σ_g the bulk conductivity of the gas-charged sediment section (both derived by inversion from EM data). Assuming the widely used gas saturation parameter $n = 2.0$ one can estimate the gas-saturation from electric conductivity anomalies without actual porosity determination, although local sediment compaction or dilution is omitted.

4.2.3. Water sampling

The hydro-geochemistry (e.g., temperature, oxygen saturation, fluorescence, and transmission) was analyzed and samples were taken using a CTD SBE911plus and carousel water sampler SBE32 equipped with additional sensors including oxygen sensors (SBE43), fluorometer (Wetlabs, EcoFLR), transmissiometer (Webtabs CStar, 25 cm). Bottom waters were sampled with a Mini-Multicorer (MIC). Samples from the water sampler were taken immediately and bubble free after retrieval using a silicon tube. Samples were directly transferred into 118 ml glass bottles and were acidified with 2 ml 37% HCl. The bottles were sealed with a Teflon coated butyl rubber seal and were closed with aluminum crimp caps. Dissolved gas concentrations were determined applying a headspace equilibration technique described in detail by Schloemer et al. (2018). 25 ml of the water samples were replaced by laboratory grade Helium (5.9) and the samples equilibrated to ambient temperature varying from 23 to 28C (since the laboratory was not air-conditioned) for at least 2 h on a laboratory shaker. After equilibration, the total headspace pressure was measured using a pressure transducer (range 0 to 160, 0.8 kPa accuracy). For gas chromatography analysis of methane and higher hydrocarbons up to i/n-butane in the headspace a Shimadzu 14B gas chromatograph with splitless injection was used and 1 ml of the equilibrated gas was injected with a gas-tight syringe. Compounds were separated on a 3 m packed column (1/8" Porapak Q) using nitrogen as carrier gas and detected on a flame ionization detector. Methane was calibrated with a 10 ppm standard air (Linde Minican) and laboratory air diluted with helium down to 0.09 ppm CH₄. The concentrations of the dissolved methane, and if present of higher hydrocarbons, were calculated using the partial pressure, derived from fractional concentration and total headspace pressure, temperature of the sample, volume of headspace gas (25 ml) and remaining water (93 ml) applying the Henry's Law-constant of methane. A correction for the salting-out effect was applied using a total salinity of 0.59 mol/L and the Setchenow constant for the analyzed components. The relative error of the GC analysis is around +/- 3% and for the total analyses ~ +/- 10%.

4. Seafloor methane seepage related to salt diapirism in the northwestern part of the German North Sea

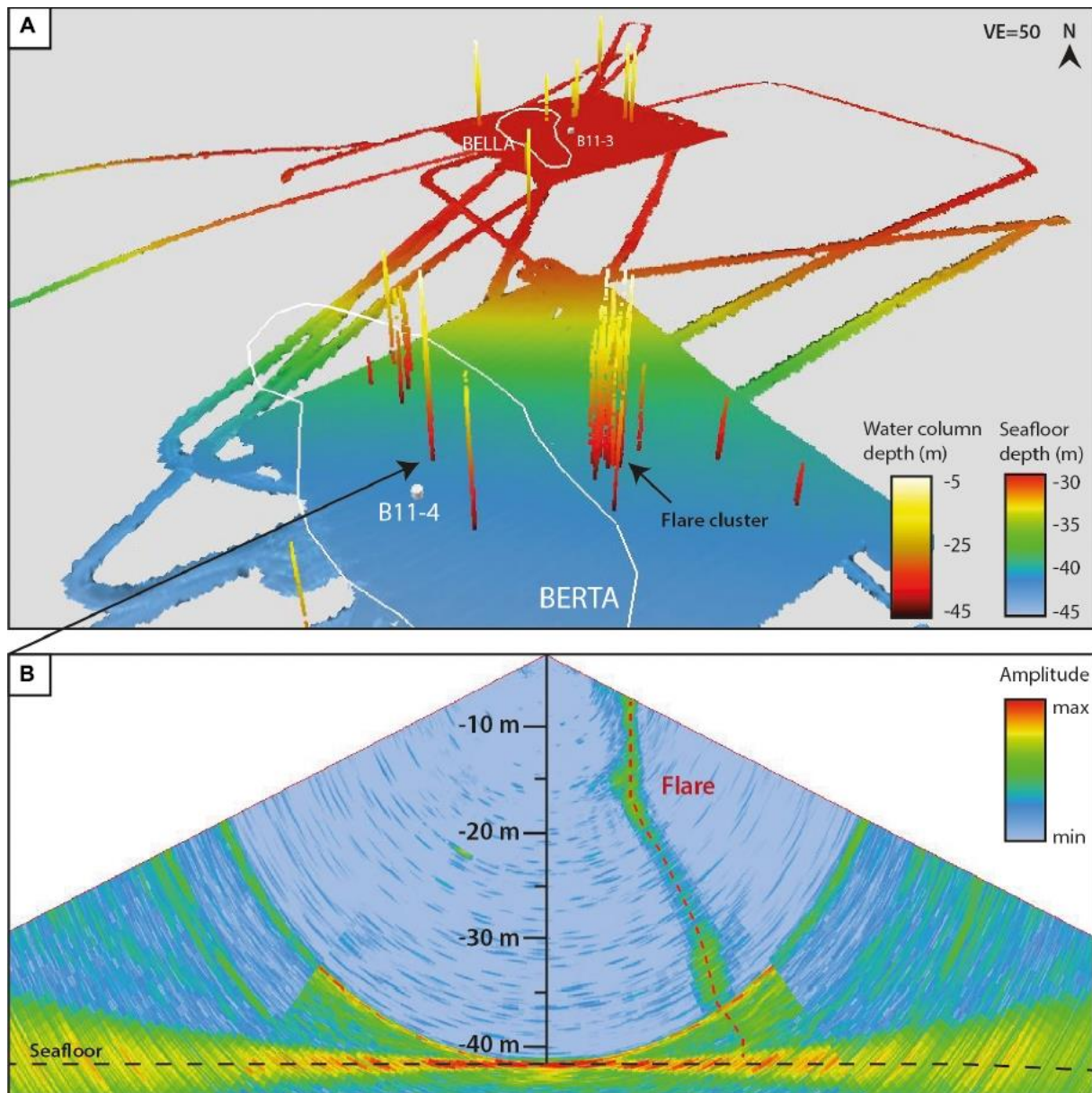


Fig. 24 (A) Flares extracted from the water column data imaged with the bathymetric data, recorded by ship-based multibeam echosounder Kongsberg EM710 during R/V Heincke cruise HE537. White outline: subsurface salt diapirs (Arfai et al. (2014), white dots: abandoned well sites (from Lower Saxony's borehole database: www.lbeg.niedersachsen.de). (B) Swath image of the water column data illustrating a flare detected above salt diapir Berta. The flare represents the pathway of gas bubbles released in 42 m water depth through almost the entire water column.

4.2.4. Methane sensor deployment

The METS from the company Franatech was mounted at a frame (together with CTD, video cameras, forward looking sonar, altimeter, and USBL transponder), which was towed 0.5–2 m above the sea floor at tow speeds of only 0.5–1 knots. The detector is a semiconductor, which is in contact with a gas-filled chamber that is separated from the surrounding water by a sintered disk supporting a gas-permeable membrane. This allows for the separation of dissolved gases from the water where the gas flow is driven by diffusion following Fick's Law. To support a

constant flow of water at the outside of the membrane, a Seabird 5M pump is used. The listed measuring range of the METS is 1–500 nM, which covers methane maxima as well as open ocean background values. The reaction time of the sensor is limited by the diffusion through the membrane. Accuracy and precision of calculated concentrations are further dependent on the response time of the temperature sensor (Pt100), listed with $T_{90} = 1–30$ min as the response of a semiconductor exposed to a target gas is highly temperature sensitive. Since the frame was towed in a nearly horizontal direction, temperatures were comparably stable and an equilibrium reached shortly after descending the frame. The sensor was calibrated by Franatech just before the HE537 cruise. Excluding the temperature dependency, the measured conductivity has a linear relationship with gas concentration. The precision of a Pt100 sensor is commonly ± 0.05 °C, which induces an error of 5 nM at temperatures between 9.0 and 9.8 °C as measured in the bottom water of the working area in bottom depths of 40–44 m.

4.3. Results and discussion

4.3.1. Gas flare occurrence in the “Entenschnabel”-area

Gas emissions were detected and identified as flares in water column echograms of the MBES. Due to the limited coverage of the swath for water column observations, the total area covered for flare imaging was roughly 65 km². In total, 315 water column anomalies were recorded in the “Entenschnabel,” in the northwestern part of the German North Sea (Supplementary Table 1). Flare observations were classified according to their appearance being certainly caused by gas bubble emissions or having an uncertainty of being misinterpreted and caused by schools of fish, which may have a similar appearance in the echogram as a flare. Relatively weak appearing anomalies or anomalies with anomalous shapes (deviant from a continuous linear feature) were therefore classified as uncertain. This uncertainty increases during bad weather conditions causing enhanced noise in the echogram or when gas emissions occur in pulses of bubble release that show up as single anomalies within the water column instead of continuous linear flares that are connected to the seafloor. Consequently, 210 flares were classified as certain flare observations, whereas 105 anomalies appeared too weak or unclear for being undoubtedly interpreted to be caused by gas bubbles. As some areas were studied multiple times, flare observations were partly repeated and flare numbers have been corrected for probable double counting. The numbers reduce to 269 detected water column anomalies of which 166 were classified as certain flare observations and 103 uncertain anomalies. Although double detection during different survey times suggests that most flares may be spatially and temporally stable, about 50 certain flares (30%) that were passed more than once were non-recurring. Natural gas emissions have often been observed to be highly transient in a variety of time scales in both the marine and freshwater settings (e.g., Tryon et al., 1999; Boles et al., 2001; Torres et al., 2002; Varadharajan and Hemond, 2012; Kannberg et al., 2013; Römer et al., 2016). It was argued that the variability of methane fluxes might be controlled by fluid flow rates mediated by microbial processes or physical changes in bottom pressure by, e.g., tides, bottom water currents, storms, swell, or earthquakes (Fechner-Levy and Hemond, 1996; Leifer and Boles, 2005; Scandella et al., 2011). Long-term monitoring or repeated observations would allow for evaluation of the

4. Seafloor methane seepage related to salt diapirism in the northwestern part of the German North Sea

variability of gas emissions and provide evidence for the controlling mechanisms in our study area.

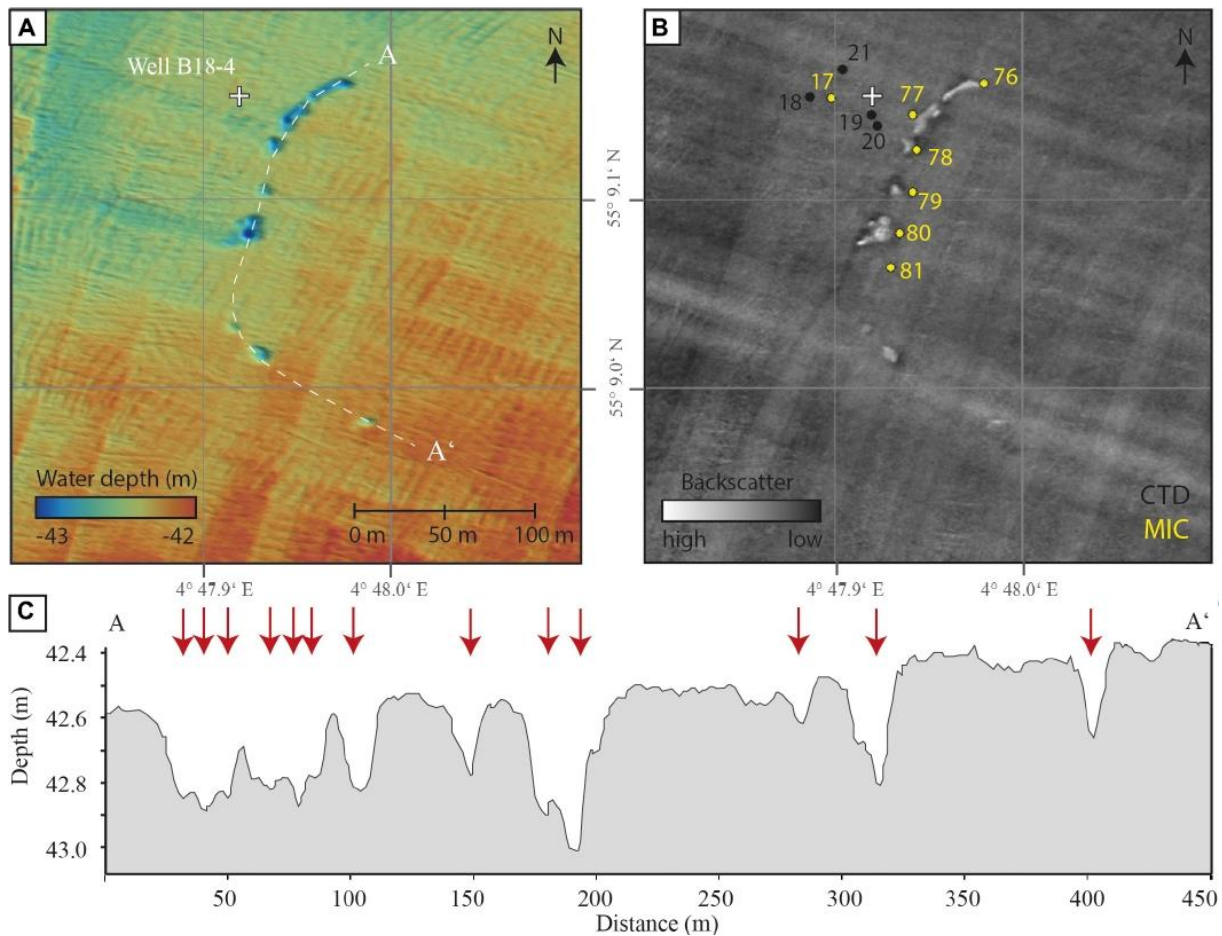


Fig. 25 (A) Bathymetric map of the area at salt diapir Britta, where several depressions were detected. Grid cell size is 2 m. Note: linear features in cm-scale vertically are artifacts. (B) The backscatter map shows that depressions are characterized by high backscatter signals (white patches). The area around well B18-4 and the depressions have been sampled for water (CTD casts) and bottom water (MIC stations) with station numbers (Supplementary Table 2). (C) Bathymetric profile crossing the depressions (marked by red arrows) from A to A' (A), indicating their sizes, depths, and shapes.

Flare height determination is generally limited by the swath geometry, and the upper parts of most flares detected in this study are cut off in about 5–15 m below surface. Flares were detected in heights from less than 10 m and ending within the water column (as seen in Fig. 24A) to more than 30 m to shallow water depths (e.g., the flare shown in Fig. 24B would have probably reached the surface, if a full view would allow imaging the upper parts). Flares were detected at seafloor depths of 31 to 48 m. Bubbles released in such shallow depths are expected to reach the surface and contain some fraction of their initial methane content when reaching the sea surface, where the bubbles burst and directly contribute to the atmospheric methane inventory (Leifer and Patro, 2002). This has been measured and visually observed, e.g., at the nearby Dutch Dogger Bank seep area with a water depth of ~ 40 m. In this seep area, flares were observed to reach the surface, and air measurements above some of the seep sites confirmed a

4. Seafloor methane seepage related to salt diapirism in the northwestern part of the German North Sea

transport of methane into the atmosphere (Römer et al., 2017). During the HE537 cruise, measurements of dissolved methane confirmed an oversaturation of methane in surface waters at the Dutch Dogger Bank seep area (see below). Surface water and atmospheric underway measurements reported in earlier studies from Rehder et al. (1998) and Judd (2015) passing through our “Entenschnabel” study area as well as our own measurements also detected elevated methane concentrations in surface waters (as described in section “Dissolved methane in the water column and bottom waters”), which would support the suggestion that the detected flares transport methane from the seafloor to the atmosphere.

Bathymetric mapping of the study area revealed that flare locations are not related to morphological seafloor indications (e.g., mounds, pockmarks, and linear cracks) or seafloor backscatter anomalies (due to, e.g., authigenic carbonate precipitation or colonization) that might be indicative for gas seepage. The seafloor is generally flat, between 30 and 50 m deep and smoothly slopes down from the Schillgrund High in the SE toward the Central Graben and further up at the northern part of the study area NW of the Central Graben. In the area of salt diapir Britta, however, we found several depressions that could have been formed by fluid release. No flares were detected in the Britta area despite several site surveys and station work. Nevertheless, the current lack or inactivity of gas release may not restrict its presence in the past forming such depressions. More than 17 depressions have been detected of which 13 appear in a semi-circular arrangement southeast of well B18–4 (Fig. 25A). Some are partly intercalated, forming linear or composite depressions. Four other depressions were detected in distances between 460 and 980 m southwest and east of the well site (not shown). The depressions are circular to subcircular in shape with dimension of a few meters to maximal 25 m cross sections. Their shape is funnel-like with slopes of 1–5° and depths of up to ~50 cm (Fig. 25C).

Backscatter mapping additionally revealed elevated backscatter patches related to the depressions (Fig. 25B). Although most prominent hydrocarbon seeps have surface relief manifestations such as pockmarks (Judd and Hovland, 2007), other examples of seep areas lacking morphological features were described from the North Sea, including the Dutch Dogger Bank seep area (Schroot et al., 2005; Römer et al., 2017) and the “Heincke” seep area [Gullfaks in the Norwegian North Sea, Hovland (2007)]. It has been speculated that coarse-grained material of gravel/sand beach deposits might prevent pockmark formation (Hovland, 2007). Known natural seep sites in the North Sea correlated with pockmark formation include the large pockmarks in the Witch Ground Basin (Judd et al., 1994; Böttner et al., 2019), complex pockmarks in the Nyegga area (Hovland et al., 2005), the temporally dynamic Helgoland Reef pockmark field (Krämer et al., 2017), and small depressions at the Tommeliten seep area (Schneider Von Deimling et al., 2011). In addition, artificially created blowout events formed large depressions in the North Sea. Examples are the well site 22/4b, which displays a 50 m wide and 20 m deep depression formed in 1990 (Schneider Von Deimling et al., 2007; Leifer and Judd, 2015), and the so-called “Figge-Maar” with a depression of 400 m width and an initial depth of 30 m depth after a carbon dioxide eruption in 1964 (Thatje et al., 1999; see location in Fig. 23A). The depressions detected in this study at salt diapir Britta are located in distances of 30 to 750 m of the abandoned well site B18–4, which does not exclude nor prove a generic relationship.

4. Seafloor methane seepage related to salt diapirism in the northwestern part of the German North Sea

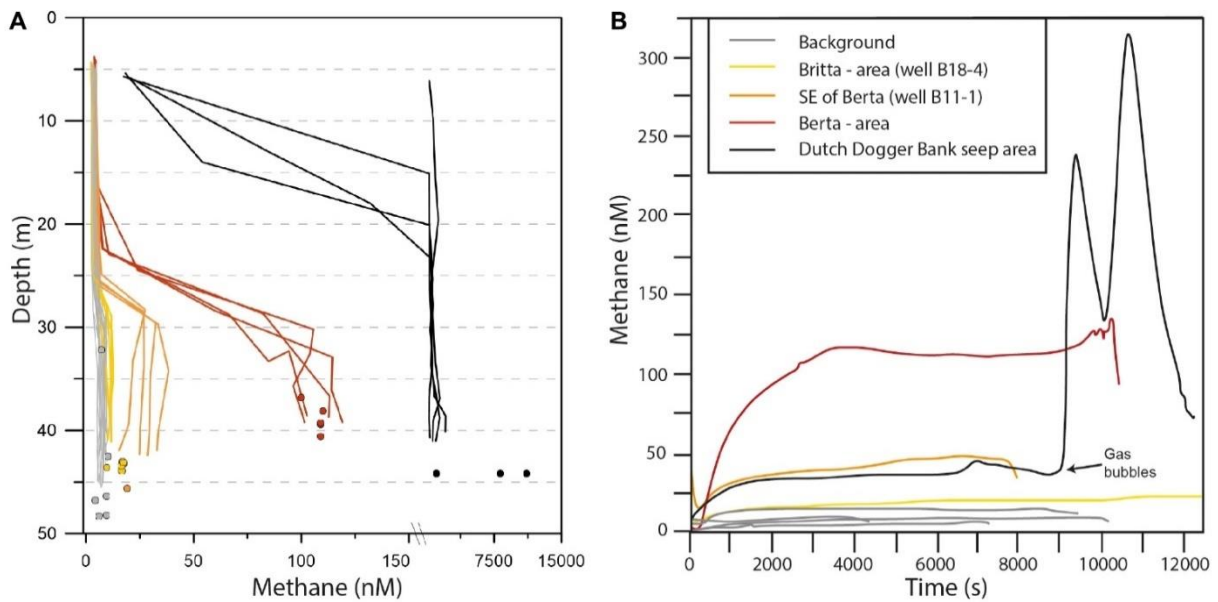


Fig. 26 (A) Profiles of methane in the water column of the “Entenschnabel” study area and for comparison of the Dutch Dogger Bank seep area (Please note break in the x-axis to address the different ranges of methane concentrations) as well as of concentrations in bottom waters (dots, MIC water samples) close to water column stations. Light gray samples represent background values at the reference site at salt diapir Birgit and four abandoned wells (wells B15–1, B15–2, B15–3, and B11–3). (B) Methane concentrations measured with the METS during towed deployments in seven areas in the “Entenschnabel” and the Dutch Dogger Bank seep area while passing a known flare cluster for comparison.

4.3.2. Dissolved methane in the water column and bottom waters

Dissolved methane concentrations measured in bottom waters (sampled with MIC) and waters below the pycnocline (sampled with CTD) at the salt diapir Berta (close to well B11–4) were 10 to 13 times higher (max. 120 nM) than background values of about 9 nM detected in the “Entenschnabel” (Fig. 26A and Supplementary Table 2). These elevated methane concentrations extended approximately 500 m to the east and west of the well site and did not increase toward the well. Slightly increased methane values of 20–30 nM also existed southeast of Berta close to abandoned well site B11–1. Well B11–1 is unlikely the origin of methane seepage, since no flares were detected near the site by hydroacoustics (coverage: 1,000 x 300 m), and we consider that diffuse seafloor venting would have led to a different methane profile with the highest amounts in the bottom water layer. However, the measured methane profiles showed slightly decreasing values with increasing depth and lower concentrations in the bottom water (Figure 4A and Supplementary Table 2). Since the most distant CTD cast from B11–1 exhibited highest methane concentrations in the deep water layer, and area B11–1 is 3 km apart from salt diapir Berta, a horizontal input from, e.g., the Berta seep area is feasible. Data extracted from the Operational Circulation Model of the BSH (Dick et al., 2001) show that a transport of water masses originating from the Berta area is feasible due the strong tidal currents. At the time of sampling, the current had only just switched directions after a period (5 h) of steady easterly currents (up to 24 cm/s). Compared to the Berta area the methane concentrations at the nearby Dutch Dogger Bank seep area were much higher and more variable. Here, values in the deepest water samples reached up to 2,085 nM (Fig. 26A), which is 200 times the background value

4. Seafloor methane seepage related to salt diapirism in the northwestern part of the German North Sea

and compares well with the published concentrations of up to 1,628 nM by Mau et al. (2015). Bottom water samples, taken from MIC sampling, reached values of up to 11.14 nM. This compares to 113 nM measured at the Berta seep area (Fig. 26A).

Tab. 2 Mean values of dissolved methane in the studied areas and in the water column zones.

Area Name (well site)	Above pycnocline			Surface waters			Bottom waters		
	$\bar{\text{O}} \text{ CH}_4$ (nM)	1 σ (nM)	<i>n</i>	$\bar{\text{O}} \text{ CH}_4$ (nM)	1 σ (nM)	<i>n</i>	$\bar{\text{O}} \text{ CH}_4$ (nM)	1 σ (nM)	<i>n</i>
Bella (B11-3)	4.2	0.5	12	4.1	0.5	4	7.0	na	2
Berta (B11-4)	5.0	1.1	18	4.5	0.5	5	106.4	4.9	10
SE of Berta (B11-1)	5.1	0.9	16	4.4	0.6	4	17.8	na	2
Belinda (B15-1)	2.6	0.2	19	2.7	0.3	4	4.2	na	2
Belinda (B15-3)	3.3	0.5	16	3.7	0.3	4	6.1	na	2
Britta	2.6	0.1	8	2.7	0.1	2	10.2	na	2
Britta (B18-4)	2.8	0.2	10	2.6	0.1	2	15.2	3.4	8
Birgit	4.0	0.5	16	3.8	0.4	4	9.5	na	3
E of Belinda (B15-2)	3.5	0.3	12	3.6	0.1	4	8.5	na	2
Dutch Dogger Bank seep area	349.7	362.7	16	79.8	106.5	4	3491.9	4149.2	7

"Above pycnocline" combines all concentrations above the thermocline, *"surface"* between 3 and 6 m and *"bottom"* the bottom water samples from MIC deployments and the deepest sample from CTD casts (for data see **Supplementary Table 2**).

The water column methane profiles generally decrease quickly in the CTD casts toward the surface but methane concentrations vary between areas. Tab. 2 shows mean values for each studied area and zones of the water column (above pycnocline, surface and bottom waters). By far the highest surface water concentrations of methane are restricted to the Dutch Dogger Bank. Here, methane concentrations at 3–6 m water depth were about 18 nM in three CTD casts (Fig. 26A) but reached up to 263 nM at one station, clearly indicating gas emissions reaching surface waters. No shallower samples were taken due to rough weather conditions. Based on water temperature, salinity and the current atmospheric methane concentration of 1,877 ppb (Nov 2019; https://esrl.noaa.gov/gmd/ccgg/trends_ch4/; last visited 27.03.2020), methane concentrations in equilibrium with the overlaying air (air saturated sea water; ASSW) are in the range of 2.6 nM calculated after Wiesenberg and Guinasso (1979). In the southern "Entenschnabel" area with water sampling above salt diapirs Britta and Belinda, methane surface values were only very slightly oversaturated (Supplementary Table 1). The observed oversaturation increased slightly toward this northwestern part of the working area, reaching up to 5 nM at locations Berta and Bella (Supplementary Figure 2), representing a small source of methane to the atmosphere. This is in agreement with the increased numbers of gas flares found here compared to the southern working area and measurements by Rehder et al. (1999) of slightly elevated surface concentrations in the region.

4. Seafloor methane seepage related to salt diapirism in the northwestern part of the German North Sea

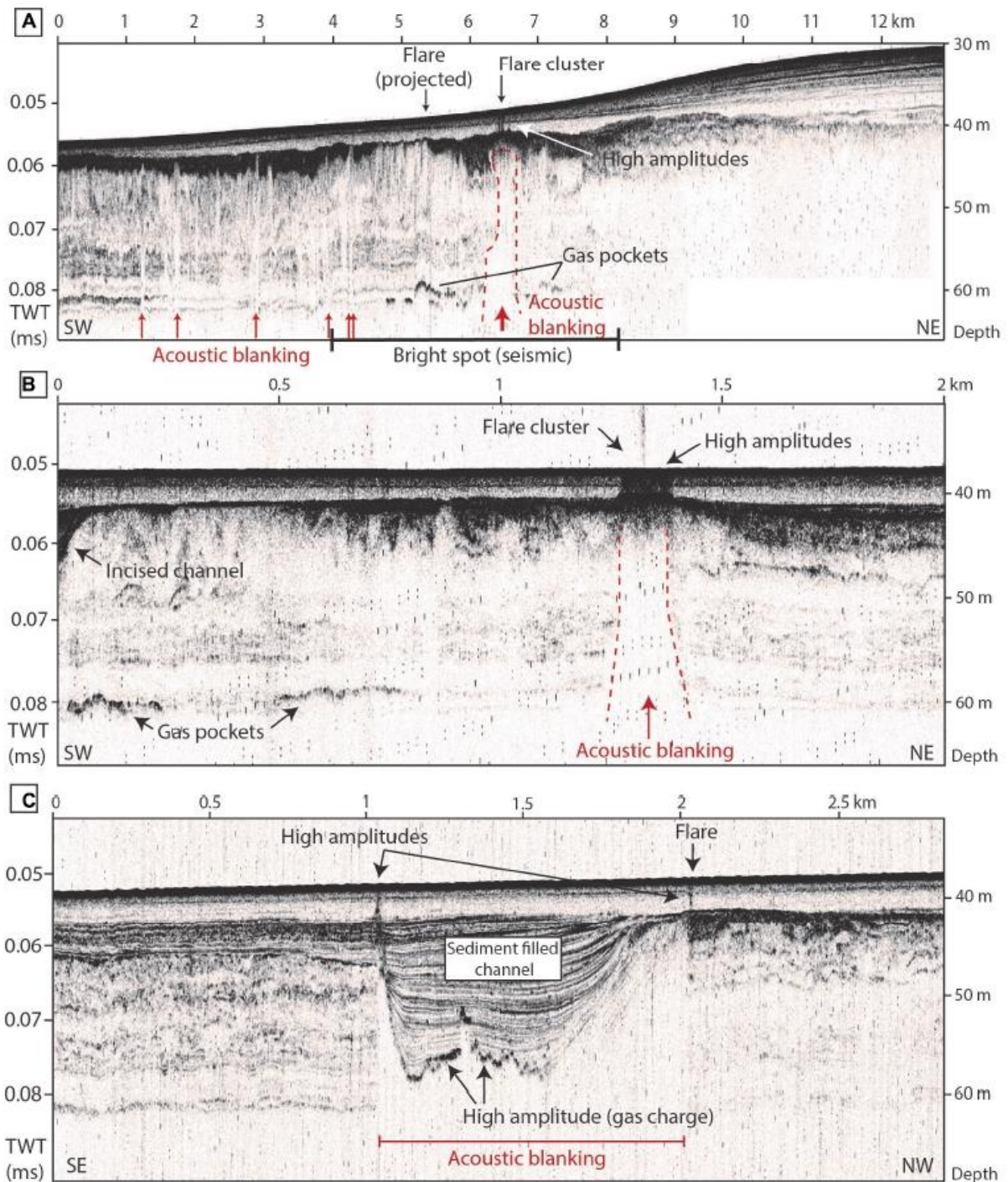


Fig. 27 Subbottom profiles recorded with the sediment echosounder Innomar SES-2000 during R/V Heincke cruise HE537 in the area close to salt diapir Berta. See Figure 6B for locations. Depth conversion has been estimated using a sound velocity of 1,500 m/s. (A) Profile covering the bright spot mapped in the deeper subsurface above salt diapir Berta. Acoustic blanking forming chimneys are indicated with red arrows, with the widest chimney below the flare cluster detected in the water column (red dashed line marks the outline). (B) Detailed profile focusing on the chimney (red dashed line), in which the high amplitudes between acoustic blanking and water column flare cluster becomes visible. (C) Detailed profile showing a sediment-filled channel with columnar acoustic blanking and high amplitude reflectors below, indicating increased gas concentrations migrating along the flanks of the channel up to the seafloor.

Ethane, the only higher hydrocarbon detected, was found in trace amounts at two sites, one of them the Dutch Dogger Bank site. The second site is located above the Britta salt diapir in the

4. Seafloor methane seepage related to salt diapirism in the northwestern part of the German North Sea

southern part of the “Entenschnabel.” Here, bottom water samples collected from all six MIC cores contained traces of ethane. The MIC sample taken close to well site B18–4 was devoid of ethane and showed methane concentrations close to the background (9.8 nM). The MICs with ethane originated from a series of depressions occurring in a linear array near the well site B18–4, extending further to the south (as described above, see Fig. 25B). In addition, methane values of bottom and deep water samples were slightly elevated with concentrations of 18 nM and 12 nM, respectively. Flares were absent in the region of these depressions, and considering the very low absolute concentrations, we assume the depressions to be pockmarks characterized by diffuse fluid transport or episodically occurring gas emissions. Trace amounts of ethane are common in biogenic gases in different environments and usually methane/ethane ratios in such samples are high ($\gg 100$). We assume that the low observed methane/ethane ratios found in the depressions at Britta (~40) are the result of the preferential oxidation of methane compared to ethane occurring during a slow diffusive ascend of the fluid. Equally low methane/ethane ratios were assigned to partly oxidized biogenic gases in ground waters based on enrichments in ^{13}C isotopes of methane (Schloemer et al., 2018). Propane, which would be an indicator for a migrated deeper sourced thermal (natural) gas, was not found, neither in the samples from the depressions in the Britta area nor in bottom waters at the Dogger Bank seep site.

The METS data are in good agreement with discrete water sampling from vertical CTD casts. Like the CTD casts, the METS profiles do not indicate any seepage of methane at salt diapir Belinda (well sites B15–3 and B15–2) and salt diapir Bella (well site B11–3; light gray lines in Fig. 26B). At salt diapir Britta the deployments crossing the line of pockmarks detected slightly elevated methane concentrations of up to 20 nM in relatively flat time-series (Fig. 26B) confirming a small methane flux into the water column. The pattern is similar close to well B11–1 with elevated concentrations of up to 40 nM. At Berta, where numerous gas flares were observed, the METS detected methane concentrations of ~120 nM throughout most of the deployment (Fig. 26B), indicating a strong oversaturation with methane over a wider area despite no active seepage having been crossed. The METS time series at Berta is relatively flat with no spikes. This is unlike a profile measured at the Dutch Dogger Bank seep area, where two clear peaks occurred during the crossing of a prominent flare cluster (Fig. 26B). The METS data not only confirm the results from the discrete water sampling but show, that methane oversaturation extend beyond the small grid covered by the CTD stations.

4. Seafloor methane seepage related to salt diapirism in the northwestern part of the German North Sea

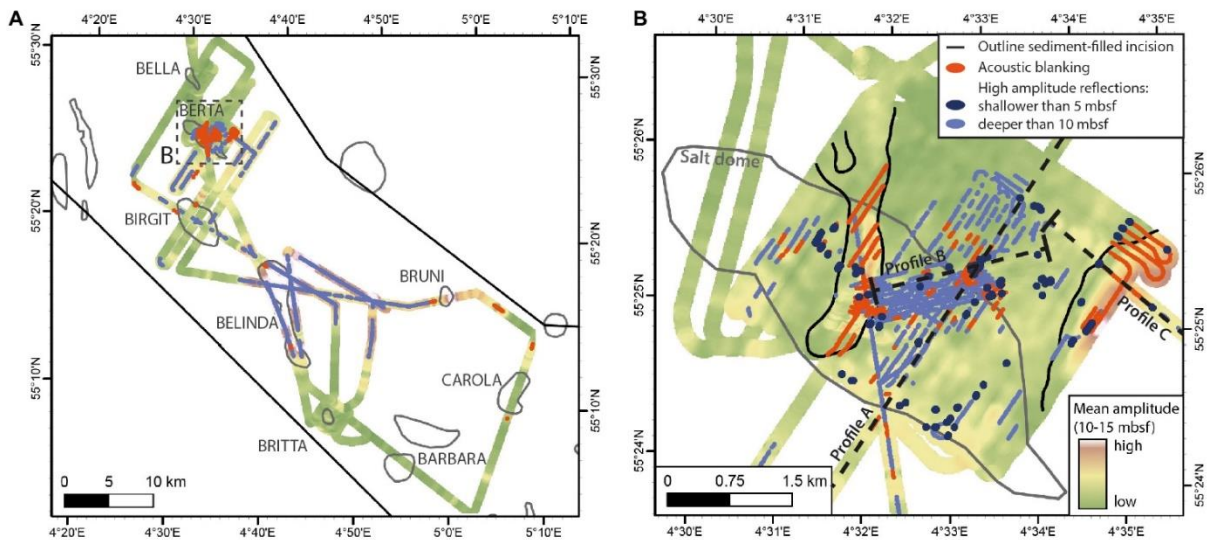


Fig. 28 Subbottom analysis maps showing mean amplitude values between 10 and 15 mbsf throughout the entire dataset acquired, the locations of high-amplitude reflections (blue) and acoustic blanking (red). (A) Overview map (interpolated raster surface from track points using kriging, grid cell size is 50 m and maximum point distance is 500 m), (B) detailed map of the area mapped at salt diapir Berta (interpolated raster surface from track points using kriging, grid cell size is 10 m and maximum point distance is 100 m).

4.3.3. Subsurface gas indications

4.3.3.1. Sediment echosounder profiling

Due to increased impedance contrasts resulting from enriched free gas content in the pore-space, gas in the subsurface becomes visible in sediment echosounder profiles as enhanced reflectors with high amplitudes and acoustic signal blanking appearing as vertical zones lacking any reflectors underneath these high amplitude reflections. Subsurface gas indications such as acoustic blanking and high amplitude reflections interpreted as gas pockets have been widely found and described in the Dutch North Sea sector including the nearby Dutch Dogger Bank seep area (Schroot et al., 2005; Römer et al., 2017). Subsurface acoustic blanking in our study area has been observed as (1) narrow vertical chimneys (examples shown with red arrows in Fig. 27A,B), and (2) below subsurface seafloor incisions filled by sediments (Fig. 27C). Chimneys were documented to reach within 3m of the seafloor and are commonly few tens of meters wide. The most prominent chimney has been detected below the flare cluster at salt diapir Berta with a width of about 200 to 300 m (Fig. 27A,B). Acoustic blanking below sediment-filled channels or basins becomes visible below the incised structure and follows the flanks up to the shallow subsurface (Fig. 27C). This type of acoustic blanking is generally more extensive than the narrow chimneys. Acoustic blanking interpreted to result from increased free gas content were described also in relation to Pleistocene glacial valley-fills in the Netherlands EEZ (Schroot and Schüttenhelm, 2003; Schroot et al., 2005). In several sediment-filled incisions, blanking also pierces through the bottom of the channel or basin and is accompanied by high amplitude reflections at their upper limit (Fig. 27C), where the gas appears to be hindered from further upward migration and accumulated. High amplitude reflections also occur in areas close to acoustic blanking in about 20m depth below seafloor and were interpreted to represent gas

4. Seafloor methane seepage related to salt diapirism in the northwestern part of the German North Sea

pockets (Fig. 27A,B). Another type of high amplitude reflections was frequently observed close to the seafloor connecting gas chimneys with flare observations in the water column (Fig. 27A–C), appearing as narrow vertical lineations.

Gas indications in shallow sediments are most concentrated at but not restricted to the area at salt diapir Berta. The mean amplitude calculated in a sediment depth interval between 10 and 15 meters below seafloor (mbsf) illustrates differences in the “Entenschnabel” (Fig. 28A). Whereas the northernmost part of the study area (around salt diapirs Bella and Berta) as well as the southern part (around salt diapirs Britta, Barbara, and Carola) shows lowest mean amplitudes, the central part shows overall higher values indicating better sound penetration. Besides being influenced by higher gas concentrations, such differences could be also related to sedimentological differences of the deposits. However, in the central part, areas of highest mean amplitudes are related to the presence of high amplitude reflections in sediments deeper than 10 mbsf, possibly illustrating the occurrence of free gas, which rather accumulated in the sub-surface and not percolated throughout the shallowest deposits. Mapping of high amplitude reflections further indicates that their occurrence is restricted to the northern and central parts (blue lines in Fig. 28A), suggesting that these areas are influenced by higher gas concentrations. Furthermore, focused acoustic blanking zones were mapped revealing several occurrences apart from salt diapir Berta (red areas in Fig. 28A). With few exceptions, acoustic blanking was observed close to the outlines of salt diapirs, e.g., of Birgit, Belinda, Bruni, and Carola. However, the highest abundance of acoustic blanking was detected in the area of salt diapir Berta (Fig. 28B). In part, these were related to two sediment-filled incisions (black outlines in Fig. 28B), which also show up as elevated mean amplitudes when deeper incised than 10 mbsf. High amplitude reflections and acoustic blanking not related to the sediment-filled incisions were concentrated in the northeastern part of the salt diapir.

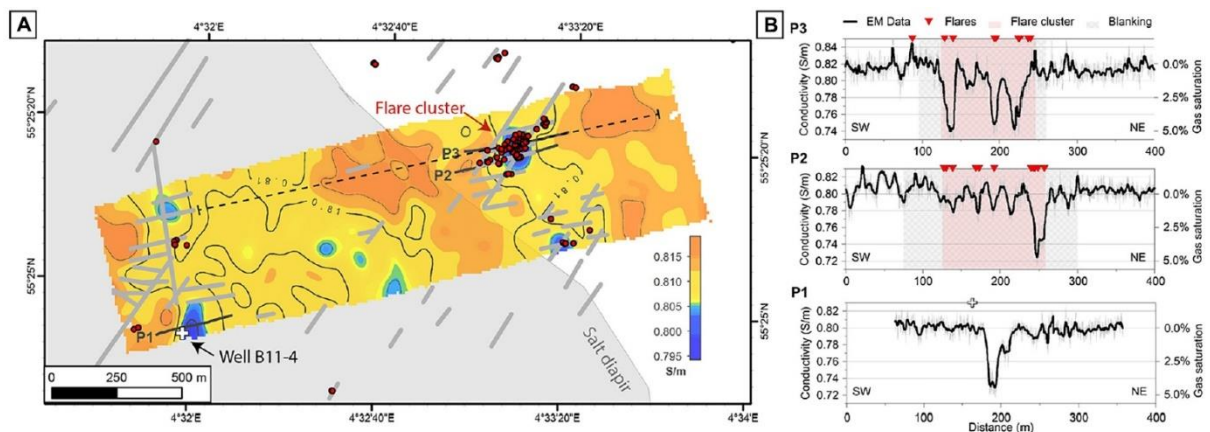


Fig. 29 Sediment electric conductivity data of the benthic EM Profiler. (A) Gridded 10 kHz EM conductivity data with flare locations (red dots), acoustic blanking from subbottom data (gray lines), and transect of subbottom profile B Fig. 27B; dashed line). (B) Selected profiles crossing conductivity minima (indicated by black lines in a; gray: raw data, black: median filtered) with projected flare locations. Background colors indicate areas of high flare density and acoustic blanking. Gas saturation estimates are based on the conductivity contrast (Eq. 1). A white cross marks the location of borehole B11-4 in both figures.

4.3.3.2. Electromagnetic seabed mapping

Free gas is considered to reduce the electric conductivity of the subsurface by replacing conductive pore-fluid with resistive gas and blocking of conduction paths through the sediment (Evans et al., 1999). EM methods are therefore used to derive volume estimates of free gas in the sediment (Cheesman et al., 1993; Schwalenberg et al., 2017). However, the sediment electric conductivity is controlled by other factors as well, such as pore-water salinity and temperature, lithology, clay content, grain-size, and sorting (e.g., Winsauer et al., 1952; Jackson et al., 1978).

The survey area at salt diapir Berta including borehole B11–4 (Fig. 29A) is dominated by fine sands, with higher (11–20%) clay and silt content in the west, and medium to coarse sands in the northeastern section (Laurer et al., 2012). Apparent electric conductivities of the sediments are in the range of 0.711– 0.953 S/m and follow the general sedimentary units with slightly lower values in fine sands in the western part and highest values in coarser sands in the eastern half of the survey area. This trend is interpreted to result from sediment sorting, where porosity is reduced with increasing content of fine particles. The largescale sedimentary units are interrupted by several distinct electric conductivity lows. A prominent low is associated with acoustic blanking visible in subbottom data (see above) below the flare cluster (Fig. 29A and profiles P2 and P3 in Fig. 29B). The profile view (Fig. 29B) depicts several focused conductivity minima, less than 50 m in diameter, which are smoothed by the gridding interpolation. In profile P3, three local minima are observed, where conductivity drops from background values of 0.82 to 0.74 S/m. Neglecting the saturation term in Eq. 1 we can derive a mean porosity for the study area of approx. 40% from the background conductivity outside the anomaly using Archie coefficients $a = 1$ and $m = 1.6$ for medium-fine to coarse sands (e.g., Evans et al., 1999), and a CTD-derived pore water conductivity of 3.7 S/m. According to Eq. 2, the drop in conductivity at the flare cluster relates to a free-gas saturation up to 5% of the pore-space. Similar patterns are observed in profile P2 although less developed and frequent.

Another minimum has been mapped further south that appears to follow a SSE trending structure, which roughly mimics the boundary of the salt diapir. Profile P1 identifies a bimodal conductivity anomaly with a similar drop in amplitude, about 30 m to the east of the location of borehole B11–4. Video transects did not reveal changes (e.g., small-scale morphologies or sediment characteristics) of the seafloor sediments in this region. Due to the absence of acoustic blanking in the sediment echosounder profiles, we do not expect free gas to cause this conductivity low and assume over consolidated or contaminated sediments as a result of the drilling operation that took place in 2001. Note that we made the assumption that the sediment matrix (hence porosity) does not change for gas-charged sediments, thereby the gas saturation is a pure function of the conductivity difference and the empirical saturation exponent n , and hence independent from porosity, pore-water conductivity and grainsize. However, Szpak et al. (2012) and Garcia et al. (2014) even observed higher conductivities with highest volumes of gas within pockmarks which they explain by an increase in porosity and fining of the sediment in consequence of gas migration (and potentially by gas-driven microbial activity). Consequently, even higher free-gas concentrations are required to explain the drop in conductivity below the flare clusters. The impact of gas migration on the sediment fabric may be resolved combining electric

4. Seafloor methane seepage related to salt diapirism in the northwestern part of the German North Sea

conductivity mapping with, e.g., high resolution sediment sampling, magnetic susceptibility mapping, or joint inversion with seismic data (e.g., Müller et al., 2011; Baasch et al., 2017; Attias et al., 2020), which is out of scope in this publication.

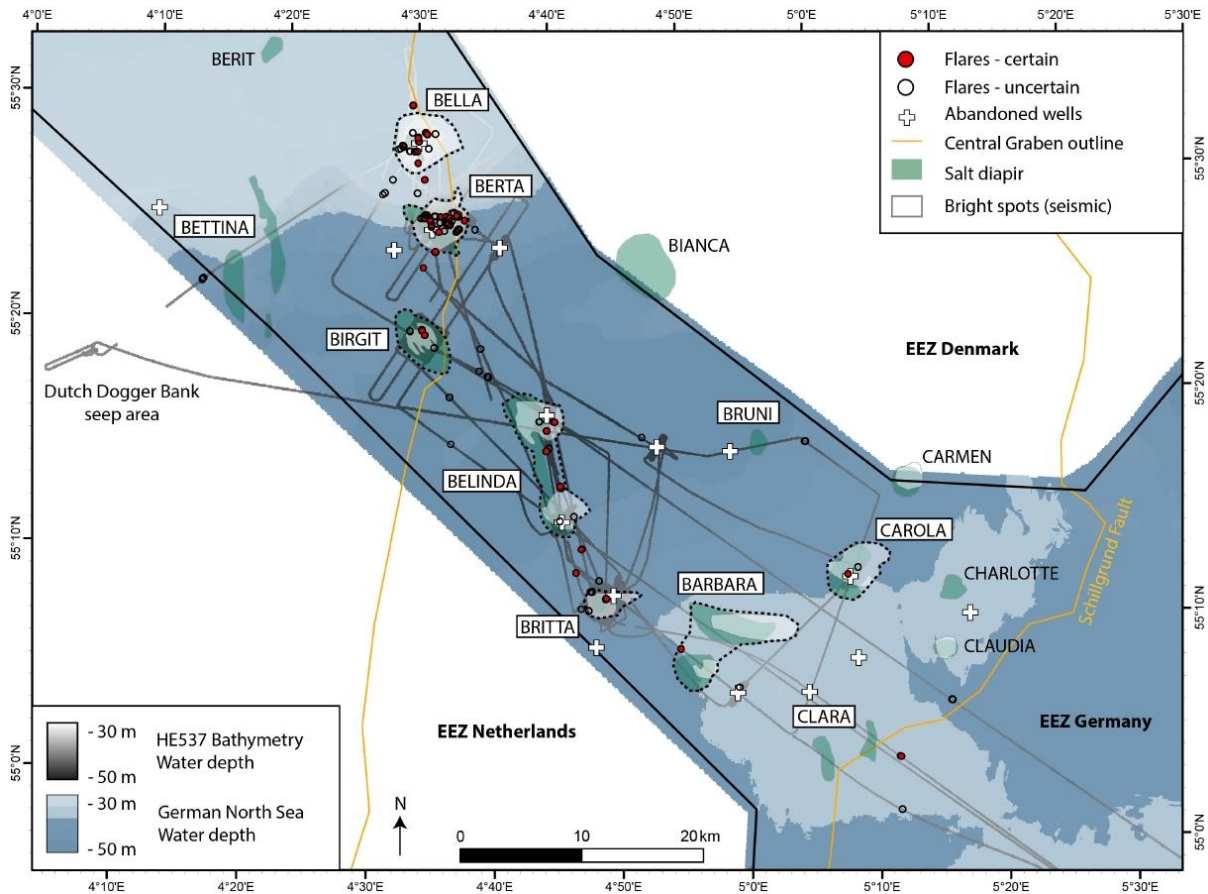


Fig. 30 Map compiling flare detections in relation to subsurface salt diapirs and bright spots as well as abandoned wells. Almost 90% of all detected flares were found in the vicinity of subsurface salt diapir structures [depicted from Arfai et al. (2014)]. Note that salt diapir and bright spot areas are slightly transparent to illustrate their extents were overlapping each other. Bathymetry downloaded from www.gpdn.de.

4.3.4. Gas distribution and the shallow gas system in the “Entenschnabel”-area

4.3.4.1. Flare distribution in the study area

The flares detected during R/V Heincke cruise HE537 were not randomly distributed in the study area. Most flares (149 out of 166 certain flares) were found in the vicinity of subsurface salt diapir structures (Fig. 30 and Tab. 3). Highest abundance of flares were located at or around salt diapir Berta (104 flares) and Bella (19 flares). Five other salt diapirs revealed the presence of 1 to 13 flares. Salt diapirs Clara, Brunni and Bettina did not show any sign of gas bubble seepage. However, they were not mapped with a larger coverage, but passed during transits with partly increased vessel speeds of 5–10 knots, limiting the data quality. In order to account

4. Seafloor methane seepage related to salt diapirism in the northwestern part of the German North Sea

for the different coverage in the study area, the fraction of each defined area that has been mapped for the presence of flares was calculated and related to the number of flare findings (Tab. 3). The results show that the flare abundance at those salt diapirs with only 1 to 13 flares are similar or only very slightly elevated in relation to transits (areas between salt diapirs). However, even when accounting for the coverage, Bella and especially Berta exhibit elevated flare abundances. The relation of gas seepage to salt diapirs is also known from closely located seep areas: the Tommeliten seep area (Hovland and Judd, 1988) and the Dutch Dogger Bank seep area (Schroot et al., 2005). Seismic studies revealed that shallow gas accumulations seem to be concentrated above salt structures, which act as focal structures for migration (Schroot et al., 2005; Müller et al., 2018). Distances of flare findings related to the outlines of subsurface salt diapirs show a clear peak in flare abundance in a distance of 1 to 500 m (Fig. 31A, B). Most flares are actually not located directly above salt diapirs, but just around them. This observation might be interpreted to result from a certain lateral migration of gas along weakening zones or gas migration that is focused along the flanks of the diapir, probably depending on the deformation pattern above the salt diapir. Buoyant gas migrates upward to the seafloor, either along diapir-induced faults or at locations where the gas columns are tall enough that the pressure of the accumulated gas is higher than the capillary entry pressure of the unconsolidated sediments above (Müller et al., 2018). Faults are common structures at the crest of salt diapirs. They form during the growth of salt structures as a result of the deformation of the overburden (Jackson and Hudec, 2017). Shallow gas reservoirs have been detected and imaged as bright spots in about 300 to 800 mbsf (Müller et al., 2018). Distances of flare positions detected during this study were also plotted in relation to bright spot detections revealing a clear relation, with the majority of flares located directly above a bright spot (Fig. 31A, B). Only 21% of all detected flares and 13% of flares classified as certain were found without a bright spot in the subsurface, whereas the maximum distance of a certain flare to the closest bright spot was 1.8 km.

Tab. 3 Spatial analysis of flare findings at different areas including coverage for water column mapping.

Area (name)	Area (km²)	Coverage (km²)	Area covered (%)	Number of certain flares	Number of flares – normalized	Flares per coverage
Bella	20.3	5.4	27	19	0.71	3.52
Berta	17.7	8.4	47	104	2.19	12.38
Birgit	15.5	4.7	30	3	0.10	0.64
Britta	7.3	4.6	63	8	0.13	1.74
Belinda	35.5	5.9	17	13	0.78	2.20
Barbara	36.5	0.9	2	1	0.41	1.11
Carola	16.4	1.4	9	1	0.12	0.71
Transit	1750.8	33.7	2	17	8.83	0.50
Entire study area	1900	65	3	166	48.52	2.55

Flare numbers were normalized accounting for the area covered during HE537. The calculated values for flares per coverage illustrate that areas Bella and Berta are above the average of other areas and the entire study area.

4. Seafloor methane seepage related to salt diapirism in the northwestern part of the German North Sea

It was examined if faults play a role as migration pathways for fluids in the “Entenschnabel” area by passing the Schillgrund Fault four times during transits. This fault is the southeastern boundary of the Central Graben to the Schillgrund High (Fig. 30). Faults and fractures were reported to relate in different ways to fluid flow patterns: acting as seals [i.e., Ligtenberg and Connolly (2003)] or providing temporally efficient migration pathways, as observed, e.g., in the Sea of Marmara (Dupré et al., 2015), the Sea of Okhotsk (Jin et al., 2011), and the Black Sea (Riboulot et al., 2017). The Schillgrund Fault has been shown to provide a pathway for salt diapirism, as salt intrusions south of salt diapirs Clara and Claudia rise up along this fault zone (Arfai et al., 2014). Salt diapirism in the Central Graben area is connected to pre-Zechstein faults (Davison et al., 2000; ten Veen et al., 2012; Duffy et al., 2013; Arfai et al., 2014). Our water column mapping detected flares during three of the four crossings of the Schillgrund Fault zone, however, only two of the four detected flares were classified as certain. Since the two flares were closely located to salt diapir Clara, a relation of the Schillgrund Fault as active fluid migration pathway might be indicated but not proven.

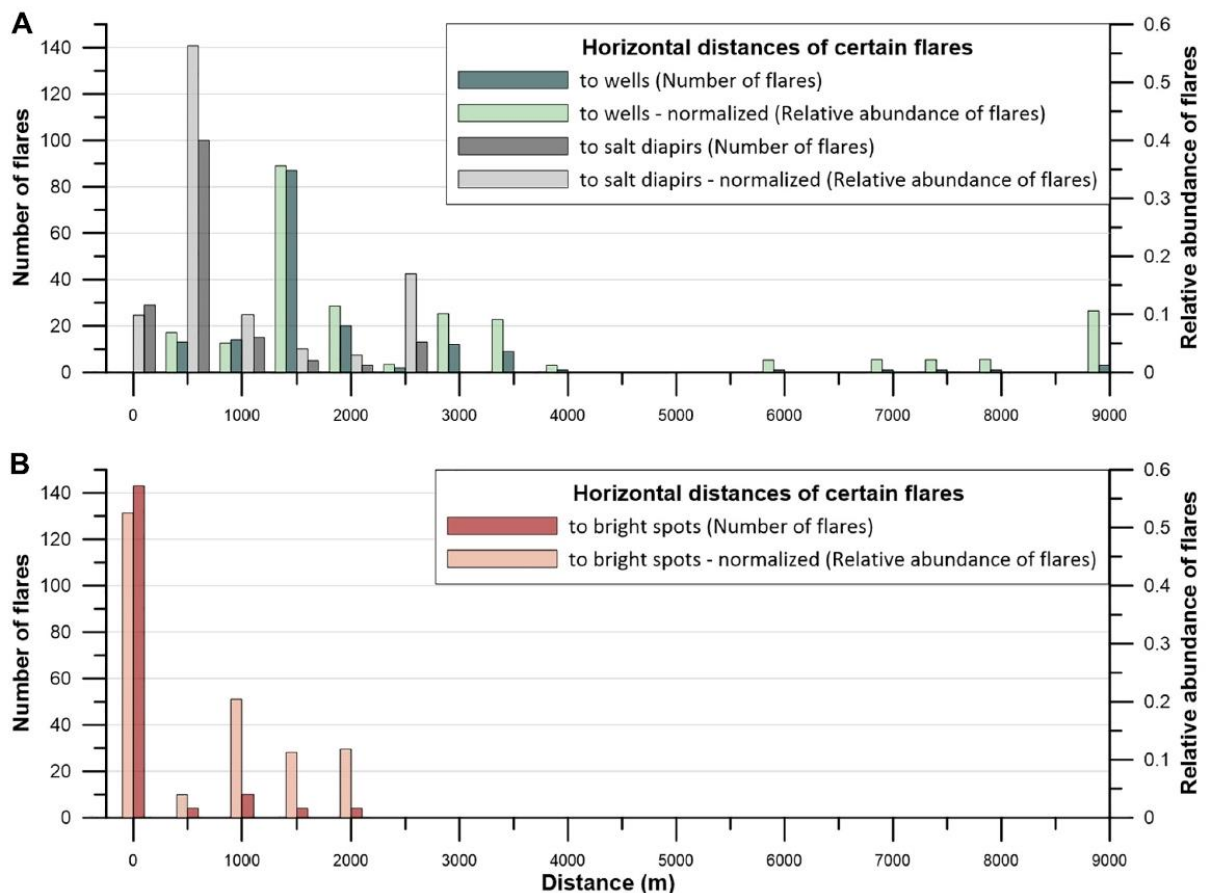


Fig. 31 Histogram plots showing the distances of flares to (A) salt diapirs, abandoned wells sites, and (B) bright spots (seismically identified). Only flares classified as certain were included. The histograms were binned at 500 m intervals, with the first bin = 0 m (flares plot above a salt diapir or bright spot area), second bin >0–500 m, third bin >500–1,000 m, ect. Darker colored bars illustrate the total numbers of flares, whereas the lighter colored bars indicate the relative abundance of flares including a normalization by the ship track coverage. The normalization corrects for the non-uniform mapping strategy in the study area.

4.3.4.2. Potential gas release related to abandoned wells

Near distance analysis of flares to abandoned well sites showed a widespread distribution between 125 and 9,500 m (Fig. 31A). Most flares were found in a distance of 1 to 1.5 km to a well site. When normalizing the distribution with the coverage during cruise HE537, individual flare findings in larger distances get amplified and the resulting distribution did not suggest a positive correlation with distance to abandoned well sites. No flare has been detected while exactly crossing one of the ten well sites surveyed during R/V Heincke cruise HE537 in the German North Sea. The closest distance of a flare to a well site is 125 m and only 13 certain flares were found in a distance of less than 500 m. However, seismic data acquired at a blowout in a Norwegian North Sea hydrocarbon exploration well indicated that gas entered into a shallow tunnel valley complex and migrated horizontally (Landrø et al., 2019), illustrating the complexity of shallow gas migration. Hence, the lack of correlation of flares with abandoned wells does not exclude any relationship particularly in complex geological settings, but we consider this to argue against a direct or indirect well-origin of gas emissions.

Six of ten wells were located in areas underlain by a bright spot, thus could be potential sites for release of shallow gas from the seafloor. Water column mapping revealed that flares were found in the vicinity of these six wells, but no flares were observed close to the four wells that are not related to a bright spot. Water column methane concentrations measured from samples at seven wells only showed clearly elevated concentrations at well B11–4 (located at salt diapir Berta). However, methane concentrations measured 500 m east and west of the well had similar values, pointing to a rather widespread gas release system above the salt diapir that is not focused at the well site. Methane concentrations were slightly above background (9 nM) in the bottom waters in the areas of wells B11–1 and B18–4 (Tab. 2 and Fig. 26), but leakage at the well sites appears unlikely due to the lack of flares and dissolved methane concentrations in the water column did not increase toward the well positions (see above).

Abandoned wells can act as migration pathways for gas through the sediment column as shown in several studies at onshore wells (Kang et al., 2014; Boothroyd et al., 2016; Townsend-Small et al., 2016; Schout et al., 2019). However, much less is known about their importance as leakage sites of methane release into the water column and subsequently into the atmosphere. In contrast to a study by Vielstädte et al. (2015), who focused on gas release at abandoned wells in the central North Sea, our study suggests that surveyed abandoned wells did not provide clear evidence for fluid release along the wells. The flares found near abandoned well sites in this study were rather interpreted to relate to a system of natural migration pathways. Vielstädte et al. (2017) discuss that one-third of all wells may potentially leak and bring the awareness of a probably unrecognized methane emission pathway contributing to the greenhouse gas inventory. Supporting this estimate, Böttner et al. (2020) could show that 28 out of 43 investigated wells in the United Kingdom sector of the North Sea release gas from the seafloor into the water column. Although our data including abandoned wells in the German EEZ do not replicate these findings, our observations were limited to ten wells and base on infrequent crossing of the wells decades after drilling. Hence, we cannot entirely exclude methane seepage from the well sites nor can we confirm it.

4. Seafloor methane seepage related to salt diapirism in the northwestern part of the German North Sea

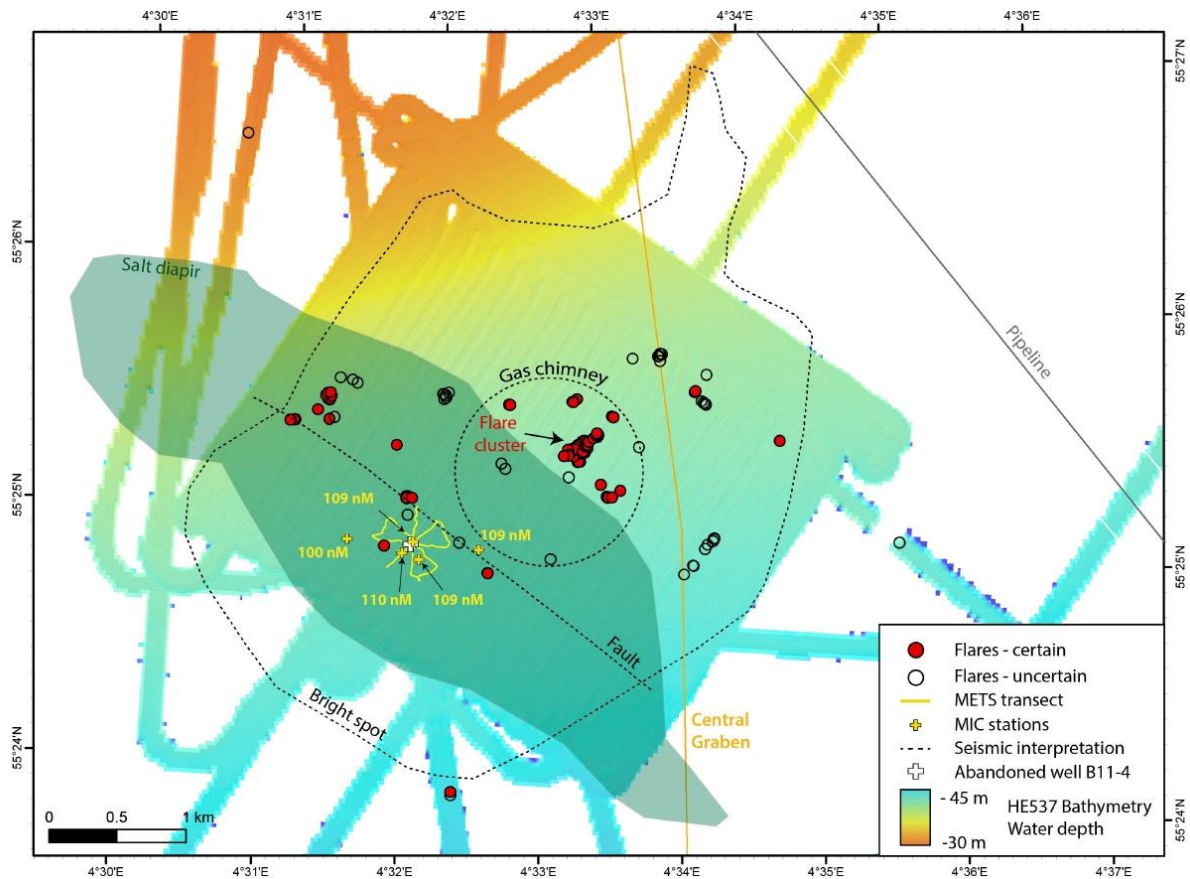


Fig. 32 Map compiling data acquired at salt diapir Berta, where most of the flare findings were concentrated. Seismic interpretation (bright spot extent, subsurface fault indication, and gas chimney) was depicted from Figure 7 in Müller et al. (2018 [Fig. 18 in this work]). Bottom water methane concentrations (yellow numbers) do not increase toward the well site.

4.3.4.3. Specific gas system at salt diapir Berta

Flare abundance analysis has shown that the main seepage area in the “Entenschnabel” is located close to salt diapir Berta. In total, 104 flares (out of 166 flares classified as certain) were detected in this area covering about 8.4 km². The flare distribution shows that gas seepage is not homogeneous across the area but is concentrated in specific areas. Most prominent is a flare cluster comprising more than half of all detected flares (66 flares) in a small area of about 300 x 100 m (Fig. 32). All flares are located above or in the vicinity (with a maximum distance of 1.3 km) of the subsurface salt diapir. The top of the salt diapir is located in approximately 2,000 mbsf (Müller et al., 2018). Whereas 20 flares are located directly above the salt diapir, the flare cluster is about 150 to 450 m northeast of the diapir outline. Seismic interpretation including bright spots, faults and gas chimneys [depicted from Figure 7 (Fig. 18 this work) in Müller et al. (2018)] reveal good correlation to flare locations mapped in this study (Fig. 32). Except for one flare, all flares are located in the area underlain by seismically detected stacked bright spots. Eight flares align along the fault plane intersection with the seafloor. Müller et al. (2018) described that the horizons above the salt diapir intersect with a NW-SE striking normal fault. In addition, increased amplitudes at the flank of the fault and at the uppermost reflections above

the fault indicated gas migration from the fault toward the seafloor. The flare cluster and 15 other flares (80% of all flares at Berta) plot in the area interpreted by Müller et al. (2018) as a gas chimney, which is indicated by discontinuous low amplitude reflections from the top of the salt diapir to the center of the bright spots. Hence, seepage found at Berta appears mainly focused through naturally evolved pathways related to salt diapirism.

4.4. Conclusion and outlook

Our results show that methane seepage is not uncommon in the German “Entenschnabel” region in the North Sea. An extensive mapping campaign has proven the presence of at least 166 flares. As flares were not observed closer than 125 m to a well site, we conclude that the seepage is focused on naturally evolved pathways related to salt diapirism rather than drill holes and related mechanical sediment disruption. The majority of flares were located at salt diapir Berta, which is characterized by subsurface gas indications such as acoustic blanking, high amplitude reflectors, and sediment electric conductivity anomalies. Geochemical analyses of water samples suggest a shallow, microbial origin of the gas. However, additional deep subsurface imaging is needed to interpret the relation between salt diapirism and seepage into the water column. Our hydroacoustic flare observations imaged gas bubbles rising close to the sea surface and methane concentrations in surface waters were slightly elevated, both suggesting that gas bubbles might be a pathway to transport fractions of methane from the seafloor to the atmosphere. Based on this study, we suggest to further characterize the nature of the active gas system in the German North Sea including the quantity of emitted methane, the gas source and address the following questions:

1. How much methane is released in form of gas bubbles and dissolved in pore water from the seafloor? Although our study did not systematically investigate the temporal variability, first results do indicate that flares are not stable over times of hours and days. Better understanding this variability and the controlling factors would be crucial to evaluate the gas quantities released.
2. Are the depressions detected at salt diapir Britta formed by fluid release? Are they related to the drilling activities at this site?
3. What is the origin of the methane emissions detected? If related to subsurface gas accumulations above salt diapirs, why is seepage mainly focused on salt diapir Berta?
4. Does methane released from the seafloor in the “Entenschnabel” reach the sea-air interface and contribute to the atmospheric inventory?
5. Is the Schillgrund Fault providing efficient fluid migration pathways

A better knowledge about shallow seep systems along continental shelf margins would be needed to evaluate the importance for gas exchange and fluid fluxes from the seafloor into the water column and eventually into the atmosphere.

Data availability statement

The datasets analyzed for this study can be found in the Open Access library PANGAEA (<https://www.pangaea.de/>). Data associated with the article:

Ship's track HE537: <https://doi.pangaea.de/10.1594/PANGAEA.905303>.

Station list HE537: <https://doi.pangaea.de/10.1594/PANGAEA.905303>.

Sediment echosounder data: <https://doi.pangaea.de/10.1594/PANGAEA.910739>.

Multibeam echosounder data: <https://doi.pangaea.de/10.1594/PANGAEA.912849>.

CTD hydrocast data: <https://doi.pangaea.de/10.1594/PANGAEA.907544>.

METS data: <https://doi.pangaea.de/10.1594/PANGAEA.915769>, <https://doi.pangaea.de/10.1594/PANGAEA.915770>, <https://doi.pangaea.de/10.1594/PANGAEA.915771>, <https://doi.pangaea.de/10.1594/PANGAEA.915772>, <https://doi.pangaea.de/10.1594/PANGAEA.915773>, <https://doi.pangaea.de/10.1594/PANGAEA.915774>, <https://doi.pangaea.de/10.1594/PANGAEA.915775>, <https://doi.pangaea.de/10.1594/PANGAEA.915776>, <https://doi.pangaea.de/10.1594/PANGAEA.915777>, <https://doi.pangaea.de/10.1594/PANGAEA.915778>, and <https://doi.pangaea.de/10.1594/PANGAEA.915779>.

Electromagnetic data: <https://doi.pangaea.de/10.1594/PANGAEA.915602>, <https://doi.pangaea.de/10.1594/PANGAEA.915605>, and <https://doi.pangaea.de/10.1594/PANGAEA.915610>.

Funding

This study was funded through the Cluster of Excellence “The Ocean Floor – Earth’s Uncharted Interface.” Open access publication fees are funded by the University of Bremen. Grant GPF 18-2_18 MESSENGER ship time R/V Heincke.

Acknowledgments

We greatly appreciate the shipboard support from the masters and crew of R/V Heincke cruise HE537 and the Leitstelle Deutsche Forschungsschiffe as well as the Gutachterpanel Forschungsschiffe for support to realize the cruise. We kindly acknowledge help onboard by Christian Seeger, Dennis Hagedorn, and Konstantin Reeck, and laboratory support by Daniela Graskamp and Dietmar Laszinski. We would also like to thank four reviewers for their constructive suggestions that helped to improve and strengthen our manuscript.

References

- Archie, G. E., 1942. The electrical resistivity log as an aid in determining some reservoir characteristics. *J. Pet. Technol.* 146, 54–62. doi: 10.2118/942054-g
- Arfai, J., Jahne, F., Lutz, R., Franke, D., Gaedicke, C. & Kley, J., 2014. Late Paleozoic to early Cenozoic geological evolution of the northwestern German North Sea (Entenschnabel): new results and insights. *Netherlands J. Geosci.* 93, 147–174. doi: 10.1017/njg.2014.22
- Attias, E., Amalokwu, K., Watts, M., Falcon-Suarez, I. H., North, L., Hu, G. W., et al., 2020. Gas hydrate quantification at a pockmark offshore Norway from joint effective medium modelling of resistivity and seismic velocity. *Mar. Pet. Geol.* 113:104151. doi: 10.1016/j.marpetgeo.2019.104151
- Baasch, B., Müller, H., Dobeneck, T. V. & Oberl, F. K. J., 2017. Determination of grain-size characteristics from electromagnetic seabed mapping data: a NW Iberian shelf study. *Cont. Shelf Res.* 140, 75–83. doi: 10.1016/j.csr.2017.04.005
- Boles, J. R., Clark, J. F., Leifer, I., & Washburn, L., 2001. Temporal variation in natural methane seep rate due to tides, Coal Oil Point area, California. *J. Geophys. Res.* 106, 27077–27086. doi: 10.1029/2000jc000774
- Boothroyd, I. M., Almond, S., Qassim, S. M., Worrall, F. & Davies, R. J., 2016. Fugitive emissions of methane from abandoned, decommissioned oil and gas wells. *Sci. Total Environ.* 547, 461–469. doi: 10.1016/j.scitotenv.2015.12.096
- Böttner, C., Berndt, C., Reinardy, B. T. I., Geersen, J., Karstens, J., Bull, J. M., et al., 2019. Pockmarks in the witch ground basin, central North Sea. *Geochem. Geophys. Geosyst.* 20, 1698–1719. doi: 10.1029/2018gc008068
- Böttner, C., Haeckel, M., Schmidt, M., Berndt, C., Vielstädte, L., Kutsch, J. A., et al., 2020. Greenhouse gas emissions from marine decommissioned hydrocarbon wells: leakage detection, monitoring and mitigation strategies. *Int. J. Greenh. Gas Control* 100:103119. doi: 10.1016/j.ijggc.2020.103119
- Caress, D. W. & Chayes, D. N., 2017. MB-System: Mapping the Seafloor. Available online at: <https://www.mbari.org/products/research-software/mbsystem> (accessed July 1, 2019).
- Cheesman, S. J., Law, L. K. & Louis, B. S., 1993. A porosity mapping survey in hecate strait using a seafloor electro-magnetic profiling system. *Mar. Geol.* 110, 245–256. doi: 10.1016/0025-3227(93)90087-c
- Davison, I., Alsop, I., Birch, P., Elders, C., Evans, N., Nicholson, H., et al., 2000. Geometry and late-stage structural evolution of central Graben salt diapirs, North Sea. *Mar. Pet. Geol.* 17, 499–522. doi: 10.1016/s0264-8172(99) 00068-9

4. Seafloor methane seepage related to salt diapirism in the northwestern part of the German North Sea

- Dick, S., Kleine, E. & Müller-Navarra, S. H., 2001. "The operational circulation model of BSH (BSH cmod). model description and validation," in *Berichte des Bundesamtes für Seeschiffahrt und Hydrographie*. 29/2001, 48 (Hamburg, Germany: Bundesamtes für Seeschiffahrt und Hydrographie).
- Duffy, O. B., Gawthorpe, R. L., Docherty, M. & Brocklehurst, S. H., 2013. Mobile evaporite controls on the structural style and evolution of rift basins: Danish central Graben, North Sea. *Basin Res.* 25, 310–330. doi: 10.1111/bre. 12000
- Dupré, S., Scalabrin, C., Grall, C., Augustin, J.-M., Henry, P., Sengör, A. M. C., et al., 2015. Tectonic and sedimentary controls on widespread gas emissions in the Sea of Marmara: results from systematic, shipborne multibeam echo sounder water column imaging. *J. Geophys. Res. Solid Earth Res.* 120, 2891–2912. doi: 10.1002/2014jb011617
- Evans, R. L., Law, L. K., St. Louis, B., Cheesman, S. & Sananikone, K., 1999. The shallow porosity structure of the Eel shelf, northern California: results of a towed electromagnetic survey. *Mar. Geol.* 154, 211–226. doi: 10.1016/s0025- 3227(98)00114-5
- Fechner-Levy, E. J. & Hemond, H. F., 1996. Trapped methane volume and potential effects on methane ebullition in a northern peatland. *Limnol. Oceanogr.* 41, 1375–1383. doi: 10.4319/lo.1996.41.7.1375
- Flanders Marine and Institute, 2019. *Maritime Boundaries Geodatabase: Maritime Boundaries and Exclusive Economic Zones (200NM)*, version 11.
- Garcia, X., Monteys, X., Evans, R. L. & Szpak, M., 2014. Constraints on a shallow offshore gas environment determined by a multidisciplinary geophysical approach: the Malin Sea, NW Ireland. *Geochem. Geophys. Geosyst.* 15, 867–885. doi: 10.1002/2013gc005108
- Hovland, M., 1993. Submarine gas seepage in the North Sea and adjacent areas. *Pet. Geol. Conf. Proc.* 4, 1333–1338. doi: 10.1144/0041333
- Hovland, M., 2007. Discovery of prolific natural methane seeps at Gullfaks, northern North Sea. *Geo Mar. Lett.* 27, 197–201. doi: 10.1007/s00367-007- 0070-6
- Hovland, M. & Judd, A. G., 1988. *Seabed Pockmarks and Seepages*. London: Graham and Trotman.
- Hovland, M., Svensen, H., Forsberg, C. F., Johansen, H., Fichler, C., Fosså, J. H., et al., 2005. Complex pockmarks with carbonate-ridges off mid-Norway: products of sediment degassing. *Mar. Geol.* 218, 191–206. doi: 10.1016/j. margeo.2005.04.005
- Jackson, M. P. A. & Hudec, M. R., 2017. *Salt Tectonics: Principles and Practice*. Cambridge: Cambridge University Press.
- Jackson, P. D., Taylor Smith, D. & Stanford, P. N., 1978. Resistivity-porosity particle shape relationships for marine sands. *Geophysics* 43, 1250–1268. doi: 10.1190/1.1440891
- Jin, Y. K., Kim, Y., Baranov, B., Shoji, H. & Obzhirov, A., 2011. Distribution and expression of gas seeps in a gas hydrate province of the northeastern Sakhalin continental slope, sea of Okhotsk. *Mar. Pet. Geol.* 28, 1844–1855. doi: 10.1016/j.marpetgeo.2011.03.007

4. Seafloor methane seepage related to salt diapirism in the northwestern part of the German North Sea

- Judd, A., 2015. The significance of the 22/4b blow-out site methane emissions in the context of the North Sea. *Mar. Pet. Geol.* 68, 836–847. doi: 10.1016/j.marpetgeo.2015.07.031
- Judd, A. & Hovland, M., 2007. *Seabed Fluid Flow. The Impact on Geology, Biology and the Marine Environment*. Cambridge: Cambridge University Press, 475.
- Judd, A., Long, D. & Sankey, M., 1994. Pockmark formation and activity, UK block 15/25, North Sea. *Bull. Geol. Soc. Denmark* 41, 34–49.
- Kang, M., Kanno, C. M., Reid, M. C., Zhang, X., Mauzerall, D. L., Celia, M. A., et al., 2014. Direct measurements of methane emissions from abandoned oil and gas wells in Pennsylvania. *Proc. Natl. Acad. Sci. U. S. A.* 111, 18173–18177. doi: 10.1073/pnas.1408315111
- Kannberg, P. K., Tréhu, A. M., Pierce, S. D., Paull, C. K. & Caress, D. W., 2013. Temporal variation of methane flares in the ocean above Hydrate Ridge, Oregon. *Earth Planet. Sci. Lett.* 368, 33–42. doi: 10.1016/j.epsl.2013.02.030
- Krämer, K., Holler, P., Herbst, G., Bratek, A., Ahmerkamp, S., Neumann, A., et al., 2017. Abrupt emergence of a large pockmark field in the German bight, southeastern North Sea. *Sci. Rep.* 7:5150.
- Landrø, M., Wehner, D., Vedvik, N., Ringrose, P., Løhre, N. L. & Berteussen, K., 2019. Gas flow through shallow sediments—a case study using passive and active seismic field data. *Int. J. Greenh. Gas Control* 87, 121–133. doi: 10.1016/j.ijggc.2019.05.001
- Laurer, W. U., Naumann, M. & Zeiler, M., 2012. Erstellung der Karte zur Sedimentverteilung auf dem Meeresboden in der deutschen Nordsee nach der Klassifikation von Figge (1981). *Geopotenzial Deutsche Nordsee, Hannover/Hamburg*, 19 S. Available online at: <https://www.gpdn.de/gpdn/wilma.aspx?pgId=337&WilmaLogonActionBehavior=Default> (accessed April 14, 2020).
- Leifer, I., 2015. Seabed bubble flux estimation by calibrated video survey for a large blowout seep in the North Sea. *Mar. Pet. Geol.* 68, 743–752. doi: 10.1016/j.marpetgeo.2015.08.032
- Leifer, I. & Boles, J., 2005. Turbine tent measurements of marine hydrocarbon seeps on sub-hourly timescales. *J. Geophys. Res. Oceans* 110, 1–12. doi: 10.1007/978-3-030-34827-4_1
- Leifer, I. & Judd, A., 2015. The UK22/4b blowout 20 years on: investigations of continuing methane emissions from sub-seabed to the atmosphere in a North Sea context. *Mar. Pet. Geol.* 68, 706–717. doi: 10.1016/j.marpetgeo.2015.11.012
- Leifer, I. & Patro, R. K., 2002. The bubble mechanism for methane transport from the shallow sea bed to the surface: a review and sensitivity study. *Cont. Shelf Res.* 22, 2409–2428. doi: 10.1016/s0278-4343(02)00065-1
- Ligtenberg, H. & Connolly, D., 2003. Chimney detection and interpretation, revealing sealing quality of faults, geohazards, charge of and leakage from reservoirs. *J. Geochem. Explor.* 78–79, 385–387. doi: 10.1016/s0375-6742(03)00095-5
- Little, R., Bayer, U., Gajewski, D. & Nelskamp, S., 2008. *Dynamics of Complex Intracontinental Basins: The Central European Basin System*. Berlin: Springer.

4. Seafloor methane seepage related to salt diapirism in the northwestern part of the German North Sea

- Lutz, R., Kalka, S., Gaedicke, C., Reinhardt, L. & Winsemann, J., 2009. Pleistocene tunnel valleys in the German North Sea: spatial distribution and morphology. *Zeitschrift der Deutschen Gesellschaft für Geowissenschaften* 160, 225–235. doi: 10.1127/1860-1804/2009/0160-0225
- Mau, S., Gentz, T., Körber, J. H., Torres, M. E., Römer, M., Sahling, H., et al., 2015. Seasonal methane accumulation and release from a gas emission site in the central North Sea. *Biogeosciences* 12, 5261–5276. doi: 10.5194/bg-12-5261-2015
- Müller, H., Von Dobeneck, T., Hilgenfeldt, C., SanFilipo, B., Rey, D. & Rubio, B., 2012. Mapping the magnetic susceptibility and electric conductivity of marine surficial sediments by benthic EM profiling. *Geophysics* 77, 1JF–Z19.
- Müller, H., von Dobeneck, T., Nehmiz, W. & Hamer, K., 2011. Near-surface electromagnetic, rock magnetic, and geochemical fingerprinting of submarine freshwater seepage at Eckernförde Bay (SW Baltic Sea). *Geo Mar. Lett.* 31, 123–140. doi: 10.1007/s00367-010-0220-0
- Müller, S., Reinhardt, L., Franke, D., Gaedicke, C. & Winsemann, J., 2018. Shallow gas accumulations in the German North Sea. *Mar. Pet. Geol.* 91, 139–151. doi: 10.1016/j.marpetgeo.2017.12.016
- Niemann, H., Elvert, M., Hovland, M., Orcutt, B., Judd, A., Suck, I., et al., 2005. Methane emission and consumption at a North Sea gas seep (Tommeliten area). *Biogeosciences* 2, 335–351. doi: 10.5194/bg-2-335-2005
- Pletsch, T., Appel, J., Botor, D., Clayton, C. J., Duin, E. J. T., Faber, E., et al., 2010. *Petroleum Geological Atlas of the Southern Permian Basin Area*. Houten: EAGE Publications.
- Rehder, G., Keir, R. S., Suess, E. & Pohlmann, T., 1998. The multiple sources and patterns of methane in North Sea waters. *Aquat. Geochem.* 4, 403–427.
- Rehder, G., Keir, R. S., Suess, E. & Rhein, M., 1999. Methane in the northern Atlantic controlled by microbial oxidation and atmospheric history. *Geophys. Res. Lett.* 26, 587–590. doi: 10.1029/1999gl1900049
- Riboulot, V., Cattaneo, A., Scalabrin, C., Gaillot, A., Jouet, G., Ballas, G., et al., 2017. Control of the geomorphology and gas hydrate extent on widespread gas emissions offshore Romania. *Bull. Soc. Geol. Fr.* 188, 12–26.
- Römer, M., Riedel, M., Scherwath, M., Heesemann, M. & Spence, G. D., 2016. Tidally controlled gas bubble emissions: a comprehensive study using long-term monitoring data from the NEPTUNE cabled observatory offshore Vancouver Island. *Geochem. Geophys. Geosyst.* 17, 1312–1338.
- Römer, M., Wenau, S., Bohrmann, G., Mau, S., Veloso, M., Greinert, J., et al., 2017. Assessing marine gas emission activity and contribution to the atmospheric methane inventory: a multi-disciplinary approach from the Dutch Dogger Bank seep area (North Sea). *Geochem. Geophys. Geosyst.* 18, 2617–2633. doi: 10.1002/2017gc006995

4. Seafloor methane seepage related to salt diapirism in the northwestern part of the German North Sea

- Scandella, B. P., Varadharajan, C., Hemond, H. F., Ruppel, C. & Juanes, R., 2011. A conduit dilation model of methane venting from lake sediments. *Geophys. Res. Lett.* 38, 1–6.
- Schloemer, S., Oest, J., Illing, C. J., Elbracht, J. & Blumenberg, M., 2018. Spatial distribution and temporal variation of methane, ethane and propane background levels in shallow aquifers – a case study from Lower Saxony (Germany). *J. Hydrol. Reg. Stud.* 19, 57–79. doi: 10.1016/j.ejrh.2018.07.002
- Schmale, O., Schneider, von Deimling, J., Gülzow, W., Nausch, G., Waniek, J. J., et al., 2010. Distribution of methane in the water column of the Baltic Sea. *Geophys. Res. Lett.* 37:L12604.
- Schneider Von, Deimling, J., Brockhoff, J. & Greinert, J., 2007. Flare imaging with multibeam systems: data processing for bubble detection at seeps. *Geochem. Geophys. Geosyst.* 8, 1–7. doi: 10.1109/joe.2021.3056910
- Schneider Von, Deimling, J., Rehder, G., Greinert, J., Mcginnnis, D. F., Boetius, A., et al., 2011. Quantification of seep-related methane gas emissions at Tommeliten. *North Sea. Cont. Shelf Res.* 31, 867–878. doi: 10.1016/j.csr.2011.02.012
- Schout, G., Griffioen, J., Hassanizadeh, S. M., Cardon, de Lichtbuer, G., and Hartog, N., 2019. Occurrence and fate of methane leakage from cut and buried abandoned gas wells in the Netherlands. *Sci. Total Environ.* 659, 773–782. doi: 10.1016/j.scitotenv.2018.12.339
- Schroot, B. M., Klaver, G. T. & Schüttenhelm, R. T. E., 2005. Surface and subsurface expressions of gas seepage to the seabed - examples from the Southern North Sea. *Mar. Pet. Geol.* 22, 499–515. doi: 10.1016/j.marpetgeo.2004.08.007
- Schroot, B. M. & Schüttenhelm, R. T. E., 2003. Expressions of shallow gas in the Netherlands North Sea. *Netherlands J. Geosci.* 82, 91–105. doi: 10.1017/s0016774600022812
- Schwalenberg, K., Gehrman, R. A. S., Bialas, J. & Rippe, D., 2020. Analysis of marine controlled source electromagnetic data for the assessment of gas hydrates in the Danube deep-sea fan, Black Sea. *Mar. Pet. Geol.* 120. doi: 10.1016/j.marpetgeo.2020.104650
- Schwalenberg, K., Rippe, D., Koch, S. & Scholl, C., 2017. Marine-controlled source electromagnetic study of methane seeps and gas hydrates at opouawe bank, hikurangi margin, New Zealand. *J. Geophys. Res. Solid Earth* 122, 3334–3350. doi: 10.1002/2016jb013702
- Sommer, S., Schmidt, M. & Linke, P., 2015. Continuous inline mapping of a dissolved methane plume at a blowout site in the central North Sea UK using a membrane inlet mass spectrometer – water column stratification impedes immediate methane release into the atmosphere. *Mar. Pet. Geol.* 68, 766–775. doi: 10.1016/j.marpetgeo.2015.08.020
- Szpak, M. T., Monteys, X., O'Reilly, S., Simpson, A. J., Garcia, X., Evans, R. L., et al., 2012. Geophysical and geochemical survey of a large marine pockmark on the Malin Shelf, Ireland. *Geochem. Geophys. Geosyst.* 13:Q01011.
- ten Veen, J. H., Van Gessel, S. F. & den Dulk, M., 2012. Thin and thick-skinned salt tectonics in the Netherlands; a quantitative approach. *Netherlands J. Geosci.* 91, 447–464. doi: 10.1017/s001677460000330

4. Seafloor methane seepage related to salt diapirism in the northwestern part of the German North Sea

Thatje, S., Gerdes, D. & Rachor, E., 1999. A seafloor crater in the German bight and its effects on the benthos. *Helgol. Mar. Res.* 53, 36–44. doi: 10.1007/ pl00012136

Torres, M. E., Mcmanus, J., Hammond, D. E., Angelis, M. A., De, Heeschen, K. U., et al., 2002. Fluid and chemical fluxes in and out of sediments hosting methane hydrate deposits on Hydrate Ridge, or, i?: hydrological provinces. *Earth Planet. Sci. Lett.* 201, 525–540. doi: 10.1016/s0012-821x(02) 00733-1

Townsend-Small, A., Ferrara, T. W., Lyon, D. R., Fries, A. E. & Lamb, B. K., 2016. Emissions of coalbed and natural gas methane from abandoned oil and gas wells in the United States. *Geophys. Res. Lett.* 43, 2283–2290. doi: 10.1002/2015gl067623

Tryon, M. D., Brown, K. M., Torres, M. E., Tréhu, A. M., McManus, J. & Collier, R. W., 1999. Measurements of transience and downward fluid flow near episodic methane gas vents, hydrate ridge, cascadia. *Geology* 27, 1075–1078. doi: 10.1130/0091-7613(1999)027<1075:motadf>2.3.co;2

Varadharajan, C. & Hemond, H. F., 2012. Time-series analysis of high resolution ebullition fluxes from a stratified, freshwater lake. *J. Geophys. Res. Biogeosci.* 117, 1–15. doi: 10.15504/fmj.2016.18

Vielstädte, L., Haeckel, M., Karstens, J., Linke, P., Schmidt, M., Steinle, L., et al., 2017. Shallow gas migration along hydrocarbon wells-an unconsidered, anthropogenic source of biogenic methane in the North Sea. *Environ. Sci. Technol.* 51, 10262–10268. doi: 10.1021/acs.est.7b02732

Vielstädte, L., Karstens, J., Haeckel, M., Schmidt, M., Linke, P., Reimann, S., et al., 2015. Quantification of methane emissions at abandoned gas wells in the central North Sea. *Mar. Pet. Geol.* 68, 848–860. doi: 10.1016/j.marpetgeo.2015. 07.030

White, J. E., 1975. Computed seismic speeds and attenuation in rocks with partial gas saturation. *Geophysics* 40, 224–232. doi: 10.1190/1.1440520

Wiesenberg, D. A. & Guinasso, N. L., 1979. Equilibrium solubilities of methane, carbonmonoxide and hydrogen in water and seawater. *J. Chem. Eng. Data* 24, 356–360. doi: 10.1021/je60083a006

Winsauer, W. O., Shearin, H. M., Masson, P. H. & Williams, M., 1952. Resistivity of brine saturated sands in relation to pore geometry. *Am. Assoc. Pet. Geol. Bull.* 36, 253–277.

Woodbury, H. O., Murray, I. B. & Osborne, R. E., 1980. “Diapirs and their relation to hydrocarbon accumulation,” in: *Facts and Principles of World Petroleum Occurrence*, ed. A.D. Miall. Calgary: Canadian Society of Petroleum Geologists

Wong, D. A., 2007. “Jurassic,” in *Geology of the Netherlands*. Royal Netherlands Academy of Arts and Sciences, (eds.) T. E. Wong, D. A. J. Batjes, and J. de Jager (Amsterdam: Elsevier), 107–125.

4. Seafloor methane seepage related to salt diapirism in the northwestern part of the German North Sea

Supplementary material

Supplementary table 1: Time, location, and certainty assessment of detected flares in water column echograms of the MBES.

Date/Time	Area	Lon (°E)	Lat (°N)	Seafloor depth (m)	Classification	Distance to well (m)
14.07.2019 01:17:29	Transit	5,18894441	55,0061245	-40,2	uncertain (weak)	12410
14.07.2019 08:29:57	Berta	4,53943974	55,3986456	-43,7	uncertain (anomalous)	1870
14.07.2019 08:30:06	Berta	4,53945501	55,398842	-43,6	certain	1849
14.07.2019 08:45:41	Berta	4,53221117	55,4180105	-41,5	certain	335
14.07.2019 09:12:15	Transit	4,51940506	55,4515648	-31,8	certain	3071
14.07.2019 09:32:06	Bella	4,50857131	55,479787	-31,5	certain	145
14.07.2019 09:50:27	Bella	4,49851648	55,505818	-31,5	certain	3112
14.07.2019 09:50:29	Bella	4,49861568	55,5058868	-31,5	certain	3118
14.07.2019 09:50:30	Bella	4,49869316	55,505912	-31,5	certain	3120
14.07.2019 09:50:37	Bella	4,49854422	55,5060568	-31,5	certain	3138
14.07.2019 09:50:37	Bella	4,49845367	55,5060587	-31,5	certain	3139
14.07.2019 09:50:38	Bella	4,49840594	55,5060771	-31,5	certain	3142
14.07.2019 09:50:38	Bella	4,49856647	55,5060945	-31,5	certain	3141
14.07.2019 09:50:38	Bella	4,49863985	55,5060991	-31,5	certain	3141
14.07.2019 13:29:16	Bella	4,50935743	55,4796119	-31,5	certain	125
14.07.2019 13:29:19	Bella	4,5094841	55,4796442	-31,5	certain	130
14.07.2019 13:38:03	Bella	4,51731933	55,4865017	-31,5	certain	1034
14.07.2019 13:38:05	Bella	4,51725422	55,4866117	-31,5	certain	1042
14.07.2019 13:51:53	Bella	4,50763199	55,4720924	-31,5	certain	720
14.07.2019 21:22:16	Berta	4,53220625	55,4180376	-41,5	certain	338
14.07.2019 21:22:24	Berta	4,53227303	55,4181663	-41,5	certain	351
14.07.2019 21:57:26	Berta	4,53218324	55,4180385	-41,5	certain	338
14.07.2019 23:51:14	Berta	4,54339205	55,4246036	-40,7	certain	1253
14.07.2019 23:51:15	Berta	4,54342309	55,424618	-40,7	certain	1256
14.07.2019 23:51:17	Berta	4,54350346	55,4245778	-40,7	certain	1255
15.07.2019 06:40:24	Belinda (South)	4,72326711	55,2049858	-46,4	uncertain (anomalous)	182
15.07.2019 10:39:13	Transit	4,7488608	55,1672942	-43,9	certain	3573
15.07.2019 16:29:37	B18-5	4,96916126	55,0899005	-38,9	certain	474
15.07.2019 19:37:22	Carola	5,10159265	55,1785848	-40,7	certain	235
15.07.2019 20:46:51	Carola	5,11419521	55,1840138	-40,8	uncertain (weak)	997
16.07.2019 02:54:13	Britta	4,78891	55,1490415	-42,5	certain	735
16.07.2019 02:54:22	Britta	4,78919575	55,1491527	-42,4	certain	713
16.07.2019 02:54:31	Britta	4,78929448	55,1493375	-42,4	certain	697
16.07.2019 02:54:38	Britta	4,78941028	55,1494511	-42,4	certain	684
16.07.2019 02:54:45	Britta	4,79005198	55,1494686	-42,4	certain	649
16.07.2019 02:54:45	Britta	4,78949574	55,1496055	-42,5	certain	671
16.07.2019 02:54:50	Britta	4,78956499	55,1496957	-42,5	certain	662
16.07.2019 02:54:54	Britta	4,79000668	55,1496786	-42,4	certain	639

4. Seafloor methane seepage related to salt diapirism in the northwestern part of the German North Sea

16.07.2019 14:44:27	Britta	4,79482822	55,1536142	-42,6	uncertain (anomalous)	275
16.07.2019 17:53:41	Transit	4,77937115	55,1624229	-43,1	uncertain (weak)	1648
16.07.2019 18:21:52	Belinda (South)	4,72287181	55,2292396	-47,7	certain	2772
16.07.2019 18:21:57	Belinda (South)	4,72269248	55,229437	-47,7	certain	2795
16.07.2019 18:21:59	Belinda (South)	4,72244341	55,2294679	-47,7	certain	2800
16.07.2019 18:22:13	Belinda (South)	4,72176576	55,2299579	-47,7	certain	2858
16.07.2019 18:22:29	Belinda (South)	4,72117973	55,2305563	-47,7	certain	2928
16.07.2019 18:22:29	Belinda (South)	4,72123002	55,2305913	-47,7	certain	2931
16.07.2019 18:22:29	Belinda (South)	4,72126649	55,2306012	-47,7	certain	2932
16.07.2019 19:19:44	Belinda (North)	4,68878628	55,2776068	-47,6	uncertain (anomalous)	829
16.07.2019 19:19:49	Belinda (North)	4,68907124	55,277684	-47,7	uncertain (anomalous)	810
16.07.2019 19:19:49	Belinda (North)	4,68918218	55,2776716	-47,7	uncertain (anomalous)	806
17.07.2019 02:42:34	Belinda (South)	4,74151213	55,2089052	-45,9	uncertain (weak)	1112
17.07.2019 02:50:38	Transit	4,75414146	55,18519	-44,2	certain	2793
17.07.2019 02:50:41	Transit	4,7535998	55,1849264	-44,1	certain	2794
17.07.2019 03:01:22	Transit	4,77089776	55,1537416	-42,7	uncertain (weak)	1775
17.07.2019 19:19:46	Transit	4,56999828	55,2915343	-46,9	uncertain (weak)	8178
17.07.2019 19:19:50	Transit	4,56983562	55,2916987	-46,9	uncertain (weak)	8190
17.07.2019 20:34:48	Birgit	4,51337861	55,338754	-45,8	uncertain (anomalous)	6847
17.07.2019 20:34:52	Birgit	4,51301558	55,3389656	-45,7	uncertain (anomalous)	6819
17.07.2019 22:50:33	Birgit	4,52801309	55,3405607	-45,5	certain	6958
17.07.2019 23:24:42	Birgit	4,52883074	55,3396978	-45,4	certain	7067
18.07.2019 00:33:15	Birgit	4,53288752	55,3364025	-45,5	certain	7506
18.07.2019 04:38:12	Birgit	4,54587594	55,3276533	-45,6	uncertain (anomalous)	8736
18.07.2019 04:38:13	Birgit	4,54587345	55,3276713	-45,6	uncertain (anomalous)	8734
18.07.2019 08:16:28	Transit	4,60631405	55,3121489	-46,6	uncertain (weak)	6659
18.07.2019 08:19:09	Transit	4,61808376	55,308661	-46,8	uncertain (anomalous)	5818
18.07.2019 08:19:14	Transit	4,61854091	55,3086501	-46,8	uncertain (anomalous)	5792
18.07.2019 08:19:22	Transit	4,61923873	55,3085634	-46,8	uncertain (anomalous)	5748
18.07.2019 12:09:02	Belinda (North)	4,69900748	55,2712331	-47,7	certain	1309
18.07.2019 12:09:03	Belinda (North)	4,69907316	55,2712015	-47,7	certain	1313
18.07.2019 12:09:04	Belinda (North)	4,69914857	55,2711699	-47,7	certain	1316
18.07.2019 12:15:29	Transit	4,70360189	55,2586929	-47,9	uncertain (anomalous)	2728
18.07.2019 15:25:56	Transit	4,70003148	55,2561906	-47,9	certain	2985
18.07.2019 17:40:22	Belinda (North)	4,70693905	55,2782749	-47,5	certain	780
18.07.2019 17:40:41	Belinda (North)	4,70850138	55,2779361	-47,6	certain	880
18.07.2019 19:33:31	Transit	5,24526213	55,0899634	-40,5	uncertain (anomalous)	7345
18.07.2019 19:33:36	Transit	5,24564067	55,0897834	-40,5	uncertain (anomalous)	7361
18.07.2019 19:33:39	Transit	5,24584207	55,0896784	-40,5	uncertain (anomalous)	7371
20.07.2019 03:38:25	Transit	4,57562076	55,2568171	-46,0	uncertain (weak)	8296
20.07.2019 20:29:09	Transit	4,23806908	55,3669927	-43,1	uncertain (anomalous)	6956
20.07.2019 20:29:09	Transit	4,2381287	55,366953	-43,1	uncertain (anomalous)	6962
20.07.2019 20:29:18	Transit	4,23837345	55,3674972	-43,1	uncertain (anomalous)	6921
20.07.2019 20:29:18	Transit	4,23833949	55,3675197	-43,1	uncertain (anomalous)	6918
20.07.2019 20:29:19	Transit	4,23880721	55,3673201	-43,1	uncertain (anomalous)	6953

4. Seafloor methane seepage related to salt diapirism in the northwestern part of the German North Sea

20.07.2019 20:29:38	Transit	4,239649	55,3682017	-43,0	uncertain (anomalous)	6904
20.07.2019 23:55:40	Bella	4,48312804	55,4730021	-31,6	uncertain (weak)	1747
20.07.2019 23:58:41	Bella	4,48569929	55,4736872	-31,5	uncertain (weak)	1568
21.07.2019 00:00:16	Bella	4,48794511	55,475632	-31,4	certain	1370
21.07.2019 00:00:18	Bella	4,48807111	55,4756721	-31,4	certain	1361
21.07.2019 00:00:21	Bella	4,4881489	55,4757353	-31,4	certain	1354
21.07.2019 00:00:22	Bella	4,48787528	55,4758206	-31,4	certain	1369
21.07.2019 00:00:22	Bella	4,48776161	55,4758679	-31,4	certain	1375
21.07.2019 00:00:25	Bella	4,48798466	55,4758923	-31,4	certain	1361
21.07.2019 00:00:25	Bella	4,4880645	55,4758714	-31,4	certain	1356
21.07.2019 00:00:26	Bella	4,4879536	55,4759328	-31,4	certain	1362
21.07.2019 00:00:26	Bella	4,48800986	55,4759225	-31,4	certain	1358
21.07.2019 00:27:14	Bella	4,50043676	55,4858627	-31,5	uncertain (weak)	982
21.07.2019 00:36:10	Bella	4,48930275	55,4753211	-31,4	uncertain (weak)	1295
21.07.2019 00:36:20	Bella	4,48912208	55,4751047	-31,4	uncertain (weak)	1313
21.07.2019 02:40:49	Bella	4,50814822	55,4828066	-31,5	uncertain (anomalous)	482
21.07.2019 02:40:52	Bella	4,50831829	55,4826354	-31,5	uncertain (anomalous)	462
21.07.2019 02:40:55	Bella	4,50805603	55,4826695	-31,5	uncertain (anomalous)	467
21.07.2019 02:57:38	Bella	4,49797512	55,4720119	-31,5	uncertain (anomalous)	1005
21.07.2019 02:57:39	Bella	4,49812557	55,4720049	-31,5	uncertain (anomalous)	999
21.07.2019 02:57:43	Bella	4,49841153	55,4720131	-31,5	uncertain (anomalous)	986
21.07.2019 02:57:43	Bella	4,49844141	55,4720044	-31,5	uncertain (anomalous)	985
21.07.2019 03:29:33	Bella	4,50859905	55,4798326	-31,5	certain	150
21.07.2019 03:59:02	Bella	4,51724126	55,4863738	-31,5	uncertain (weak)	1019
21.07.2019 04:23:12	Bella	4,50457513	55,4720046	-31,5	uncertain (weak)	776
21.07.2019 04:46:45	Bella	4,51967238	55,4851564	-31,5	certain	1001
21.07.2019 04:46:52	Bella	4,51940946	55,4853935	-31,6	certain	1010
21.07.2019 05:09:19	Bella	4,50797214	55,4720263	-31,5	certain	725
21.07.2019 06:02:05	Transit	4,53861678	55,4153003	-42,0	uncertain (anomalous)	359
21.07.2019 08:30:38	Berta	4,53290065	55,4180282	-41,5	certain	333
21.07.2019 08:31:21	Berta	4,53284638	55,4180292	-41,4	certain	334
21.07.2019 10:24:07	Berta	4,53006826	55,415064	-41,9	certain	184
21.07.2019 10:24:23	Berta	4,53031989	55,4151249	-41,8	certain	168
21.07.2019 17:07:43	Berta	4,58966806	55,417174	-42,2	uncertain (weak)	2494
21.07.2019 17:11:17	Berta	4,57504333	55,4233548	-41,4	certain	2821
21.07.2019 18:45:49	Bella	4,52960994	55,4861288	-31,5	uncertain (weak)	1555
21.07.2019 19:34:25	Bella	4,52244965	55,47479	-31,5	uncertain (anomalous)	946
21.07.2019 19:34:29	Bella	4,52238963	55,4747032	-31,5	uncertain (anomalous)	946
21.07.2019 19:44:34	Bella	4,50974383	55,4634893	-31,5	certain	1673
21.07.2019 21:17:09	Transit	4,51116241	55,4413873	-32,4	uncertain (weak)	3243
21.07.2019 21:37:00	Berta	4,52127445	55,4234689	-39,8	certain	1196
21.07.2019 21:37:36	Berta	4,52256673	55,4241635	-39,7	certain	1211
21.07.2019 21:37:37	Berta	4,52252866	55,4241975	-39,7	certain	1216
21.07.2019 21:37:37	Berta	4,52232335	55,4242484	-39,6	certain	1227
21.07.2019 21:37:40	Berta	4,52266831	55,4242368	-39,7	certain	1215

4. Seafloor methane seepage related to salt diapirism in the northwestern part of the German North Sea

21.07.2019 21:37:44	Berta	4,52211481	55,4244764	-39,5	certain	1256
21.07.2019 21:37:48	Berta	4,52269128	55,4244554	-39,6	certain	1234
21.07.2019 21:37:51	Berta	4,52231279	55,4246159	-39,5	certain	1262
21.07.2019 21:37:55	Berta	4,52265901	55,4246591	-39,5	certain	1255
21.07.2019 21:38:42	Berta	4,52365075	55,4256988	-39,1	uncertain (weak)	1326
21.07.2019 22:00:42	Berta	4,52565942	55,4254229	-39,5	uncertain (weak)	1246
21.07.2019 22:00:44	Berta	4,52508508	55,4256014	-39,4	uncertain (weak)	1278
21.07.2019 22:02:38	Berta	4,52324895	55,4230628	-40,1	uncertain (weak)	1085
21.07.2019 22:02:52	Berta	4,52266631	55,422914	-40,1	certain	1093
22.07.2019 00:08:59	Berta	4,53634155	55,425135	-40,3	uncertain (weak)	1145
22.07.2019 00:09:10	Berta	4,53598165	55,424965	-40,3	uncertain (weak)	1122
22.07.2019 00:09:12	Berta	4,53574739	55,4250113	-40,2	uncertain (weak)	1125
22.07.2019 00:09:13	Berta	4,53564116	55,4250167	-40,3	uncertain (weak)	1124
22.07.2019 00:09:16	Berta	4,5360146	55,4248136	-40,4	uncertain (weak)	1106
22.07.2019 00:09:22	Berta	4,53584385	55,4247023	-40,4	uncertain (weak)	1092
22.07.2019 00:59:09	Berta	4,5322736	55,4181683	-41,5	certain	352
22.07.2019 00:59:13	Berta	4,53214591	55,4181209	-41,5	certain	348
22.07.2019 00:59:16	Berta	4,53217171	55,4180449	-41,5	certain	339
22.07.2019 00:59:17	Berta	4,5321975	55,418023	-41,5	certain	336
22.07.2019 02:55:48	Berta	4,5511866	55,425237	-40,7	certain	1619
22.07.2019 02:55:57	Berta	4,55083583	55,4250878	-40,7	certain	1592
22.07.2019 02:55:59	Berta	4,55070566	55,4250563	-40,7	certain	1583
22.07.2019 02:55:59	Berta	4,55079821	55,4250258	-40,8	certain	1585
22.07.2019 03:33:04	Berta	4,55738852	55,4281502	-40,3	uncertain (anomalous)	2127
22.07.2019 03:37:56	Berta	4,55168656	55,4222423	-41,3	certain	1431
22.07.2019 03:38:02	Berta	4,55153345	55,4221247	-41,3	certain	1416
22.07.2019 03:38:09	Berta	4,55136465	55,4219717	-41,3	certain	1398
22.07.2019 03:38:10	Berta	4,55118971	55,4219981	-41,3	certain	1390
22.07.2019 03:38:21	Berta	4,5505396	55,4218961	-41,3	certain	1350
22.07.2019 03:38:30	Berta	4,55072151	55,4215761	-41,4	certain	1340
22.07.2019 03:38:34	Berta	4,55056415	55,4215135	-41,4	certain	1327
22.07.2019 03:38:34	Berta	4,55061938	55,4214974	-41,4	certain	1329
22.07.2019 03:38:41	Berta	4,55010408	55,4214597	-41,3	certain	1300
22.07.2019 03:45:16	Berta	4,54213319	55,4134071	-42,2	certain	608
22.07.2019 03:45:16	Berta	4,54216647	55,4133974	-42,2	certain	610
22.07.2019 04:03:29	Berta	4,55233533	55,4217149	-41,4	certain	1434
22.07.2019 04:03:30	Berta	4,55225836	55,4217763	-41,4	certain	1434
22.07.2019 04:03:31	Berta	4,55241974	55,4217308	-41,4	certain	1440
22.07.2019 04:03:32	Berta	4,55231066	55,4218009	-41,4	certain	1438
22.07.2019 04:03:47	Berta	4,55255386	55,422169	-41,3	certain	1473
22.07.2019 04:03:48	Berta	4,55260064	55,4221891	-41,3	certain	1477
22.07.2019 04:03:49	Berta	4,55263852	55,4221932	-41,3	certain	1479
22.07.2019 04:03:49	Berta	4,55264609	55,4222093	-41,3	certain	1480
22.07.2019 04:03:53	Berta	4,55279672	55,422263	-41,3	certain	1491
22.07.2019 04:04:02	Berta	4,55291244	55,4224785	-41,3	certain	1511

4. Seafloor methane seepage related to salt diapirism in the northwestern part of the German North Sea

22.07.2019 04:04:16	Berta	4,5533789	55,4227275	-41,2	certain	1551
22.07.2019 04:04:27	Berta	4,55377658	55,4229106	-41,2	certain	1583
22.07.2019 04:04:28	Berta	4,55388432	55,4228871	-41,2	certain	1587
22.07.2019 04:04:31	Berta	4,55389675	55,4229874	-41,2	certain	1594
22.07.2019 04:04:31	Berta	4,55396074	55,4229736	-41,2	certain	1596
22.07.2019 04:04:33	Berta	4,55377333	55,4230951	-41,1	certain	1594
22.07.2019 04:04:33	Berta	4,55385723	55,4230739	-41,2	certain	1597
22.07.2019 04:05:31	Berta	4,55539307	55,4242469	-41,1	certain	1752
22.07.2019 04:05:32	Berta	4,55558344	55,4242132	-41,1	certain	1759
22.07.2019 04:12:09	Berta	4,56075376	55,4285729	-40,4	uncertain (anomalous)	2317
22.07.2019 04:12:09	Berta	4,56052837	55,4285941	-40,4	uncertain (anomalous)	2308
22.07.2019 04:12:10	Berta	4,56057576	55,4285829	-40,4	uncertain (anomalous)	2309
22.07.2019 04:12:10	Berta	4,56050357	55,4285815	-40,4	uncertain (anomalous)	2305
22.07.2019 04:12:10	Berta	4,56055329	55,4285757	-40,4	uncertain (anomalous)	2307
22.07.2019 04:12:21	Berta	4,56043571	55,4284326	-40,4	uncertain (anomalous)	2291
22.07.2019 04:12:24	Berta	4,56030912	55,4283981	-40,4	uncertain (anomalous)	2283
22.07.2019 04:12:38	Berta	4,56052966	55,4281183	-40,5	uncertain (anomalous)	2273
22.07.2019 04:38:47	Berta	4,54931573	55,414582	-42,2	uncertain (anomalous)	1037
22.07.2019 04:42:49	Berta	4,55458974	55,4197076	-41,6	certain	1465
22.07.2019 05:01:38	Berta	4,55544267	55,4188611	-41,7	certain	1486
22.07.2019 05:01:39	Berta	4,55554594	55,4187926	-41,7	uncertain (weak)	1490
22.07.2019 05:31:13	Berta	4,56478313	55,4261985	-40,9	certain	2367
22.07.2019 05:31:16	Berta	4,56485974	55,4262685	-40,9	certain	2375
22.07.2019 05:32:52	Berta	4,56606718	55,4274181	-40,7	uncertain (anomalous)	2509
22.07.2019 05:35:07	Berta	4,56566277	55,4256491	-41,0	uncertain (anomalous)	2384
22.07.2019 05:35:09	Berta	4,56590446	55,4255482	-41,0	uncertain (anomalous)	2392
22.07.2019 05:35:10	Berta	4,5660879	55,4254927	-41,0	uncertain (anomalous)	2399
22.07.2019 05:35:10	Berta	4,56623507	55,4254454	-41,0	uncertain (anomalous)	2404
22.07.2019 07:50:22	Berta	4,56819466	55,416662	-42,1	uncertain (anomalous)	2238
22.07.2019 07:50:23	Berta	4,56812005	55,4166627	-42,1	uncertain (anomalous)	2234
22.07.2019 07:50:25	Berta	4,56811971	55,4166019	-42,1	uncertain (anomalous)	2233
22.07.2019 07:50:30	Berta	4,56799907	55,416489	-42,1	uncertain (anomalous)	2224
22.07.2019 07:50:48	Berta	4,56745609	55,4162123	-42,1	uncertain (anomalous)	2188
22.07.2019 07:51:01	Berta	4,56717611	55,41594	-42,2	uncertain (anomalous)	2169
22.07.2019 07:51:58	Berta	4,56601742	55,4147629	-42,3	uncertain (anomalous)	2093
22.07.2019 07:51:59	Berta	4,56591657	55,4147733	-42,3	uncertain (anomalous)	2087
22.07.2019 07:52:34	Berta	4,56491514	55,4141542	-42,4	uncertain (anomalous)	2026
22.07.2019 11:50:49	Transit	4,52534255	55,3861533	-44,5	certain	2862
22.07.2019 12:20:41	Transit	4,60618252	55,3289833	-46,1	uncertain (anomalous)	7754
22.07.2019 14:39:27	Britta	4,76907917	55,1539018	-42,8	uncertain (anomalous)	1892
22.07.2019 14:39:30	Britta	4,76964493	55,1538166	-42,7	uncertain (anomalous)	1855
22.07.2019 15:10:45	Britta	4,75859526	55,1406552	-42,3	uncertain (anomalous)	2879
22.07.2019 17:12:37	Britta	4,76836149	55,1398383	-42,2	uncertain (anomalous)	2396
23.07.2019 03:39:38	Transit	4,82314113	55,2705273	-47,8	uncertain (anomalous)	1462
23.07.2019 16:52:54	Barbara	4,89095699	55,1157464	-40,4	certain	5920

4. Seafloor methane seepage related to salt diapirism in the northwestern part of the German North Sea

23.07.2019 20:29:20	Transit	5,03643998	55,2753222	-44,9	uncertain (weak)	6321
23.07.2019 20:29:36	Transit	5,03518471	55,2750631	-44,9	uncertain (anomalous)	6237
24.07.2019 04:20:49	Berta	4,53215856	55,4180207	-41,5	certain	336
24.07.2019 04:22:44	Berta	4,53067566	55,4214724	-40,9	certain	731
24.07.2019 11:26:01	Berta	4,55537952	55,4189416	-41,7	certain	1484
24.07.2019 11:26:07	Berta	4,55550161	55,4188954	-41,7	certain	1490
24.07.2019 11:26:09	Berta	4,55554717	55,4189131	-41,7	certain	1494
24.07.2019 11:26:30	Berta	4,55601489	55,4189341	-41,7	certain	1523
24.07.2019 11:42:48	Berta	4,5587859	55,4223556	-41,4	uncertain (weak)	1827
24.07.2019 11:47:23	Berta	4,55205033	55,4211473	-41,5	certain	1387
24.07.2019 11:47:29	Berta	4,55187831	55,4211531	-41,4	certain	1378
24.07.2019 12:00:13	Berta	4,53216703	55,4180265	-41,5	certain	337
24.07.2019 12:25:37	Berta	4,55693556	55,4194096	-41,7	certain	1594
24.07.2019 12:42:51	Berta	4,55279001	55,4220542	-41,3	certain	1479
24.07.2019 12:43:16	Berta	4,55243134	55,4217372	-41,4	certain	1441
24.07.2019 12:43:18	Berta	4,55235088	55,4217627	-41,4	certain	1438
24.07.2019 12:43:21	Berta	4,5520438	55,4219964	-41,3	certain	1435
24.07.2019 12:43:27	Berta	4,55189044	55,421987	-41,3	certain	1427
24.07.2019 12:43:53	Berta	4,55155948	55,4216273	-41,4	certain	1387
24.07.2019 12:44:07	Berta	4,55111826	55,4216712	-41,3	certain	1366
24.07.2019 12:44:08	Berta	4,55129551	55,4214818	-41,4	certain	1365
24.07.2019 12:44:11	Berta	4,55123792	55,4214766	-41,4	certain	1361
24.07.2019 12:44:19	Berta	4,55092245	55,4215689	-41,4	certain	1350
24.07.2019 12:44:25	Berta	4,55084876	55,4214797	-41,4	certain	1341
24.07.2019 12:57:03	Berta	4,53217209	55,4180245	-41,5	certain	337
24.07.2019 12:57:04	Berta	4,53215748	55,4180279	-41,5	certain	337
24.07.2019 13:45:45	Berta	4,55282773	55,4222807	-41,3	certain	1494
24.07.2019 13:45:47	Berta	4,55281238	55,4222495	-41,3	certain	1491
24.07.2019 13:45:49	Berta	4,55259927	55,4224304	-41,3	certain	1491
24.07.2019 13:45:53	Berta	4,55266323	55,4222153	-41,3	certain	1481
24.07.2019 13:45:57	Berta	4,55259037	55,4221684	-41,3	certain	1475
24.07.2019 13:45:59	Berta	4,55252731	55,422189	-41,3	certain	1473
24.07.2019 13:46:00	Berta	4,55233075	55,422377	-41,3	certain	1474
24.07.2019 13:46:05	Berta	4,55219337	55,4223926	-41,3	certain	1467
24.07.2019 13:46:11	Berta	4,55216805	55,4222123	-41,3	certain	1455
24.07.2019 13:46:14	Berta	4,55216109	55,4221402	-41,3	certain	1450
24.07.2019 13:46:17	Berta	4,55219405	55,4219865	-41,3	certain	1443
24.07.2019 13:46:18	Berta	4,55220172	55,4219451	-41,3	certain	1441
24.07.2019 13:46:23	Berta	4,55209879	55,4219058	-41,3	certain	1433
24.07.2019 13:46:23	Berta	4,55201202	55,4219879	-41,3	certain	1433
24.07.2019 13:46:24	Berta	4,55205556	55,4218978	-41,3	certain	1430
24.07.2019 13:46:28	Berta	4,55189237	55,4219802	-41,3	certain	1426
24.07.2019 13:46:28	Berta	4,55186697	55,4220021	-41,3	certain	1426
24.07.2019 13:46:30	Berta	4,55181195	55,4220232	-41,3	certain	1425
24.07.2019 13:46:41	Berta	4,55155535	55,4219462	-41,3	certain	1406

4. Seafloor methane seepage related to salt diapirism in the northwestern part of the German North Sea

24.07.2019 13:46:46	Berta	4,55139957	55,4219733	-41,3	certain	1400
24.07.2019 13:46:50	Berta	4,55137369	55,4218546	-41,3	certain	1391
24.07.2019 13:46:56	Berta	4,55115054	55,4219104	-41,3	certain	1383
24.07.2019 13:52:29	Berta	4,54343808	55,4203727	-41,4	uncertain (weak)	890
24.07.2019 13:52:39	Berta	4,54296445	55,4206862	-41,4	uncertain (weak)	893
24.07.2019 14:48:33	Berta	4,55396917	55,4230669	-41,2	certain	1603
24.07.2019 14:48:36	Berta	4,55400538	55,422947	-41,2	certain	1597
24.07.2019 14:48:40	Berta	4,55392761	55,4228954	-41,2	certain	1590
24.07.2019 14:48:43	Berta	4,55389631	55,4228495	-41,2	certain	1585
24.07.2019 14:49:05	Berta	4,55344814	55,422662	-41,2	certain	1550
24.07.2019 14:49:30	Berta	4,55276361	55,4225599	-41,2	certain	1508
24.07.2019 14:49:39	Berta	4,55253411	55,4225154	-41,2	certain	1493
24.07.2019 14:49:40	Berta	4,55258067	55,4224579	-41,3	certain	1492
24.07.2019 14:49:44	Berta	4,55239647	55,4225162	-41,3	certain	1486
24.07.2019 14:49:44	Berta	4,55237616	55,422536	-41,2	certain	1486
24.07.2019 14:49:45	Berta	4,55241033	55,4224726	-41,3	certain	1484
24.07.2019 14:49:45	Berta	4,55241094	55,4224498	-41,3	certain	1482
24.07.2019 14:49:46	Berta	4,55232683	55,4225	-41,3	certain	1481
24.07.2019 14:49:47	Berta	4,55234427	55,4224543	-41,3	certain	1479
24.07.2019 14:49:52	Berta	4,55218678	55,4224647	-41,3	certain	1472
24.07.2019 14:49:53	Berta	4,55213458	55,4224841	-41,3	certain	1470
24.07.2019 14:50:01	Berta	4,55203868	55,4223426	-41,3	certain	1456
24.07.2019 15:26:23	Berta	4,55081152	55,4200635	-41,5	uncertain (weak)	1261
24.07.2019 16:11:58	Berta	4,5324665	55,4169207	-41,6	uncertain (weak)	212
24.07.2019 21:21:52	Berta	4,51870243	55,4227447	-40,0	certain	1246
24.07.2019 21:21:53	Berta	4,51860855	55,4227415	-40,0	certain	1250
24.07.2019 21:22:00	Berta	4,51815691	55,4227033	-40,0	certain	1268
24.07.2019 23:29:53	Berta	4,55280837	55,422563	-41,2	certain	1510
24.07.2019 23:29:56	Berta	4,5527898	55,422455	-41,3	certain	1503
24.07.2019 23:29:57	Berta	4,55263382	55,4224647	-41,3	certain	1495
24.07.2019 23:29:59	Berta	4,55236845	55,4224767	-41,3	certain	1482
24.07.2019 23:30:02	Berta	4,55260568	55,4222771	-41,3	certain	1482
24.07.2019 23:30:03	Berta	4,55266154	55,4222293	-41,3	certain	1482
24.07.2019 23:30:04	Berta	4,55261298	55,4221972	-41,3	certain	1478
24.07.2019 23:30:05	Berta	4,55262657	55,4221393	-41,3	certain	1475
24.07.2019 23:30:10	Berta	4,55248378	55,4220266	-41,3	certain	1461
24.07.2019 23:30:13	Berta	4,55231598	55,421962	-41,3	certain	1448
24.07.2019 23:30:16	Berta	4,55254475	55,4217527	-41,4	certain	1448
24.07.2019 23:30:17	Berta	4,55202718	55,4219443	-41,3	certain	1431
24.07.2019 23:30:17	Berta	4,55236971	55,4218102	-41,4	certain	1442
24.07.2019 23:30:17	Berta	4,55225961	55,4218533	-41,3	certain	1438
24.07.2019 23:30:18	Berta	4,55244039	55,4217301	-41,4	certain	1441
24.07.2019 23:30:40	Berta	4,55175639	55,4211224	-41,4	certain	1369
25.07.2019 00:46:34	Berta	4,53217101	55,4180181	-41,5	certain	336
25.07.2019 02:00:43	Bella	4,50760594	55,4821146	-31,5	certain	411

4. Seafloor methane seepage related to salt diapirism in the northwestern part of the German North Sea

25.07.2019 02:14:17	Transit	4,47809806	55,4501411	-32,1	uncertain (anomalous)	3714
25.07.2019 02:18:37	Transit	4,46857452	55,4401877	-33,0	uncertain (anomalous)	4799
25.07.2019 02:19:27	Transit	4,46629446	55,4384403	-33,3	uncertain (anomalous)	4645
25.07.2019 07:21:56	Britta	4,80271641	55,1524092	-42,4	uncertain (weak)	267
25.07.2019 11:32:58	Transit	5,18272786	55,0454961	-39,0	certain	8885
25.07.2019 11:33:05	Transit	5,18334799	55,0453613	-39,0	certain	8916
25.07.2019 11:33:07	Transit	5,18349998	55,0452552	-39,0	certain	8931

Station-no.	Area	Device	Latitude (°N)	Longitude (°E)	Depth (m)	Methane (nM)	Ethane (nM)
HE537_05	Bella (B11-3)	MIC	55,478254	4,508487	32,2	7,11	bdl
HE537_05	Bella (B11-3)	MIC	55,478254	4,508487	32,2	6,88	bdl
HE537_06	Bella (B11-3)	CTD	55,478562	4,508615	31	5,48	bdl
HE537_06	Bella (B11-3)	CTD	55,478562	4,508615	24,9	4,22	bdl
HE537_06	Bella (B11-3)	CTD	55,478562	4,508615	20,1	3,83	bdl
HE537_06	Bella (B11-3)	CTD	55,478562	4,508615	14,9	4,92	bdl
HE537_06	Bella (B11-3)	CTD	55,478562	4,508615	10,6	3,98	bdl
HE537_06	Bella (B11-3)	CTD	55,478562	4,508615	5,9	3,42	bdl
HE537_07	Bella (B11-3)	CTD	55,478180	4,508713	29,8	6,58	bdl
HE537_07	Bella (B11-3)	CTD	55,478180	4,508713	28,5	6,95	bdl
HE537_07	Bella (B11-3)	CTD	55,478180	4,508713	24,5	3,65	bdl
HE537_07	Bella (B11-3)	CTD	55,478180	4,508713	19,4	4,70	bdl
HE537_07	Bella (B11-3)	CTD	55,478180	4,508713	13,7	4,67	bdl
HE537_07	Bella (B11-3)	CTD	55,478180	4,508713	8,8	5,12	bdl
HE537_07	Bella (B11-3)	CTD	55,478180	4,508713	4,5	4,74	bdl
HE537_08	Bella (B11-3)	CTD	55,478528	4,509063	28,8	5,89	bdl
HE537_08	Bella (B11-3)	CTD	55,478528	4,509063	24,7	6,09	bdl
HE537_08	Bella (B11-3)	CTD	55,478528	4,509063	18,8	4,77	bdl
HE537_08	Bella (B11-3)	CTD	55,478528	4,509063	14	3,77	bdl
HE537_08	Bella (B11-3)	CTD	55,478528	4,509063	9,3	3,94	bdl
HE537_08	Bella (B11-3)	CTD	55,478528	4,509063	5,5	4,14	bdl
HE537_09	Bella (B11-3)	CTD	55,478654	4,508841	30,6	5,44	bdl
HE537_09	Bella (B11-3)	CTD	55,478654	4,508841	25,5	5,70	bdl
HE537_09	Bella (B11-3)	CTD	55,478654	4,508841	20,4	4,47	bdl
HE537_09	Bella (B11-3)	CTD	55,478654	4,508841	15	4,31	bdl
HE537_09	Bella (B11-3)	CTD	55,478654	4,508841	10	3,96	bdl
HE537_09	Bella (B11-3)	CTD	55,478654	4,508841	5	4,01	bdl
HE537_11	Belinda (B15-1)	MIC	55,204356	4,727089	46,8	4,13	bdl
HE537_11	Belinda (B15-1)	MIC	55,204356	4,727089	46,8	4,32	bdl
HE537_12	Belinda (B15-1)	CTD	55,204379	4,725371	41,9	6,78	bdl
HE537_12	Belinda (B15-1)	CTD	55,204379	4,725371	38,6	7,19	bdl
HE537_12	Belinda (B15-1)	CTD	55,204379	4,725371	34,3	6,92	bdl
HE537_12	Belinda (B15-1)	CTD	55,204379	4,725371	28,8	6,34	bdl
HE537_12	Belinda (B15-1)	CTD	55,204379	4,725371	23,7	2,76	bdl
HE537_12	Belinda (B15-1)	CTD	55,204379	4,725371	17,7	2,39	bdl
HE537_12	Belinda (B15-1)	CTD	55,204379	4,725371	12,8	3,00	bdl
HE537_12	Belinda (B15-1)	CTD	55,204379	4,725371	7,4	2,56	bdl
HE537_12	Belinda (B15-1)	CTD	55,204379	4,725371	5,5	2,39	bdl
HE537_13	Belinda (B15-1)	CTD	55,204384	4,725750	44,4	5,56	bdl
HE537_13	Belinda (B15-1)	CTD	55,204384	4,725750	38,8	5,15	bdl
HE537_13	Belinda (B15-1)	CTD	55,204384	4,725750	34,2	5,45	bdl
HE537_13	Belinda (B15-1)	CTD	55,204384	4,725750	28,4	3,33	bdl
HE537_13	Belinda (B15-1)	CTD	55,204384	4,725750	23,8	2,74	bdl
HE537_13	Belinda (B15-1)	CTD	55,204384	4,725750	18,7	2,49	bdl
HE537_13	Belinda (B15-1)	CTD	55,204384	4,725750	13,1	2,30	bdl
HE537_13	Belinda (B15-1)	CTD	55,204384	4,725750	7,7	2,55	bdl
HE537_13	Belinda (B15-1)	CTD	55,204384	4,725750	4,3	2,70	bdl
HE537_14	Belinda (B15-1)	CTD	55,204367	4,725980	42,4	6,22	bdl

4. Seafloor methane seepage related to salt diapirism in the northwestern part of the German North Sea

HE537_14	Belinda (B15-1)	CTD	55,204367	4,725980	40	6,37	bdl
HE537_14	Belinda (B15-1)	CTD	55,204367	4,725980	37,6	5,25	bdl
HE537_14	Belinda (B15-1)	CTD	55,204367	4,725980	33,1	6,09	bdl
HE537_14	Belinda (B15-1)	CTD	55,204367	4,725980	30	5,97	bdl
HE537_14	Belinda (B15-1)	CTD	55,204367	4,725980	24,1	2,39	bdl
HE537_14	Belinda (B15-1)	CTD	55,204367	4,725980	18	2,25	bdl
HE537_14	Belinda (B15-1)	CTD	55,204367	4,725980	13,5	2,47	bdl
HE537_14	Belinda (B15-1)	CTD	55,204367	4,725980	4,7	2,48	bdl
HE537_15	Belinda (B15-1)	CTD	55,204662	4,725698	43,6	5,73	bdl
HE537_15	Belinda (B15-1)	CTD	55,204662	4,725698	42	5,16	bdl
HE537_15	Belinda (B15-1)	CTD	55,204662	4,725698	39,5	6,57	bdl
HE537_15	Belinda (B15-1)	CTD	55,204662	4,725698	35	6,19	bdl
HE537_15	Belinda (B15-1)	CTD	55,204662	4,725698	30,3	5,65	bdl
HE537_15	Belinda (B15-1)	CTD	55,204662	4,725698	24,6	2,63	bdl
HE537_15	Belinda (B15-1)	CTD	55,204662	4,725698	19	2,74	bdl
HE537_15	Belinda (B15-1)	CTD	55,204662	4,725698	14,1	2,92	bdl
HE537_15	Belinda (B15-1)	CTD	55,204662	4,725698	9,1	2,89	bdl
HE537_15	Belinda (B15-1)	CTD	55,204662	4,725698	6,5	3,05	bdl
HE537_17	Britta (B18-4)	MIC	55,152445	4,798311	43,6	9,77	bdl
HE537_18	Britta (B18-4)	CTD	55,152562	4,798113	40,9	9,92	bdl
HE537_18	Britta (B18-4)	CTD	55,152562	4,798113	39	10,94	bdl
HE537_18	Britta (B18-4)	CTD	55,152562	4,798113	34,4	9,41	bdl
HE537_18	Britta (B18-4)	CTD	55,152562	4,798113	25,9	4,87	bdl
HE537_18	Britta (B18-4)	CTD	55,152562	4,798113	24,4	2,77	bdl
HE537_18	Britta (B18-4)	CTD	55,152562	4,798113	19,3	2,70	bdl
HE537_18	Britta (B18-4)	CTD	55,152562	4,798113	13,8	2,67	bdl
HE537_18	Britta (B18-4)	CTD	55,152562	4,798113	9,2	2,94	bdl
HE537_18	Britta (B18-4)	CTD	55,152562	4,798113	5,2	2,48	bdl
HE537_19	Britta (B18-4)	CTD	55,152418	4,798695	41,1	11,77	bdl
HE537_19	Britta (B18-4)	CTD	55,152418	4,798695	38,8	11,65	bdl
HE537_19	Britta (B18-4)	CTD	55,152418	4,798695	34,8	11,68	bdl
HE537_19	Britta (B18-4)	CTD	55,152418	4,798695	28,9	11,82	bdl
HE537_19	Britta (B18-4)	CTD	55,152418	4,798695	24,7	3,34	bdl
HE537_19	Britta (B18-4)	CTD	55,152418	4,798695	19,5	2,88	bdl
HE537_19	Britta (B18-4)	CTD	55,152418	4,798695	14,5	2,76	bdl
HE537_19	Britta (B18-4)	CTD	55,152418	4,798695	9,3	2,65	bdl
HE537_19	Britta (B18-4)	CTD	55,152418	4,798695	5,5	2,75	bdl
HE537_20	Britta (B18-4)	CTD	55,152323	4,798688	38,9	11,03	bdl
HE537_20	Britta (B18-4)	CTD	55,152323	4,798688	36,8	11,18	bdl
HE537_20	Britta (B18-4)	CTD	55,152323	4,798688	35,1	11,77	bdl
HE537_20	Britta (B18-4)	CTD	55,152323	4,798688	28	9,65	bdl
HE537_20	Britta (B18-4)	CTD	55,152323	4,798688	24,6	2,85	bdl
HE537_20	Britta (B18-4)	CTD	55,152323	4,798688	19,1	2,50	bdl
HE537_20	Britta (B18-4)	CTD	55,152323	4,798688	14,2	2,78	bdl
HE537_20	Britta (B18-4)	CTD	55,152323	4,798688	9,4	2,86	bdl

4. Seafloor methane seepage related to salt diapirism in the northwestern part of the German North Sea

HE537_20	Britta (B18-4)	CTD	55,152323	4,798688	5,4	2,31	bdl
HE537_21	Britta (B18-4)	CTD	55,152828	4,798419	38,8	10,94	bdl
HE537_21	Britta (B18-4)	CTD	55,152828	4,798419	36,6	11,89	bdl
HE537_21	Britta (B18-4)	CTD	55,152828	4,798419	34,9	12,59	0,21
HE537_21	Britta (B18-4)	CTD	55,152828	4,798419	30,3	11,99	0,25
HE537_21	Britta (B18-4)	CTD	55,152828	4,798419	24,8	3,44	bdl
HE537_21	Britta (B18-4)	CTD	55,152828	4,798419	20,1	2,49	bdl
HE537_21	Britta (B18-4)	CTD	55,152828	4,798419	14,6	2,87	bdl
HE537_21	Britta (B18-4)	CTD	55,152828	4,798419	9,3	2,59	bdl
HE537_21	Britta (B18-4)	CTD	55,152828	4,798419	4,3	2,29	bdl
HE537_23	Britta (Flare site)	MIC	55,149380	4,790106	42,5	10,25	bdl
HE537_23	Britta (Flare site)	MIC	55,149380	4,790106	42,5	10,10	bdl
HE537_24	Britta (Flare site)	CTD	55,149433	4,790000	41,7	9,26	bdl
HE537_24	Britta (Flare site)	CTD	55,149433	4,790000	39,5	7,90	bdl
HE537_24	Britta (Flare site)	CTD	55,149433	4,790000	34,6	8,77	bdl
HE537_24	Britta (Flare site)	CTD	55,149433	4,790000	30,8	8,54	bdl
HE537_24	Britta (Flare site)	CTD	55,149433	4,790000	24,4	2,52	bdl
HE537_24	Britta (Flare site)	CTD	55,149433	4,790000	19,3	2,46	bdl
HE537_24	Britta (Flare site)	CTD	55,149433	4,790000	13,9	2,81	bdl
HE537_24	Britta (Flare site)	CTD	55,149433	4,790000	9	2,42	bdl
HE537_24	Britta (Flare site)	CTD	55,149433	4,790000	4,6	2,52	bdl
HE537_25	Britta (Flare site)	CTD	55,149281	4,790000	40,2	9,49	bdl
HE537_25	Britta (Flare site)	CTD	55,149281	4,790000	38,8	8,79	bdl
HE537_25	Britta (Flare site)	CTD	55,149281	4,790000	35,5	7,85	bdl
HE537_25	Britta (Flare site)	CTD	55,149281	4,790000	31,4	9,78	bdl
HE537_25	Britta (Flare site)	CTD	55,149281	4,790000	24,9	2,66	bdl
HE537_25	Britta (Flare site)	CTD	55,149281	4,790000	20	2,63	bdl
HE537_25	Britta (Flare site)	CTD	55,149281	4,790000	14,6	2,50	bdl
HE537_25	Britta (Flare site)	CTD	55,149281	4,790000	9,4	2,66	bdl
HE537_25	Britta (Flare site)	CTD	55,149281	4,790000	5,2	2,78	bdl
HE537_29	Birgit	CTD	55,327605	4,546512	43,2	9,05	bdl
HE537_29	Birgit	CTD	55,327605	4,546512	41,5	8,71	bdl
HE537_29	Birgit	CTD	55,327605	4,546512	38,5	8,49	bdl
HE537_29	Birgit	CTD	55,327605	4,546512	33,2	8,48	bdl
HE537_29	Birgit	CTD	55,327605	4,546512	29,1	8,20	bdl
HE537_29	Birgit	CTD	55,327605	4,546512	22,9	4,74	bdl
HE537_29	Birgit	CTD	55,327605	4,546512	23	3,99	bdl
HE537_29	Birgit	CTD	55,327605	4,546512	12,8	4,21	bdl
HE537_29	Birgit	CTD	55,327605	4,546512	4,4	3,98	bdl
HE537_30	Birgit	CTD	55,327484	4,546492	43	8,97	bdl
HE537_30	Birgit	CTD	55,327484	4,546492	38,3	8,81	bdl
HE537_30	Birgit	CTD	55,327484	4,546492	33,1	8,42	bdl
HE537_30	Birgit	CTD	55,327484	4,546492	29,2	8,75	bdl
HE537_30	Birgit	CTD	55,327484	4,546492	25,9	3,69	bdl
HE537_30	Birgit	CTD	55,327484	4,546492	23,1	4,36	bdl

4. Seafloor methane seepage related to salt diapirism in the northwestern part of the German North Sea

HE537_30	Birgit	CTD	55,327484	4,546492	17,8	4,67	bdl
HE537_30	Birgit	CTD	55,327484	4,546492	12,7	4,00	bdl
HE537_30	Birgit	CTD	55,327484	4,546492	4,4	4,33	bdl
HE537_31	Birgit	CTD	55,327399	4,546079	43	9,81	bdl
HE537_31	Birgit	CTD	55,327399	4,546079	40,7	8,70	bdl
HE537_31	Birgit	CTD	55,327399	4,546079	38,5	9,52	bdl
HE537_31	Birgit	CTD	55,327399	4,546079	33,3	8,70	bdl
HE537_31	Birgit	CTD	55,327399	4,546079	28,7	9,11	bdl
HE537_31	Birgit	CTD	55,327399	4,546079	23,2	3,31	bdl
HE537_31	Birgit	CTD	55,327399	4,546079	18,1	3,92	bdl
HE537_31	Birgit	CTD	55,327399	4,546079	12,9	3,56	bdl
HE537_31	Birgit	CTD	55,327399	4,546079	4,5	3,28	bdl
HE537_32	Birgit	CTD	55,327735	4,546074	42,7	7,85	bdl
HE537_32	Birgit	CTD	55,327735	4,546074	41,1	9,74	bdl
HE537_32	Birgit	CTD	55,327735	4,546074	38	9,50	bdl
HE537_32	Birgit	CTD	55,327735	4,546074	33,3	9,43	bdl
HE537_32	Birgit	CTD	55,327735	4,546074	29,1	9,40	bdl
HE537_32	Birgit	CTD	55,327735	4,546074	22,9	4,83	bdl
HE537_32	Birgit	CTD	55,327735	4,546074	17,6	3,84	bdl
HE537_32	Birgit	CTD	55,327735	4,546074	12,3	3,76	bdl
HE537_32	Birgit	CTD	55,327735	4,546074	4,1	3,73	bdl
HE537_33	Birgit	MIC	55,327873	4,546048	46,4	9,50	bdl
HE537_33	Birgit	MIC	55,327873	4,546048	46,4	9,81	bdl
HE537_33	Birgit	MIC	55,327873	4,546048	46,4	9,18	bdl
HE537_37	Belinda (B15-3)	CTD	55,282989	4,697848	45	5,62	bdl
HE537_37	Belinda (B15-3)	CTD	55,282989	4,697848	42,4	7,62	bdl
HE537_37	Belinda (B15-3)	CTD	55,282989	4,697848	38,2	6,52	bdl
HE537_37	Belinda (B15-3)	CTD	55,282989	4,697848	33,7	7,39	bdl
HE537_37	Belinda (B15-3)	CTD	55,282989	4,697848	29,5	7,24	bdl
HE537_37	Belinda (B15-3)	CTD	55,282989	4,697848	22,9	2,52	bdl
HE537_37	Belinda (B15-3)	CTD	55,282989	4,697848	18,2	2,61	bdl
HE537_37	Belinda (B15-3)	CTD	55,282989	4,697848	14,8	3,34	bdl
HE537_37	Belinda (B15-3)	CTD	55,282989	4,697848	4,6	3,20	bdl
HE537_38	Belinda (B15-3)	CTD	55,282934	4,697809	45,2	6,20	bdl
HE537_38	Belinda (B15-3)	CTD	55,282934	4,697809	42,8	6,47	bdl
HE537_38	Belinda (B15-3)	CTD	55,282934	4,697809	40	6,68	bdl
HE537_38	Belinda (B15-3)	CTD	55,282934	4,697809	30,2	6,64	bdl
HE537_38	Belinda (B15-3)	CTD	55,282934	4,697809	23,5	2,38	bdl
HE537_38	Belinda (B15-3)	CTD	55,282934	4,697809	16	2,83	bdl
HE537_38	Belinda (B15-3)	CTD	55,282934	4,697809	12,8	2,80	bdl
HE537_38	Belinda (B15-3)	CTD	55,282934	4,697809	10	2,78	bdl
HE537_38	Belinda (B15-3)	CTD	55,282934	4,697809	4,8	3,68	bdl
HE537_39	Belinda (B15-3)	CTD	55,282918	4,698132	45	6,67	bdl
HE537_39	Belinda (B15-3)	CTD	55,282918	4,698132	43	6,37	bdl
HE537_39	Belinda (B15-3)	CTD	55,282918	4,698132	38,9	6,25	bdl

4. Seafloor methane seepage related to salt diapirism in the northwestern part of the German North Sea

HE537_39	Belinda (B15-3)	CTD	55,282918	4,698132	33,9	6,08	bdl
HE537_39	Belinda (B15-3)	CTD	55,282918	4,698132	29,5	5,62	bdl
HE537_39	Belinda (B15-3)	CTD	55,282918	4,698132	23,5	3,20	bdl
HE537_39	Belinda (B15-3)	CTD	55,282918	4,698132	18	3,70	bdl
HE537_39	Belinda (B15-3)	CTD	55,282918	4,698132	13,1	3,65	bdl
HE537_39	Belinda (B15-3)	CTD	55,282918	4,698132	4,8	3,70	bdl
HE537_40	Belinda (B15-3)	CTD	55,282958	4,697861	44,9	5,39	bdl
HE537_40	Belinda (B15-3)	CTD	55,282958	4,697861	42,6	5,59	bdl
HE537_40	Belinda (B15-3)	CTD	55,282958	4,697861	38,6	7,66	bdl
HE537_40	Belinda (B15-3)	CTD	55,282958	4,697861	33,5	7,73	bdl
HE537_40	Belinda (B15-3)	CTD	55,282958	4,697861	30,9	5,56	bdl
HE537_40	Belinda (B15-3)	CTD	55,282958	4,697861	28,3	3,24	bdl
HE537_40	Belinda (B15-3)	CTD	55,282958	4,697861	21	2,95	bdl
HE537_40	Belinda (B15-3)	CTD	55,282958	4,697861	10,5	4,00	bdl
HE537_40	Belinda (B15-3)	CTD	55,282958	4,697861	4,5	4,08	bdl
HE537_41	Belinda (B15-3)	MIC	55,282791	4,697832	48,3	6,10	bdl
HE537_41	Belinda (B15-3)	MIC	55,282791	4,697832	48,3	6,18	bdl
HE537_52	Berta	CTD	55,414338	4,533693	38,6	102,70	bdl
HE537_52	Berta	CTD	55,414338	4,533693	32,3	94,28	bdl
HE537_52	Berta	CTD	55,414338	4,533693	33,3	84,78	bdl
HE537_52	Berta	CTD	55,414338	4,533693	28,8	66,63	bdl
HE537_52	Berta	CTD	55,414338	4,533693	22,4	7,88	bdl
HE537_52	Berta	CTD	55,414338	4,533693	15,7	5,20	bdl
HE537_52	Berta	CTD	55,414338	4,533693	12,6	5,04	bdl
HE537_52	Berta	CTD	55,414338	4,533693	4,2	4,64	bdl
HE537_53	Berta	CTD	55,415070	4,532533	38,7	112,64	bdl
HE537_53	Berta	CTD	55,415070	4,532533	36,7	113,22	bdl
HE537_53	Berta	CTD	55,415070	4,532533	33,2	99,78	bdl
HE537_53	Berta	CTD	55,415070	4,532533	28,7	82,38	bdl
HE537_53	Berta	CTD	55,415070	4,532533	22,9	10,42	bdl
HE537_53	Berta	CTD	55,415070	4,532533	15,8	4,76	bdl
HE537_53	Berta	CTD	55,415070	4,532533	12,9	4,08	bdl
HE537_53	Berta	CTD	55,415070	4,532533	4	4,06	bdl
HE537_54	Berta	CTD	55,415052	4,532729	39,2	119,08	bdl
HE537_54	Berta	CTD	55,415052	4,532729	36,1	114,10	bdl
HE537_54	Berta	CTD	55,415052	4,532729	32,9	114,50	bdl
HE537_54	Berta	CTD	55,415052	4,532729	28,4	59,80	bdl
HE537_54	Berta	CTD	55,415052	4,532729	22,4	7,56	bdl
HE537_54	Berta	CTD	55,415052	4,532729	16	4,81	bdl
HE537_54	Berta	CTD	55,415052	4,532729	12,6	4,33	bdl
HE537_54	Berta	CTD	55,415052	4,532729	4,1	4,44	bdl
HE537_55	Berta	CTD	55,415074	4,532834	39,2	101,56	bdl
HE537_55	Berta	CTD	55,415074	4,532834	35,7	96,24	bdl
HE537_55	Berta	CTD	55,415074	4,532834	32,6	103,98	bdl
HE537_55	Berta	CTD	55,415074	4,532834	30,2	105,68	bdl

4. Seafloor methane seepage related to salt diapirism in the northwestern part of the German North Sea

HE537_55	Berta	CTD	55,415074	4,532834	24,5	24,20	bdl
HE537_55	Berta	CTD	55,415074	4,532834	16,1	4,88	bdl
HE537_55	Berta	CTD	55,415074	4,532834	12,1	3,49	bdl
HE537_55	Berta	CTD	55,415074	4,532834	3,8	3,83	bdl
HE537_56	Berta	MIC	55,415217	4,533232	43,4	109,80	bdl
HE537_56	Berta	MIC	55,415217	4,533232	43,4	107,54	bdl
HE537_64	Berta	MIC	55,415151	4,525568	38	94,83	bdl
HE537_64	Berta	MIC	55,415151	4,525568	38	104,10	bdl
HE537_65	Berta	MIC	55,414461	4,532076	38,1	105,07	bdl
HE537_65	Berta	MIC	55,414461	4,532076	38,1	113,80	bdl
HE537_66	Berta	MIC	55,413917	4,534117	40,1	107,16	bdl
HE537_66	Berta	MIC	55,413917	4,534117	40,1	109,88	bdl
HE537_67	Berta	MIC	55,414860	4,541235	40,6	106,39	bdl
HE537_67	Berta	MIC	55,414860	4,541235	40,6	110,52	bdl
HE537_68	Berta	CTD	55,415330	4,531604	38,9	114,94	bdl
HE537_68	Berta	CTD	55,415330	4,531604	35,6	114,88	bdl
HE537_68	Berta	CTD	55,415330	4,531604	32,7	113,05	bdl
HE537_68	Berta	CTD	55,415330	4,531604	25,9	5,69	bdl
HE537_68	Berta	CTD	55,415330	4,531604	19,4	5,17	bdl
HE537_68	Berta	CTD	55,415330	4,531604	14	5,33	bdl
HE537_68	Berta	CTD	55,415330	4,531604	7	5,42	bdl
HE537_59	SE of Berta (B11-1)	CTD	55,404974	4,623159	41,9	32,92	bdl
HE537_59	SE of Berta (B11-1)	CTD	55,404974	4,623159	40,2	33,46	bdl
HE537_59	SE of Berta (B11-1)	CTD	55,404974	4,623159	34,2	38,34	bdl
HE537_59	SE of Berta (B11-1)	CTD	55,404974	4,623159	29,7	33,43	bdl
HE537_59	SE of Berta (B11-1)	CTD	55,404974	4,623159	25,9	5,76	bdl
HE537_59	SE of Berta (B11-1)	CTD	55,404974	4,623159	16,2	5,18	bdl
HE537_59	SE of Berta (B11-1)	CTD	55,404974	4,623159	9,7	4,60	bdl
HE537_59	SE of Berta (B11-1)	CTD	55,404974	4,623159	5,5	4,87	bdl
HE537_60	SE of Berta (B11-1)	CTD	55,404993	4,622496	42,4	28,64	bdl
HE537_60	SE of Berta (B11-1)	CTD	55,404993	4,622496	40,4	29,39	bdl
HE537_60	SE of Berta (B11-1)	CTD	55,404993	4,622496	35	29,81	bdl
HE537_60	SE of Berta (B11-1)	CTD	55,404993	4,622496	29,6	32,38	bdl
HE537_60	SE of Berta (B11-1)	CTD	55,404993	4,622496	25,5	6,48	bdl
HE537_60	SE of Berta (B11-1)	CTD	55,404993	4,622496	18,3	5,98	bdl

4. Seafloor methane seepage related to salt diapirism in the northwestern part of the German North Sea

HE537_60	SE of Berta (B11-1)	CTD	55,404993	4,622496	10,9	4,93	bdl
HE537_60	SE of Berta (B11-1)	CTD	55,404993	4,622496	5,9	4,80	bdl
HE537_61	SE of Berta (B11-1)	CTD	55,405135	4,622721	42,3	24,86	bdl
HE537_61	SE of Berta (B11-1)	CTD	55,405135	4,622721	39,7	25,24	bdl
HE537_61	SE of Berta (B11-1)	CTD	55,405135	4,622721	33,8	26,87	bdl
HE537_61	SE of Berta (B11-1)	CTD	55,405135	4,622721	28,5	26,78	bdl
HE537_61	SE of Berta (B11-1)	CTD	55,405135	4,622721	25,5	4,98	bdl
HE537_61	SE of Berta (B11-1)	CTD	55,405135	4,622721	18,2	5,01	bdl
HE537_61	SE of Berta (B11-1)	CTD	55,405135	4,622721	10,8	4,19	bdl
HE537_61	SE of Berta (B11-1)	CTD	55,405135	4,622721	4,8	4,56	bdl
HE537_62	SE of Berta (B11-1)	CTD	55,405225	4,622337	41,9	15,51	bdl
HE537_62	SE of Berta (B11-1)	CTD	55,405225	4,622337	39,4	19,88	bdl
HE537_62	SE of Berta (B11-1)	CTD	55,405225	4,622337	33,2	21,83	bdl
HE537_62	SE of Berta (B11-1)	CTD	55,405225	4,622337	28,3	27,47	bdl
HE537_62	SE of Berta (B11-1)	CTD	55,405225	4,622337	24,9	7,29	bdl
HE537_62	SE of Berta (B11-1)	CTD	55,405225	4,622337	17,9	4,44	bdl
HE537_62	SE of Berta (B11-1)	CTD	55,405225	4,622337	10,6	4,91	bdl
HE537_62	SE of Berta (B11-1)	CTD	55,405225	4,622337	4,6	3,39	bdl
HE537_63	SE of Berta (B11-1)	MIC	55,404938	4,622884	45,6	19,06	bdl
HE537_63	SE of Berta (B11-1)	MIC	55,404938	4,622884	45,6	16,58	bdl
HE537_70	E of Belinda (B15-2)	CTD	55,261548	4,848015	45,4	7,45	bdl
HE537_70	E of Belinda (B15-2)	CTD	55,261548	4,848015	43,7	8,16	bdl
HE537_70	E of Belinda (B15-2)	CTD	55,261548	4,848015	38,6	8,57	bdl
HE537_70	E of Belinda (B15-2)	CTD	55,261548	4,848015	32	9,12	bdl
HE537_70	E of Belinda (B15-2)	CTD	55,261548	4,848015	22,8	3,97	bdl

4. Seafloor methane seepage related to salt diapirism in the northwestern part of the German North Sea

HE537_70	E of Belinda (B15-2)	CTD	55,261548	4,848015	13	3,77	bdl
HE537_70	E of Belinda (B15-2)	CTD	55,261548	4,848015	4,6	3,70	bdl
HE537_71	E of Belinda (B15-2)	CTD	55,264395	4,844014	45,1	7,90	bdl
HE537_71	E of Belinda (B15-2)	CTD	55,264395	4,844014	42,9	8,14	bdl
HE537_71	E of Belinda (B15-2)	CTD	55,264395	4,844014	38,8	8,23	bdl
HE537_71	E of Belinda (B15-2)	CTD	55,264395	4,844014	30,2	8,17	bdl
HE537_71	E of Belinda (B15-2)	CTD	55,264395	4,844014	22,2	3,26	bdl
HE537_71	E of Belinda (B15-2)	CTD	55,264395	4,844014	14	3,45	bdl
HE537_71	E of Belinda (B15-2)	CTD	55,264395	4,844014	4,8	3,63	bdl
HE537_72	E of Belinda (B15-2)	CTD	55,264587	4,843626	45,5	6,96	bdl
HE537_72	E of Belinda (B15-2)	CTD	55,264587	4,843626	43,2	7,12	bdl
HE537_72	E of Belinda (B15-2)	CTD	55,264587	4,843626	38,9	7,59	bdl
HE537_72	E of Belinda (B15-2)	CTD	55,264587	4,843626	32,1	7,99	bdl
HE537_72	E of Belinda (B15-2)	CTD	55,264587	4,843626	19,3	2,95	bdl
HE537_72	E of Belinda (B15-2)	CTD	55,264587	4,843626	14,3	3,26	bdl
HE537_72	E of Belinda (B15-2)	CTD	55,264587	4,843626	5,2	3,77	bdl
HE537_73	E of Belinda (B15-2)	CTD	55,264468	4,843396	45,1	7,74	bdl
HE537_73	E of Belinda (B15-2)	CTD	55,264468	4,843396	38,4	8,24	bdl
HE537_73	E of Belinda (B15-2)	CTD	55,264468	4,843396	33,1	8,29	bdl
HE537_73	E of Belinda (B15-2)	CTD	55,264468	4,843396	21,7	3,60	bdl
HE537_73	E of Belinda (B15-2)	CTD	55,264468	4,843396	13,2	3,60	bdl
HE537_73	E of Belinda (B15-2)	CTD	55,264468	4,843396	4,1	3,44	bdl
HE537_74	E of Belinda (B15-2)	MIC	55,264309	4,843238	48,2	9,54	bdl
HE537_74	E of Belinda (B15-2)	MIC	55,264309	4,843238	48,2	7,51	bdl
HE537_76	Britta (B18-4)	MIC	55,152676	4,799657	43,2	17,66	0,39
HE537_77	Britta (B18-4)	MIC	55,152402	4,799021	43,9	16,86	0,32
HE537_78	Britta (B18-4)	MIC	55,152088	4,799046	43,2	17,43	0,42

4. Seafloor methane seepage related to salt diapirism in the northwestern part of the German North Sea

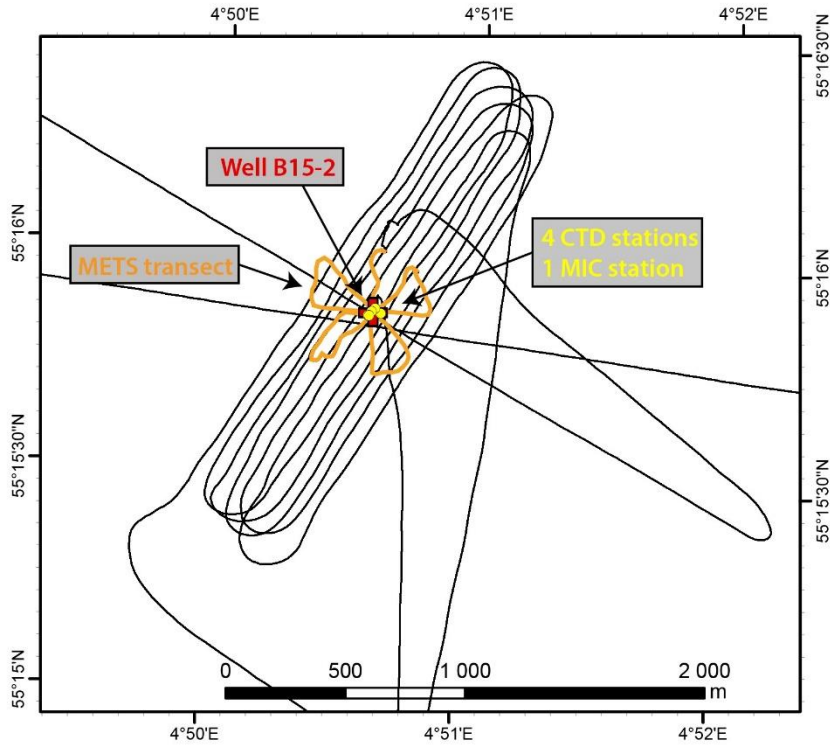
HE537_79	Britta (B18-4)	MIC	55,151712	4,799036	43	16,91	0,41
HE537_80	Britta (B18-4)	MIC	55,151356	4,798932	43,4	16,45	0,40
HE537_81	Britta (B18-4)	MIC	55,151047	4,798815	43,1	17,44	0,45
HE537_45	Dutch Dogger Bank	CTD	55,304485	4,094171	41	644,31	bdl
HE537_45	Dutch Dogger Bank	CTD	55,304485	4,094171	39,1	686,28	bdl
HE537_45	Dutch Dogger Bank	CTD	55,304485	4,094171	36,9	1454,99	bdl
HE537_45	Dutch Dogger Bank	CTD	55,304485	4,094171	33,4	942,14	bdl
HE537_45	Dutch Dogger Bank	CTD	55,304485	4,094171	25,8	464,86	2,30
HE537_45	Dutch Dogger Bank	CTD	55,304485	4,094171	19,6	1263,84	0,55
HE537_45	Dutch Dogger Bank	CTD	55,304485	4,094171	15,5	936,50	bdl
HE537_45	Dutch Dogger Bank	CTD	55,304485	4,094171	9,8	683,84	bdl
HE537_45	Dutch Dogger Bank	CTD	55,304485	4,094171	6,1	264,32	bdl
HE537_45	Dutch Dogger Bank	CTD	55,304485	4,094171	41	983,21	bdl
HE537_46	Dutch Dogger Bank	CTD	55,305832	4,092236	38,8	1435,59	bdl
HE537_46	Dutch Dogger Bank	CTD	55,305832	4,092236	36,7	1046,43	bdl
HE537_46	Dutch Dogger Bank	CTD	55,305832	4,092236	33,7	436,32	bdl
HE537_46	Dutch Dogger Bank	CTD	55,305832	4,092236	27,8	704,72	bdl
HE537_46	Dutch Dogger Bank	CTD	55,305832	4,092236	23,3	402,68	bdl
HE537_46	Dutch Dogger Bank	CTD	55,305832	4,092236	18	132,12	bdl
HE537_46	Dutch Dogger Bank	CTD	55,305832	4,092236	13,1	85,75	bdl
HE537_46	Dutch Dogger Bank	CTD	55,305832	4,092236	5,7	19,17	bdl
HE537_47	Dutch Dogger Bank	CTD	55,305681	4,091218	40,1	2037,79	bdl
HE537_47	Dutch Dogger Bank	CTD	55,305681	4,091218	38,6	2084,50	bdl
HE537_47	Dutch Dogger Bank	CTD	55,305681	4,091218	36,7	844,11	bdl
HE537_47	Dutch Dogger Bank	CTD	55,305681	4,091218	33,5	556,09	bdl
HE537_47	Dutch Dogger Bank	CTD	55,305681	4,091218	30	499,05	bdl
HE537_47	Dutch Dogger Bank	CTD	55,305681	4,091218	25,5	287,05	bdl

4. Seafloor methane seepage related to salt diapirism in the northwestern part of the German North Sea

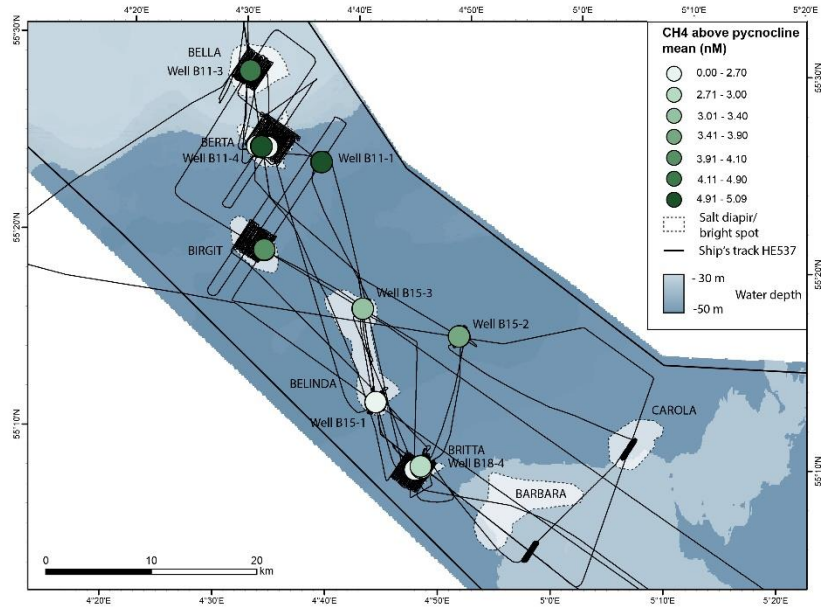
HE537_47	Dutch Dogger Bank	CTD	55,305681	4,091218	20,1	274,34	bdl
HE537_47	Dutch Dogger Bank	CTD	55,305681	4,091218	14	54,03	bdl
HE537_47	Dutch Dogger Bank	CTD	55,305681	4,091218	5,4	18,27	bdl
HE537_48	Dutch Dogger Bank	CTD	55,305527	4,090916	40,7	345,21	bdl
HE537_48	Dutch Dogger Bank	CTD	55,305527	4,090916	39	221,25	bdl
HE537_48	Dutch Dogger Bank	CTD	55,305527	4,090916	36,8	241,18	bdl
HE537_48	Dutch Dogger Bank	CTD	55,305527	4,090916	33,2	636,12	bdl
HE537_48	Dutch Dogger Bank	CTD	55,305527	4,090916	30,3	368,97	bdl
HE537_48	Dutch Dogger Bank	CTD	55,305527	4,090916	25,3	672,73	bdl
HE537_48	Dutch Dogger Bank	CTD	55,305527	4,090916	20	250,59	bdl
HE537_48	Dutch Dogger Bank	CTD	55,305527	4,090916	15,1	232,45	bdl
HE537_48	Dutch Dogger Bank	CTD	55,305527	4,090916	5,7	17,36	bdl
HE537_49	Dutch Dogger Bank	MIC	55,305835	4,091021	44,2	1096,73	bdl
HE537_49	Dutch Dogger Bank	MIC	55,305835	4,091021	44,2	11135,75	1,46
HE537_49	Dutch Dogger Bank	MIC	55,305835	4,091021	44,2	8200,56	1,58

Supplementary table 2: Water (CTD casts) and bottom water (MIC stations) with station numbers and methane and ethane values.

4. Seafloor methane seepage related to salt diapirism in the northwestern part of the German North Sea



Supplementary figure 1: Example of a METS survey and sampling strategy.



Supplementary figure 2: Observed CH₄ oversaturation in the working area.

5. Source rocks of the German Central Graben

This chapter has been published as Müller, S., Arfai, J., Jähne-Klingberg, F., Bense, F., & Weniger, P., 2020. Source rocks of the German Central Graben. *Marine and Petroleum Geology*, 113, 104-120.

Abstract

Jurassic to Lower Cretaceous formations are the most important source rocks for hydrocarbons in the southern Central Graben area. Within the Dutch Central Graben, the Lower Jurassic Posidonia Shale Formation is the most prolific source for hydrocarbons, while the Upper Jurassic to Lowermost Cretaceous Bo Member of the Farsund Formation plays this role in the Danish Central Graben. Oil and gas discoveries in the Norwegian, Dutch and Danish part of the Central Graben proved a prolific petroleum system. Despite limited success of hydrocarbon exploration in the German part of the Central Graben, various indications suggest migration of gas out of active thermogenic source rocks that are closely related to potential shallow gas accumulations. These indications include the restricted location of the bright spots above the Jurassic graben system, the occurrence of gas chimneys underneath these accumulations and geochemical data from offshore The Netherlands, which support contribution of thermogenic gas. The purpose of this study is to assess the potential for generating thermogenic hydrocarbons from Upper Triassic to Lower Cretaceous formations. For this reason, prominent source rocks of the Southern North Sea, i.e., the Posidonia Shale Formation and the Upper Jurassic to Lower Cretaceous “Hot Shales” (namely Clay Deep Member offshore The Netherlands and Bo Member offshore Denmark), were mapped in detail. These and other potential formations from the Late Triassic to the Early Cretaceous are integrated into an existing petroleum system model of the Northern German North Sea, which was modified for the new requirements. The results showed that the main source rocks of the southern Central Graben, the Posidonia Shale Formation, and the Upper Jurassic – Lower Cretaceous “Hot Shales” are insignificant as sources for commercial hydrocarbon accumulations within the German Central Graben area. That is either due to marginal occurrence or to low maturity. However, Lower to Upper Jurassic formations such as marine claystones of the Aalburg Formation and the lower parts of the Kimmeridge Clay Formation, as well as coaly intervals of the Central Graben Subgroup, are likely to have generated, and still generate, hydrocarbons.

5.1. Introduction

The Central Graben area is an important province for the petroleum industry of The Netherlands and Denmark. Gas produced in The Netherlands, the third largest gas producer in the EU (BP, 2018), is mainly sourced from Upper Carboniferous coals and shales (mostly Westphalian B), which vanish in the northern Dutch offshore towards the German border (Lokhorst, 1998; Gerling et al., 1999; van Buggenum and den Hartog Jager, 2007). Other potential gas source rocks in the Dutch Central Graben are coals of the Central Graben Subgroup, and Viséan coals in the northern offshore area (de Jager and Geluk, 2007). There are ambiguous indications for either a microbial or a thermogenic origin of shallow gas in the Dutch Central and Step Graben area (ten Veen et al., 2013).

A significant part of the Dutch oil - and some of the gas - production derives from reservoirs of the Central Graben, which are primarily sourced by the Lower Jurassic Posidonia Shale Formation. In the northern Dutch Central Graben, the Clay Deep Member of the Upper Jurassic

Lutine Formation (Upper Jurassic to Lower Cretaceous Scruff Group), which today is over-mature, likely generated oil in the past (de Jager and Geluk, 2007). The time equivalent Bo Member of the Farsund Formation in the Danish Central Graben is regarded as the main source rock for hydrocarbons in offshore Denmark (Ineson et al., 2003). Because the Bo Member itself is not sufficient to explain the volumes of hydrocarbons in the area, new research explores other potential sources of the hydrocarbons in place (Ponsaing et al., 2018). These additional sources include the lower sections of the Upper Jurassic Farsund Formation, which is less rich in organic matter, but shows potential to generate gas and oil (Petersen et al., 2017; Ponsaing et al., 2018) and Middle Jurassic coals (Bryne and Lulu Fms.). Petersen and Hertle (2018) and Petersen et al. (2018) recently discussed the potential of Middle Jurassic coals as an additional source for gas and oil in the Danish Central Graben.

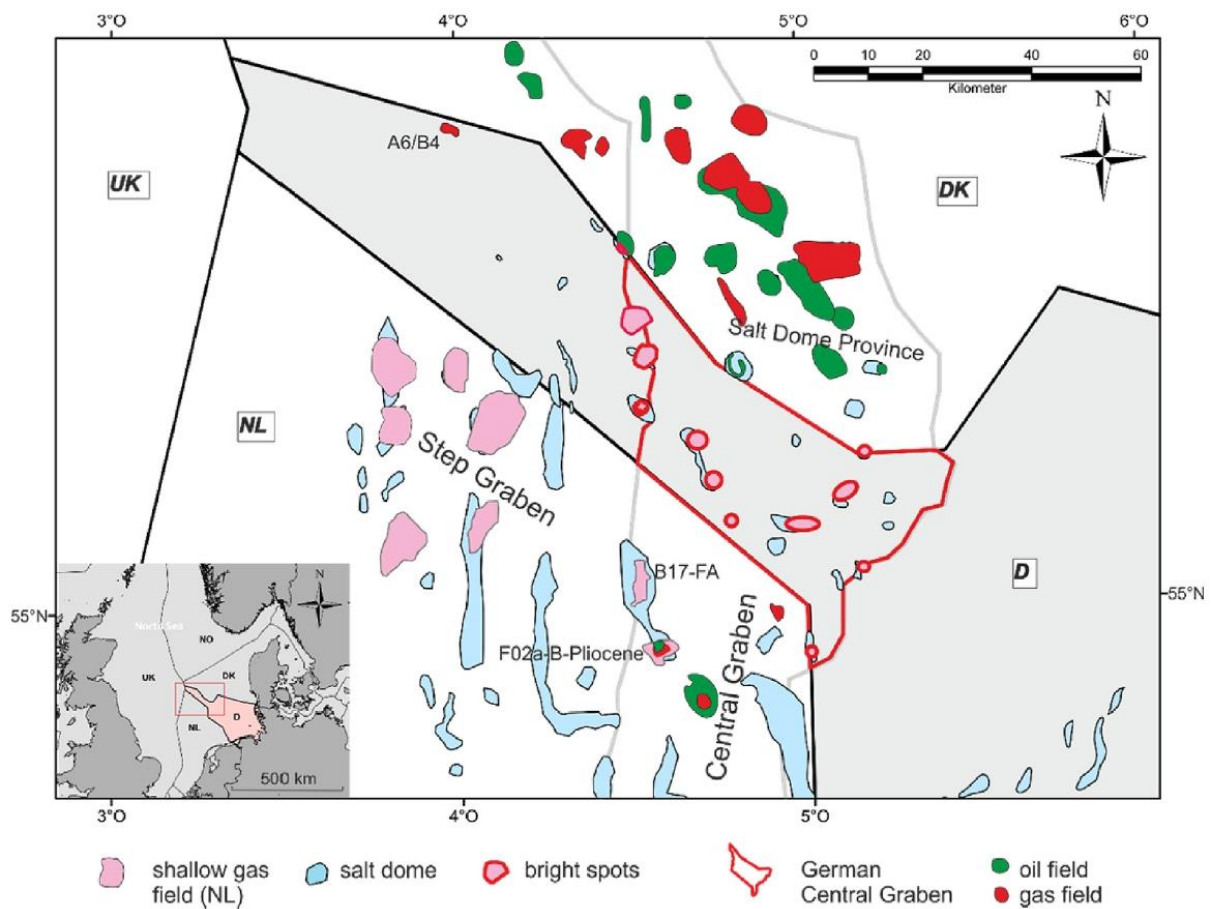


Fig. 33 Location of bright spot indicators of shallow gas accumulations in the German Central Graben, and location of oil and gas fields in adjacent Dutch and Danish parts of the Graben (EBN, 2016; Müller et al., 2018). Note that shallow gas fields in the Dutch sector and bright spots in the German Central Graben are located above Zechstein salt domes. The outlines of the salt structures are modified from Reinhold et al. (2008) and Arfai et al. (2014), the outline of the Central Graben from Pharaoh et al. (2010) and Arfai et al. (2014).

Even though it forms the geographic link between the Dutch and the Danish part of the graben, where rich oil and gas accumulations were discovered, almost no hydrocarbons were found in the German Central Graben. Potential shallow gas accumulations above Zechstein salt domes,

indicated by high amplitude reflections (bright spots), are an exception that may suggest the presence of an active thermogenic source rock in the area (Fig. 33). Amplitude anomalies on reflection seismic data, so-called “gas chimneys”, underneath bright spots indicate vertical gas migration from a deeper source (Müller et al., 2018, Fig. 38). In addition, the geographic limitation of the shallow gas accumulations in the area hypothesizes a source within the Jurassic graben system. Furthermore, adsorbed gases from cuttings from the nearby field B17-FA in the Dutch Central Graben (Fig. 33) are of a mixed thermogenic-microbial origin and the F02a-B-Pliocene shallow gas field is located directly above an oil field that is sourced by the Lower Jurassic Posidonia Shale Formation (Kombrink et al., 2012). Arfai and Lutz (2017) investigated the potential for petroleum generation for the northern German North Sea, including the Central Graben. Their petroleum system model, which constitutes a basis for this work, included three source rocks. The Namurian- Viséan, as the most probable source rock for the A6/B4 gas field in the northernmost German North Sea.

Additionally, the Posidonia Shale Formation and the Upper Jurassic – Lower Cretaceous ‘Hot Shales’ (time equivalent to the Clay Deep Member in the Dutch Central Graben, the Bo Member in the Danish Central Graben and the Mandal Formation in the Norwegian Central Graben) as the two most important oil source rocks in the southern North Sea. Their distribution maps of these source rocks were deduced from the top Lower Jurassic (Posidonia Shale Formation) and Upper Jurassic (“Hot Shales”), which were mapped. Main objectives of the present publication were to present new distribution maps of the Posidonia Shale Formation and the Clay Deep Member, based on all available geophysical data, and to discuss potential contribution from additional source rocks, including Middle Jurassic coals and Upper Triassic shales. The focus of this study is on potentially active source rocks from the Uppermost Triassic to the Lowermost Cretaceous. The tectonic history of the Central Graben was most active during the Jurassic, which led to the deposition and preservation of significant Jurassic sediments. Older Paleozoic formations are over-mature, though, and therefore constitute no active hydrocarbon system (Arfai and Lutz, 2017). The results are intended to advance the discussion of the exploration potential of the German North Sea.

5.2. Geology of the Central Graben

The Central Graben is one of the most prominent Mesozoic rift structures within the Central European Basin system and a major hydrocarbon province in the North Sea (Littke et al., 2008; Pletsch et al., 2010). It is the southern arm of a triple junction rift system, which shows first extensional pulses during the break-up of the supercontinent Pangea from the Permian to the Triassic (Ziegler, 1990; Stemmerik et al., 2000). The German Central Graben takes an exceptional position as the link between the NW-SE trending Danish and the NE-SW trending Dutch Central Graben. Compared to parts of the graben in the Dutch and Danish offshore area, the German Central Graben takes a structurally higher position, which is probably mainly related to a more distinct structural inversion during the Late Cretaceous (Arfai et al., 2014). The high intense structural inversion greatly affected the sedimentation and hydrocarbon genesis of this part of the graben during the Late Cretaceous. Despite its exceptional position, the lithofacies

of most of the Mesozoic is equivalent and genetically related to the lithology of the adjacent Dutch and Danish Central Graben (Fig. 34). The Central Graben is genetically a half-graben, whose eastern flank is formed by a major fault array, the Schillgrund Fault (also called Coffee Soil Fault in the Danish offshore), and whose western flank is dominated by a series of horst and graben structures (Step Graben System) (Ter Borgh et al., 2018). Within its German part, the Central Graben has a differentiated internal structure, which features several sub-basins and –grabens (Fig. 35). During the Late Triassic and the Early Jurassic, the southern North Sea area was dominated by a shallow epicontinental sea, which is manifested by the deposition of fine-grained mudstones of the Altena Group offshore The Netherlands and its equivalents like the Fjerritslev

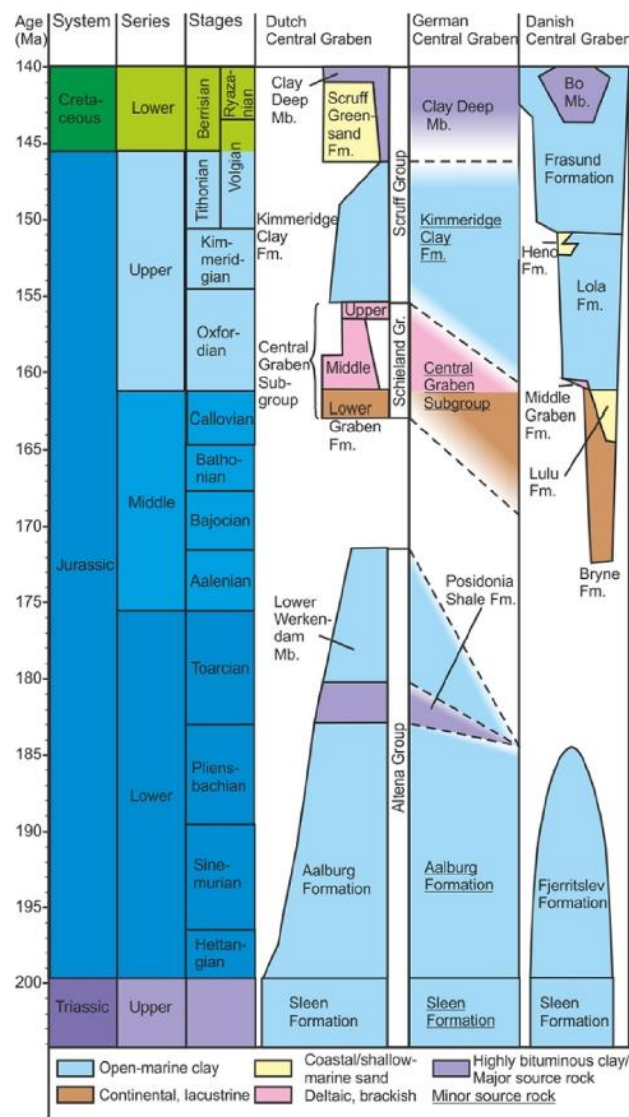


Fig. 34 Lithostratigraphic column of the Jurassic in the southern Central Graben (modified from Lott et al. (2010) for the Dutch and Danish Central Graben). The Dutch nomenclature is adopted for the formations of the German Central Graben. The presence of the formations in the German Central Graben is endorsed by well and reflection seismic data, but there is uncertainty about their place in time and lithological/facial composition as well as the distributional pattern. From the Late Triassic to the Middle Jurassic, the area was characterized by a shallow epicontinental sea, which resulted in the deposition of marine clay. During the Middle Jurassic, erosion and non-deposition was the consequence of the appearance of the Mid-North Sea Dome (Underhill and Partington, 1993). After its collapse, deposition and subsidence started again. At first with continental and deltaic sediments of the Central Graben Subgroup, then with the marine clays of the Scruff Group (Wong, 2007).

Formation offshore Denmark. (Lott et al., 2010, Fig. 34). After the Mid- Jurassic uplift of the central North Sea area during the Late Aalenian to Bajocian, which is attributed to the development of the Central North Sea thermal dome (Ziegler, 1992; Graversen, 2006), main rifting of the Central Graben started at the Callovian (Michelsen et al., 2003; Møller and Rasmussen, 2003). The uplift event marked the end of a laminar depositional system, which dominated in the Lower and Middle Jurassic and resulted in the regional Mid-Cimmerian Unconformity. Within the German Central Graben, the uplift stopped the deposition of the Altena Group and even resulted in erosion at structural highs. Especially the area of the Clemens Basins and the Clemens Graben were affected by the uplift (Fig. 35; Fig. 37). The end of the thermal uplift and a resuming subsidence is manifested at first by the deposition of continental and deltaic sediments of the Central Graben Subgroup (equivalent to the Bryne, Lulu, and Middle Graben Formation offshore Denmark) and then of the marine claystones of the Scruff Group (equivalent to the Lola and Farsund Formation offshore Denmark) (Fig. 34). A more complex system of platforms and basins evolved due to increased rifting and intensified halokinesis during the Late Jurassic, including the Johannes Graben, John Graben, Clemens Graben, and Clemens Basin offshore Germany (Fig. 35). While platform areas were subject to erosion or sediment starvation, major rifting resulted in differential subsidence and rapid deposition of Upper Jurassic sediments in the Central Graben (Herngreen et al., 2003; Andsbjerg and Dybkjaer, 2003). Especially structural lows, like the John Graben and the developing Clemens Graben, experienced intense subsidence and sedimentation (Fig. 35; Fig. 37). Rifting ceased after the Late Cimmerian II pulse in the Late Ryazanian (Wong, 2007). In the following post-rift thermal sag phase, a more even sedimentation replaced the differential subsidence. During the Early Cretaceous, the region was subject to a long-term transgression (Herngreen and Wong, 2007), leading to the deposition of the Rijnland Group in the Dutch and of the Cromer Knoll Group in the Danish Central Graben. Contraction and transpression during the Late Cretaceous resulted in a highly active sedimentary environment and the deposition of shallow marine carbonates (Chalk Group). The compressional phase ceased until the Early Paleocene, after much of the Cretaceous within the now inverted Jurassic basins was eroded and redistributed (Herngreen and Wong, 2007). During the Paleogene, an intracratonic sag basin developed on top, but without reactivating the Mesozoic rift structures of the Central Graben (Huuse and Clausen, 2001), and the North Sea Basin reached its present-day condition.

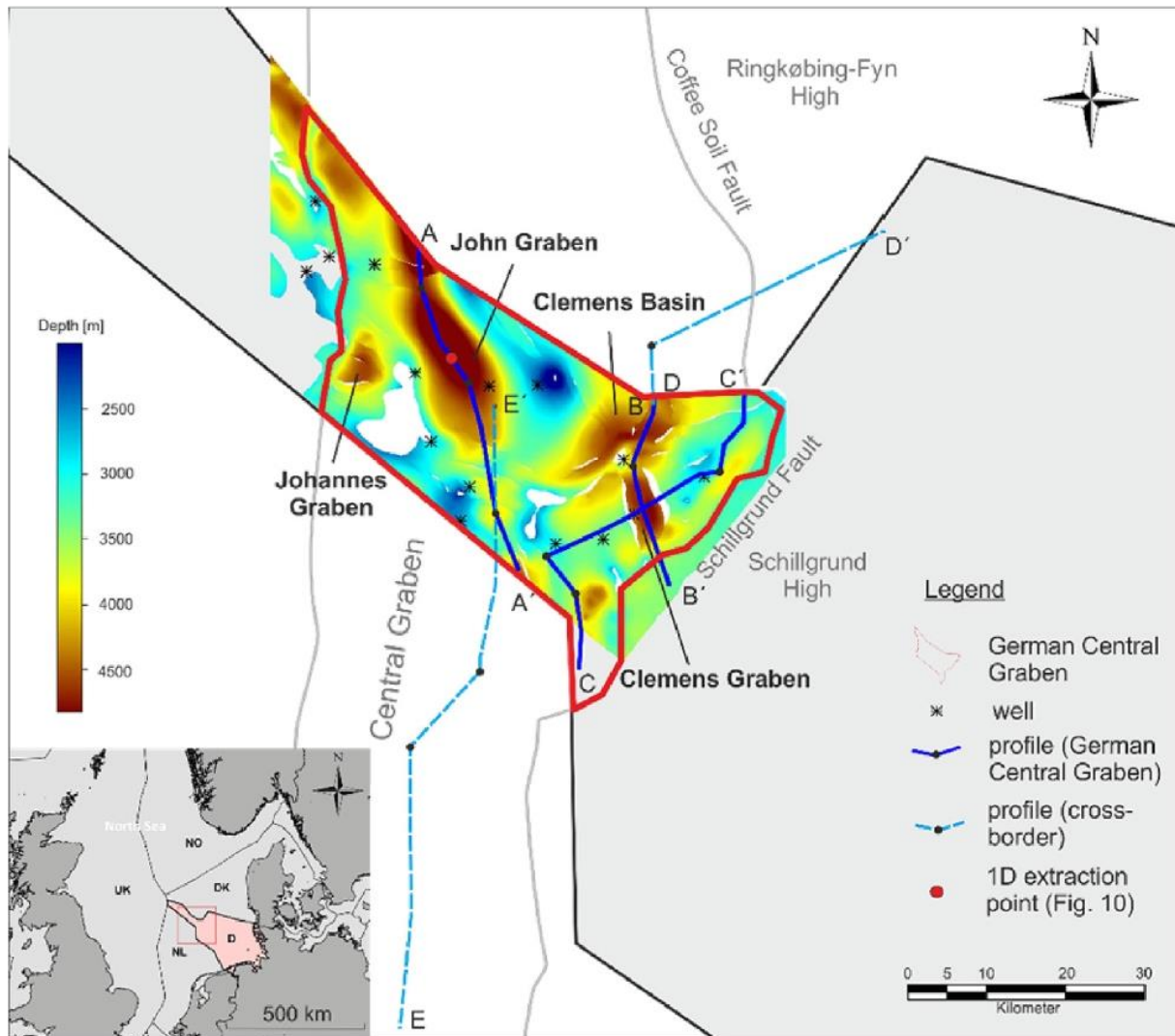


Fig. 35 Map of the base Upper Jurassic of the German Central Graben. Increased rifting and intense halotectonics during the Late Jurassic resulted in a differentiated structural relief of various sub-basins and – grabens. These structures mainly affect the distribution and thickness distribution of Jurassic formations, which may act as source rocks for hydrocarbons. Profiles along the extend of some significant Jurassic depocenters (Profile A - C) and into the Dutch and Danish Central Graben are presented in Fig. 37 and Fig. 38

5.3.Potential source rocks

5.3.1. Major source rocks

Within this study, we adopted the Dutch nomenclature for the lithology in the German Central Graben due to the depositional relation of the sediments, the traceability of important horizons from the Dutch to the German Central graben, and the bulk of publicly available data in The Netherlands. All potential source rocks, major and minor, are encountered by wells, either in the German Central Graben itself or in the neighboring Dutch Central Graben and confirmed by log data and cuttings (Fig. 36). Due to the lack of published geochemical data from the German Central Graben, their hydrocarbon potential is confirmed only by data from its Dutch or Danish counterpart (Tab. 4 TOC (Total Organic Carbon) and HI (Hydrogen Index) values of

the Upper Triassic to Lower Cretaceous formations that were investigated on their source rock potential and the kinetics used for the petroleum system modeling. The average values served as input for the potential source rock intervals (from: Thomsen et al., 1983; Damtoft et al., 1987; Ostfeldt, 1987; Gašparík et al., 2012).). The Posidonia Shale Formation within the Upper Altona Group is the most important source rock for oil in the Netherlands (Herngreen et al., 2003; Wong, 2007). It consists of dark grey, laminated and bituminous marlstones with mostly type II kerogen. The average TOC (Total Organic Carbon) content in the Dutch Central Graben is about 8 wt % and reaches up to 15 wt % (Pletsch et al., 2010). Stratified bottom conditions associated with the global Toarcian oceanic anoxic event (Jenkyns, 1988) promoted preservation of organic matter during deposition of the Posidonia Shale Formation. In the southern North Sea area, the formation is only preserved in main Mesozoic rift basins and deeper subsided basin parts such as the Central Graben. (Lokhorst, 1998). In contrast to the Dutch Central Graben, the Posidonia Shale Formation is not confirmed by a well in the German Central Graben. It is a dominantly oil-prone source rock, but also generated gas in NW Germany and the Netherlands, where it reached higher thermal maturity (Lokhorst, 1998; Herngreen et al., 2003).

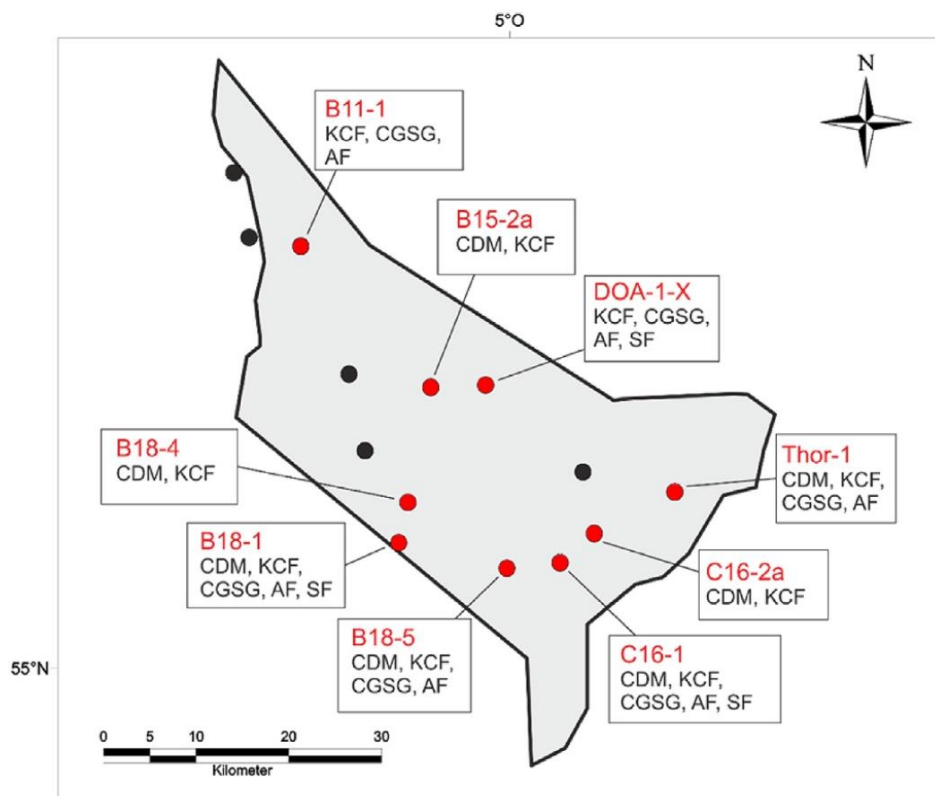


Fig. 36 Wells in the German Central Graben and the encountered Upper Triassic to Lower Cretaceous formations. The red points show the location of wells that confirm the presence of the investigated horizons by well logs and cuttings. The wells represented by the black dots are located at the crest of salt domes and did not encounter any of the investigated strata. Abbreviations: CDM = Clay Deep Member; KCF = Kimmeridge Clay Formation; CGSG = Central Graben Subgroup; AF=Aalburg Formation; SF = Sleen Formation.

The Upper Jurassic ‘Hot Shales’ are bituminous claystones and mudstones deposited near the Jurassic – Cretaceous boundary (Tithonian/Volgian – Berriassian/Ryazanian), overlying the

5. Source rocks of the German Central Graben

Kimmeridge Clay Formation. (Gautier, 2005; Ineson et al., 2003). They are called Clay Deep Member in the Dutch Central Graben, Bo Member in the Danish Central Graben and Mandal Formation in the Norwegian Central Graben and are time-equivalent to the Draupne Formation in the Northern North Sea. The Bo Member is the most important oil and gas source rock in the Danish Central Graben (Ineson et al., 2003; Pletsch et al., 2010). The term ‘Hot Shale’ is attributed to high levels of radioactivity, which facilitates their recognizability on gamma-ray logs. The higher GR-log readings, low sonic velocities and the absence of dolomite stringers distinguish the Clay Deep Member from the underlying Kimmeridge Clay Formation. The Clay Deep Member is confirmed by seven wells in the German Central Graben (Fig. 36). The ‘Hot Shales’ were deposited under euxinic marine conditions resulting from stagnation of basin circulation in parts of the southern North Sea (Cayley, 1987; Erratt, 1993; Wong, 2007).

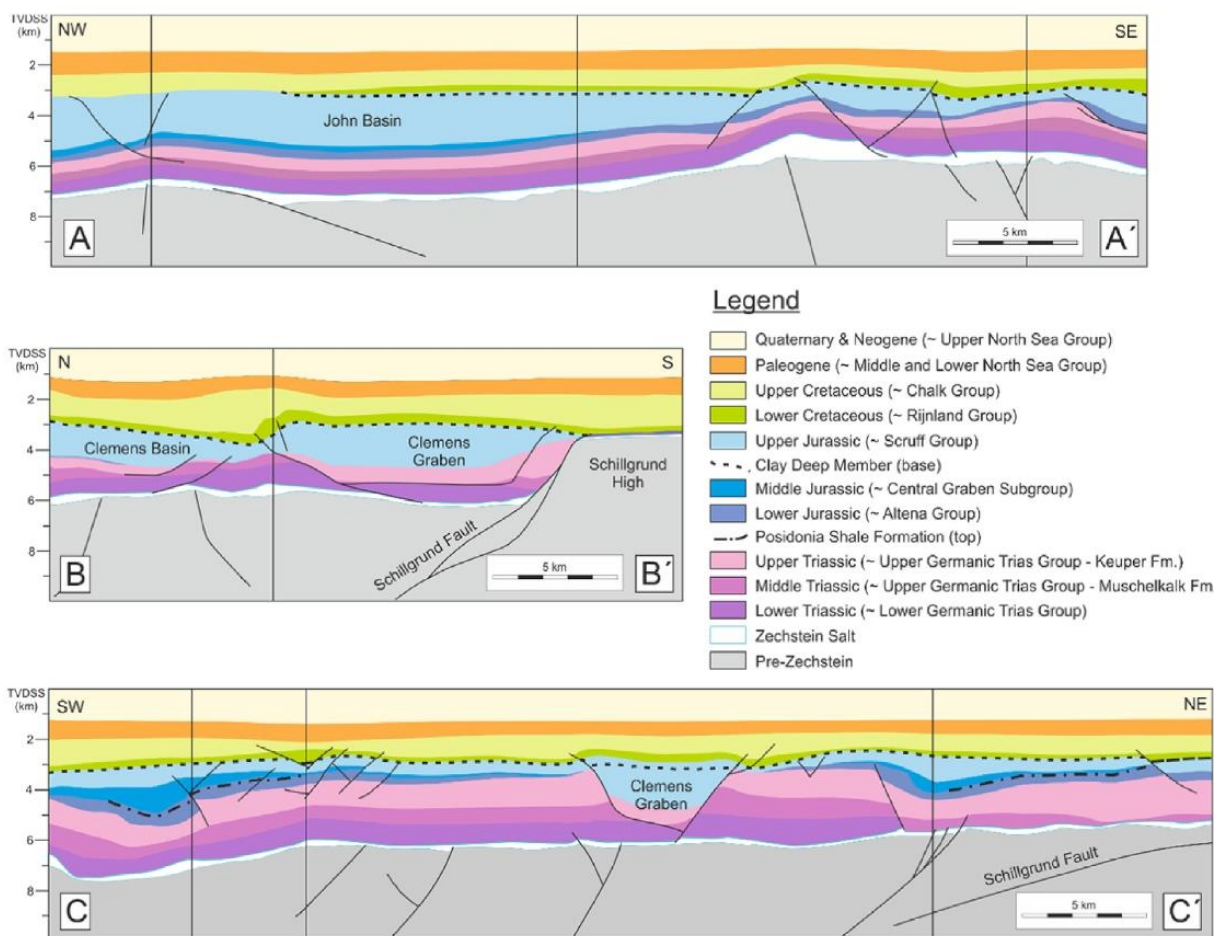


Fig. 37 Profiles across the German Central Graben mainly along graben/basin axes and along the main depocenters of the Jurassic to Cretaceous sediments. Due to profile orientations perpendicular to the dip of the main faults some unusual fault geometries are shown. (A) Profile across the John Graben. Within the John Graben in the NW, Lower Jurassic sediments of the Altena Group as well as Middle Jurassic sediments of the Central Graben Subgroup are present. Despite the presence of the Altena Group, the Posidonia Shale facies seems to be absent. The distribution of the Clay Deep Member ends unconformable in the north of the John Graben. (B) Profile from the Danish border across the Clemens Basin and the Clemens Graben to the Schillgründ Fault. Due to the raised position between the Late Triassic to the Middle Jurassic, no or almost no Lower and Middle Jurassic sediments were deposited. However, syn-tectonic sedimentation in the Late Jurassic was far more intense. (C) Profile from the Dutch to the Danish border along the Schillgründ Fault, crossing the Clemens Graben. Relatively thick Lower and Middle Jurassic sediments of the Altena and Central Graben Subgroup, including the Posidonia Shale Formation, were deposited and are preserved in deeper subsided graben parts near the Schillgründ Fault.

5.3.2. Minor source rocks

Besides the major source rocks, other formations with a significant amount of TOC are taken into account as potential source rocks, including the Rhaetian Sleen Formation, the Lower Jurassic Aalburg Formation and Callovian-Oxfordian coal-bearing sequences of the Central Graben Subgroup. The values of the TOC and the Hydrogen Index (HI), which is a measure of the hydrogen richness and therefore an indicator of the hydrocarbon generative capacity of a source rock, are generally lower than for the major source rocks (Tab. 4 TOC (Total Organic Carbon) and HI (Hydrogen Index) values of the Upper Triassic to Lower Cretaceous formations that were investigated on their source rock potential and the kinetics used for the petroleum system modeling. The average values served as input for the potential source rock intervals (from: Thomsen et al., 1983; Damtoft et al., 1987; Ostfeldt, 1987; Gašparík et al., 2012).). The Rhaetian Sleen Formation was deposited in a shallow, openmarine environment after the Early Cimmerian extensional phase in the earliest Rhaetian and represents the lowest part of the Altena Group in the Dutch offshore (Wong, 2007).

Tab. 4 TOC (Total Organic Carbon) and HI (Hydrogen Index) values of the Upper Triassic to Lower Cretaceous formations that were investigated on their source rock potential and the kinetics used for the petroleum system modeling. The average values served as input for the potential source rock intervals (from: Thomsen et al., 1983; Damtoft et al., 1987; Ostfeldt, 1987; Gašparík et al., 2012).

Lithostratigraphy	Equivalent Danish lithostratigraphy	TOC wt %		Hydrogen Index		Kinetics
		Average	Range	Average	Range	
Clay Deep Member	Bo Member	7.0	1.2–13.5	314	187–610	Vandenbroucke et al. (1999) TII (NorthSea)
Kimmeridge Clay Formation	Farsund/Lola Formation	1.2	1–3.3	99	54–270	
Central Graben Subgroup	Middle Graben/Bryne Formation	7.5	1–65	108	76–299	Ungerer (1990) TIII (North Sea)
Posidonia Shale Formation	–	9.7	3.2–10.5	560	124–684	Pepper and Corvi (1995a,b) TII (B)
Aalburg Formation	Fjerritslev Formation	1.3	1.2–10.8	180	92–493	
Sleen Formation	Sleen Formation	2.2	0.8–4.8	162	38–285	

After a basin-wide transgression in the Late Triassic, it rests unconformably (Early Cimmerian II Unconformity) on the older Upper Germanic Trias Group in the southern North Sea. In the southern Central Graben area, its base forms an excellent marker on both seismic and well-log data (Geluk, 2007). Its facies in the area shows at its bottom grey fossiliferous marine claystones, overlain by brown, locally sandy, claystones with a considerable amount of megaspores, and some open marine argillaceous greensand (Geluk, 2007). The formation contains mostly <5 wt % organic matter of type II-III kerogen with good petroleum potential (Clark-Lowes et al., 1987; de Jager and Geluk, 2007; Gašparík et al., 2012). The Sleen Formation is confirmed by three wells in the German Central Graben (Fig. 36). The Lower Jurassic Aalburg Formation consists mostly of dark grey or black silty claystones of an open-marine origin and occasionally of some shallow marine sandy limestones (Herngreen et al., 2003). It was deposited during the continuing transgression after the Early Cimmerian extensional phase (Wong, 2007). In the Dutch offshore, it is a uniform section of up to 700m and is of a Hettangian to earliest Toarcian age (Herngreen et al., 2003). Its equivalent in the Danish Central Graben is the Hettangian to Lower Pliensbachian Fjerritslev Formation. According to Michelsen et al. (2003), it occurs only

as an erosional remnant in the southern part of the Danish Central Graben. The bituminous sections (mainly type II kerogen) of the Aalburg Formation are assumed to have contributed to hydrocarbon accumulations in the Dutch Central Graben (Wong et al., 1989; Wong, 2007; de Jager and Geluk, 2007). The Aalburg Formation is confirmed by six wells in the German Central Graben (Fig. 36). The thermal uplift, related to the establishment of the Mid North Sea Dome, meant for the southern North Sea area a phase of non-deposition and erosion. After its collapse and the subsequent onset of rifting, continental and paralic sediments were deposited in the southern Central Graben (Herngreen et al., 2003; Wong, 2007). These sediments include the coal-bearing Middle Callovian to Oxfordian Central Graben Subgroup in the northernmost Dutch Central Graben, which are time-equivalent to the Bryne Formation in the Danish Central Graben and the Heather Formation in the Norwegian North (Michelsen et al., 2003; Pletsch et al., 2010). The coal seams of the Central Graben Subgroup with its type III kerogen may have locally generated gas (Wong, 2007; Herngreen et al., 2003; de Jager and Geluk, 2007). Especially gas in Upper Jurassic and Lower Cretaceous reservoirs is assumedly derive from coal measures from the Central Graben Subgroup or the Lower Jurassic Aalburg Formation (de Jager and Geluk, 2007). The Central Graben Subgroup is confirmed by six wells in the German Central Graben (Fig. 36). After the paralic environment of the Central Graben Subgroup, open marine conditions were re-established in the southern Central Graben. This resulted in the accumulation of thick open marine clay deposits in the Kimmeridgian and the Portlandian (Herngreen et al., 2003). In the Dutch Central Graben this succession is called the Kimmeridge Clay Formation, with the Lola and the Farsund Formation as its equivalents in the Danish Central Graben (Ineson et al., 2003). Most of the Kimmeridge Clay in the southern Central Graben is not characterized as a “Hot Shale” (as e.g., the Clay Deep Member or the Bo Member), but still contains significant amounts of TOC (type II-III kerogen) and may constitute an additional source of hydrocarbons (Pletsch et al., 2010). The Kimmeridge Clay Formation is confirmed by nine wells in the German Central Graben (Fig. 36).

5. Source rocks of the German Central Graben

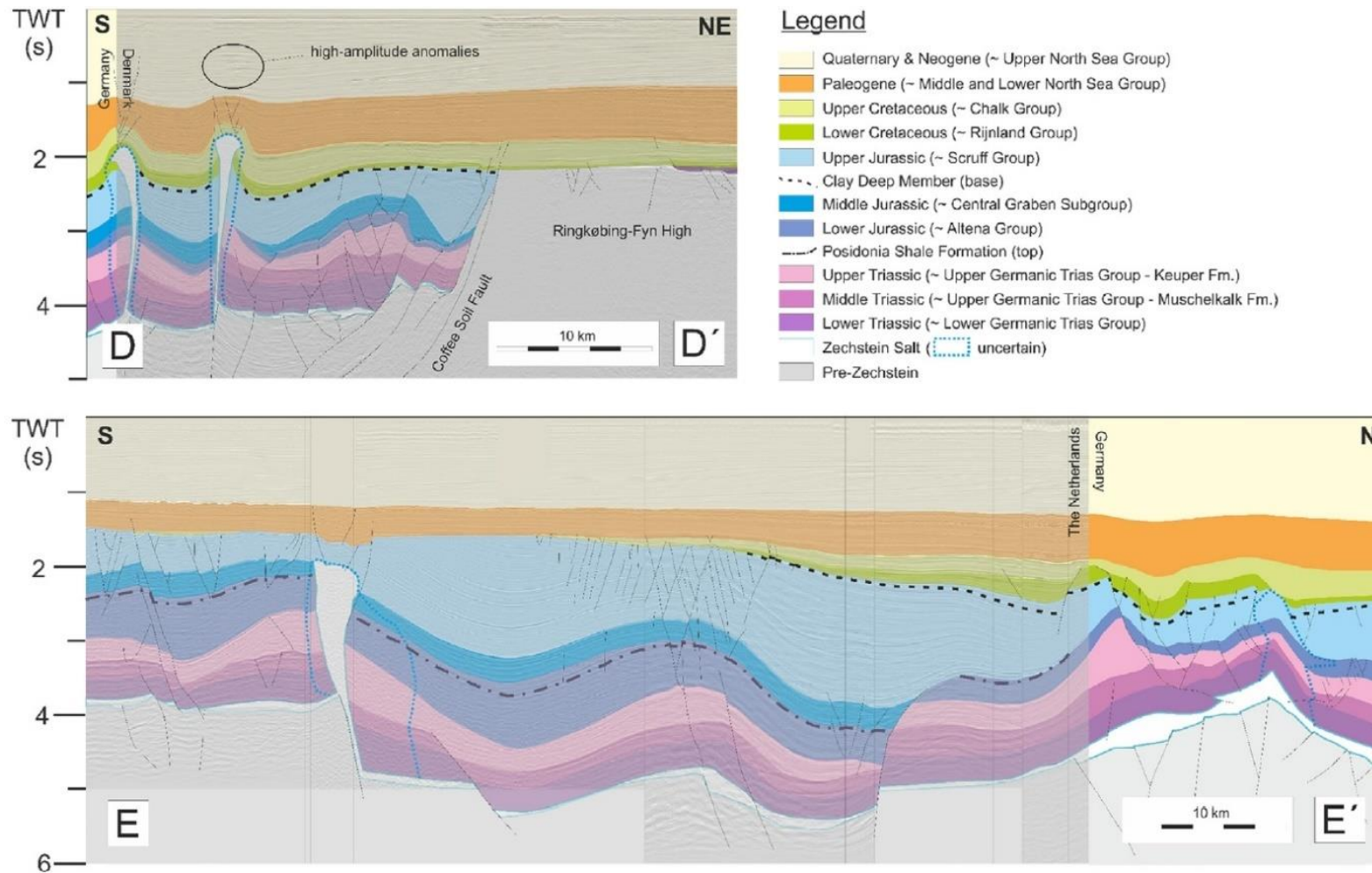


Fig. 38 Profiles from the German Central Graben into the Danish (D) and the Dutch Central Graben (E). The profiles highlight the continuity of most of the Jurassic formations in the neighboring parts of the Central Graben. The Posidonia Shale Formation is prevalent in the Dutch Central Graben but missing in the Danish part. The occurrence of the Clay Deep Member continues from the Dutch Central Graben, across its German part, and into the Danish Central Graben. Profile D shows high amplitude anomalies above a Zechstein salt dome, indicating shallow gas accumulations in the Danish Central Graben. Interpretation is based on seismic data from surveys DK95-ANJ and CGD85 for profile D and on publicly available data from surveys Z3FUG2002A, Z3NAM1982A, Z3NAM1989E, Z3PET1992F, and Z3OXY1994A for profile E. Seismic profiles from the German graben part is excluded from the figure due to confidentiality of the data.

5.4. Data and methodology

5.4.1. Mapping

Due to the absence of reliable mapped horizons in the German Central Graben of the Posidonia Shale Formation and Clay Deep Member, these important regional source rocks had to be mapped anew based on seismic and well data with Schlumberger's GeoFrame software. The mapping was conducted within the TUNB-project (Deeper Underground North German Basin), in succession of the GPDN-project (Geo-Potential German North Sea; www.gpdn.de). Within the previous project, horizons were mapped that correlate with the remaining potential source rocks that are investigated in this study. For the mapping of the Posidonia Shale Formation and the Clay Deep Member, one 3D seismic survey that covers the north-western part of the German Central Graben, several 2D seismic surveys, and the data of 14 wells in northern offshore Germany were available. Checkshot data were used to fit well- data with seismic data in time domain as well as with the help of synthetic seismograms for a more accurate well tie. Mapping of the Posidonia Shale Formation, as well as the Clay Deep Member, started in the northern Dutch Central Graben. There, the occurrence of these two source rocks is well documented by the data of several wells.

The Posidonia Shale Formation is easy to identify on well logs from offshore The Netherlands due to high gamma ray and resistivity values and a lower interval transit time. On reflection seismic data, the top of the formation is marked by a distinct positive (SEG reverse polarity) reflection, which results from a decrease in seismic velocity at the transition from the Lower Werkendam Member to the bituminous Posidonia Shale Formation (Fig. 39 A). Within the German Central Graben, no well penetrates the Posidonia Shale Formation. Therefore, the mapping concentrates on the specific seismic character of the formation, i.e., along a distinct positive reflection horizon in the otherwise relatively uniform Lower Jurassic succession. If such a reflection is missing, the source rock is assumed to be absent, either due to nondeposition or later erosional events, or due to a lithology change to a non-source rock facies.

The Clay Deep Member is recognizable on well logs due to their high GR-values, which indicate a high organic content of the formation. The high GR values are the result of preferred attachment of uranium to organic material (Mann et al., 1986). The presence of the Clay Deep Member in the German Central Graben is affirmed by seven wells (Fig. 36). On reflection seismic data, the top of the Clay Deep Member is a distinct positive (SEG reverse polarity) seismic reflection (Fig. 39 B). It reflects the transition from the claystones of the Upper Cretaceous Rijnland Group to the bituminous Clay Deep Member. If its thickness is great enough that the distinct reflection is traceable, the base of the Clay Deep Member appears as a negative reflection (SEG reverse polarity) on the transition to the Scruff Greensand Formation (especially strong reflection due to the change in lithology; only in the Dutch Central Graben) or the Kimmeridge Clay Formation (much less distinctive; in the German Central Graben).

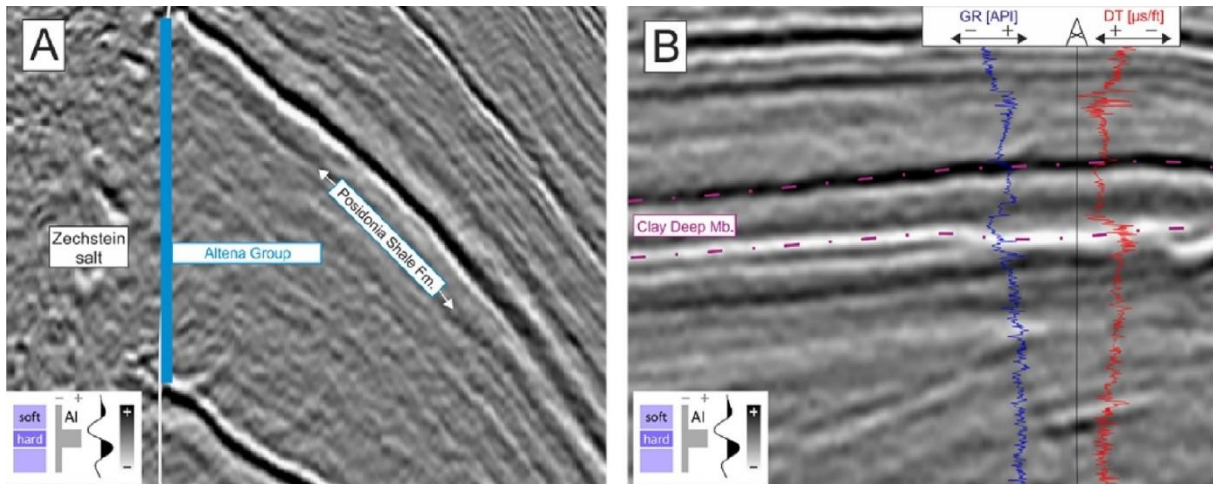


Fig. 39 Exemplary seismic views of the Posidonia Shale Formation (A) and the Clay Deep Member (B) in the northern Dutch Central Graben. (A) The top of the Posidonia Shale Formation appears as a relatively strong positive reflection (SEG-reverse polarity). Just below the top of the Altena Group, which features an otherwise uniform low-amplitude reflection pattern. (B) The Clay Deep Member features significantly higher gamma ray (GR) readings and a lower sonic velocity (higher DT-readings) than the surrounding claystones of the Rijnland Group (at the top) and the Scruff Greensand Formation at the base or the Kimmeridge Clay Formation (German Central Graben), respectively. This different in sonic velocity appears on reflection seismic data as a distinct positive reflection at its top and a distinct negative reflection at its base (SEG-reverse polarity).

5.4.2. Petroleum model

To decipher the origin of near-surface accumulated gas within the study area a 3D basin and petroleum system model was built on the basis of the model from Arfai and Lutz (2017) and analyzed within the software PetroMod® V. 16 to reconstruct the thermal history, maturity and petroleum generation of the before mentioned potential source rocks. The software calculates the evolution of a sedimentary environment from the oldest to the youngest event (forward modeling), and the processes of petroleum generation and migration (Hantschel and Kauerauf, 2009). For the calculation of vitrinite reflectance from temperature histories, the EASY%Ro algorithm of Sweeney and Burnham (1990) is used. This calculation method follows a kinetic reaction scheme and is valid for calculated reflectance values between 0.3 and 4.5%. Hydrocarbon generation for the oil-prone source rocks was calculated using the kinetic dataset in PetroMod, TII North Sea of Vandenbroucke et al. (1999). Hydrocarbon generation for the gas-prone source rocks was calculated with the TIII kinetic after Burnham (1989). The 3D model includes the present-day geological and stratigraphic framework, erosional maps, boundary conditions and generalized lithologies from a recently published 3D basin and petroleum system model covering an area of 4000 km² in the NW German North Sea (Arfai and Lutz, 2017).

The model of Arfai and Lutz (2017) was modified with regard to the new requirements for shallow gas. The modification includes new layers for the newly mapped Clay Deep Member and Posidonia Shale Formation. Furthermore, layers from the Arfai and Lutz (2017) model, as the Upper, Middle, and Lower Jurassic, were split or redefined and provided with their source rock properties like HI and TOC values (Tab. 1). The petroleum model now investigates six different potential source rocks for shallow gas, instead of three different source rock in the

original model. The area of interest was reduced to the German Central Graben according to the research object. Accordingly, new model input consists of 29 stratigraphic layers covering a time interval from the Devonian to the Present (358–0 Ma). The 3D model includes six defined potential source rocks. The Jurassic is subdivided into one oil-prone and one mixed oil-gas-prone Upper Jurassic layer, one gas-prone Middle-Upper Jurassic layer and three Lower Jurassic - Rhaetian layers, which are induced as oil-prone and mixed oil-gas-prone source rocks, respectively. The petroleum system model is a simplification of the actual geology of the German Central Graben after Arfai et al. (2014). The average TOC values were adopted for the bulk of the investigated formations. Some of these formations, like the Kimmeridge Clay Formation, have gross thicknesses of several hundred meters. Also, the Kimmeridge Clay Formation features distinct dolomite stringers, and the Central Graben Subgroup is very heterogeneous, including coal, shale, silt, and sand.

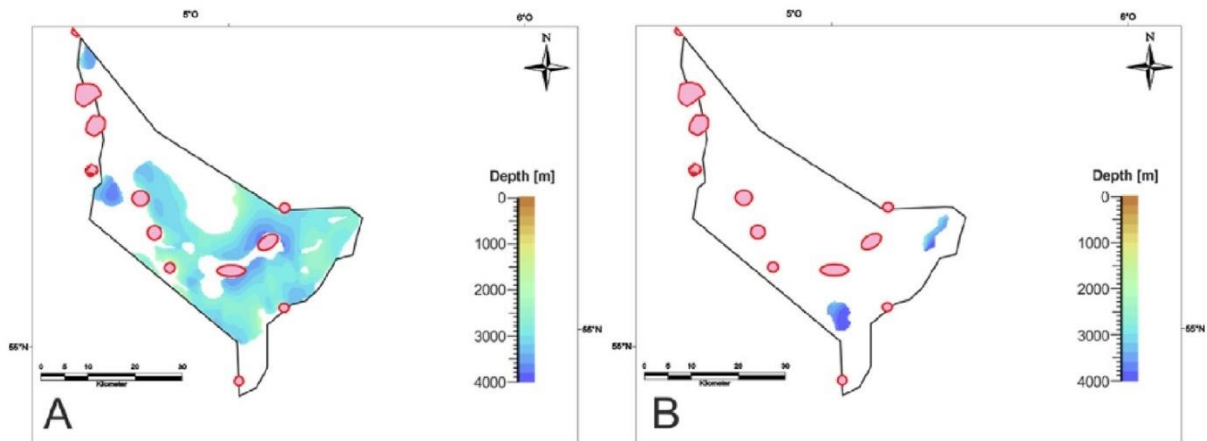


Fig. 40 Distribution of the Clay Deep Member (A) and the Posidonia Shale Formation (B) in the German Central Graben. The Clay Deep Member is present in large parts of the graben, especially in its south, and there it is continuously traceable from the Dutch to the Danish graben parts. In contrast to the Clay Deep Member, only two relatively small, isolated areas of the seismic Posidonia facies are preserved in deep subsided parts near the Schillgrund fault.

5.5. Results

5.5.1. Mapping of the Posidonia Shale Formation and the Clay Deep Member

The Clay Deep Member is present in most of the German Central Graben (Fig. 40). In the north of its distribution area, the reflection horizon that highlights the Clay Deep Member is eroded in the north of the John Graben (Fig. 37A). Well data further in the NW of the John Graben do not indicate its presence (Fig. 36). Well control of the Clay Deep Member is best in the south near offshore The Netherlands and in the John Graben. In the North-East towards offshore Denmark, there is no well control. However, the Clay Deep Member was mapped towards the Danish-German border due to the continuity of its reflection horizon. The results of the mapping of the Posidonia Shale Formation differs considerably from previous maps of its distribution

within the German North Sea sector (e.g., Lott et al., 2010; Arfai and Lutz, 2017). Mapping showed that the seismic facies, which is associated with the Posidonia Shale Formation, is preserved only in two relatively small isolated areas (Fig. 40B). Reflections that are interpreted as Posidonia Shale Formation are found just north of the border to offshore The Netherlands and near the border to offshore Denmark in deeper subsided basin parts. There is, however, no well control that affirms ultimately the presence of the Posidonia Shale Formation in the mapped areas. The mapping is solely adapted from seismic characteristics of the horizons and there is still uncertainty.

5.5.2. Petroleum Model

The results of petroleum modeling show that all investigated horizons are in parts or overall at a maturity state that is favorable for the generation of hydrocarbons at the present day. Because vitrinite is a terrigenous maceral and therefore rare to absent in marine sediments, all vitrinite reflectance maps consist of calculated values. The 1D burial history from the John Graben indicates that deepest burial of sediments, including the source rocks units, occurs at the present day. This is associated with the maximum maturity of the source rocks in the study area (Fig. 43).

The uppermost potential source rock, the Clay Deep Member, is currently for the most part in the main oil window (Fig. 41). The transformation of the type II kerogen to hydrocarbons is generally low for the Clay Deep Member (< 20%). A higher transformation ratio is reached at areas of a deeper burial, like the John Graben (> 30%) and the Clemens Basin (> 40%) or at areas of high thermal conductivity around the salt domes (up to 80%). For the transformation of type III kerogen to gas, the Clay Deep Member is still immature.

The top of the Kimmeridge Clay is for the most part in the main oil window (Fig. 41). Within the deeper parts of the Central Graben (John Graben, Johannes Graben, Clemens Basin), most of its type II kerogen has been transformed to hydrocarbons (> 90%). In structurally higher positions outside the deep subsided sub-basins, the transformation ratio varies from <5 to >40%. Due to the relatively low maturity, most of the type III kerogen of the top of the Kimmeridge Clay has not been transformed to hydrocarbons yet (between 0 and 5%). Only in the deep parts the gas-prone type III kerogen may have been transformed (up to 60%).

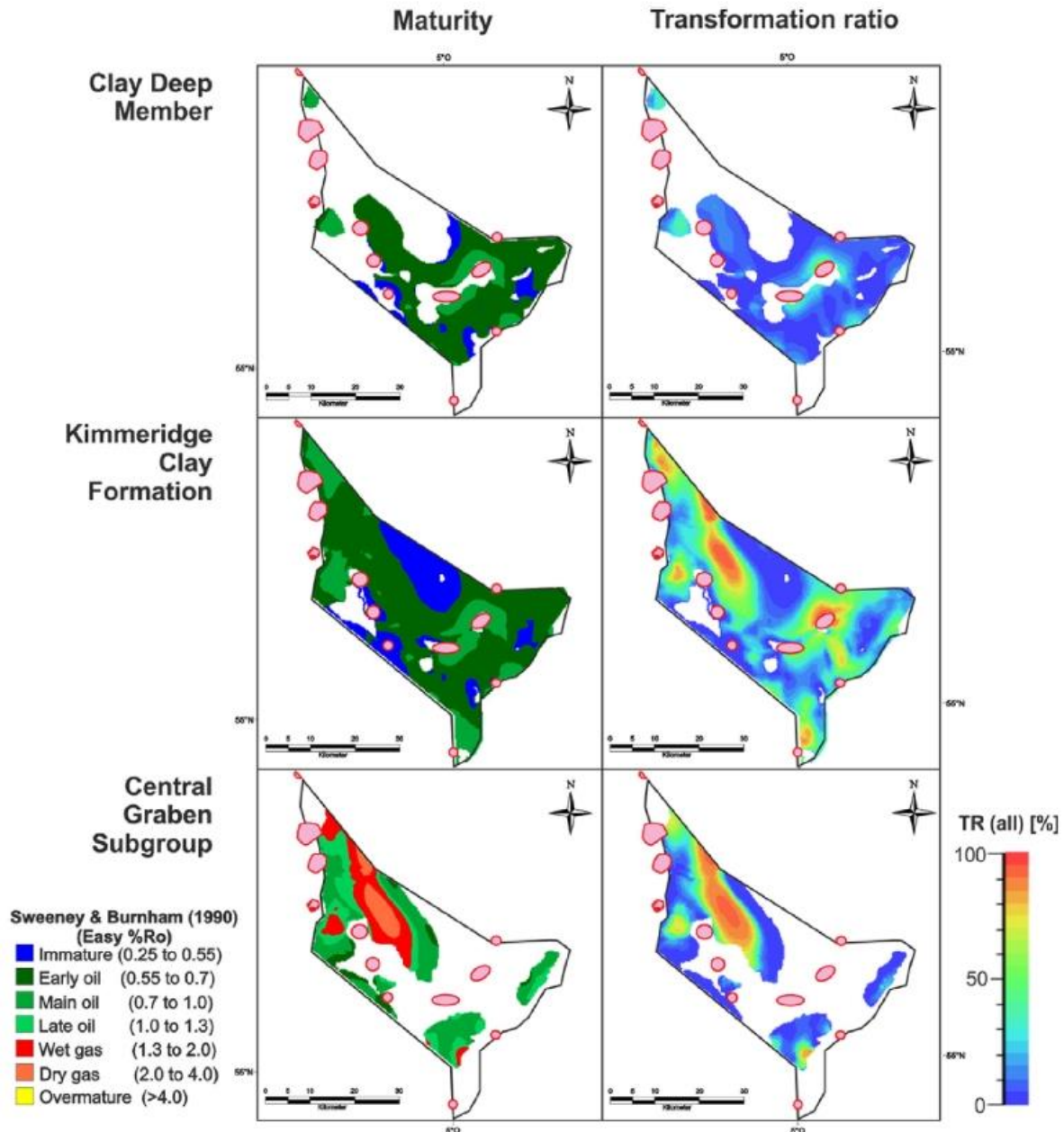


Fig. 41 Results of the petroleum system modeling. Present-day maturities and transformation ratios (type II kerogen for the Clay Deep Member and the Kimmeridge Clay Formation, type III kerogen for the Central Graben Subgroup) of the Lower Cretaceous to Middle Jurassic formations that were investigated as potential thermal source rocks for shallow gas. The distribution of the Clay Deep Member based on a new mapping study.

The Middle to Upper Jurassic Central Graben Subgroup has reached the gas window in the John and the Johannes Graben (Fig. 41). Between 50 and 85% of the gas-prone type III kerogen of the subgroup's coal measures have been transformed to gas at the present time.

The two isolated patches of the mapped Posidonia Shale Formation differ in their maturity and transformation ratio (Fig. 42). The southern patch at the border to offshore The Netherlands varies from the main oil to the wet gas window. Most of its type II kerogen has already been transformed to hydrocarbon. The northern patch at the border to offshore Denmark on the other

hand is in the main oil window, but the greatest part of its kerogen has not been transformed yet.

The results of the petroleum model reveal a similar picture for the Lower Jurassic Aalburg and the Rhaetian Sleen Formation (Fig. 42). The two formations have reached the gas window in the John and Johannes Graben, as well as in deeper buried areas at the border to offshore The Netherlands and Denmark. In the Clemens Basin, the Lower Jurassic is not present. In other areas of the German Central Graben, the formations are in the main or late oil window. The transformation ratio of type II and type III kerogen differs significantly. The type II kerogen is already transformed within the greatest part of the formations' areal extent. The transformation ratio of type III kerogen on the other hand has reached high levels in the areas within the gas window ($> 80\%$). However, substantial amounts of kerogen are not transformed to hydrocarbons yet.

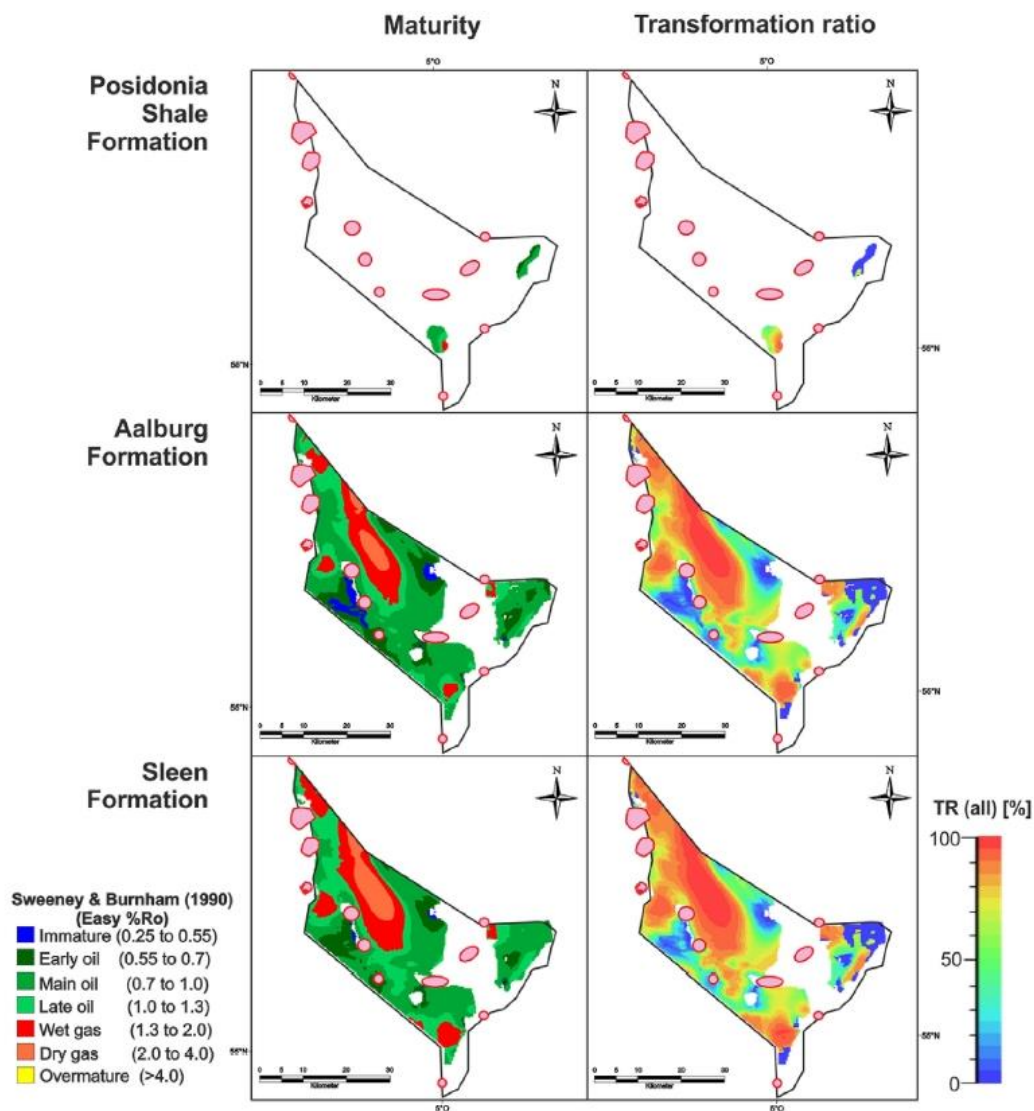


Fig. 42 Results of the petroleum system modeling. Present-day maturities and transformation ratios (type II kerogen) of Jurassic to Upper Triassic potential source rocks that were investigated as potential source rocks for shallow gas. The distribution of the Posidonia Shale Formation based on a new mapping study.

5.6. Discussion

5.6.1. Potential as source rocks

The Clay Deep Member in the North of the Dutch Central Graben is highly bituminous but immature (Herngreen et al., 2003). The gross thickness of its Danish counterpart, the organic-rich Bo Member of the upper Farsund Formation, varies from over 100m in the northern Tail End Graben and less than 10m in the southern Salt Dome Province (Ineson et al., 2003). It constitutes a prolific source rock for oil that has presumably charged most of the fields in the Danish North Sea (Petersen et al., 2017). The German section of these “Hot Shales” lies between the thick, but immature Dutch Clay Deep Member, and the likewise immature and thin Bo Member of the Salt Dome Province. For the German part, we estimate the kerogen composition and amount of the organic matter to be comparable with the Dutch and Danish “Hot Shales”. The gross thickness varies from several tens of meters at the Dutch-German border to less than 10m (no distinct seismic reflection on available data) at the German-Danish border. The new interpretation delivers insight into the distribution of the organic rich rocks, but the results from the updated petroleum system model confirm the immaturity as their close Dutch and Danish counterparts as well as the results of Arfai and Lutz (2017).

The non-“Hot Shale”-section of the Kimmeridge Clay differs in part significantly from the Clay Deep Member regarding its thickness, maturity, and organic content. At its top section, the Kimmeridge Clay Formation is in the oil window according to the calculated vitrinite reflection (Fig. 41). Its base on the other hand is, similar to the top of the Central Graben Subgroup, especially in deeper subsided sub-basins, in the gas window. Here, a significant fraction of the kerogen is transformed to hydrocarbons. Because of the marine origin, we assigned a type-II-kerogen kinetic to the Kimmeridge Clay Formation. However, the source rock quality of the Danish Kimmeridge Clay equivalents varies significantly in depth as well as with lateral distribution (Ponsaing et al., 2018). In the upper parts of the Farsund Formation, close to the Bo Member, the organic content consists of predominantly oil-prone Type II kerogen of a marine origin. In the lower parts of the Farsund Formation, the source rock quality decreases. This decrease results from a more oxic depositional environment as well as from a larger input of terrigenous organic matter into the older sediments (Ineson et al., 2003; Petersen et al., 2017). However, several isolated anoxic events resulted in oil-prone intervals in the lower part of the Farsund Formation (Petersen et al., 2010). The marine claystones of the older Lola Formation below the Farsund Formation average 2 wt % TOC and an HI value of 118 (Damtoft et al., 1987). However, its kerogen is dominated by gas-prone organic matter and inertinite (Thomsen et al., 1983). In the Danish Salt Dome Province, the kerogen quality of the Farsund Formation deteriorates significantly, due to a higher portion of siliciclastic and inert terrigenous matter (Ineson et al., 2003). Hereby, the kerogen type changes from predominantly type II or type II-III to predominantly type III in the Salt Dome Province (Damtoft et al., 1987). Because of this change in source rock quality from oil-to gas-prone, we expect this trend to continue into the German Central Graben. Despite its maturity in the oil window, this alteration in the composition of the organic matter could explain the fact that there were no oil shows in the wells within

the German Central Graben. However, the base of the Kimmeridge Clay Formation may constitute a gas-prone source rock of minor quality. It may have contributed to the potential shallow gas accumulations in the area. Significant amounts of hydrocarbons from this source alone are not expected.

Middle Jurassic coals are regarded as the second most prolific source rock in the greater North Sea area that have sourced fields in the UK Central North Sea, the Danish-Norwegian Søgne Basin, and the Viking Graben (Isaksen et al., 2002; Mouritzen et al., 2018; Petersen et al., 2018). However, in the southern Central Graben the coals and coaly shales of the Central Graben Subgroup and its Danish equivalents did not receive much attention until recently. Within the Dutch Central Graben, the coals and coaly shales of the Central Graben Subgroup are assumed to have locally generated gas (Herngreen et al., 2003; de Jager and Geluk, 2007; Wong, 2007). Their equivalents of the Middle Graben, Bryne, and Lulu Formations in the Danish Central Graben are described as gas-prone source rocks with a good generation potential that is only restricted to the thickness of its coaly intervals (Damtoft et al., 1987). Recent literature dedicated itself to these Middle Jurassic coals and describes them as an overlooked and underexplored petroleum system south of the Norwegian-Danish border (Petersen and Hertle, 2018; Petersen et al., 2018). In the northern Danish Central Graben Middle Jurassic coals are the source rocks for gas and condensate fields. The coals are primarily gas-prone, but frequently also contain oil-prone lacustrine algal kerogen that provides them with a high hydrogen index (~280 mg HC/g TOC) that enables them to generate liquids like condensate and oil (Petersen et al., 2000; Petersen and Hertle, 2018). Within the German Central Graben, the presence of the Middle Jurassic coals is confirmed by several wells. The Central Graben Subgroup is at the present in the gas window in the John and Johannes Graben and transformed a considerable percentage of its kerogen to hydrocarbons. Based on our data, we assumed a lower hydrogen index (Tab. 4) than Petersen and Hertle (2018) and used another kinetic (TIII North Sea of Ungerer (1990) instead of Pepper and Corvi (1995a, 1995b)). Therefore, the Central Graben Subgroup produced exclusively gaseous hydrocarbons in our model. However, a continuation of the lacustrine, more liquid-prone facies is possible. The coals of the Central Graben Subgroup pose a potentially good source for gaseous and even liquid hydrocarbons. Its potential depends on the lateral and vertical extent of the coaly intervals.

5. Source rocks of the German Central Graben

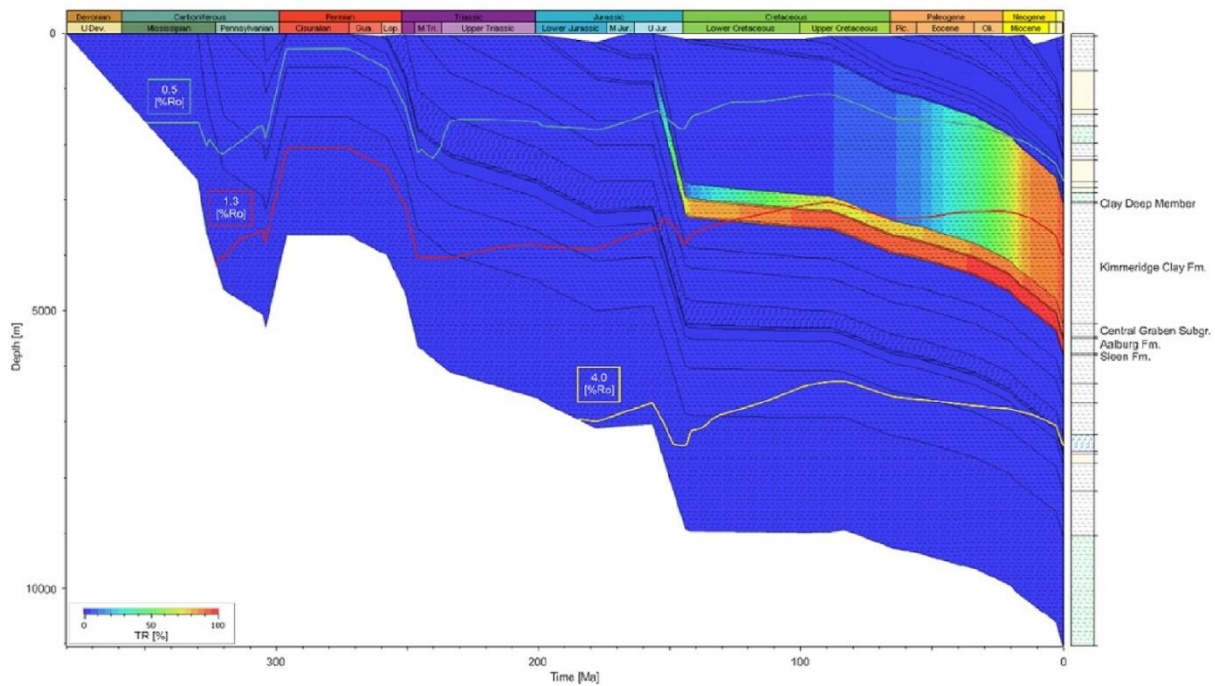


Fig. 43 1D extraction of the PetroMod model at the point of the deepest burial within the German Central Graben, located in the John Graben-subbasin. The location of the extraction point is shown in Fig. 35. The figure connects the local burial history with the kerogen transformation ratio (TR, in %) of the investigated source rocks and the state of maturation of the organic matter (green line: oil window; red line: gas window; yellow line: overmature; after Sweeney and Burnham, 1990). Significant transformation of kerogen to hydrocarbons started for the Sleen and Aalburg Formation in the Late Jurassic, for the Central Graben Subgroup in the Early Cretaceous, for the Kimmeridge Clay Formation in the Eocene. The Clay Deep Member did not generate significant amounts of hydrocarbons.

Besides its significance as a prolific source for hydrocarbons in the Dutch Central Graben only residual deposits of the Posidonia Shale Formation remain in the German Central Graben. The occurrence close to the Dutch-German border is currently in a depth sufficient to produce oil and, in its deeper part, gas. The second occurrence at the Schillgrund Fault is at present not in the gas or oil window. Further north in the Danish Central Graben, no occurrences of the Posidonia Shale Formation are known and it is assumed to be eroded during the Mid- Cimmerian uplift (Damtoft et al., 1987). However, due to its maturity and its excellent source rock quality, the Posidonia Shale Formation has probably generated hydrocarbons at its occurrence on the Dutch- German border. This assumption is supported by shows of residual oil in the area (EBN, 2016; Arfai and Lutz, 2017). Due to its limited distribution, these hydrocarbons will only have marginal and local relevance. The residual oil may also indicate later stage gas-flushing and remigration of earlier oil accumulations (O'Brien et al., 2002).

The marine claystones of the Aalburg and the Sleen Formation are probably distributed over most of the German Central Graben. The Aalburg Formation is assumed to have contributed to hydrocarbon accumulations in the southern Dutch Central Graben (Wong et al., 1989). The Sleen Formation is also believed to be a fair source rock for oil that is present in most parts of the Central Graben (Clark-Lowes et al., 1987). Geochemical analyses of both formations affirmed their source rock potential for onshore The Netherlands (Gašparík et al., 2012). The Aalburg Formation equivalent in offshore Denmark, the Fjerritslev Formation, has an average

TOC of 2.1% (Damtoft et al., 1987). Results from geochemical analyses yielded that its kerogen is predominantly gas-prone (Damtoft et al., 1987). However, due to the marine origin of the claystones, we applied a Type II kinetic (Pepper and Corvi, 1995b) in our model. Presently, large parts of both formations are within the gas window, structurally higher parts still in the oil window. In our model, most of the kerogen is already transformed. However, the transformation ratio may be too advanced due to the applied kinetics, and gas generations may still be ongoing due to gas-prone kerogen and low HI-values. The potential kitchen areas comprise the John and Johannes Graben in the West, as well as extensions from the Dutch Central Graben and the Tail End Graben in the south- and north-east of the German Central Graben.

5.6.2. Thermogenic contribution to shallow gas accumulations

Potential shallow gas accumulations in the area of the German Central Graben and phenomena related to vertical fluid migration, such as gas chimneys, may indicate an active hydrocarbon source rock. Shallow gas is produced in economic quantities in the northern Dutch offshore from Plio-Pleistocene reservoirs along the Dutch Step Graben and Central Graben. Anticlinal uplifts of the crest of salt domes provide in most cases structural traps for the gas (ten Veen et al., 2013). The potential shallow gas accumulations in the neighboring German Central Graben are equivalent to the Dutch fields with respect to geological setting and trapping mechanism (Müller et al., 2018). The origin of shallow gas in offshore The Netherlands is still a matter of debate (ten Veen et al., 2013). Verweij et al. (2018) suggests a predominantly microbial origin of the shallow gas in the Dutch North Sea due to favorable conditions for microbial activity in the Plio-Pleistocene source and reservoir horizons and geochemical data from the Step Graben System. Generally, two different mechanisms for methane generation in the underground are possible: microbial gas generation and thermogenic gas generation. Microbial gas in shallow depth is produced by a variety of anaerobic methanogens (archaea) (Rice and Claypool, 1981). Microbial methane generation involves different metabolic pathways, including acetate fermentation and CO₂ reduction (Thauer, 1998). Both processes are associated with kinetic isotope effects that result in generation of ¹³C depleted (isotopically light) methane (Whiticar et al., 1986). Thermogenic gas is produced by thermocatalytic cracking of kerogen or bitumen, mostly during catagenesis at temperatures exceeding 60 °C, which usually occur at greater depths (Hunt, 1991). Thermogenic gas is isotopically “heavier” (less ¹³C depleted) and the gas wetness (abundance of C₂₊ hydrocarbons) is higher than in microbial gas (Schoell, 1980). Published geochemical data of shallow gas is scarce and originates exclusively from the shallow gas fields in offshore The Netherlands. Most shallow gas accumulated at the top of the Dutch Step Graben is very dry (> 99% methane) and depleted in heavy carbon isotopes, indicating a microbial origin (ten Veen et al., 2013).

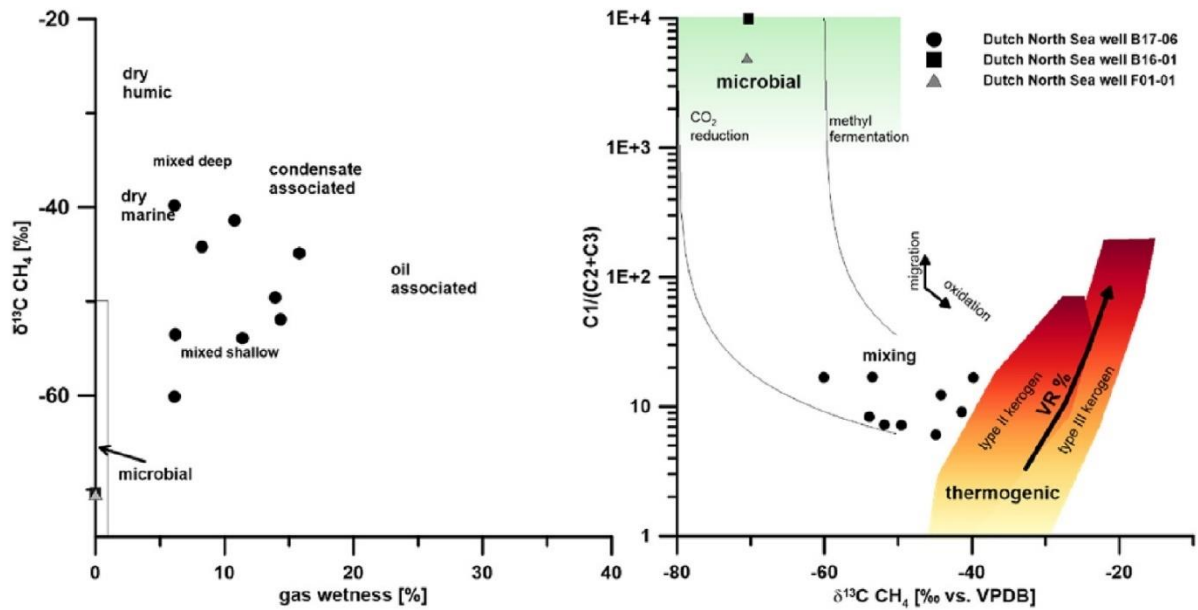


Fig. 44 Diagnostic plots modified after Bernard et al. (1976, left) and Schoell (1983, right) indicating variable contribution of thermogenic gas to shallow gas in well B17-06. Gas wetness calculated after Jenden et al. (1993).

However, there are several locations, where the geochemical data indicate at least an admixture of thermogenic gas. One of those locations is the B17-shallow gas field that is located in the Dutch part of the Central Graben (Fig. 33). The molecular and stable carbon isotope composition of gases desorbed from drilling cuttings (~300m–800m interval) indicates a mixing of gases from thermogenic and microbial origin (Fig. 44). ten Veen et al. (2013) interpret these data as indicative of a thermogenic source. However, the analysis of free gas collected during a production test from the same shallow gas field indicates a predominantly microbial origin (Verweij et al., 2018). The reason for this apparent ambiguity is not yet resolved, but may be attributed to strong biodegradation of the free gas or a different origin of the free and adsorbed gases. Due to these indications for the presence of thermogenic derived shallow gas in the nearby Dutch Central Graben and the indications for gas migration from greater depths to the shallow potential reservoirs in the German Central Graben (Müller et al., 2018), we assume that thermogenic derived gas also contributed to potential shallow gas accumulations in the German Central Graben. However, the contribution of microbial gas in the shallow reservoirs cannot be excluded and further geochemical data are required to test the hypothesis of admixture of thermogenic gas in the German Central Graben. Based on results of the petroleum system modeling and comparison with the distribution of potential shallow gas accumulations, the lower section of the Kimmeridge Clay Formation, the coaly intervals of the Central Graben Subgroup, and the upper section of the Aalburg Formation as the most probable sources of thermogenic gas.

5.6.3. Migration and accumulation

While the formations of the Quaternary and Neogene (Upper North Sea Group) are at hydrostatic or close-to-hydrostatic pressure, older formations underneath the Mid-Miocene Unconformity (MMU) are overpressured in the area of the southern Central Graben (Verweij et al., 2012). The overpressure is related to the rapid Neogene and Quaternary sedimentation and its depocenters (Mudford et al., 1991; Verweij et al., 2012; Lamb et al., 2017). The overpressure decreases towards the salt domes, which indicates that fluid flow and pressure relief takes place towards these structures (Verweij et al., 2012). Consequentially, hydrocarbon migration below the MMU probably follows pressure gradients, additionally to buoyant and capillary forces, from the source rocks towards the salt domes. According to this, Thomsen et al. (1990) suggested hydrocarbon migration from areas of high excess fluid pressures to areas of low excess fluid pressures in the northern Danish Central Graben. In the German Central Graben, we assume primary migration of hydrocarbons to take place out of the Upper to Lower Jurassic source rocks (claystones and coals) into permeable silty and sandy layers of the Central Graben Subgroup (Fig. 45). The gas then migrates buoyancy-driven and bed parallel towards the salt domes, which form a lateral seal. Here, at the flanks and underneath of salt dome overhangs, hydrocarbons can accumulate. These potential exploration targets are often not drilled yet. For this particular play, the Central Graben Subgroup is simultaneously source rock, migration conduit, and potential reservoir rock. Along deformed and fractured sediments at the rim of the salt domes gas can migrate vertical (Cornford, 1994). Müller et al. (2018) suggest that the weakened sediment structure along the salt domes (faults and fractures due to halotectonic processes) serves as a drain for pressure dissipation and fluid escape out of the overpressured sediments into the normally pressured Upper North Sea Group. In addition, the reduced effective stress due to the overpressure increases the permeability of the polygonal fault network of the Paleocene and Lower Miocene mudstones potentially form fluid conduits and facilitate hydrocarbon migration (Cartwright, 1994; Müller et al., 2018). Above the MMU, in the hydrostatic or close-to-hydrostatic pressured sediments of the Upper North Sea Group, fluid migration is driven by buoyant and capillary forces. Due to the pressure drop, dissolved gas exsolves from water invading the strata above the salt domes. Isolated bubbles of gas, stuck in the post-MMU sediments underneath the potential shallow gas accumulations, appear as a gas chimney on reflection seismic data. The bulk of the gas accumulates in shallow strata. The potential mechanisms of fluid migration from Mesozoic to Plio-Pleistocene sediments in the surrounding of diapirs, and further into the atmosphere, has to be taken into account for any considerations of seal integrity regarding CCS (Carbon Capture and Storage) in the Central Graben area.

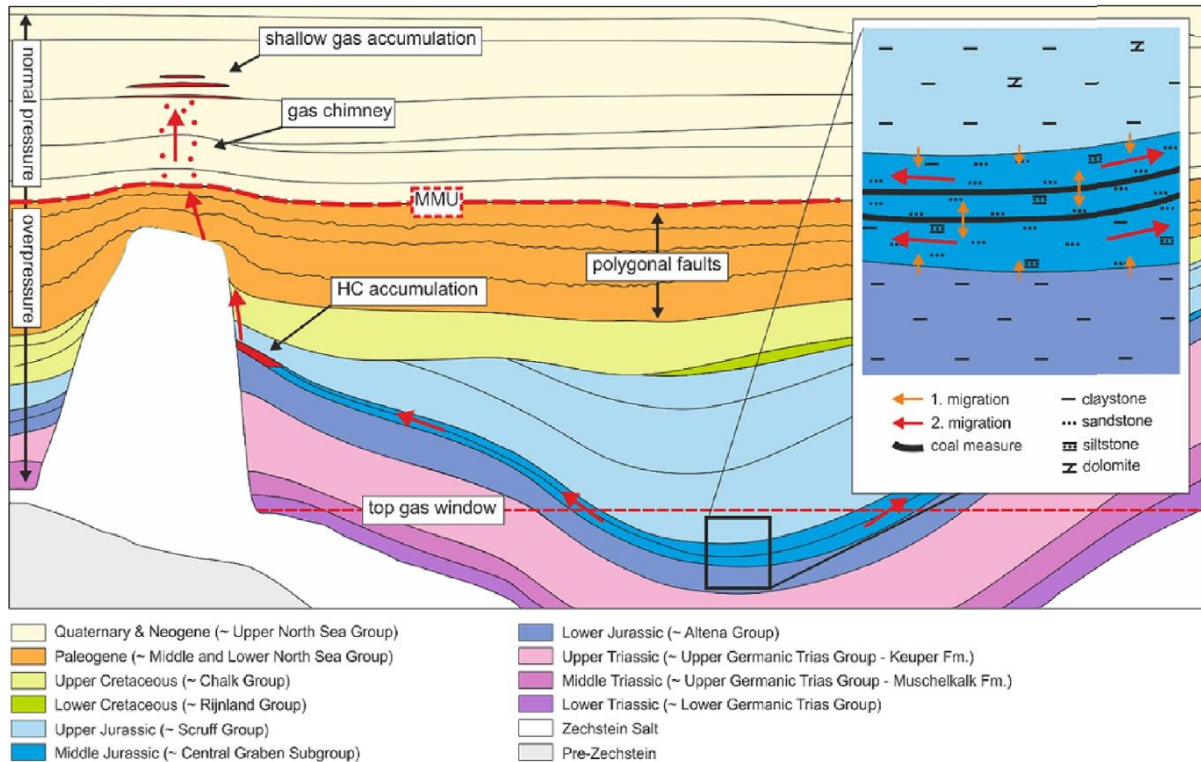


Fig. 45 Sketch of hydrocarbon generation, migration, and accumulation in the German Central Graben. Hydrocarbons are generated from the Upper and Lower Jurassic marine claystones, as well as from Middle Jurassic coals. The hydrocarbons migrate buoyancy-driven up-dip and along a pressure gradient probably within Middle Jurassic sandstones. Where these sandstones are in contact with Zechstein salt domes or onlap on claystones, hydrocarbons may have accumulated. A part of the accumulated gas may have migrated vertically along deformed sediments at the rim of the salt domes and Paleogene polygonal faults towards shallow reservoirs.

5.6.4. Influence of glaciations and deglaciations

The study area was affected by several glaciations and deglaciations during the Late Pleistocene (Ehlers, 1990; Litt et al., 2008). During this period, ice sheets with thicknesses of several hundred meters covered the southern North Sea, including the area of the German Central Graben (Mahaney, 1995). These ice sheets are not integrated into the petroleum system model, but the additional load and its subsequent removal potentially affected the investigated petroleum system. Sachse and Littke (2018) investigated the influence of the Pleistocene ice loads and their retreat on a similar petroleum system onshore northern Germany, including salt domes, the Posidonia Shale as a source rock, and Middle Jurassic sandstones as a potential reservoir rock. Their model indicates a cooling effect of several degrees of the ice on the temperature of source and reservoir rocks, especially near salt domes due to their high thermal conductivity (Mello, 1995; Neunzert et al., 1996). This observation confirms the matching results of Grassmann et al. (2010) for the nearby Mittelplate oil field. The ice sheets also changed the porosities and the pore pressures of the underlying formations (Sachse and Littke, 2018). If these changes are only valid for the period of glaciation or if they are irreversible is not yet resolved definitively and may depend on the ice thickness and the duration of the glaciation. The ice-induced overpressure triggers a process called “glacial pumping” (Sachse and Littke, 2018). The increased pore

pressure leads to microfracturing of source rocks or sealing shales, which facilitates enhanced hydrocarbon migration out of the source rock and out of the reservoir, respectively. Besides microfracturing, the ice-load may also influence rock mechanics in a greater scale. The change in the pressure regime may decrease the stability of the faults, thus creating pathways for hydrocarbon migration (Johnston et al., 1998; Lund and Näslund, 2009).

5.7. Conclusions

For this study, important source rocks of the southern North Sea, the Posidonia Shale Formation and the Clay Deep Member, were mapped in the German Central Graben using reflection seismic and well log data. To assess the hydrocarbon potential of the area, they were integrated into a petroleum system model, together with four other potential source rocks. The modeling showed the following results:

- The elsewhere prolific Posidonia Shale Formation is only locally significant in the German Central Graben.
- The Clay Deep Member is present in large parts of the German Central Graben but is probably immature for hydrocarbon generation.
- The non-“Hot Shale” Kimmeridge Clay Formation (Farsund/Lola equivalent in the Danish sector) is generally a poor source rock, but may have generated gas at its lower section.
- The Aalburg and Sleen Formation are currently in the gas window and the transformation of kerogen to hydrocarbons is advanced. However, the quality as a prolific source rock is uncertain.
- The coaly intervals of the Central Graben Subgroup are now in the maturity window of gas generation. Its humic kerogen type III is gas-prone and is likely to have generated gaseous and potentially liquid hydrocarbons.

The silty and sandy sections of the Central Graben Subgroup are also likely migration conduits and potential reservoir rocks for hydrocarbons generated by the coaly intervals and surrounding marine claystones. These hydrocarbons may have accumulated in the porous and permeable sections of the Central Graben Subgroup at contacts with salt domes or in anticlinal structures. Thermogenic methane from these sources is likely to have contributed to potential shallow gas accumulations in the German Central Graben. Indications that are related to potential shallow gas accumulations point to an active thermogenic petroleum system in the German Central Graben, which is supported by the results of the petroleum system modeling. The connection of the graben evolution and the halotectonics to the distribution of source rock facies in the area is still not established and worth more attention in the future.

Acknowledgments

The presented research was done in the project “Tieferer Untergrund Norddeutsches Becken (TUNB) within the Federal Institute for Geosciences and Natural Resources of Germany (BGR). We thank our colleagues Christoph Gaedicke, Dieter Franke, Lutz Reinhardt, Rüdiger Lutz, Stefan Ladage and Heidrun Stück who provided expertise that greatly assisted the research. We thank Hanneke Verweij from TNO and Jutta Winsemann from the Leibniz University Hannover for their helpful input. We also want to acknowledge the support from Franziska-Sabine Müller and Tilda Müller-Thiel, which was invaluable. Last not least, we also thank the associate editor Jonathan Craig, the reviewer Friedemann Baur, and an anonymous reviewer for their helpful and detailed comments, which improved this article.

References

- Andsbjerg, J. & Dybkjær, K., 2003. Sequence stratigraphy of the Jurassic of the Danish central graben. In: Surlyk, F., Ineson, J.R. (eds.), *The Jurassic of Denmark and Greenland*. Geological Survey of Denmark and Greenland Bulletin, vol. 1. pp. 265–300.
- Arfai, J. & Lutz, R., 2017. 3D basin and petroleum system modeling of the NW German North Sea (Entenschnabel). In: Bowman, M., Levell, B. (Eds.), *Petroleum Geology of NW Europe: 50 Years of Learning – Proceedings of the 8th Petroleum Geology Conference*. Geological Society, London, pp. 8–35.
- Arfai, J., Jähne, F., Lutz, R., Franke, D., Gaedicke, C. & Kley, J., 2014. Late Palaeozoic to early Cenozoic geological evolution of the northwestern German North Sea (Entenschnabel): new results and insights. *Neth. J. Geosci.* 93 (4), 147–174.
- Bernard, B.B., Brooks, J.M. & Sackett, W.M., 1976. Natural gas seepage in the Gulf of Mexico. *Earth Planet. Sci. Lett.* 31, 48–54.
- BP, 2018. *Statistical Review of World Energy*.
- Burnham, A.K., 1989. A Simple Kinetic Model of Petroleum Formation and Cracking. Internal report of Lawrence Livermore National Laboratory, Report UCID 21665. Lawrence Livermore National Laboratory, Livermore, CA.
- Cartwright, J.A., 1994. Episodic basin-wide hydrofracturing of overpressured early Cenozoic mudrock sequences in the North Sea Basin. *Mar. Pet. Geol.* 11 (5), 587–607.
- Cayley, G.T., 1987. Hydrocarbon migration in the Central North Sea. In: Brooks, J., Glennie, K. (eds.), *Petroleum Geology of North West Europe*. Graham & Trotman, London, pp. 549–555.
- Clark-Lowes, D.D., Kuzemko, N.C.J. & Scott, D.A., 1987. Structure and petroleum prospectivity of the Dutch Central Graben and neighbouring platform areas. In: Brooks, J., Glennie, K. (eds.), *Petroleum Geology of North West Europe*. Graham & Trotman, London, pp. 337–356.
- Cornford, C., 1994. Mandal-ekofisk (!) petroleum system in the central graben of the North Sea. In: Magoon, L.B., Dow, W.G. (eds.), *The Petroleum System – from Source to Trap*, vol. 60. AAPG Memoir, pp. 537–571.
- Damtoft, K., Andersen, C. & Thomsen, E., 1987. Prospectivity and hydrocarbon plays of the Danish central trough. In: Brooks, J., Glennie, K. (eds.), *Petroleum Geology of North West Europe*. Graham & Trotman, London, pp. 403–417.
- de Jager, J.D. & Geluk, M., 2007. *Petroleum Geology. Geology of the Netherlands*. Royal Netherlands Academy of Arts and Sciences, Amsterdam, pp. 241–264.
- EBN, 2016. *Focus on Dutch Oil and Gas 2016*. EBN B.V., Utrecht.
- Ehlers, J., 1990. Reconstructing the dynamics of the north-west European Pleistocene ice sheets. *Quat. Sci. Rev.* 9, 71–83.

- Erratt, D., 1993. Relationship between basement faulting, salt withdrawal and Late Jurassic rifting, UK, central North Sea. In: Parker, J.R. (ed.), *Petroleum Geology of Northwest Europe: Proceedings from the 4th Conference*. The Geological Society, London, pp. 1211–1219.
- Gašparík, M., Ghanizadeh, A., Bertier, P., Gensterblum, Y., Bouw, S. & Krooss, B.M., 2012. High-pressure methane sorption isotherms of black shales from The Netherlands. *Energy Fuels* 26, 4995–5004.
- Gautier, D.L., 2005. *Kimmeridgian Shales total Petroleum System of the North Sea Graben Province (No. 2204-C)*. Geological Survey (US).
- Geluk, M.C., 2007. Triassic. In: Wong, T.E., Batjes, D.A.J., de Jager, J. (eds.), *Geology of the Netherlands*. Royal Netherlands Academy of Arts and Sciences, Amsterdam, pp. 85–106.
- Gerling, P., Geluk, M.C., Kockel, F., Lokhorst, A., Lott, G.K. & Nicholson, R.A., 1999. NW European gas Atlas'—new implications for the Carboniferous gas plays in the western part of the southern permian basin. In: *Petroleum Geology Conference Series*, vol. 5. Geological Society, London, pp. 799–808 1.
- Grassmann, S., Cramer, B., Delisle, G., Hantschel, T., Messner, J. & Winsemann, J., 2010. pT-effects of Pleistocene glacial periods on permafrost, gas hydrate stability zones and reservoir of the Mittelplate oil field, northern Germany. *Mar. Pet. Geol.* 27, 298–306.
- Graversen, O., 2006. The Jurassic-Cretaceous North Sea rift dome and associated basin evolution. In: *American Association of Petroleum Geologists Annual Convention*, Calgary, Alberta, June 19-22, 2005.
- Hantschel, T. & Kauerauf, A.I. (eds.), 2009. *Fundamentals of Basin and Petroleum Systems Modeling*. Springer-Verlag, Berlin.
- Herngreen, G.F.W. & Wong, T.E., 2007. Cretaceous. In: Wong, T.E., Batjes, D.A.J., de Jager, J. (eds.), *Geology of the Netherlands*. Royal Netherlands Academy of Arts and Sciences, Amsterdam, pp. 127–150.
- Herngreen, G.W., Kouwe, W.F. & Wong, T.E., 2003. The Jurassic of The Netherlands. *Geol. Surv. Den. Greenl. Bull.* 1, 217–229.
- Hunt, J.M., 1991. Generation of gas and oil from coal and other terrestrial organic matter. *Org. Geochem.* 17, 673–680.
- Huuse, M. & Clausen, O.R., 2001. Morphology and origin of major Cenozoic sequence boundaries in the eastern North Sea Basin: top Eocene, near-top Oligocene and the mid-Miocene unconformity. *Basin Res.* 13 (1), 17–41.
- Ineson, J.R., Bojesen-Koefoed, J.A., Dybkjær, K. & Nielsen, L.H., 2003. Volgian–Ryazanian 'hot shales' of the Bo member (Farsund Formation) in the Danish central graben, North Sea: stratigraphy, facies and geochemistry. In: Surlyk, F., Ineson, J.R. (eds.), *The Jurassic of Denmark and Greenland*, vol. 1. Geological Survey of Denmark and Greenland Bulletin, pp. 403–436.

- Isaksen, G.H., Patience, R., Van Graas, G. & Jenssen, A.I., 2002. Hydrocarbon system analysis in a rift basin with mixed marine and nonmarine source rocks: the South Viking Graben, North Sea. *AAPG Bull.* 86 (4), 557–592.
- Jenden, P.D., Drazan, D.J. & Kaplan, I.R., 1993. Mixing of thermogenic natural gases in northern Appalachian basin. *AAPG Bull.* 77, 980–998.
- Jenkyns, H., 1988. The early Toarcian (Jurassic) anoxic event-stratigraphic, sedimentary, and geochemical evidence. *Am. J. Sci.* 288 (2), 101–151.
- Johnston, P., Wu, P. & Lambeck, K., 1998. Dependence of horizontal stress magnitude on load dimension glacial rebound models. *Int. Geophys. J.* 132, 41–60.
- Kombrink, H., ten Veen, J.H. & Geluk, M.C., 2012. Exploration in The Netherlands, 1987-2012. *Netherlands Journal of Geosciences - Geologie en Mijnbouw* 91 (4), 403–418.
- Lamb, R.M., Huuse, M. & Stewart, M., 2017. Early Quaternary sedimentary processes and paleoenvironments in the central North Sea. *J. Quat. Sci.* 32 (2), 127–144.
- Litt, T., Schmincke, H.-U., Frechen, M. & Schlüchter, C., 2008. Quaternary. In: McCann, T. (ed.), *The Geology of Central Europe. Volume 2: Mesozoic and Cenozoic.* Geological Society, London, pp. 1287–1340.
- Littke, R., Bayer, U., Gajewski, D. & Nelskamp, S. (eds.), 2008. *Dynamics of Complex Intracontinental Basins: the Central European Basin System.* Springer Science & Business Media, Berlin, Heidelberg 519 pp.
- Lokhorst, A. (ed.), 1998. *NW European Gas Atlas.* NITG-TNO (Haarlem) 154 pp.
- Lott, G.K., Wong, T.E., Duser, M., Andsbjerg, J., Mönnig, E., Feldman-Olszewska, A. & Verreussel, R.M.C.H., 2010. Jurassic. In: Doornenbal, J.C., Stevenson, A.G. (eds.), *Petroleum Geological Atlas of the Southern Permian Basin Area.* EAGE Publications b.v. (Houten), pp. 175–193.
- Lund, B. & Näslund, J.O., 2009. Glacial isostatic adjustment: implications for glacially induced faulting and nuclear waste repositories. In: Connor, C.B., Chapman, N.A., Connor, L.J. (eds.), *Volcanic and Tectonic Hazard Assessment for Nuclear Facilities.* Cambridge Press, Cambridge.
- Mahaney, W.C., 1995. Pleistocene and Holocene glacier thicknesses, transport histories and dynamics inferred from SEM microtextures on quartz particles. *Boreas* 24, 293–304.
- Mann, U., Leythaeuser, D. & Müller, P.J., 1986. Relation between source rock properties and wireline log parameters: an example from Lower Jurassic Posidonia Shale, NW Germany. *Org. Geochem.* 10 (4), 1105–1112.
- Mello, U.T., 1995. Role of salt in restraining the maturation of subsalt source rocks. *Mar. Pet. Geol.* 12, 697–716.
- Michelsen, O., Nielsen, L.H., Johannessen, P.N., Andsbjerg, J. & Surlyk, F., 2003. Jurassic lithostratigraphy and stratigraphic development onshore and offshore Denmark. In: Surlyk, F.,

- Ineson, J.R. (eds.), The Jurassic of Denmark and Greenland. Geological Survey of Denmark and Greenland Bulletin, vol. 1. pp. 147–216.
- Møller, J.J. & Rasmussen, E.S., 2003. Middle Jurassic – early Cretaceous rifting of the Danish central graben. In: In: Surlyk, F., Ineson, J.R. (eds.), The Jurassic of Denmark and Greenland. Geological Survey of Denmark and Greenland Bulletin, vol. 1. pp. 247–264.
- Mouritzen, C., Farris, M.A., Morton, A. & Matthews, S., 2018. Integrated Triassic stratigraphy of the greater Culzean area, UK central North sea. *Pet. Geosci.* 24 (2), 197–207.
- Mudford, B.S., Gradstein, F.M., Katsube, T.J. & Best, M.E., 1991. Modeling 1D compaction-driven flow in sedimentary basins: a comparison of the Scotian Shelf, North Sea and Gulf Coast. *Geol. Soc. Lond. Spec. Publ.* 59 (1), 65–85.
- Müller, S., Reinhardt, L., Franke, D., Gaedicke, C. & Winsemann, J., 2018. Shallow gas accumulations in the German North Sea. *Mar. Pet. Geol.* 91, 139–151.
- Neunzert, G.H., Gaupp, R. & Littke, R., 1996. Absenkungs- und Temperaturgeschichte paläozoischer und mesozoischer Formationen im Nordwestdeutschen Becken [Burial and temperature history of Paleozoic and Mesozoic formations in the northwest German Basin]. *Z. Dtsch. Geol. Ges.* 147, 183–208.
- Østfeldt, P., 1987. Oil-source rock correlation in the Danish North Sea. In: Brooks, J., Glennie, K. (eds.), *Petroleum Geology of North West Europe*. Graham & Trotman, London, pp. 419–429.
- O'Brien, G.W., Lawrence, G., Williams, A.K. & Brincat, M., 2002. Fault and top seal failure: exploration risk or rather a missed opportunity for evaluating hydrocarbon prospectivity at prospect to sub-basin scale? In: AAPG Hedberg Research Conference, 1-5 December, Barossa Valley, South Australia. Extended Abstract.
- Pepper, A.S. & Corvi, P.J., 1995a. Simple kinetic models of petroleum formation. Part I: oil and gas generation from kerogen. *Mar. Pet. Geol.* 12 (3), 291–319.
- Pepper, A.S. & Corvi, P.J., 1995b. Simple kinetic models of petroleum formation. Part III: modelling an open system. *Mar. Pet. Geol.* 12 (3), 417–452.
- Petersen, H.I. & Hertle, M., 2018. A review of the coaly source rocks and generated petroleum in the Danish North Sea: an underexplored Middle Jurassic petroleum system? *J. Pet. Geol.* 41 (2), 135–154.
- Petersen, H.I., Andsbjerg, J., Bojesen-Koefoed, J.A. & Nytoft, H.P., 2000. Coal-generated oil: source rock evaluation and petroleum geochemistry of the Lulita oilfield, Danish North Sea. *J. Pet. Geol.* 23 (1), 55–90.
- Petersen, H.I., Nytoft, H.P., Vosgerau, H., Andersen, C., Bojesen-Koefoed, J.A. & Mathiesen, A., 2010. Source rock quality and maturity and oil types in the NW Danish Central Graben: implications for petroleum prospectivity evaluation in an Upper Jurassic sandstone play area. *Geol. Soc. Lond. Petrol. Geol. Conf.* 7 (1), 95–111.

- Petersen, H.I., Hertle, M. & Sulsbrück, H., 2017. Upper Jurassic–lowermost Cretaceous marine shale source rocks (Farsund Formation), North Sea: kerogen composition and quality and the adverse effect of oil-based mud contamination on organic geochemical analyses. *Int. J. Coal Geol.* 173, 26–39.
- Petersen, H.I., Hertle, M. & Mauritzen, E., 2018. The Middle Jurassic coaly-sourced petroleum system in the Danish North Sea – an overlooked exploration target? In: 80th EAGE Conference and Exhibition, 11-14 June 2018, Copenhagen, Denmark. Extended Abstract.
- Pharaoh, T.C., Dussar, M., Geluk, M.C., Kockel, F., Krawczyk, C.M., Krzywiec, P., Scheck-Wenderoth, M., Thybo, H., Vejbæk, O.V. & Van Wees, J.D., 2010. Tectonic evolution. In: Doornenbal, J.C., Stevenson, A.G. (eds.), Permian Basin Area. EAGE Publications b.v. (Houten), pp. 25–57.
- Pletsch, T., Appel, J., Botor, D., Clayton, C.J., Duin, E.J.T., Faber, E., Górecki, W., Kombrink, H., Kosakowski, P., Kuper, G., Kus, J., Lutz, R., Mathiesen, A., Ostertag-Henning, C., Papiernek, B. & Van Bergen, F., 2010. Petroleum generation and migration. In: Doornenbal, J.C., Stevenson, A.G. (eds.), Petroleum Geological Atlas of the Southern Permian Basin Area. EAGE Publications b.v. (Houten), pp. 225–253.
- Ponsaing, L., Bojesen-Koefoed, J.A., Thomsen, E. & Stemmerik, L., 2018. Temporal organic facies variations of upper Jurassic-lowermost Cretaceous source rocks in the Danish central graben, North Sea. *Int. J. Coal Geol.* 195, 217–237.
- Reinhold, K., Krull, P. & Kockel, F., 2008. Karte der Salzstrukturen Norddeutschlands. BGR, Hannover.
- Rice, D.D. & Claypool, G.E., 1981. Generation, accumulation, and resource potential of biogenic gas. *AAPG Bull.* 65, 5–25.
- Sachse, V.F. & Littke, R., 2018. The impact of Quaternary glaciation on temperature and pore pressure in Jurassic troughs in the Southern Permian Basin, northern Germany. In: Kilhams, B., Kukla, P.A., Mazur, S., Mckie, T., Mijnlief, H.F., van Ojik, K. (eds.), Mesozoic Resource Potential in the Southern Permian Basin. Geological Society (London), vol. 469. Special Publications, pp. 371–398.
- Schoell, M., 1980. The hydrogen and carbon isotopic composition of methane from natural gases of various origins. *Geochem. Cosmochim. Acta* 44, 649–661.
- Schoell, M., 1983. Genetic characterization of natural gases. *AAPG Bull.* 67, 2225–2238.
- Stemmerik, L., Ineson, J.R. & Mitchell, J.G., 2000. Stratigraphy of the Rotliegend Group in the Danish part of the northern permian basin, North Sea. *J. Geol. Soc.* 157 (6), 1127–1136.
- Sweeney, J.J. & Burnham, A.K., 1990. Evaluation of a simple model of vitrinite reflectance based on chemical kinetics (1). *AAPG Bull.* 74 (10), 1559–1570.
- ten Veen, J., Verweij, H., Donders, T., Geel, K., de Bruin, G., Munsterman, D., Verreussel, R., Daza Cajjal, V., Harding, R. & Cremer, H., 2013. Anatomy of the Cenozoic Eridanos Delta hydrocarbon system. In: TNO Report TNO 2013 R10060. TNO, Utrecht 217 pp.

- ter Borgh, M.M., Jaarsma, B. & Rosendaal, E.A., 2018. Structural development of the northern Dutch offshore: Paleozoic to present. In: Underhill, A.A., Hewett, A.J., Marshall, J.E.A. (eds.), *Paleozoic Plays of NW Europe*. Geological Society (London), vol. 471. Special Publications, pp. 115–131.
- Thauer, R.K., 1998. Biochemistry of methanogenesis: a tribute to Marjory Stephenson. 1998 Marjory Stephenson prize lecture. *Microbiology* 144 (9), 2377–2406.
- Thomsen, E., Lindgreen, H. & Wrang, P., 1983. Investigation on the source rock potential of Denmark. *Geol. Mijnb.* 62, 221–239.
- Thomsen, R., Lerche, I. & Korstgårdt, J.A., 1990. Dynamic hydrocarbon predictions for the northern part of the Danish Central Graben: an integrated basin analysis assessment. *Mar. Pet. Geol.* 7 (2), 123–137.
- Underhill, J.R. & Partington, M.A., 1993. Jurassic thermal doming and deflation in the North Sea: implications of the sequence stratigraphic evidence. In: Parker, J.R. (ed.), *Petroleum Geology of Northwest Europe: Proceedings of the 4th Conference: the Geological Society (London)*. Petroleum Geology Conference Series, vol. 4. pp. 337–345.
- Ungerer, P., 1990. State of the art of research in kinetic modelling of oil formation and expulsion. *Org. Geochem.* 16 (1–3), 1–25.
- Van Buggenum, J.M. & den Hartog Jager, D.G., 2007. Silesian. In: Wong, T.E., Batjes, D.A.J., de Jager, J. (eds.), *Geology of the Netherlands*. Royal Netherlands Academy of Arts and Sciences, Amsterdam, pp. 43–62.
- Vandenbroucke, M., Behar, F. & Rudkiewicz, J.L., 1999. Kinetic modeling of petroleum formation and cracking: implications from the high pressure/high temperature Elgin Field (UK, North Sea). *Org. Geochem.* 30, 1105–1125.
- Verweij, J.M., Simmelink, H.J., Underschultz, J. & Witmans, N., 2012. Pressure and fluid dynamic characterisation of the Dutch subsurface. *Neth. J. Geosci.* 91 (4), 465–490.
- Verweij, J.M., Nelskamp, S.N., Ten Veen, J.H., De Bruin, G., Geel, K. & Donders, T.H., 2018. Generation, migration, entrapment and leakage of microbial gas in the Dutch part of the Southern North Sea Delta. *Mar. Pet. Geol.* 97, 493–516.
- Whiticar, M.J., Faber, E. & Schoell, M., 1986. Biogenic methane formation in marine and freshwater environments: CO₂ reduction vs. acetate fermentation-Isotope evidence. *Geochem. Cosmochim. Acta* 50, 693–709.
- Wong, D.A., 2007. Jurassic. In: Wong, T.E., Batjes, D.A.J., de Jager, J. (eds.), *Geology of the Netherlands*. Royal Netherlands Academy of Arts and Sciences, Amsterdam, pp. 107–125.
- Wong, T.E., Van Doorn, T.H. & Schroot, B.M., 1989. Late Jurassic petroleum geology of the Dutch central North Sea graben. *Geol. Rundsch.* 78 (1), 319–336.
- Ziegler, P.A., 1990. Geological Atlas of western and central Europe. In: Shell Internationale Petroleum Maatschappij B.V., second ed. Geological Society Publishing House, Bath 239 pp.

Ziegler, P.A., 1992. North Sea rift system. *Tectonophysics* 208 (1–3), 55–75.

6. Jurassic to Lower Cretaceous tectonostratigraphy of the German Central Graben, southern North Sea

This chapter has been submitted for publication as Müller, S., Jähne-Klingberg, F., Thöle, H., Jakobsen, F., Bense, F., Winsemann, J., Gaedicke, C., *in review*. Jurassic to Lower Cretaceous tectonostratigraphy of the German Central Graben, southern North Sea. Submitted to Netherlands Journal of Geosciences.

Abstract

The Central Graben is a Mesozoic sedimentary basin that is significantly influenced by rift and salt tectonics. Its southern part is located in the German and Dutch sectors of the North Sea. Even though studies exist on the tectonic and stratigraphic development of the Danish and Dutch Central Graben, the German Central Graben as an important link is less investigated. We aim to fill this gap and to investigate the sedimentary development from the Latest Triassic to the Early Cretaceous, the relative influence of salt and rift tectonics on subsidence, and how our results fit into the existing studies of the Danish and Dutch Central Graben. Knowledge of the development of the graben and its sedimentation is critical for any possible economic use like hydrocarbon exploitation or carbon capture and storage (CCS). Therefore, we mapped nine laterally traceable horizons on 2D and 3D reflection seismic data from the Lower Jurassic to the Lower Cretaceous within the German Central Graben and adjacent Danish Salt Dome Province as well as the northern Dutch Central Graben. These horizons include the base horizons of four tectonostratigraphic mega-sequences of the southern Central Graben adopted from the current Dutch tectonostratigraphic concept. Based on the mapping results, we constructed subsidence, thickness and erosion maps of the tectonostratigraphic mega-sequences and their subdivisions. The tectonostratigraphic mega-sequences were then correlated with well logs to determine the lithology. The results show that the structural and stratigraphic architecture of the German Central Graben was consecutively dominated by either subsidence controlled by rifting, salt tectonics, or by thermal uplift and subsidence. We suggest that the German Central Graben is divided by a large strike-slip fault zone, the Mid Central Graben Transverse Zone (MCGTZ), into a northern part that geologically rather belongs to the Danish and a southern part that rather belongs to the Dutch Central Graben. We discuss how this division and the tectonics influenced the regional lithology.

6.1. Introduction

The southern Central Graben, located in the southern North Sea, is an important hydrocarbon province of both The Netherlands and Denmark (Pletsch et al., 2010). Jurassic and Lower Cretaceous rocks are important as source and reservoir rocks for the hydrocarbon systems in the region. The bulk of the hydrocarbons originates from Lower Jurassic to Lower Cretaceous source rocks, of which the Lower Jurassic Posidonia Shale Formation (offshore The Netherlands) and the Upper Jurassic to Lower Cretaceous Bo Member (offshore Denmark) of the Farsund Formation are the most significant and prolific ones (Lott et al., 2010). It is assumed that some of the locally present hydrocarbons originate from secondary Jurassic source rocks, e.g., Lower Jurassic marine claystones from the Aalburg Formation and Middle Jurassic coals from the Central Graben Subgroup (de Jager & Geluk, 2007; Wong, 2007; Müller et al., 2020). Middle Jurassic sandstones of the Central Graben Subgroup also constitute reservoir rocks, e.g., the oil and condensate field F3-FB in the northern Dutch Central Graben. The southern Central Graben is a Mesozoic rift system that was most active from the Middle Jurassic to the Early Cretaceous. Its tectonostratigraphic evolution is accompanied by significant proportion of

halokinesis and halotectonics. The salt tectonics had a great impact on the basin evolution and sedimentation (ten Veen et al., 2012; Jackson & Hudec, 2017). Salt withdrawal and diapir growth, combined with active rifting, induced the segmentation of the basin into several sub-basins (Arfai et al., 2014). Sedimentation again reciprocally influenced salt mobilization by differential loading.

Due to the close relationship between rifting, salt tectonics, and sedimentation, research that links these three aspects is crucial to understand the sedimentary system of the Graben and to fully assess the economic potential of the area, regarding hydrocarbon exploitation or carbon capture and storage (CCS). A tectonostratigraphic approach that studies the relationship between stratigraphic successions and the influence of tectonic processes is therefore an appropriate procedure to investigate such an environment as the southern Central Graben.

Different authors attended to the sedimentary and tectonic evolution of the Danish Central Graben. Andsbjerg and Dybkjaer (2003) established a sequence stratigraphic framework for the Jurassic of the Danish Central Graben. Michelsen et al. (2003) examined the lithostratigraphy and the distribution of the depositional systems in the Jurassic and Early Cretaceous of the Danish Central Graben. Møller and Rasmussen (2003) did research on the tectonic evolution of the Danish Central Graben, which they differentiated into several tectonic pulses. Duffy et al. (2013) integrated the consideration of salt tectonic processes into basin evolution concepts and investigated how they influenced the structural style and the tectonostratigraphy of the Danish Central Graben.

For the Dutch Central Graben, Verreussel et al. (2018) and Bouroullec et al. (2018) developed a tectonostratigraphic model of the southern Central Graben. This paper builds on their work by adopting their concept of four tectonostratigraphic mega-sequences in the graben evolution. We will complement the missing link of the German Central Graben for more consistent tectonostratigraphic correlation of basin evolution of the NNW-SSE trending Danish Central Graben and the NNE-SSW trending Dutch Central Graben (*Fig. 46*). For this we take a closer look to changes of sedimentation patterns over time, where erosion took place, how rifting and salt tectonics influenced sedimentation, and how these influences changed in different tectonic phases. To answer these questions, we used seismic interpretation as well as well log correlation.

6. Jurassic to Lower Cretaceous tectonostratigraphy of the German Central Graben, southern North Sea

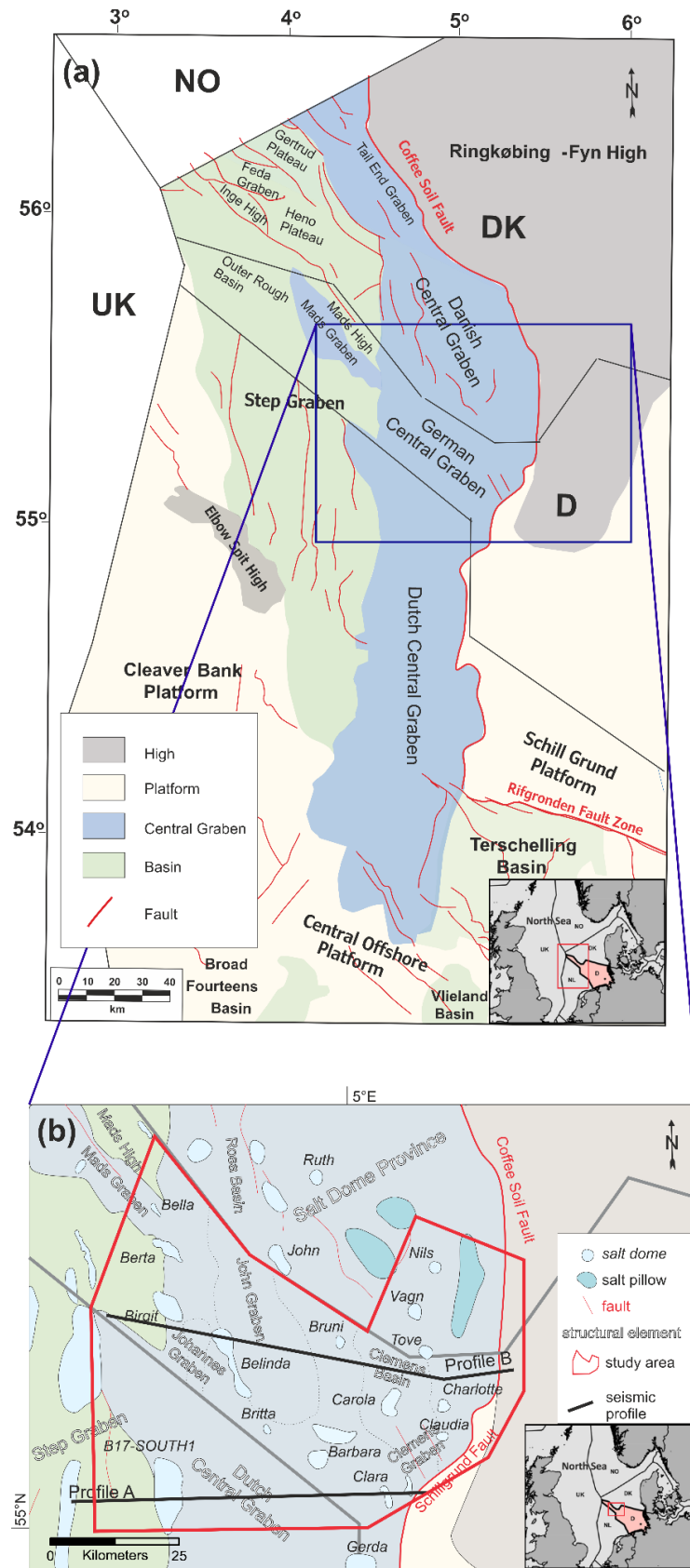


Fig. 46 (a) Structural map of the southern North Sea including the southern Central Graben (blue-grey), adjacent basins and highs, and faults (red) (modified from Jakobsen et al. (2020a)). (b) Structural map of the study area of the paper, including adjacent basins and highs, salt structures, and the main bounding fault (red). Profile A and Profile B show geological interpretations of exemplary seismic sections (Fig. 49 and Fig. 50).

6.2. Geological evolution

6.2.1. Tectonic and sedimentary evolution

The southern Central Graben, in its narrow definition without the Step Graben system, is a about 250 km long and on average about 50 km wide half-graben (Fig. 46). It is limited to its east by its eastern main bounding faults (MBF), the Coffee Soil Fault system (CSF) for the Danish part and the Schillgrund Fault system (SF) for the German and Dutch part of the graben (Thöle et al., 2021). It comprises the NNE-SSW trending Dutch Central Graben, the NNW-SSE trending Danish Central Graben to the Norwegian border, and in between the German Central Graben. Within the German Central Graben, the Mid Central Graben Transverse Zone (MCGTZ) is located, which is also known as Thor Transverse zone (Wride, 1995) and divides the study area roughly in half into a northern and southern part (Thöle et al., 2021).

The here investigated part of the southern Central Graben is located in the northwestern part of the Southern Permian Basin in transition to the East and Mid North Sea Highs. The Southern Permian Basin (SPB) is an ESE-WNW trending intracontinental basin that started to subside during the late Early Permian (Bachmann & Grosse, 1989; Bachmann & Hoffmann, 1997). During the Late Permian, cyclic deposition of marine evaporites of the Upper Permian Zechstein group took place in the basin (Geluk, 2007; Stollhofen et al., 2008).

The supercontinent Pangea broke up from the Triassic to the Early Cretaceous along a roughly SW-NE-trending line, the Arctic-North Atlantic mega-rift system, with rifting between Greenland and the Baltic Shield towards the Central Atlantic domain (Ziegler, 1992; Pharaoh et al., 2010). A southeastern part of the mega-rift system is the triple junction of the North Sea Rift System. It consists of the Viking Graben, the Moray Firth-Witch Ground graben, and the Central Graben as its southern arm, which showed major tectonic activity in the Late Triassic (Ziegler et al., 1992; Jähne-Klingberg et al., 2018). The development of the Central Graben is closely connected with the break-up of Pangea from the Triassic to the Early Cretaceous (de Jager, 2007), Nevertheless, the Central Graben presumably rests on structural precursors going back to the Rotliegend (Stemmerik et al., 2000). First prominent tectonic activity with moderate rifting, though, started not until the Middle Triassic for the German part of the Graben (Jähne-Klingberg et al., 2018) During the Mid Triassic, a roughly E-W-oriented extensional stress field developed in the study area that persisted until the Late Jurassic (Sippel, 2009).

The southern North Sea area of the Latest Triassic (Rhaetian) and the Early Jurassic was dominated by a shallow epicontinental sea in a time of relative tectonic quiescence (Pharaoh et al., 2010), except for the larger approximately N-S striking Glückstadt Graben, Horn-Graben and to a lesser extent the Central Graben. This resulted in the wide-scale deposition of fine-grained mudstones, such as the Posidonia Shale Formation, during a time of stagnant water stratification (Lott et al., 2010; Fig. 47). This depositional system ended in the Middle Jurassic with the emergence of the Central North Sea thermal dome at the center of the triple junction (Graversen, 2006). The uplift resulted in erosion of Jurassic and Triassic sediments on the platforms and marginal areas, represented by the regional Mid-Cimmerian Unconformity, while deposition

continued only in the Central basin areas like the Central Graben (Underhill & Partington, 1993). After the collapse of the thermal dome in the late Middle Jurassic, subsidence resumed, evidenced by the deposition of continental and paralic sediments and subsequently of marine claystones (Wong, 2007; Fig. 47). During the Late Jurassic, rifting increased and halotectonics intensified, which resulted in a complex system of intra basin platforms, highs and subbasins in the southern Central Graben (Arfai et al., 2014).

Rifting stopped in the late Early Cretaceous and sedimentation was more evenly distributed in the following post-rift thermal sag phase (Wong, 2007). A long-term transgression in the Early Cretaceous led to the deposition of at first open-marine clay and then marl (Herngreen & Wong, 2007). Over-regional NE/NNE compressional stresses as an effect of the Africa-Iberia-Europe convergence resulted in structural inversion of parts of the Central Graben, parallel to ongoing transgression to the deposition of shallow marine carbonates (Vejbæk & Andersen, 1987; de Jager, 2003, 2007; Kley and Voigt, 2008; Rasmussen, 2009). Compression ceased in the Paleocene and an intracontinental sag basin developed in the southern North Sea, which does not or only inconspicuously trace pre-existing structures, reaching its present-day state in the Eocene (Huuse & Clausen, 2001; Walter, 2007).

The Uppermost Triassic to Lower Cretaceous lithostratigraphy of the southern Danish, German and Dutch parts of the Central Graben is illustrated in Fig. 47. The apparent differences of the national sections originate from the diachronous development of the southern Central Graben as well as of decades of development of separate national tectonostratigraphies – which focus on different national specificities without cross-border harmonization. Denmark and The Netherlands use different national terms for lithologies from the same or a related depositional setting, e.g., Lower Jurassic open-marine clays (Fig. 47). In the following, we call these related lithostratigraphic terms “equivalents”.

6. Jurassic to Lower Cretaceous tectonostratigraphy of the German Central Graben, southern North Sea

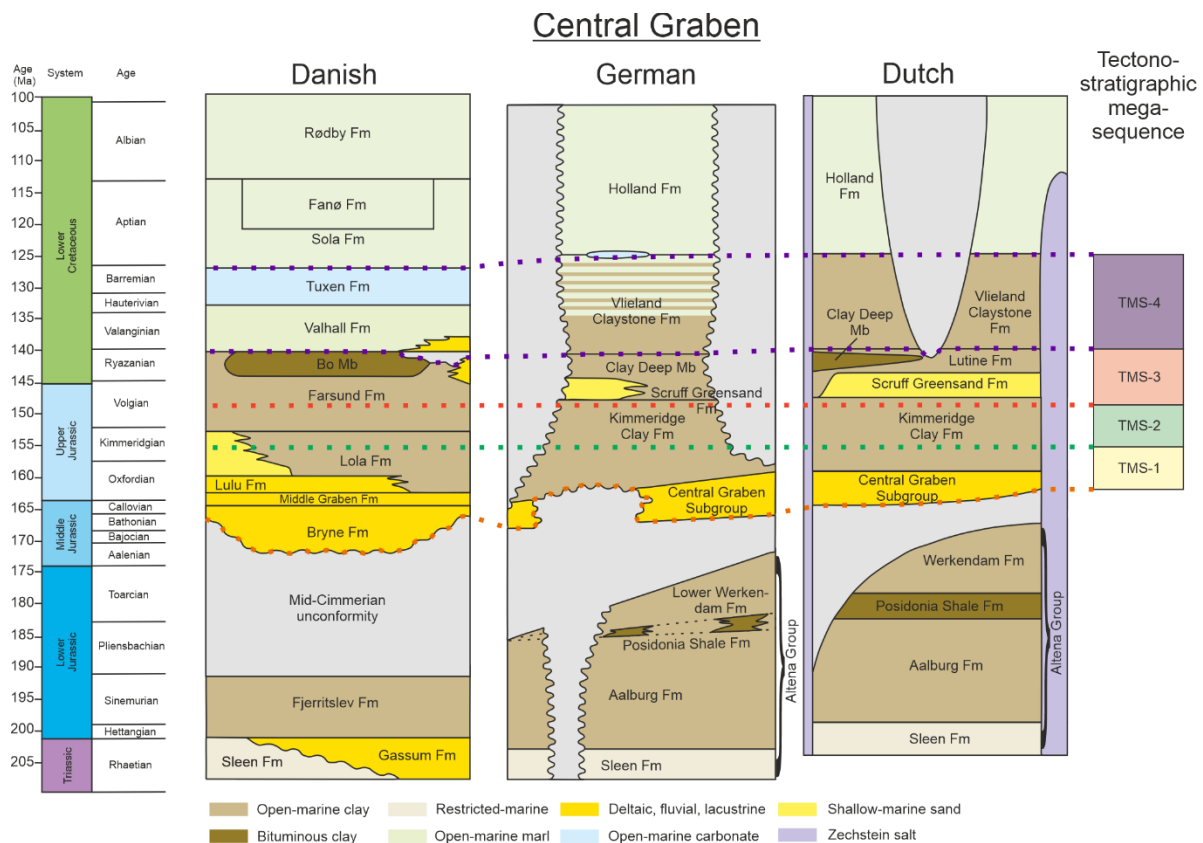


Fig. 47 Lithostratigraphy of the Danish, German, and Dutch Central Graben, covering the study period with tectonostratigraphic mega-sequences (TMS) from the Late Triassic to the Early Cretaceous including the most active phase of rifting and halotectonics. Differences between the national lithostratigraphies are the result of a diachronous development of the graben, as well as of different national research histories. Modified from Jakobsen et al. (2020b).

6.2.2. Jurassic sequence- and tectonostratigraphy in the southern Central Graben

6.2.2.1. Danish Central Graben

Andsbjerg and Dybkjaer (2003) established a sequence stratigraphic framework for the Danish Central Graben on the basis of the analysis of well logs, sedimentological core logs, lithology logs, and biostratigraphic data. They differentiated the Jurassic and Lower Cretaceous succession into 20 sequences, which are assigned to seven rifting phases. These phases range from a pre-rift stage, uplift and erosion due to the Mid-North Sea Dome, rift initiation and rift climax finally to the beginning of a post-rift stage with uniform subsidence (Tab. 5).

6. Jurassic to Lower Cretaceous tectonostratigraphy of the German Central Graben, southern North Sea

Tab. 5 The age, tectonic state, depositional environment, and associated sediments of the rift phases of the Danish Central Graben according to Andsbjerg and Dybkjaer (2003) and Møller and Rasmussen (2003).

Phase	Age	Tectonic state	Depositional environment & sediments
7	late Middle Volgian - Ryazanian	early post-rift stage; decreasing rate of subsidence; ceasing of fault activity on main boundary fault	marine conditions; organic -rich mudstones and basin axis turbidites
6	latest Late Kimmeridgian - middle Middle Volgian	rift pulses and thermal subsidence in between; NNW-SSE trending faults	marine conditions; deep-water mudstones
5	Late Kimmeridgian	waning of rift-related subsidence; activity low between two rift pulses; NNW-SSE trending faults	low-energy marine conditions, shallow marine to paralic in marginal areas; marine mudstones, shallow marine to paralic sandstones in marginal areas
4	Early Oxfordian - Early Kimmeridgian	rift pulse related transgression; rift climax	transgressive development, from paralic to fully marine; marine mudstones, locally marginal marine sandstones
3	latest Aalenian/earliest Bajocian - Late Callovian	initiation of syn-rift subsidence; increase of salt tectonics, N-S trending faults	terrestrial and marginal marine; asymmetric distribution of sediments; fluvial, estuarine, and lacustrine sand and mudstones
2	latest Pliensbachian - latest Aalenian	regional uplift and erosion	erosion; major unconformity
1	Hettangian - Pliensbachian	pre-rift; tectonically quiescent; uniform subsidence history	shallow marine; uniform lithologies; dominated by shelf mudstones

Møller and Rasmussen (2003) distinguished between three tectonic pulses that formed the Danish Central Graben. The first pulse lasted from the Callovian to the Early Oxfordian and concentrated along pre-existing N-S-trending faults. The second tectonic pulse, from the Late Kimmeridgian to the Early Volgian, created new NNW-SSE striking faults. During this pulse, salt tectonics intensified and controlled the location of depocenters away from the main boundary fault of the Central Graben. The last tectonic pulse took place in the mid-Ryazanian.

6.2.2.2. Dutch Central Graben

Abbink et al. (2006) differentiated the Middle Jurassic to Lower Cretaceous stratigraphy of the Dutch Central Graben into four large-scale stratigraphic sequences. Verreussel et al. (2018) and Bouroullec et al. (2018) then developed the concept further into a new tectonostratigraphic model. They defined four tectonostratigraphic mega-sequences (TMS) based on palynological, geochemical, sedimentological analyses as well as seismic and well log interpretation. The TMS are defined as main phases of the basin evolution that are governed by changes in the tectonic regime (Verreussel et al., 2018). TMS-1 is of Bathonian to Early Kimmeridgian age, when sedimentation was limited to the axis of the graben. The sediments of TMS-2 were deposited during the Late Kimmeridgian to the Late Volgian. TMS-2 is characterized by active faulting and salt movement and sedimentation on basins and plateaus adjacent to the graben axis. During the sedimentation of TMS-3 (Volgian to Ryazanian) fault activity ceased and sedimentation occurred also on the adjacent plateaus. The sediments of TMS-4 lasted during the Valanginian to the Barremian, when the rift phase ended, and the entire southern North Sea was subject to thermal subsidence.

6.3. Data and methods

6.3.1. Seismic interpretation

Seismic analysis was carried out on three 3D seismic reflection surveys and several 2D seismic reflection lines from different surveys, which were selected to cover the study area. The study area comprises the area of the German Central Graben and adjacent areas of the northern Dutch Central Graben and of the southern Salt Dome Province of the Danish Central Graben. The 3D seismic survey “Entenschnabel 2002” covers the Dutch part, most of the German part of the study area and originally parts of the Danish North Sea (Fig. 48). However, for this study, the data was only available as two separate Dutch and German parts, without the Danish part. Therefore, 2D seismic reflection lines were used in the Danish sector (Fig. 48). Seismic analysis was carried out with Schlumberger’s GeoFrame software. Seismic interpretation of the horizons was performed in the time domain. The horizons were subsequently depth converted using Paradigm’s SeisEarth (v.2018/2019) and SkuaGocad (v.2019) software. The depth conversion based on a harmonized v_0 -k seismic velocity modeling approach for the Central Graben area carried out as part of the GeoERA 3DGEO-EU project (Doornenbal et al., 2021a; Thöle et al. 2021).

In a first step, we adopted the tectonostratigraphic concept of Verreussel et al. (2018) and Bouroullec et al. (2018) from the Dutch Central Graben and applied it to the study area. Starting point of our seismic interpretation was a 2D seismic section (profile D from Bouroullec et al., 2018; Fig. 48) that intersects the northernmost part of the Dutch Central Graben approximately perpendicular to the graben axis and parallel to the Dutch-German border. Coming from this profile, we extended the interpretation of the base horizons of TMS-1, TMS-2, TMS-3, and TMS-4, as well as an intra-TMS-1 erosional surface to the northern Dutch Central Graben, the

6. Jurassic to Lower Cretaceous tectonostratigraphy of the German Central Graben, southern North Sea

German Central Graben without its most northwestern extension, the Mads Graben, and to the south-eastern part of the Salt Dome Province of the Danish Central Graben (Fig. 47). To investigate the tectonostratigraphic evolution of the Jurassic and Lower Cretaceous of the study area in more detail, we further subdivided the tectonostratigraphic mega-sequences regarding prominent regional seismic horizons (base TMS-1.3 intra Kimmeridge Clay Formation) or prominent lithological changes (base TMS-1.2 base Kimmeridge Clay Formation, TMS-3-2 base “Hot Shale”) that can be correlated between wells. Additionally, we mapped the base of the Lower Cretaceous Holland Formation, representing the part of the Lower Cretaceous after TMS-4, and used existing seismic interpretation data (Arfai et al., 2014) of the base of the Altena Group (Sleen, Aalborg, Posidonia Shale, and Werkendam Formation in the German and Dutch nomenclature, and Sleen and Fjerritslev Formation in the Danish nomenclature) as a combined pre-rift horizon (Fig. 49 and Fig. 50).

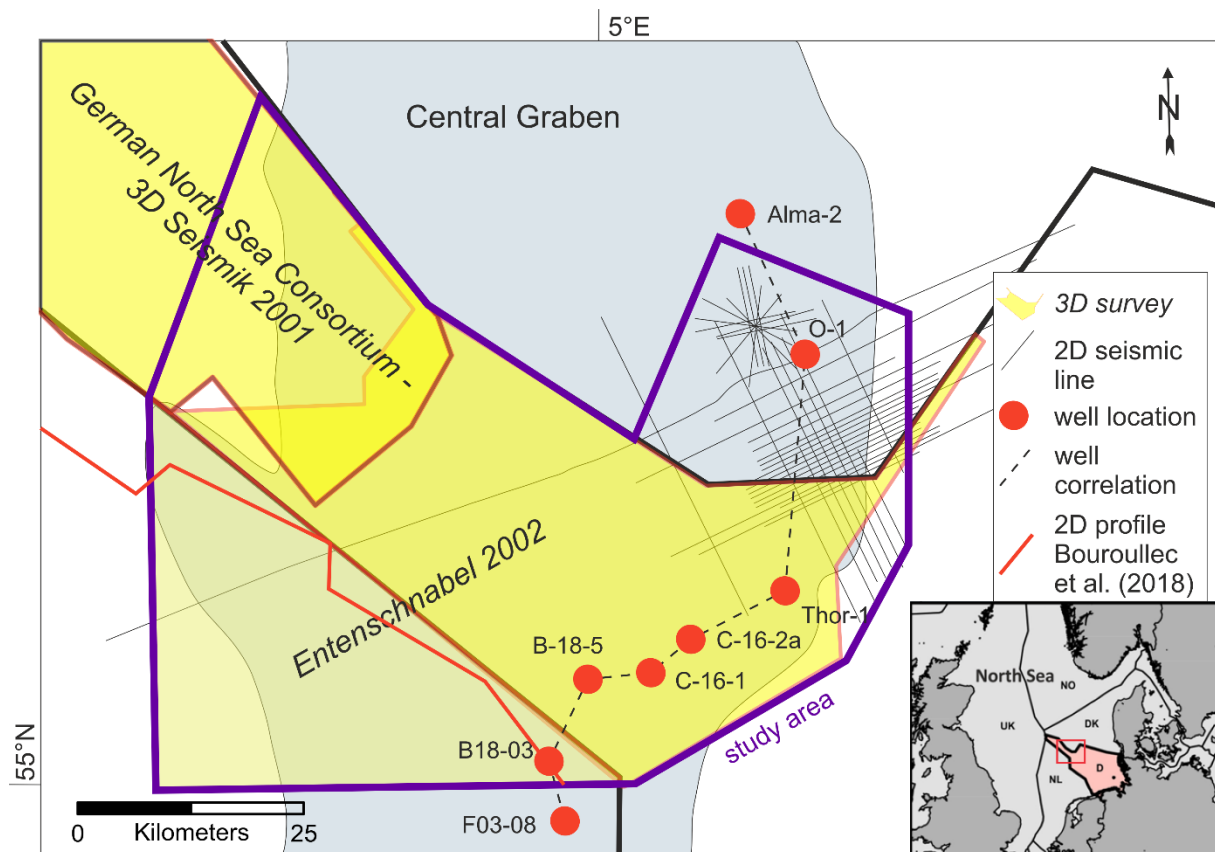


Fig. 48 Data used in the present study: Two 3D reflection seismic surveys for the German Central Graben, one 3D reflection seismic survey for the northern Dutch Central Graben, several 2D reflection seismic lines from different surveys for the southeastern part of the Salt Dome Province of the Danish Central Graben, as well as eight wells within or adjacent the study area for well correlation. The 3D survey “Entenschnabel 2002” is divided in a Dutch and German part. The 2D seismic profile from Bouroullec et al. (2018) was the initial point for the seismic interpretation.

6.3.2. Thickness and subsidence maps

The presented thickness and subsidence maps were created with Skua/Gocad (v.2019). On the base of horizon grids, originating from seismic interpretation, closed grids were created with grid mathematics to receive for every interpreted unit a top and base grid. Gridding artefacts and overlaps of the horizon grids were also finally eliminated by grid mathematic. However, especially in highly faulted areas and regions with steep dipping layers (e.g., salt rim synclines), in some cases generalizations were unavoidable. This was considered in the subsequent interpretation of the thickness distribution. Subsidence maps were created by including ages of the tectonostratigraphic mega-sequences from Bouroullec et al. (2018). The calculation of the subsidence values is based on simplified assumptions. Compactions was not taken into account, which means that the calculated subsidence values tend to be too low. Furthermore, the average was taken over the respective period of the considered tectonostratigraphic cycles. Thus, higher subsidence rates may have been achieved at times within the respective TMS-cycles. Areas of partial erosion were highlighted by putting eroded areas of the next sequence on top of the particular map (Fig. 51 and Fig. 52).

6.3.3. Well log correlation

The evident differences in the stratigraphic charts of the Dutch, German and Danish part of the southern Central Graben originate in a diachronous development of the Central Graben, in which Jurassic rifting started in the north and continued to the south. These locally different stages of basin evolution, as well as basin compartmentalization due to salt tectonics and lateral differences in rifting history, resulted in lateral variations and changes in lithofacies. Therefore, we correlated wells from structural different locations within the Central Graben (Fig. 54).

The palynological information (dinoflagellate cyst zonation) that was essential for the age determination of the TMS in the Dutch offshore was used to correlate the tectonostratigraphy of the Dutch Central Graben to the sequence stratigraphy of the Danish Central Graben by Jakobsen et al. (2020a) (Tab. 6). The integration of both approaches revealed a close correlation between the Danish sequence and the Dutch tectonostratigraphic subdivisions. Based on the comparison of the depositional units of the Dutch and the Danish Central Graben, the Dutch tectonostratigraphic nomenclature could be assigned approximately to the Danish sequence boundaries. The lower boundary of the Bat-1 sequence as well as of TMS-1 is defined by the occurrence of *Adnatosphaeridium caulleryi*. The last occurrence datum (LOD) of *Endoscrinium galeritum* at the base of the Kimm-2 sequence is found again at the top of TMS-1. The base of TMS-3 correlates to the middle to upper part of sequence Volg-4, which is evidenced by the LOD of *Egmontodinium polyplacophorum* (approximately base TMS-3) and the LOD of *Dichadogonyaulax Pannea* (approximately top TMS-2). Thus, the correlation between TMS-3 and the sequence Volg-4 has a higher uncertainty. The top of the sequence Ryaz-1 corresponds exactly to the base of TMS-4 due to the LOD of *Dingodinium spinosum*. No palynological data nor a detailed stratigraphy is available for offshore Germany. To fill the gap between the Dutch

and Danish sectors, the results of the detailed mapping of the tectonostratigraphic mega-sequences was transferred to the well logs using synthetic seismograms based on gamma ray (GR) and sonic (DT) logs as well as if available based on density logs.

Tab. 6 Correlation of the sequence boundaries of Andsbjerg and Dybkjaer (2003) of the Danish Central Graben with the tectonostratigraphy of Verreussel et al. (2018) and Bouroulllec et al. (2018). The correlation is based on LOD (last occurrence datum) Dinocyt events determined in these studies and modified from Jakobsen et al. (2020a).

Danish Central Graben	Cen-	Dutch Central Graben	Cen-	German Central Graben	Cen-	Dinocyst event (LOD)
top Ryaz-1 sequence		base TMS-4		base TMS-4		Dingodinium spinosum
middle to upper Volg-4 sequence		base TMS-3		base TMS-3		Egmontodinium polyplacophorum; Dichadogonyaulax Pannea
base Kimm-2 sequence		base TMS-2		base TMS-2		Endoscrinium galeritum
base Bat-1 sequence		base TMS-1		base TMS-1		Adnatosphaeridium caulleryi

Eight wells, each one presented by a GR and a DT log, were chosen for well log correlation. The eight wells extend from the northern Dutch Central Graben in the south (F03-08 and B18-03), across the German Central Graben (B-18-05, C-16-1, C-16-2a, and Thor-1) and into the Salt Dome Province of the southern Danish Central Graben in the North (O-1, Alma-2, at which Alma-2 is located outside of the area of investigation (Fig. 48).

6.4. Results

6.4.1. Seismic interpretation and gridding

The mapping of nine Jurassic to Lower Cretaceous horizons illustrates the tectonic and sedimentary evolution of the German Central Graben and adjacent areas. The mapped horizons include the base and top horizons of the defined tectonostratigraphic mega-sequences. We created two geological cross-sections based on depth converted seismic transects (Fig. 49 and Fig. 50) that cover the south and the center of the study area. Twelve thickness maps were constructed that comprise the pre-rift state of the Lower Jurassic Altena Group to the post-rift state of the Lower Cretaceous Holland Group (Fig. 51 and Fig. 52). The results, that are shown in these figures are described and interpreted in this section.

6. Jurassic to Lower Cretaceous tectonostratigraphy of the German Central Graben, southern North Sea

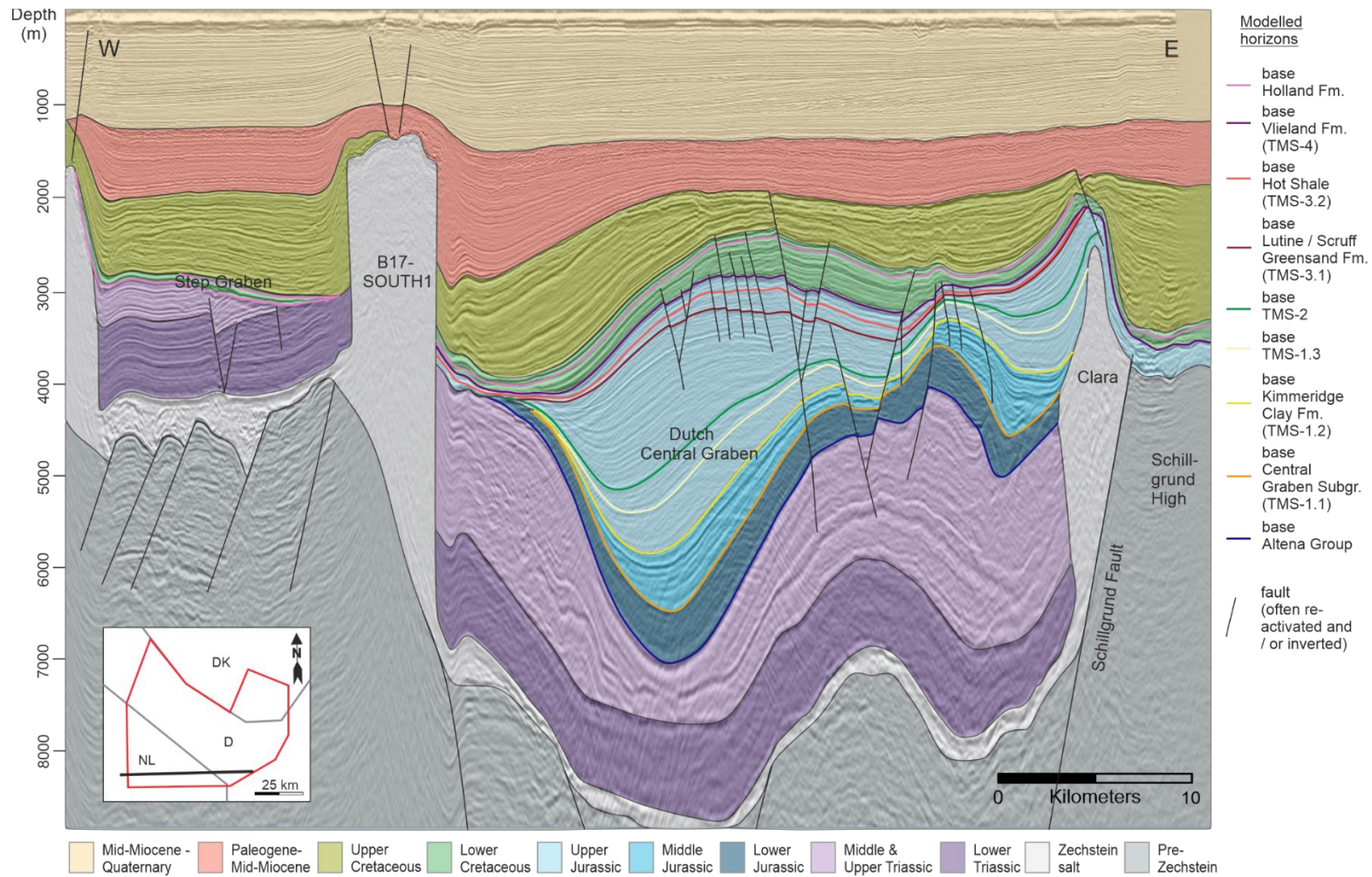


Fig. 49: Interpreted depth converted 2D seismic profile in the south of the study area. The seismic section starts on the Step Graben (the strongly dissected half-graben shoulder of the Central Graben) in the west and crosses the salt structure “B17-SOUTH1”, the northern Dutch Central Graben, the salt structure “Clara” in top of the Coffee-Soil fault and ends at the Schillgrund High outside the Central Graben. Eye-catching are the Late Jurassic depocenters in the center of the northern Dutch Central Graben and at the western flank of “Clara” in the hanging wall of the CSF, which shift steadily from TMS-1 to TMS-2 towards the salt structures, indicating an increasing influence of halotectonics during the Later Jurassic. Former topographic lows and depocenters of TMS-2 to the Lower Cretaceous in the Dutch Central Graben were structurally inverted during Late Cretaceous compression and formed an impressive turtle structure. The profile is five times vertically exaggerated.

6. Jurassic to Lower Cretaceous tectonostratigraphy of the German Central Graben, southern North Sea

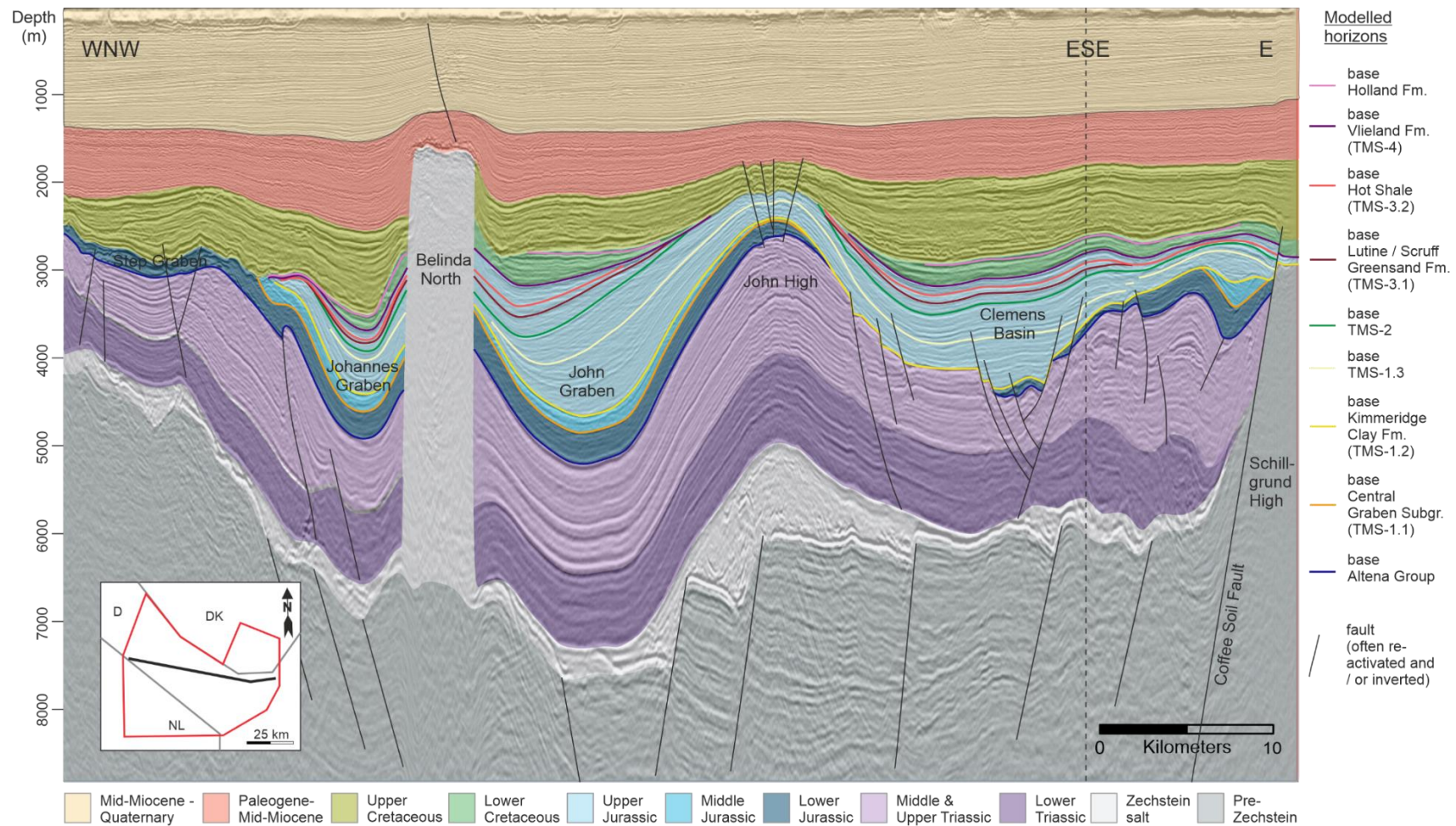


Fig. 50 Interpreted 2D seismic profile in the center of the study area. The seismic section starts at the western graben shoulder in the Step Graben System (the strongly dissected half-graben shoulder of the Central Graben), crosses the northern part of the Johannes Graben, the salt structure “Belinda”, the John Graben, then the Clemens Basin and ends at the Schillgrund High in the east outside the graben. Eye-catching is the shift of the depocenter in the John Graben east of “Belinda” from the graben center towards the salt structure, indicating a decreasing influence of rifting that was dominating from TMS-1.1 to TMS-1.2 in favor of an increasing influence of halotectonics in the subsequent TMS. Also, the erosion of Triassic and Lower Jurassic Altena Group strata and the absence of TMS-1.1 in the Clemens Basin indicates that the basin was a structural high during the emergence of the Mid North Sea Dome in the Middle Jurassic. Preservation of Lower Jurassic strata and depocenters of TMS-1 along the main boundary fault at the eastern margin of the Central Graben indicates a main rift phase in TMS-1. The rift activity decreases then steadily beginning from TMS-1.3 to TMS-4.

6.4.1.1. Pre-rift (Altena Group)

Description

The pre-rift Altena Group consists of marine claystones of the Sleen Formation, the Aalborg Formation, the Posidonia Formation and the Werkendam Formation or their Danish equivalents. Its thickness is relatively constant in the areas of the John Graben, the Johannes Graben and along the SF or the CSF, respectively, with thicknesses of about 400 m (Fig. 51). In the northern Dutch Central Graben, the thickness increases towards the center of the graben and reaches up to 800 m. The subsidence rates commonly range between 5 to 10 m/Ma, with the highest subsidence rates in the northern Dutch Central Graben and along the main boundary fault. Sediments of the Altena Group are absent around the Clemens Graben and Clemens Basin, as well as in the west of the Dutch part of the study area. The thickness of the group decreases towards the study area.

Interpretation

The relatively constant thicknesses in large parts of the study area are due to the uniform depositional environment and relative tectonic quiescence during the deposition of the Altena Group (Pharaoh et al., 2010). However, the symmetrical style of the depocenter at the center of the northern Dutch Central Graben indicates salt withdrawal to the margins in this phase (Fig. 49 and Fig. 51). The asymmetric thickness pattern in the John Graben along the John Fault and increased thicknesses and subsidence along the main boundary fault indicates fault activity. Primary thicknesses are preserved in the deeper parts of the later Central Graben, namely the northern Dutch Central Graben, the Johannes Graben, the John Graben and areas at the eastern main bounding fault of the Central Graben. Absence or thinning of the Altena Group is the result of later erosion due to the emergence of the Mid North Sea Dome, the rise of salt structures, or Cretaceous structural inversion. Proven occurrences of the Posidonia Shale Formation are described from the northern Dutch Central Graben, whereas the presence of the Posidonia Shale Formation is assumed for the southern part of the German Central Graben (Müller et al., 2020). These proven and assumed occurrences of this prolific source rock are restricted to areas south of the MCGTZ and coincide with the areas of highest subsidence. However, the subsidence rates are rather low, compared to the subsequent investigated intervals of TMS-1 and TMS-2. There are no obvious indications for the diapirism and the development of rim synclines.

6. Jurassic to Lower Cretaceous tectonostratigraphy of the German Central Graben, southern North Sea

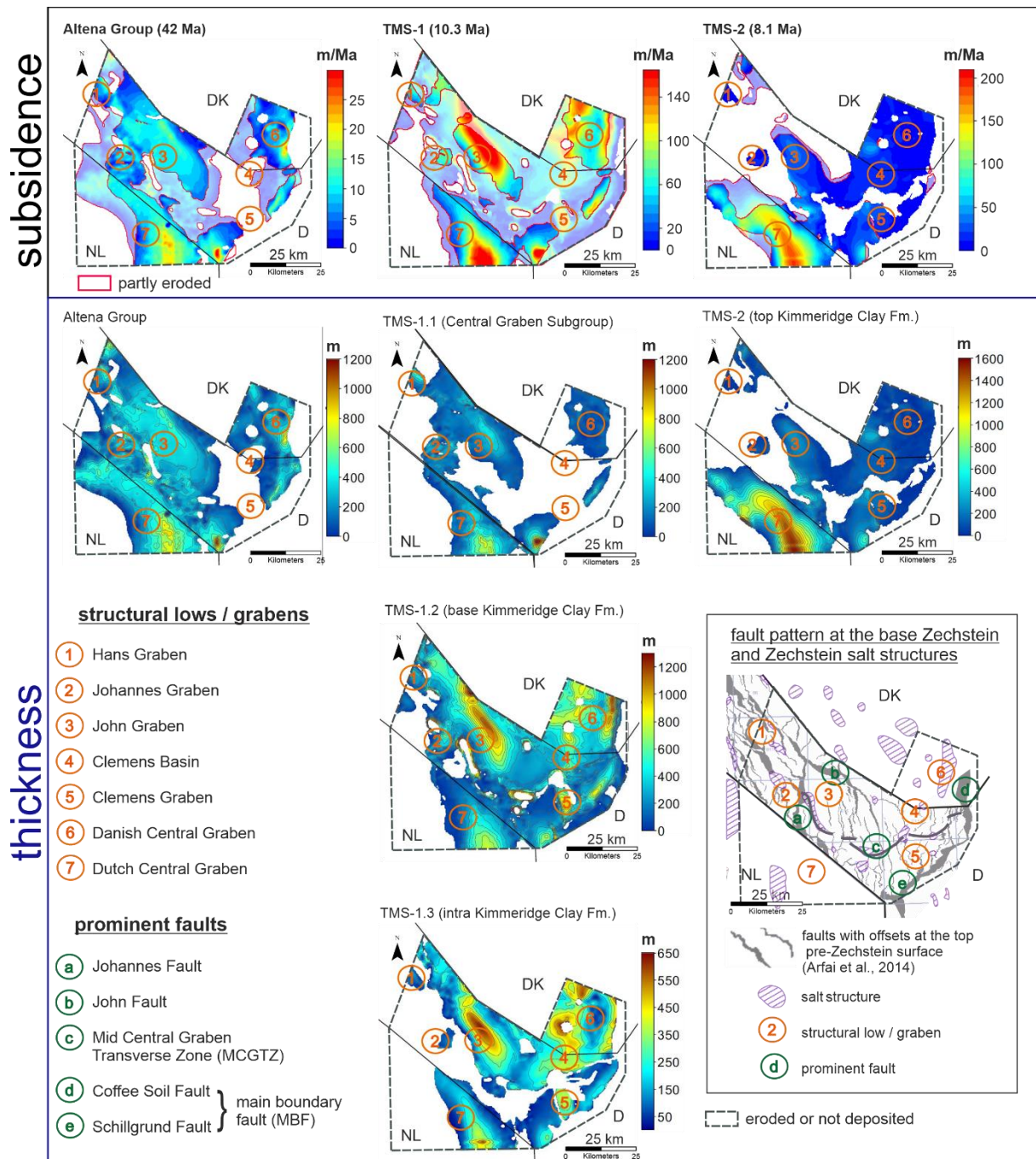


Fig. 51 Thickness and subsidence maps reconstructed from the seismic interpretation. The gridded and depth converted results focus on important phases of the graben development. During the pre-rift phase (Altena Group) sediment distribution was rather uniform. Possibly local highs like the later Clemens basin area were later partly removed by the Mid-Cimmerian erosion. Rifting resulted in sedimentation close to the main bounding faults and the basin axis (TMS-1.1 – TMS-1.2). But increasing halotectonics and decreasing rifting changed subsidence patterns to a more mini-basin-controlled style. During TMS-2, the northern Dutch Central Graben was the object of increased sedimentation.

6.4.1.2. TMS-1

Description:

The subsidence map of TMS-1 Total integrates the subsidence rates of the subsections TMS-1, namely TMS-1.1 (Central Graben Subgroup), TMS-1.2 (Lower Kimmeridge Clay Formation), and of TMS-1.3 (intra Kimmeridge Clay Formation) (Fig. 51). The subsidence rates in the study area are significantly higher than those of the Altena Group, with the highest subsidence rates up to max. 150 m/Ma in the northern Dutch Central Graben, the John Graben, along the eastern main bounding fault of the Central Graben, and within the Clemens Graben and Basin. The MCGTZ separates the area into a northern part with the John Graben, the Clemens Basin, and the southern Salt Dome Province as depocenters and a southern part with the Clemens Graben and the northern Dutch Central Graben and along the SF as depocenters. Subsidence rates and sediment thicknesses are generally higher north of the MCGTZ. Sediments of TMS-1.1 are absent in the western part of the study area, at large parts of the border area of the German and Dutch Central Graben, and around the later Clemens Graben and Clemens Basin. Depocenters of TMS-1.1 are the northern Dutch Central Graben and the center of the John Graben with thicknesses up to 800 m. The Johannes Graben connects the Dutch Central Graben with the northern German part of the study area. The depositional pattern changed during TMS-1.2. The northern Dutch Central Graben and the John Graben, as well as the areas along the eastern main bounding fault of the Central Graben remained depocenters. New depocenters emerged in the Clemens Graben and Clemens Basin along NNW-SSE trending faults. In TMS-1.3, sediments in the transition from the northern Dutch Central Graben towards the John Graben along the Johannes Graben are absent, as well as sediments along the line “Belinda” to “Carola” in the center of the study area. The relative thickness of sediments along the eastern main boundary fault of the Central Graben decreases. Depocenters remained the northern Dutch Central Graben, the John Graben and the Clemens Graben and Basin and its extension in the Danish Salt Dome Province.

Interpretation:

The depocenters of TMS-1 are predominantly determined by rifting and fault activity. They are either located along the eastern MBF or along roughly NNW-SSE trending faults that exist in the pre-Zechstein basement. TMS-1-1 represents the first sediments in the area after the collapse of the Mid North Sea Dome and after the initiation of the main rift activity. The sediments are restricted to the deeper parts of the former paleo-topography that are determined by the activity of the Schillgrund and CSF at the eastern boundary of the Central Graben and by the activity of NNW-SSE trending faults of the John Graben, the Johannes Graben, and other sections of the northern Dutch Central Graben. The areas around the later Clemens Graben and Basin, and north-east of the Dutch Central Graben were probably topographic highs and no sediment accumulation took place. The coastline and deposition of marine sediments advanced from north to south probably along the Johannes Graben that formed a connection between the Danish-German and the Dutch part of the Central Graben. In TMS-1.2, fully marine conditions were established in most of the study area and the Clemens Graben and the Clemens Basin appeared as depocenters due to continuing N-S trending fault activity. The Clemens Graben presumably

developed as a kind of pull-apart basin between the Mid-Central Graben Transverse Zone and the MBF. During the deposition of TMS-1.2, rifting of the Central Graben climaxed, which is indicated by relatively high sediment thickness and high subsidence rates along the main bounding faults as well as by decreasing thicknesses within TMS-1.3. Also, fault activity along the John Graben and the Clemens graben climaxed during TMS-1.2 and TMS-1.3, resulting in increased thicknesses. Even though rifting was the main factor for the creation of accommodation space during TMS-1, the increasing influence of salt withdrawal and the growth of salt structures is evident. From TMS-1.1 to TMS-1.3, the depocenters of the northern Dutch Central Graben and the John Graben shifted towards the salt structures on their western flanks, sedimentation around the Danish salt structures increased, and a salt pillow developed offshore Denmark between the salt structures on its western and the CSF on its eastern flank. First rim synclines developed in the Danish part of the study area in TMS-1.2 and there are subtle indications around the Barbara and Belinda salt structures. The syntectonic, persistent or reoccurring fault activity was probably the main cause of salt movement and the redistribution of the salt. The salt structures “Belinda”, “Britta”, “Barbara”, “Carola” developed probably along a major strike-slip to oblique fault (Mid Central Graben Transverse Zone; MCGTZ), in some places at crossing points with other normal faults, e.g., at the location of the salt structure “Carola”. Withdrawal of salt from underneath of a potential former high in the Clemens Basin area, triggered by the renewed tectonic activity, possibly led to the development of the Clemens Basin. Faults in the Mesozoic to Cenozoic are mostly soft-linked to thin-skinned coupled to the basement faults, the faults mostly don’t cross the Zechstein salt but clearly stimulated the salt flow (Fig. 49 and Fig. 50; ten Veen et al., 2012). Besides the obvious relation between basement faults and salt redistribution, the faults are mostly not traceable. The German Central Graben is divided by the MCGTZ and the Johannes Fault into a northern and a southern part. The division is expressed by higher subsidence rates and sediment thickness, both within the sub-basins and in general, north of the MCGTZ (Fig. 51). This northern part includes the John Basin, the Clemens Graben and the southern part of the Tail End Graben and belongs geologically rather to the Danish Central Graben. The southern part is characterized by lower subsidence rates and a lower sediment thickness during TMS-1.2 and TMS-1.3. It comprises the northern Dutch Central Graben, the Clemens Graben, and the areas along the SF. Geologically, it rather belongs to the Dutch Central Graben.

6.4.1.3. TMS-2

Description

Most of the sedimentation during TMS-2 occurred in the northern Dutch Central Graben, with thicknesses up to 1600 m in most part of the sub-basin, whereas in the rest of the investigated area thicknesses are rarely higher than 200 m (Fig. 51). The subsidence in the northern Dutch Central Graben is very high with up to 200 m/Ma, compared to mostly less than 50 m/Ma in the remaining study area (Fig. 49). There was only slightly increased subsidence in the John Graben and along the MBF. The depocenter offshore The Netherlands shifted towards the NW and loops around the salt wall B17-SOUTH1. Increased sediment thicknesses are also recorded

6. Jurassic to Lower Cretaceous tectonostratigraphy of the German Central Graben, southern North Sea

from the developing salt rim synclines “Britta” and “Belinda”, the Clemens Graben and Basin and the John Graben with thicknesses around 300 m. In most other parts of the study area, e.g., along the MBF, the sediment thickness is relatively low with about 100 m. Sediments in the area between the John Graben and the Mads Graben as well as the Danish Rosa Graben are absent.

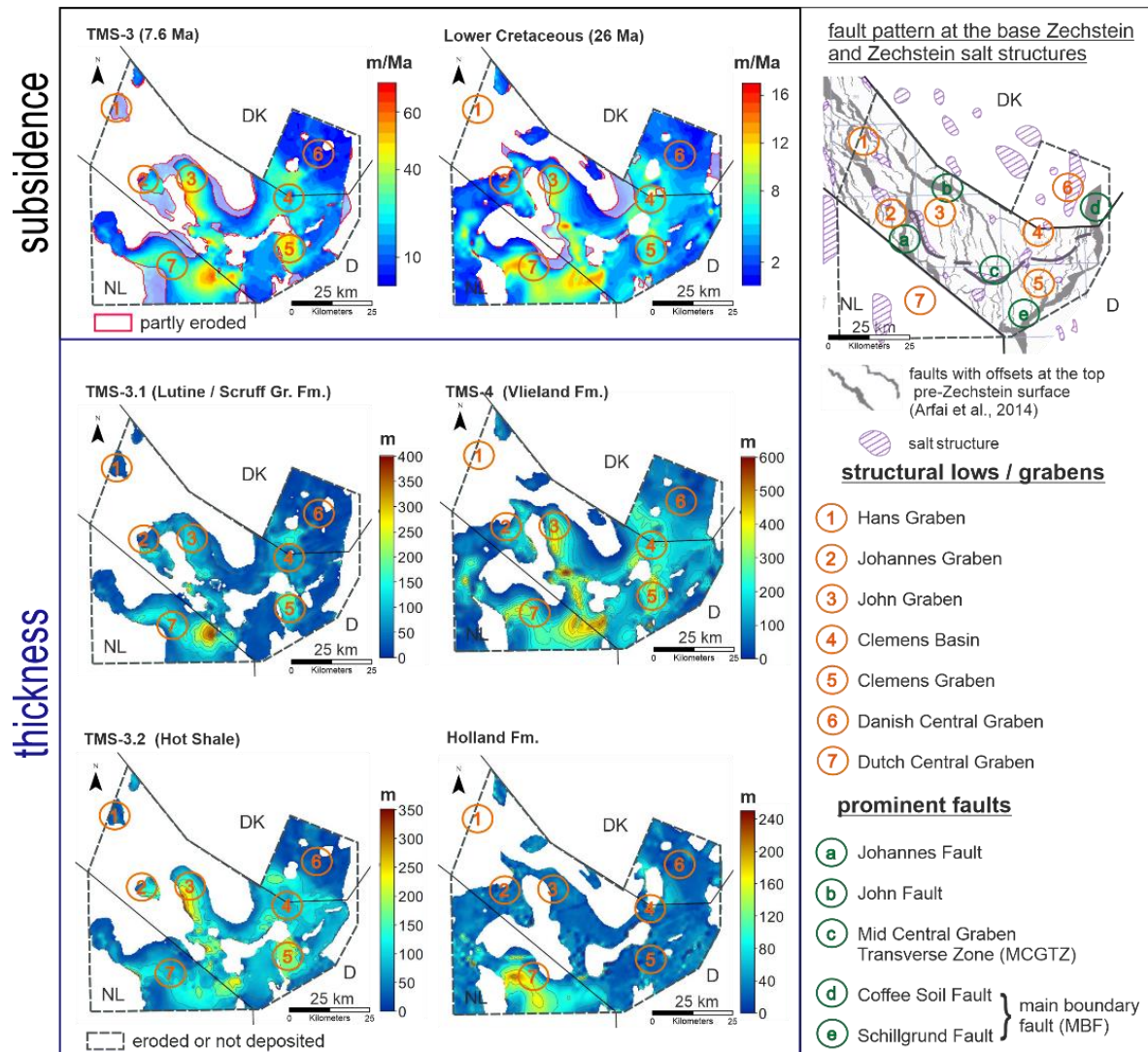


Fig. 52 Thickness and subsidence maps reconstructed from the seismic interpretation and gridding. The dominance of the northern Dutch Central Graben on sedimentation decreases in TMS-3. Halotectonics now replaced rifting as the dominating factor on deposition. The influence of salt tectonics increases during TMS-3 and still plays a role in TMS-4.1, until again a rather planar depositional system driven by thermal subsidence is established in the post-rift phase of TMS-4.2.

Interpretation

The NW-SE trending depocenters of the northern Dutch Central Graben, the John Graben, and the study area’s extension of the Mads Graben are probably related to NNW-SSE trending faults in the pre-Zechstein basement. Decreased thicknesses along the MBF, however, indicates a

ceasing activity of the MBF. The high subsidence rates in the Dutch Central Graben in comparison with the relatively low subsidence rates in the German and Danish part of the graben indicate an independent development of southern and northern Central Graben during this period.

6.4.1.4. TMS-3

Description

The dominance of the northern Dutch Central Graben as the main depocenter of the study area declined significantly during the deposition of TMS-3.1 and even further during the deposition of TMS-3.2 (Fig. 52). The subsidence in the northern Dutch Central Graben is increased around the salt structure “B17-SOUTH1” in a NW-SE direction, however, the highest subsidence rates occur south of the salt structure “Carola”. Other sites of deposition were the John Graben, where the depocenter moved further towards the salt structure “Belinda”, the Clemens Graben and Clemens Basin are, as well as the western flank of Belinda (North and South), the southern flank of Barbara, the area between salt domes, namely between Birgit and Belinda North (Johannes Graben), between Belinda South and Britta, between Britta and Barbara, and between the two southern Danish salt domes. Sediment thicknesses along the MBF are not increased and sediment thicknesses in general are low in comparison with the previous TMS-2. The subsidence rate in the study area decreased from TMS-2 to TMS-3, within the northern Dutch Central Graben even significantly from max. 200 m/Ma to max. ~ 60 m/Ma.

Interpretation

Within TMS-3, the influence of rifting on the subsidence pattern further decreased in favor of salt tectonics, which is indicated by the location of the depocenters in the close vicinity of salt structures. Fault activity seems to have been low, except for the MCGTZ and the faults of the Clemens Graben. Subsidence within the Clemens Basin, however, seems to relate to salt withdrawal towards “Bruni” and towards the southern Danish salt structures. Low sediment thicknesses along the MBF fault also indicate a further decrease in rifting activity. Deposition in salt rim synclines and salt mini-basins dominated in the study area, resulting in a complex subsidence and thickness pattern.

6.4.1.5. TMS-4 and Holland Formation (Lower Cretaceous)

Description

The overall subsidence pattern of TMS-4 is very similar to that of TMS-3 (Fig. 52). The depocenters are mainly located around the salt structures, except for the Clemens Graben. The main centers of subsidence are two roughly NNW-SSE trending areas: One from the salt structure “Belinda” to the Dutch Central Graben and the other stretch from the two southern Danish salt domes “Tove” and “Vagn” to the Clemens Grabe. The subsidence rates, though, decreased significantly to max. 16 m/Ma. In contrast to TMS-3, former areas of erosion or non-deposition,

like parts of the Dutch Step Graben in the west of the salt wall B17-SOUTH1, areas west and north of Belinda, and parts of the Schillgrund High became now covered by sediments (Fig. 5). The thicknesses of the subsequent Holland Formation are relatively uniform, with exception of increased thicknesses up to 160 m in the northern Dutch Central Graben. The average thickness of the Holland Formation is relatively low (less than 40 m).

Interpretation

The influence of salt tectonics on subsidence remained dominant in TMS-4, indicated by the depocenters around the salt structures, but ceased in the Early Cretaceous and thermal contraction and compaction became the main drivers of subsidence. Except for the faults of the Clemens Graben and potentially the MCGTZ, there are no apparent signs of fault activity. Sedimentation on former highs outside the main rift like in the west of the Dutch salt wall B17-SOUTH1 indicates a further decrease or cease in rift activity. The main control on the depocenter in the northern Dutch Central Graben, oriented WNW-ESE, seems to have been salt withdrawal towards the salt structures. The sustained folding of the northern Dutch depocenter around the salt structure B17-SOUTH1 indicates its progressive growth and impact. The thereby developed rim syncline ruptures the trend of the Johannes Fault and its Dutch extension. Influence from fault activity, e.g., the prolonged Johannes Fault or the MCGTZ is minor. During the deposition of the Holland Formation salt tectonics considerably ceased. Subsidence was now mainly driven by thermal subsidence, replacing the earlier differentiated system with rifting and salt tectonics. Salt rim synclines east of “Belinda” or along the Johannes Fault were still active during TMS-4 but ceased mainly during deposition of the Holland Formation.

6.4.2. Pillar maps

Pillar maps were created by superimposing chronologically successive horizons that illustrate the structural evolution regarding preservation, non-deposition, and erosion in the study area. We provide maps of the pre-rift, syn-rift, and main post-rift phase. The map of the pre-rift phase compiles the maps of the Lower Jurassic Altena Group and of TMS-1.1 (Fig. 53). It shows that deep subsided areas at the axis of the graben, like the John and Johannes Graben and the Dutch Central Graben, but also areas in the hanging wall of the MBF fault, were unaffected by erosion. Areas in the footwall of the MBF, outside the graben axis and the area of the Clemens Graben and Clemens Basin, though, were eroded. The erosional event that significantly affected the Altena Group was the emergence of the Mid North Sea Dome in the central North Sea that resulted in the Mid Cimmerian Unconformity. However, the relief of the study area was presumably differentiated with former lows and highs like the later Clemens Graben and Basin, where potentially erosion took place. The sediments of TMS-1-1 were deposited after the collapse of the Mid North Sea Dome. *Fig. 53b* compiles the maps of TMS-1.2, TMS-1-3, and TMS-2. It illustrates the deposition and preservation of marine claystones of the Kimmeridge Clay formation and equivalents during the main rift phase. During this phase, sediments were mainly deposited in the graben center and less on the shoulders of the graben system. *Fig. 53c* compiles the maps of TMS-3.2, TMS-4, and of the Holland Formation. It shows that areas around the salt domes were subject to erosion. Either due to ongoing diapirism in the Early

6. Jurassic to Lower Cretaceous tectonostratigraphy of the German Central Graben, southern North Sea

Cretaceous or due to regional uplift and renewed diapirism during the Late Cretaceous structural inversion (grey, orange, and green areas in Fig. 53c). Areas especially at the western Central Graben boundary in transition to the Step Graben system, but also along the CSF in the east, show strong erosion and re-distribution of sediments probably during the Late Cretaceous structural inversion.

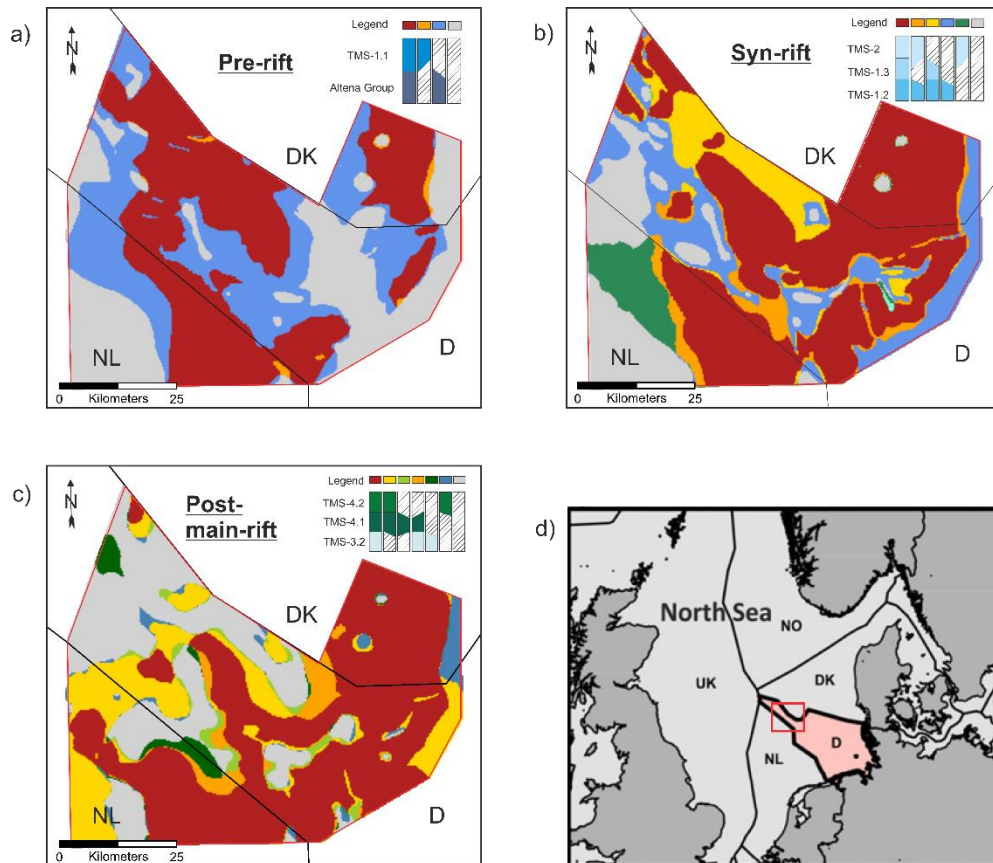


Fig. 53 Pillar maps of the study area. Figure (a) illustrates the distribution of sediments of the pre-rift phase of the Altona Group and of the early rift phase of TMS-1.1 as well as erosion due to the emergence of the Mid North Sea Dome (Mid Cimmerian Unconformity). Figure (b) illustrates the distribution of sediments of the rift phase from TMS-1.2 to TMS-2 and erosion / non-deposition due to local or regional uplift. The uplift is often related to halotectonics around the salt structures and to Late Cretaceous erosion. Figure (c) illustrates Uppermost Jurassic to Lower Cretaceous sediment distribution and corresponding erosion around salt structures due to either continuous diapirism during the Early Cretaceous or due to reactivated halotectonics during the Late Cretaceous.

6.4.3. Well log correlation

Well-log correlation with tectonostratigraphic units provides lithologic control (Fig. 54). Differences in lithology within the same sequence were identified and visualized in a time-stratigraphic panel (Fig. 55)

Each well is presented by a GR and a DT log. The national lithostratigraphic nomenclature is used in each panel and the wells were correlated using the tectonostratigraphic nomenclature of Bouroullec et al. (2018) and Verreussel et al. (2018).

Within the Danish Salt Dome Province, represented by the wells Alma-2 and O-1, the lower part of TMS-1 comprises the upper half of the Bryne Formation (Fig. 54). The Bryne Formation was deposited in an estuarine and fluvial environment and consists of interbedded sand- and mudstones (Michelsen et al., 2003; Fig. 47). The different lithologies can be identified by their log response. Sandstones feature considerably lower gamma-ray responses than the mudstones. A few (rare) intercalated coal beds are represented by a distinctly low velocity in combination with a low gamma-ray response. In the northern well, Alma-2, the Bryne Formation is overlain by the Lola Formation, which lower half forms the upper part of TMS-1 around the well (Fig. 47). The Lola formation consists of open marine mudstones, which are recognized as relatively constant and high gamma-ray responses and low velocity sonic responses, rarely intermitted by low gamma-ray and low velocity log responses of interbedded dolomites or limestones. In the southern part of the Salt Dome Province, represented by well O-1, the Bryne Formation is overlain by the Middle Graben Formation, which was deposited in a coastal swamp environment (Michelsen et al., 2003; Fig. 47). It consists mostly of mudstones that are interbedded with siltstones. Again, the Lola Formation, which thickness is significantly reduced, forms the upper part of TMS-1. In the German Central Graben, the Lower Graben formation forms the lower part of TMS-1. The Lower Graben Formation represents the onset sedimentation after the Mid Cimmerian Unconformity with alluvial plain deposits (Herngreen et al., 2003). Its log characteristic and interpreted lithology alters from north to south. In the north, represented by well Thor-1, the gamma-ray response of the Lower Graben Formation is relatively constant and high with a few lower gamma-ray peaks. The sonic log, though, is rather diversified with distinct high and low velocity peaks. The corresponding lithology is interpreted as mudstone, interbedded with siltstones and sandstones, e.g., at the upper boundary to the Kimmeridge Clay Formation, and coal beds.

To the south, visible in well C-16-1 and B18-05, the sand volume and the thickness of sandstones increases significantly. These sandstone bodies are shown as low gamma-ray and relatively high velocity log responses. In both wells, the Lower Graben Formation is overlain by the Middle Graben Formation, which shows a spiky gamma-ray and sonic log pattern, which is interpreted as an alternation of thin mud-, silt- and sandstones, interbedded with coal beds. The Middle Graben Formation reflects a shift to a lake- and swamp-dominated depositional environment (Herngreen et al., 2003). In the Dutch Central Graben (B-18-03), the Lower and Middle Graben Formation is accompanied by the Upper Graben Formation, which was formed in a coastal environment (Herngreen et al., 2003). In this area, the three formations that form the Central Graben Subgroup consist of an alternation of mud- and sandstones of various thicknesses, whereas the Middle Graben Formation almost completely consists of mudstone. These interbedded mud- and sandstones are characterized by relatively high and low gamma-ray and velocity log responses. The upper part of TMS-1 in the German as well as in the Dutch Central Graben area is formed by the lower part of the Kimmeridge Clay Formation, which shows a rather constant relatively high gamma-ray and low velocity log response (Fig. 47 & Fig. 54). Rare, thin low gamma-ray / high velocity log response peaks are interpreted as intercalated dolomite or sandstone beds with calcareous cementation.

6. Jurassic to Lower Cretaceous tectonostratigraphy of the German Central Graben, southern North Sea

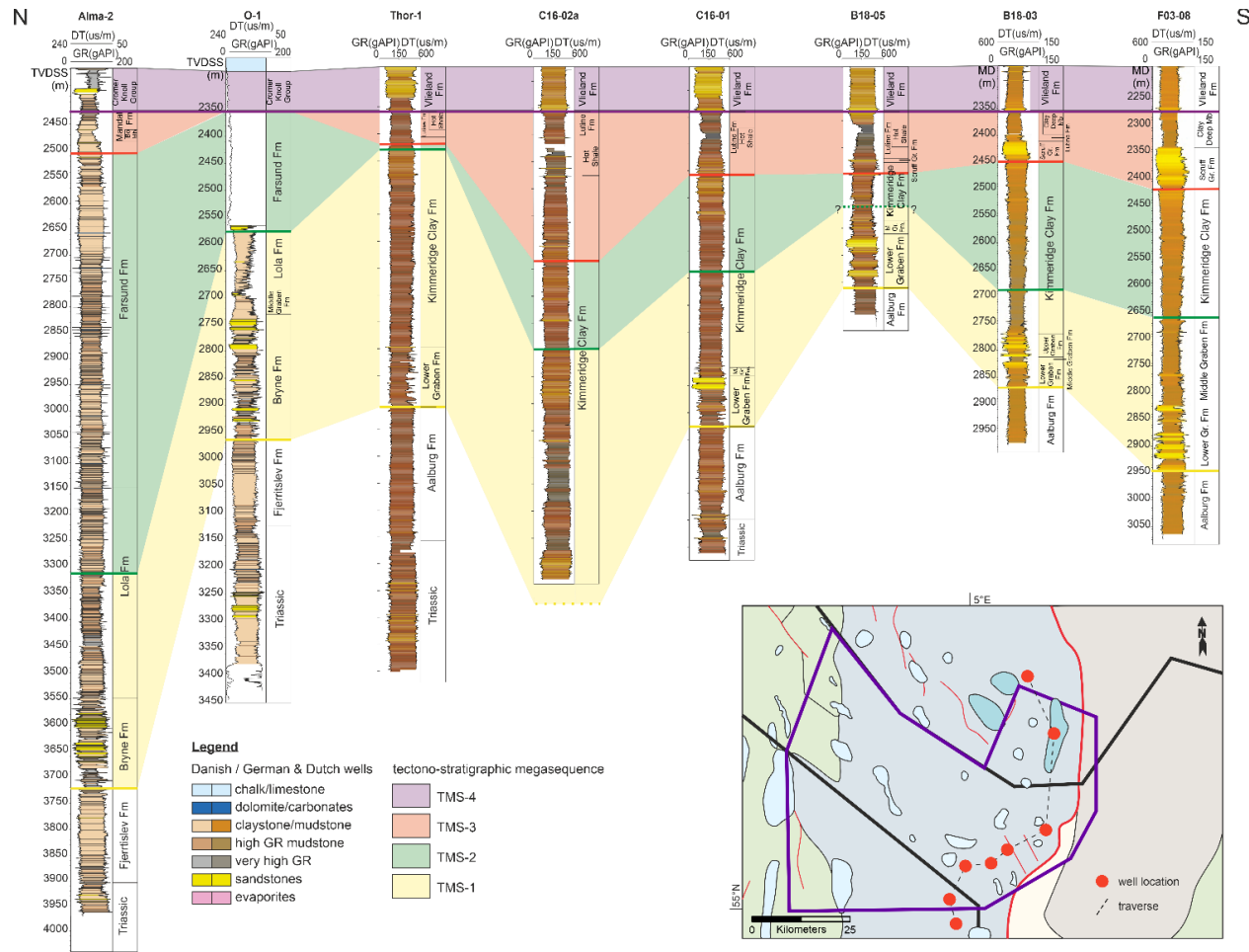


Fig. 54 Well log correlation of two Danish, four German, and two Dutch wells within or near the study area (modified after Jakobsen et al., 2020a). The wells are leveled at the base of TMS-4. TMS-1 comprises the Danish Bryne and Lola Formation, the Dutch / German equivalents Lower, Middle, and Upper Graben Group, and the lower part of the Kimmeridge Clay Formation. It reaches its maximum thickness along the traverse in the area between the German wells Thor-1 and C16-2a. TMS-2 comprises the upper part of the Lola Formation and the Farsund Formation, respectively the upper part of the Kimmeridge Clay Formation. It is almost absent at the location of Thor-1 but significantly increases in thickness towards the north of the Danish part of the study area. At the base of TMS-3, The Scruff Greensand Formation is present in the northern Dutch Central Graben but flattens out in the southern German Central Graben. Also, the “Hot Shale” is prominent in the northern Dutch Central Graben, but its radioactivity, and thereby probably its organic content, diminishes towards the Danish-German border. At the Danish well O-1 it is absent, probably because of its location on a salt structure, but reappears again at the well Alma-.2

TMS-2 starts in the Danish Central Graben with the upper half of the Lola Formation (Alma-2) whereas in the south it starts with the younger Farsund Formation (O-1) (Fig. 54). The Farsund Formation was deposited in a deep marine environment and mainly consists of calcareous claystones (Fig. 47). In Alma-2 the Farsund Formation is interbedded with thin dolomite or limestone beds, which appear as thin low gamma-ray and high velocity log responses in an otherwise relatively high gamma-ray and relatively low velocity log response background (Fig. 54). The dolomite-spikes are less prominent in O-1. In the German and Dutch Central Graben, TMS-2 is exclusively composed of the above mentioned Kimmeridge Clay Formation, which mainly consists of mudstones with a few interbedded dolomites or sandstones, as e.g., at the top of TMS-2 of well B-18-05. Notable is the significant thickness reduction in the well Thor-1 (Fig. 54).

In Alma-2 of the Danish Central Graben, TMS-3 consists of mudstones of the uppermost Farsund Formation, in which the high gamma-ray mudstones of the Bo Member occur (Fig. 47 & Fig. 54). Further in the south of the Salt Dome Province, in well O-1, TMS-3 is not present due to erosion that is caused by salt tectonics. In the German Central Graben, TMS-3 includes the uppermost Kimmeridge Clay Formation and the Lutine Formation with its Hot Shale section. The high gamma-ray response of the Hot Shale (Lutine Formation) increases steadily and significantly from the north to the south into the Dutch Central Graben (Fig. 54). TMS-3 reaches its greatest thickness with about 250 m in the Clemens Graben (well C-16-2a). In the Dutch offshore, at the base of TMS-3, the Scruff Greensand Formation is present, which consists of thick sandstones that features a blocky, low gamma ray and high velocity log response (Fig. 54). The sandstones are overlain by the high gamma ray Hot Shale ("Clay Deep Member" in the Dutch nomenclature) of the Lutine Formation (Fig. 47 & Fig. 55). The thickness of the Scruff Greensand Formation decreases significantly to the north inside the German Central Graben. Only a thin succession of the Scruff Greensand (about 10 m) is present in well B-18-05 and none in well C-16-01 (Fig. 54). However, low gamma ray and high velocity log responses near the base of TMS-3 and around the Hot Shale section of the Lutine Formation of well C-16-2a in the Clemens Basin are interpreted as a thin (less than 10 m) sandstone body.

The Lower Cretaceous sediments of the wells consist of mudstones of the Vlieland Claystone Formation or the Cromer Knoll Group, respectively.

6. Jurassic to Lower Cretaceous tectonostratigraphy of the German Central Graben, southern North Sea

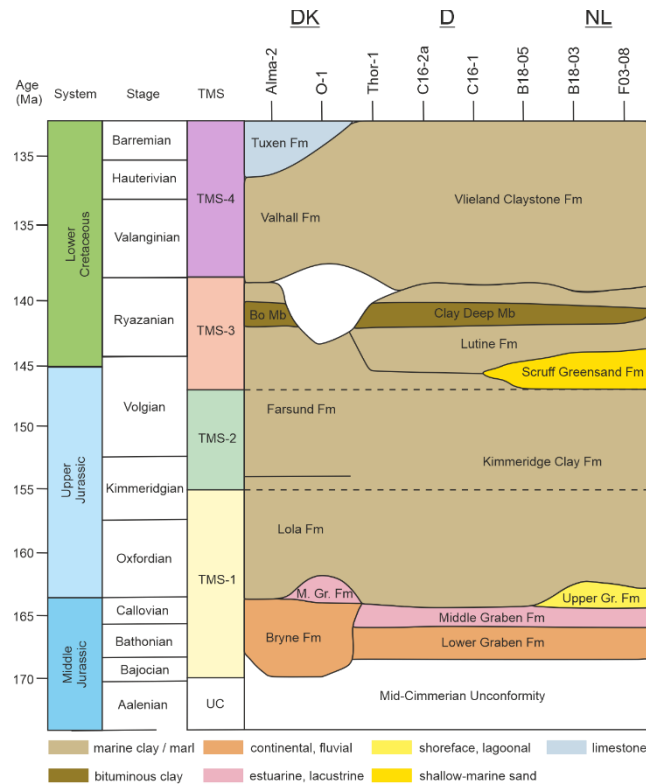


Fig. 55 Time-stratigraphic panel of the study area along the cross section shown in Fig. 54 (modified after Jakobsen et al., 2020a). The figure visualizes the TMS cycles and the associated Dutch, German, and Danish lithostratigraphy.

6.5. Discussion

Up to now, various national lithostratigraphic (Van Adrichem Boogaert & Kouwe, 1993; Michelsen et al., 2003), tectonostratigraphic (Bouroullec et al. 2018; Verreussel et al. 2018) and sequence stratigraphic (Andsbjerg & Dybkjaer, 2003) concepts exist for the Dutch and Danish parts of the Central Graben that hampers basin-wide correlation of sedimentary successions, especially because not much research on the fill and evolution of the German Central Graben has been carried out so far. For offshore Germany, traditionally a different chrono or allostratigraphic approach is used (e.g., Arfai & Lutz, 2017). In the following, we will bring together different approaches from the Dutch and Danish Central Graben and integrate our results. Additionally, we will discuss the interdependent role of rifting and salt tectonics for the evolution of the southern Central Graben as well as the influence of tectonics on the (litho-)stratigraphy in the study area.

6.5.1. Pre-rift (Altena Group)

The Early Jurassic has been commonly described as a period of relative tectonic quiescence, between rifting events in the Triassic and the Middle to Late Jurassic (Cartwright 1991; Nøttvedt et al., 1995). Hergreen et al. (2003) picture the Early Jurassic sedimentation as a very

uniform blanket and Andsbjerg & Dybkjaer (2003) regard the relatively homogenous thickness of the Lower Jurassic successions recorded in Danish wells as an indication for a uniform subsidence history for most of the Early Jurassic within the Danish Central Graben. In a tectonically quiet depositional environment without significant differential subsidence, we would assume an approximately constant original thicknesses (without erosion). During the Middle to Late Jurassic transition significant erosion took place in the area of the Central Graben, caused by the Mid North Sea Doming event (Underhill & Partington, 1993), as it is also apparent in the pillar map of the Lower Jurassic pre-rift sediment distribution (Fig. 53a). However, there are considerable thickness differences in areas that were unaffected by the Mid Cimmerian erosion, e.g., the parts of the northern Dutch Central Graben and areas along the MBF (Fig. 51 and Fig. 53). Our observation of thickness variations is in accordance with Van Winden et al. (2018), who noticed a thickening of the Lower Jurassic Altena Group towards the center of the graben. These variations in thickness may result from differential tectonic activity in the Early Jurassic. The Central Graben already experienced a first phase of major tectonic activity in the Late Triassic (Jähne-Klingberg et al., 2018). Also, we presume that the Clemens Basin and Clemens Graben constituted a topographic high in the Early Jurassic (Fig. 51). This high was then inverted to a topographic low in the Late Jurassic because of fault activity and salt withdrawal.

The division of the study area by the MCGTZ may also have a significant influence on the stratigraphy and petroleum geology. The presence of the most important source rock for hydrocarbons in the southern Central Graben, the Posidonia Shale Formation, is limited to areas south of the MCGTZ. Confirmed and prolific deposits of the Posidonia Shale Formation occur in the northern Dutch Central Graben and potentially in the southern German Central Graben (Ineson et al., 2003; Müller et al., 2020). These areas coincide with areas of highest subsidence and thicknesses in the study area (Fig. 51). North of the MCGTZ, there is no known Posidonia Shale Formation. It was assumed to have been eroded during the Mid-Cimmerian uplift (Damtoft et al., 1987). However, the pillar maps show clearly that large areas around the John Graben and in the Danish part of the study area were unaffected by later erosion (Fig. 53). Also, there are no indications for erosion, or the presence of the Posidonia Shale Formation on the reflection seismic data. This may be the result of a hiatus that is not resolvable. Other explanations are that the anoxic conditions were restricted to the areas south of the MCGTZ or that in the areas north of the MCGTZ an increased terrestrial and siliciclastic input attenuated the marine organic matter in the formation.

6.5.2. TMS-1

At the transition from the Aalenian to the Bajocian, sedimentation recurred to the Central Graben, propagating from the north to the south due to the renewed rifting following the thermal doming in the early Middle Jurassic (Andsbjerg & Dybkjaer, 2003). At first a terrestrially dominated environment developed with fluvial deposits of the Bryne Formation in the Danish Central Graben (Michelsen et al., 2003). Its base is the equivalent of the base of TMS-1 offshore Denmark. This period of the initiation of syn-rift subsidence corresponds to phase 3 of basin evolution of Andsbjerg and Dybkjaer (2003). Rifting of the Dutch Central Graben started again

a few million years later in the Late Callovian and is expressed by the deposition of fluvial and deltaic sediments of the Lower Graben Formation (*Fig. 47*). Younger sedimentary equivalents were deposited further south of the Dutch Central Graben, outside our study area, in form of the Friese Front Formation. Estuarine and lacustrine deposits of the Middle Graben Formation follow the fluvial deposits. Subsequently, marine conditions re-established in the southern Central Graben, starting with shoreface and lagoonal deposits of the Danish Lulu Formation in the Callovian and of marginal marine sediments of the Dutch Upper Graben Formation at the earliest Late Oxfordian (Michelsen et al., 2003; Bouroullec et al., 2018; Verreussel et al., 2018). The results of our mapping (TMS1-1 thickness map) indicate that the transgression propagated from the Danish to the Dutch Central Graben along the axis Rosa Basin – John Basin – Johannes Basin – northern Dutch Central Graben (*Fig. 51*). At the top of TMS-1, fully marine conditions existed in large areas of the Danish Central Graben at the Callovian-Oxfordian transition (Lola Formation; Andsbjerg & Dybkjaer, 2003). This transgression is attributed to another rift-pulse (phase 4 of Andsbjerg and Dybkjaer, 2003). Open marine conditions reached the Dutch Central Graben at the Late Oxfordian - Early Kimmeridgian, which is expressed by the deposition of the Kimmeridge Clay Formation (*Fig. 54*).

In the study area, TMS-1 and its subdivisions reflect this sedimentary development. Terrestrial and marginal marine sediments of the Bryne and Middle Graben Formations in the Danish Salt Dome Province and of the Lower, Middle, and Upper Graben Formations in the German and Dutch Central Graben are overlain by marine mudstones of the Lola and Farsund Formation in the Danish and by marine mudstones of the Kimmeridge Clay Formation in the German and Dutch Central Graben (*Fig. 54*).

The depocenters in this period were in the vicinity of the MBF, as well as in the center of the sub-basins, e.g., the John Graben, the Clemens Basin, and the Clemens Graben (*Fig. 51*). These depocenters, as well as the development of the Clemens Graben and Basin, indicate the dominance of rifting on subsidence patterns. However, the influence of salt tectonics increased steadily from TMS-1.1 to TMS-1.3, which can be recognized by increasing subsidence around salt domes, e.g., around the Johannes Basin and within the southern Salt Dome Province (*Fig. 51*). The decreasing sediment thickness from TMS-1.2 to TMS-1.3 along the MBF of the eastern Central Graben margin as well as the decreasing thickness trend of TMS-1.3 along the MBF indicate that the shift from rift-dominated subsidence towards salt-dominated subsidence, in combination with local uplift and erosion, took place within this time (*Fig. 51*). The subdivision of the German Central Graben by the MCGTZ into a southern part, rather belonging to the Dutch Central Graben, and a northern part, rather belonging to the Danish Central Graben is expressed by differences in subsidence rates and sediment thicknesses. In the Dutch Central Graben, the deposition of TMS-1 is rather limited to the graben axis (Bouroullec et al., 2018; Verreussel et al., 2018). This depositional pattern is likely related to salt withdrawal beneath the basin axis, where elongated salt structures developed (Van Winden et al., 2018). While the northern Dutch Central Graben conforms to this pattern, the depocenters along the MBF correspond to the generally asymmetric half-graben style of the Central Graben. Single sub-basins as the Clemens Graben south and the Clemens Basin north of the MCGTZ are developed rather symmetrically (*Fig. 51*).

The depocenters in the Danish Central Graben are strongly associated with faults. Either along the CSF, emphasizing the asymmetric half-graben nature of the Danish Central Graben, or along N-S striking faults like the bounding fault of the Rosa basin, which extension into the German Central Graben is represented by the John Basin (separated by a transversing structure) (*Fig. 56*). These N-S striking faults were reactivated during the first tectonic pulse during the Callovian to Early Oxfordian (Møller and Rasmussen, 2003). N-S trending faults are probably also related to depocenters of TMS-1 in the German as well as in the Dutch part of the study area (*Fig. 56*). It is also likely that the N-S trending Clemens Graben and Basin developed due to this tectonic pulse. The subdivision of the German Central Graben by the MCGTZ may have had consequences for the development of the local (litho-)stratigraphy. Higher subsidence rates during TMS-1.1 in the northern Dutch Central Graben resulted in the deposition of thick sediments of the Central Graben Subgroup. Intercalated coal seams may have locally produced gaseous hydrocarbons (Herengreen et al., 2003; de Jager and Geluk, 2007). But the Central Graben Subgroup is economically more important as reservoir rocks for oil, condensate, and gas that are predominantly sourced from the Lower Jurassic Posidonia Shale Formation in the northern Dutch Central Graben (de Jager and Geluk, 2007).

In the northern Danish Central Graben, equivalent coal-bearing deposits from the Bryne Formation have sourced gas and condensate fields (Petersen and Hertle, 2018; Petersen et al., 2000). Coaly liquids are even found within the salt dome province in the Alma field and the Tove-1 well within or near the Danish part of our study area (see *Fig. 46b* and *Fig. 48* for location). In the northern part of the study area, north of the MCGTZ, gaseous or liquid hydrocarbons from coals within TMS-1.1 may have been generated in minor quantities, as this interval lies at the present within a hydrocarbon generating temperature and depth window (Petersen and Hertle, 2018; Müller et al., 2020). However, hydrocarbons in significant accumulations, e.g., in chalk fields, probably migrated into the area from the northern part of the Danish Central Graben due to the significantly lower thickness of TMS-1.1 in the study area compared to the northern Dutch (Central Graben Subgroup) or Danish Central Graben (Bryne Formation). The marine mudstones of TMS-1.2 and TMS-1.3 consist of the lower parts of the Kimmeridge Formation, the Lola Formation, and the Farsund Formation, respectively. In the Danish Central Graben, the kerogen quality of these formations decreases towards their lower parts, which may be the result of more oxic depositional conditions and a larger input of terrestrial organic matter (Petersen et al., 2017). The marine influence increased towards the top of the formation. The ratio of siliciclastics to clay minerals is possibly higher in areas with higher subsidence rates, e.g., the John Graben area.

6. Jurassic to Lower Cretaceous tectonostratigraphy of the German Central Graben, southern North Sea

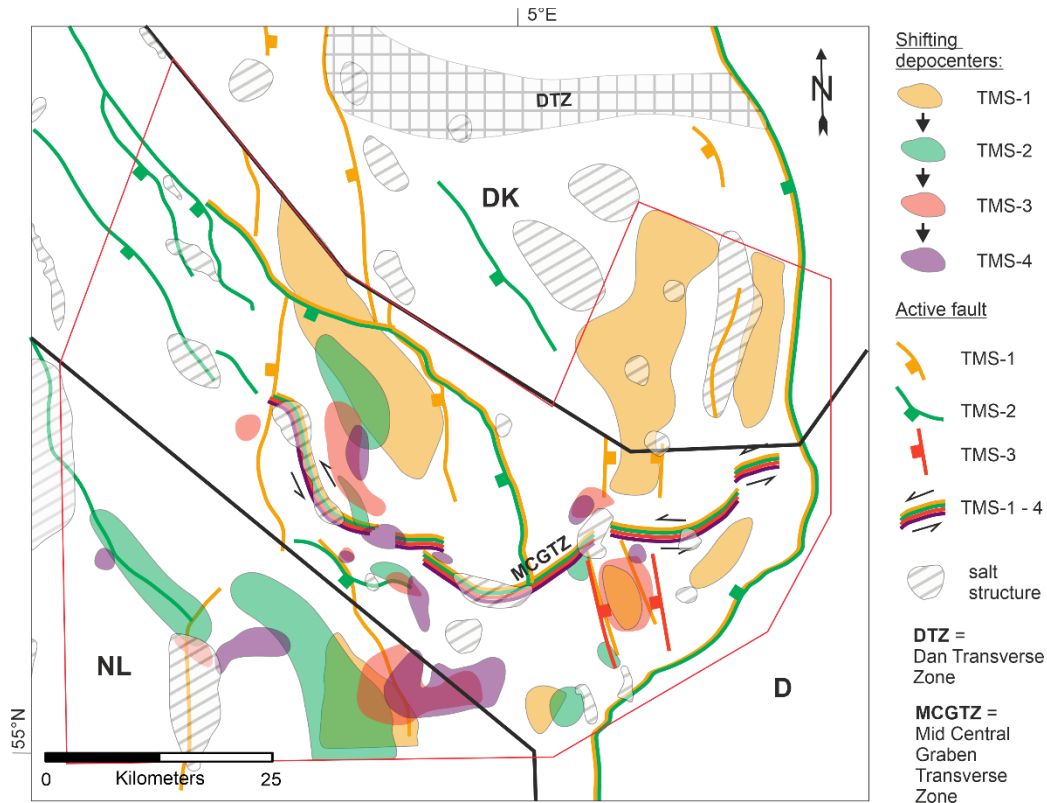


Fig. 56 illustrates the depocenters and most prominent faults within or in the vicinity of the study area for the TMS. During deposition of TMS-1 N-S trending faults were active and sediment depocenters were located at the axis of the graben structures and along the main eastern boundary fault of the Central Graben. During deposition of TMS-2, NNW-SSE trending faults were active and depocenters were oriented along these faults but also shifted towards the rising salt structures. The main eastern boundary fault of the Central Graben became less significant for the subsidence in the study area. In TMS-3 and TMS-4 rifting decreased and salt tectonics dominated subsidence. A roughly W-E trending strike-slip fault with normal fault tendencies (MCGTZ) was probably active during deposition of TMS-1 to TMS-4. The figure is compiled and modified from Cartwright (1987), Møller and Rasmussen (2003), Arfai et al. (2014).

6.5.3. TMS-2

As outlined before, the MCGTZ plays an important role for the local tectonostratigraphy and subdivides the study area in a northern part with relatively low subsidence rates and a southern part with significantly higher subsidence rates. The main depocenter during TMS-2 was in the northern Dutch Central Graben (Fig. 51). Comparable or even greater sediment thicknesses only occur in the Tail End Graben north of the Salt Dome Province in the Danish Central Graben (Møller & Rasmussen, 2003). Sediment thicknesses in the remaining study area are significantly lower, indicating that the bounding faults in the area of the Dutch Central Graben were longer active than those in the rest of the study area. A distinctive feature of TMS-2 is the initiation of subsidence in adjacent basins outside of the axis of the Central Graben. Our study area, though, does not record this development, because it mainly comprises the Central Graben. Adjacent basins and plateaus like the Terschelling Basin offshore The Netherlands, the Outer Rough Basin, or the Heno and Gertrud Plateau offshore Denmark were flooded during TMS-2 (Møller & Rasmussen, 2003; Verreussel et al., 2018). Verreussel et al. (2018) and

Bouroullec et al. (2018) therefore further subdivided TMS-2 into four tectonostratigraphic sequences related to the opening of different adjacent regions. Subsidence along the MBF mainly ceased. Fault activity influenced sediment thickness in the study area mainly in the Clemens Graben and potentially in the northern Dutch Central Graben (*Fig. 51*). In the Central Graben as a whole, the tectonic regime changed, and older roughly NW-SE trending faults were reactivated or newly created, along which depocenters in the Danish Central Graben are oriented (Møller & Rasmussen, 2003; Verreussel et al., 2018; *Fig. 56*). A roughly NW-SE trending fault also influenced the development of the depocenters of the German John Graben, at least by ultimately separating it from the Danish Rosa Graben, and the northern Dutch Central Graben (*Fig. 56*). However, the influence of salt tectonics on subsidence can be noticed clearly during deposition of TMS-2 in the study area, which is located within the area of presumed maximum initial Zechstein salt thicknesses, with up to 1000 m (*Fig. 57a*). In the northern Dutch Central Graben, however, TMS-2 reaches thicknesses of up to 1600 m. This implies that salt withdrawal, even if dominating in the German part, is not the single driving force for subsidence. At least in the Dutch part of the Central Graben, there must have been also a strong fault-driven or thermal component.

The geometry of deposits offshore Denmark is still asymmetric, with the depocenter close to the CSF, indicating continuous activity of the NW-SE trending section of the MBF in the northern Danish Central Graben (Møller & Rasmussen, 2003; *Fig. 51*). The area of the Danish Central Graben and the southwestern German Central Graben were affected by salt withdrawal and rim syncline evolution (*Fig. 51*). From the northern Dutch Central Graben to the Danish Salt Dome Province, sedimentation of marine mudstones of the Kimmeridge Clay Formation or the Lola and Farsund Formation, respectively, continued unchanged from TMS-1 to TMS-2. These predominantly deep marine sediments covered most areas of the southern Central Graben. Basin floor sands, dolomites, and terrestrial sediments of the Main Friese Front Member were deposited in the southern Dutch Central Graben and the Terschelling Basin (Bouroullec et al., 2018). Despite the apparent uniformity of the marine clays of TMS-2, we believe that tectonics influenced the local lithostratigraphy. The subsidence and thickness map of TMS-2 show that most of the study area, especially north of the MCGTZ, constituted a topographic high in contrast to the deeper subsided northern Dutch Central Graben (*Fig. 51*). This structural high extended further north into the Danish Central Graben (Thöle et al., 2021). In general, the upper parts of the Farsund Formation contain more organic matter with predominantly oil-prone Type II kerogen of marine origin (Ponsaing et al., 2018). However, the kerogen quality decreases significantly in the Danish Central Graben towards the south in the Salt Dome Province and changes from predominantly type II to type III kerogen (Damtoft et al., 1987). The decrease in kerogen quality possibly relates to a location with higher terrestrial input which possibly resulted in increased ratios of siliciclastics and inert organic matter. Also, lower subsidence rates may have led to a rather shallow marine depositional setting with potentially higher carbonate contents of the shales in contrast to a presumably rather deep marine setting within the northern Dutch Central Graben. A higher portion of marine organic material is known from the deeper, northern parts of the Danish Central Graben and we presume a similar composition of the upper Kimmeridge Formation also for the deeper subsided parts of the northern Dutch Central Graben.

6. Jurassic to Lower Cretaceous tectonostratigraphy of the German Central Graben, southern North Sea

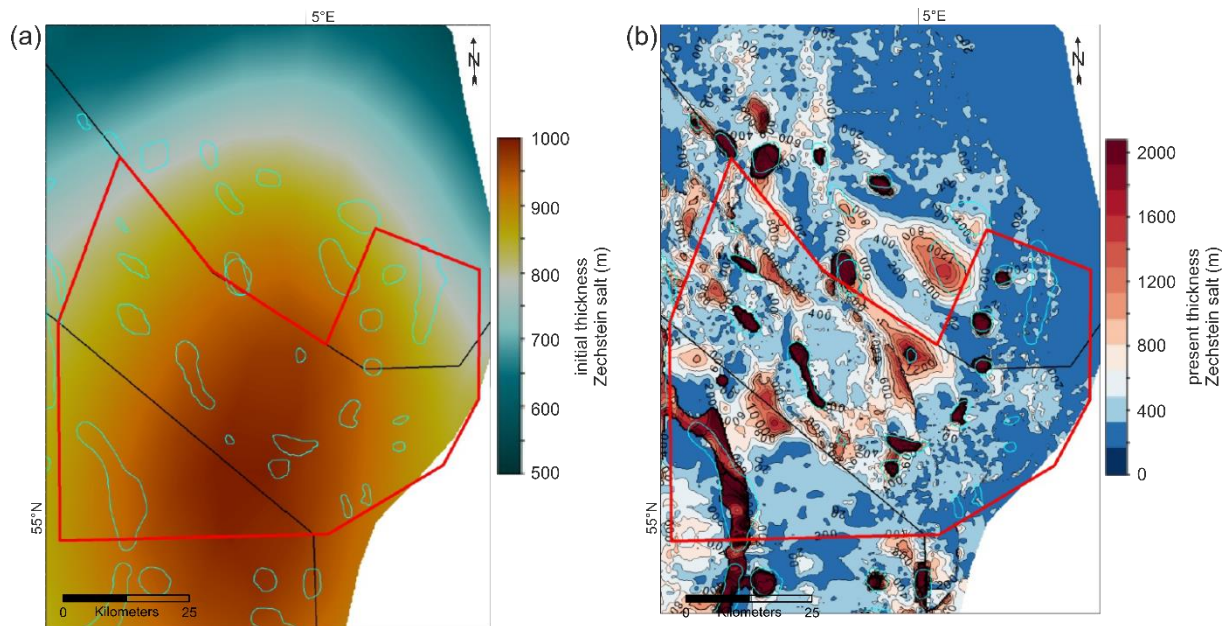


Fig. 57 (a) Interpolation of the initial Zechstein salt thickness in and around the study area. Modeled from data from Smith et al. (1993) and ten Veen et al. (2012). The presumed initial thickness of the salt reaches a maximum thickness of around 1000 m in the area of the German and the northern Dutch Central Graben and decreases towards the Danish graben part. (b) Today's thickness of the Zechstein salt in and around the study area (based on Thöle et al., 2021). Salt thicknesses of up to 6000 m are reached in the diapirs of the region.

6.5.4. TMS-3 and Lower Cretaceous

During TMS-3 sediments of the Scruff Greensand Formation and the Hot Shales were deposited in the study area. They are embedded within the mudstones of the Lutine Formation in The Netherlands (Clay Deep Member) and within the mudstones of the Mandal Formation in Denmark (Bo Member) (Fig. 47 & Fig. 55).

The occurrence of the shallow marine sandstones of the Scruff Greensand Formation is mostly restricted to the area of the northern Dutch Central Graben (Fig. 55). Only thin deposits extend into the southernmost German Central Graben (see well B18-05 in Fig. 54). The Hot Shales were mostly deposited in a hemipelagic environment with anoxic bottom water conditions (Ineson et al., 2003). They are present in the Central Graben over the entire area from the Danish Central Graben into the northern Dutch Central Graben (Müller et al., 2020). The Hot Shales form part of TS-3.2 of Bouroullec et al. (2018) and Verreussel et al. (2018) and correspond to phase seven of basin development defined by Andsbjerg and Dybkjaer (2003). They replace or overly the sandstones of the Scruff Greensand Formation and were deposited during the Late Cimmerian II pulse (Wong, 2007). The typical high gamma-ray (GR) reading, which closely correlates with the content of organic material, thickness, and maturity of the Hot Shales vary greatly within its area of distribution. The distribution of TMS-3.2 and the Hot Shale demonstrate again the impact of tectonics (especially the MCGTZ) on stratigraphy. The Hot Shale reaches the highest thickness in the northern Dutch Central Graben and in the northern Dutch Tail End Graben with up to 100 (Ineson et al., 2003). While the GR-readings and probably the organic content is well developed in the northern Dutch Central Graben, they decrease further

north across the German Central Graben. The GR-readings increase again in the Danish Salt Dome Province (Fig. 54). While they form a prolific source rock in the Danish Tail End Graben, the Hot Shales are mostly thermally immature to early mature in the German part of the Central Graben. (Ponsaing et al., 2018; Müller et al., 2020;). The subsidence pattern of TMS-3 is rather complex and local tectonics may have caused significantly more local hiatuses and variations in siliciclastic content (Fig. 52).

Tectonically, the southern Central Graben reached an early post-rift stage (Andsbjerg & Dybkjaer, 2003) and TMS-3 corresponds to a phase of tectonic quiescence between the tectonic pulses 2 and 3 of Møller and Rasmussen (2003). During this phase the organic rich Hot Shales were deposited. Subsidence rates strongly decreased in the second half of the Volgian, which is recorded by the reconstructed subsidence rates and subsidence pattern of the northern Dutch Central Graben from TMS-2 to TMS-3 (Fig. 51 & Fig. 52). But even if subsidence in total began to fade, subsidence affected not only the graben axis and adjacent basin, but the entire region (Andsbjerg & Dybkjaer, 2003; Verreussel et al., 2018). Activity of the MBF ceased, while the influence of salt tectonics on sedimentation climaxed, expressed by the formation of and deposition within rim synclines close to salt structures (Fig. 52).

During the Early Cretaceous, rifting as well as salt tectonics ceased while regional thermal subsidence became important, resulting in a regional transgression and the deposition of the Vlieland Claystone Formation (TMS-4) and the Holland Formation (Herngreen & Wong, 2007). This deposition followed the third tectonic pulse according to Møller and Rasmussen (2003). The transgressive sediments were originally deposited in large areas of the southern North Sea but were partly eroded during the Late Cretaceous inversion of the southern Central Graben (Herngreen & Wong, 2007). Our thickness maps show that the influence of salt tectonics was still significant during the deposition of the Vlieland Claystone Formation (TMS-4), while a tectonic influence at the main bounding faults was minor (Fig. 52). In comparison to the Vlieland Claystone Formation, the distribution of the Holland Formation is more uniform, reflecting the decrease in differential subsidence and salt tectonics. The low subsidence rates in the marine setting may have produced a relative homogenous distribution of the lithofacies. Increased thicknesses at the basin axis of the northern Dutch Central Graben may indicate continuous activity of sub-salt faults in this area.

6. Jurassic to Lower Cretaceous tectonostratigraphy of the German Central Graben, southern North Sea

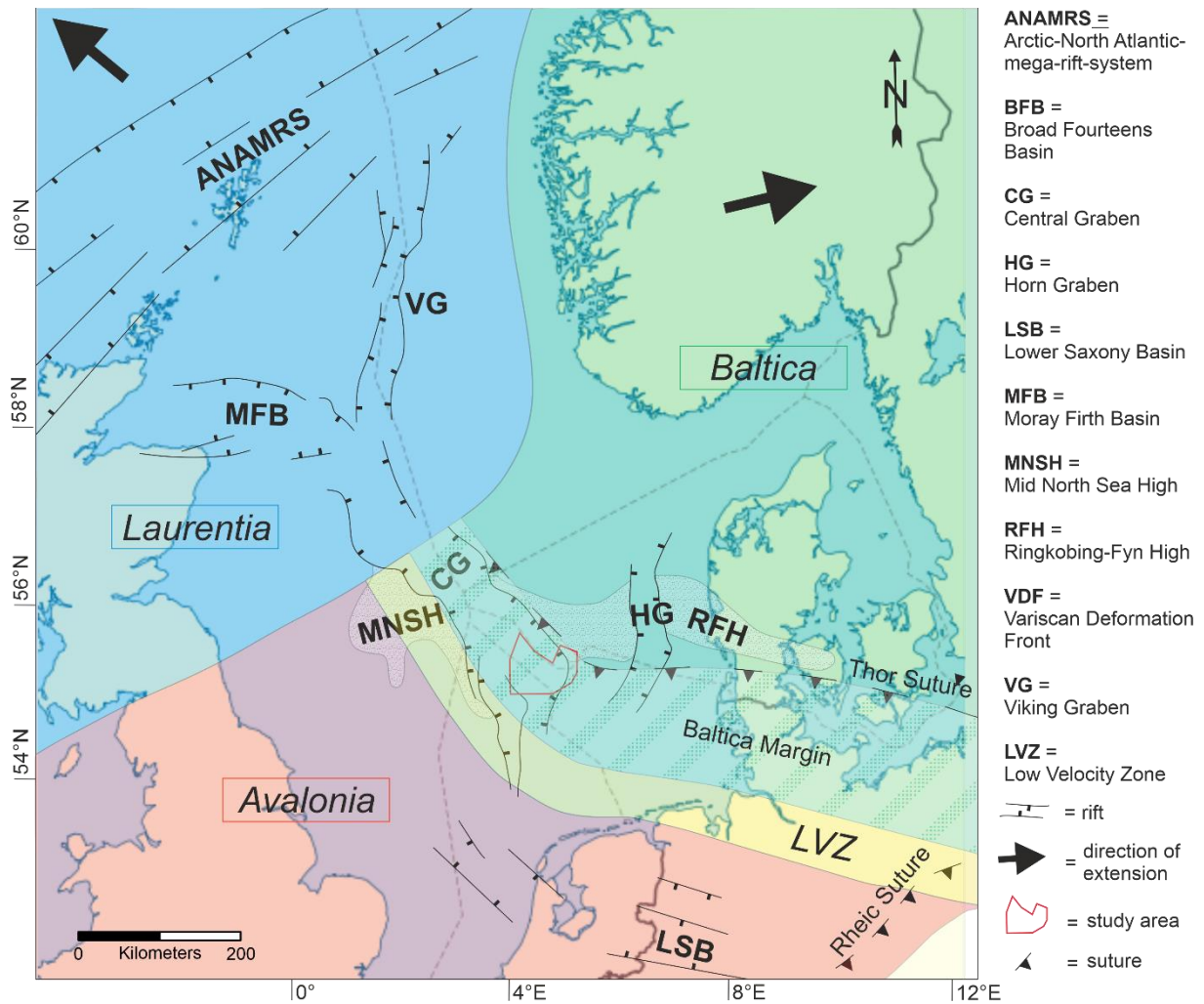


Fig. 58 Simplified structural overview map of the North Sea area during the Middle Jurassic. The area is affected by the ongoing break-up of the supercontinent Pangea which led to roughly NW-SE extension in the Arctic-North Atlantic mega-rift-system and to roughly E-W extension in the Central Graben. The Central Graben is located at the triple collision zone of the terranes Laurentia in the northwest, Baltica in the northeast, and Avalonia in the south. It cuts the transition of Laurentia to Avalonia and follows roughly the margin of Avalonia. The figure is compiled and modified from Lyngsø et al. (2007), Pharaoh et al. (2010), and Smit et al. (2016).

6.5.5. Influence of supra-regional tectonics

Initial salt mobilization in the Central Graben is probably connected to first rifting pulses during the break-up of Pangea (Stollhofen et al., 2008; Maystrenko et al., 2013). In the process, the study area was not uniformly deformed, resulting in a dichotomy in the structural pattern. Salt structures south of and within the MCGTZ, including the Dutch Central Graben, started to form in the Middle to Late Triassic (van Winden et al., 2018; Warsitzka et al., 2018). During this period, initial salt mobilization concentrated on major fault zones and graben structures as the Dutch Central Graben, the Horn Graben, and the Glückstadt Graben (Grassmann et al., 2005; Warsitzka et al., 2018). The rifting pulses led to differential gravitational unloading of the Zechstein salt due to the extension of its overburden, in combination with differential loading due to

accelerated subsidence in the evolving grabens (Scheck-Wenderoth et al., 2008; Warsitzka et al., 2018).

Salt movement north of the MCGTZ, in the German Central Graben and the Danish Salt Dome Province, initiated in the Late Triassic (Warsitzka et al., 2018). It was the Triassic main phase of salt mobilization in the Southern Permian Basin and affected also structurally higher areas (Warsitzka et al., 2018). The SPB is dominated by two structural trends, a roughly N-S and a roughly NW-SE orientation of basement faults and depocenters (Kley et al., 2008). These two main structural patterns are also reflected in the pattern of the salt structures (Kley et al., 2008; Scheck-Wenderoth et al., 2008). Many elongated salt structures follow the roughly N-S striking structural trend that is dominant for the Dutch Central Graben, e.g., B17-SOUTH1 (*Fig. 46b*). Directly after the collapse of the Mid North Sea Dome, roughly N-S trending faults were active during the deposition of TMS-1, potentially resulting from reactivation of older structures (*Fig. 56*; Pharaoh et al., 2010). The trend of these faults conforms to the general E-W extension of the area, as well as the Viking Graben and the Dutch Central Graben, but cross-cuts the roughly NW-SE trend of the Danish Central Graben. NW-SE elongated salt structures developed over pre-Zechstein basement faults. These structures were reactivated during the Late Jurassic to the Early Cretaceous (Scheck-Wenderoth et al., 2008), which may be reflected in the change from roughly N-S to NW-SE oriented faults from TMS-1 to TMS-2 in the German and Danish part of the Central Graben (*Fig. 56*). This structural trend is common in the wider area, e.g., the Broad Fourteens Basin offshore The Netherlands, the Polish Trough, and the Lower Saxony Basin onshore Germany (Kley et al., 2008).

The Central Graben is located at the collision triangle of three terranes, Laurentia in the northwest, Baltica in the northeast, Avalonia in the south (Maystrenko et al., 2008; Smit et al., 2016; *Fig. 58*). Despite the general E-W direction of extension the trend of the Danish Central Graben is roughly NW-SE oriented. We suggest that the graben follows roughly a deep-seated zone of crustal weakness, the Thor suture which separates the two terranes Avalonia and Baltica (Smit et al., 2016; *Fig. 58*). A similar relation of a Mesozoic sub-basin to deep-seated crustal structure is presumed for the Polish Trough in the east of the SPB, whose roughly NW-SE striking structural trend follows the Teisseyre-Tornquist-Zone (TTZ), a major geologic structure and zone of deformation (Narkiewicz et al., 2015; Grad & Polkowski, 2016). Especially the NW-SE trending part of the Central Graben in German and Danish offshore which cut the Mid North Sea High and Ringkøbing-Fyn High show several ENE-WSW striking transverse zones (Cartwright, 1987; Wride 1995). The MCGTZ is the furthest south of this sequence of transverse zones (Wride, 1995) and shows clear evidence for influencing the Jurassic tectonostratigraphy in the study area. It is possible that the transverse zones follow precursors in the crust. However, they may also be a consequence of the influence of a E-W directed supra-regional extension on an already existing NW-SE striking graben segment.

The main activity of salt tectonics in the German and Dutch Central Graben was in the Late Jurassic to Early Cretaceous (e.g., ten Veen et al., 2012; Arfai et al., 2014), in contrast to other grabens of the SPB, e.g., the Gückstadt Graben, where the main activity was in the Late Triassic (Grassmann et al., 2005; Warsitzka et al., 2016). This corresponds with our results, which imply that during the deposition of TMS-2 to TMS-3 the influence of salt tectonics dominated the depositional pattern (*Fig. 51 & Fig. 52*). Salt tectonics ceased during the Lower Cretaceous and

some of the salt structures have already formed welds. Due to Late Cretaceous to Paleocene compressional tectonics, salt mobilization was renewed in the study area as well as in other parts of the SPB (e.g., Mazur et al., 2005; Ahlrichs et al., 2022). The accompanying structural deformation partly complicates the analysis of the Jurassic to Early Cretaceous tectonostratigraphy in the study area.

6.6. Conclusions

- Rift tectonics dominated subsidence in the study area during the deposition of TMS-1. Subsidence took place along N-S and NW-SE trending faults. The influence of salt tectonics increased steadily until it dominated subsidence pattern during the deposition of TMS-2. Locally, salt tectonics remained the dominating factor of subsidence during deposition of TMS-3 and TMS-4.
- The paleo-topography of the Early Jurassic Central Graben area was more differentiated than assumed, with lows like the northern Dutch central Graben and highs like the Clemens Graben and Basin area.
- The German Central Graben is subdivided by the Mid Central Graben Transverse Zone (MCGTZ), a fault zone with a prominent present-day sinistral offset. Regarding their tectonostratigraphic development from the Altena Group to TMS-3, the northern part belongs rather to the Danish Central Graben and the southern part rather to the Dutch Central Graben.
- During deposition of TMS-2, the subdivision of the study area into a high-subsidence area (Dutch Central Graben) and a comparatively low-subsidence area (German and Danish Central Graben) is most pronounced.
- Active faulting and salt tectonics had a significant impact on the regional (litho-)stratigraphic evolution of the Lower Jurassic to the Lower Cretaceous sedimentary successions. E.G., the distribution of the Posidonia Shale Formation and of the high-GR Clay Deep Member is probably restricted to areas south and partly east of the MCGTZ.
- Major parts of the German Central Graben and of the Danish Salt Dome Province constituted a topographic high during deposition of TMS-1 to TMS-3 in comparison to the Dutch Central Graben in the south and the Danish Tail End Graben in the north. The elevated location presumably influenced lithology and source rock quality regarding its organic matter, siliciclastic and carbonate contents.

Acknowledgements

The presented research was done in the projects “Tieferer Untergrund Norddeutsches Becken (TUNB) and „Establishing the European geological surveys research area to deliver a geological service for Europe (GeoERA)“ at the Federal Institute for Geosciences and Natural Resources of Germany (BGR). We thank our colleagues Jashar Arfai, Dieter Franke, Lutz Reinhardt, Rüdiger Lutz, Stefan Ladage, and Heidrun Stück who provided expertise that greatly assisted the research. We also want to acknowledge the support from Franziska- Sabine Müller, Felix Müller, and Tilda Müller-Thiel, which was invaluable.

References

- Abbink, O. A., Mijndieff, H. F., Munsterman, D. K., & Verreussel, R. M. C. H., 2006. New stratigraphic insights in the 'Late Jurassic' of the southern Central North Sea Graben and Terschelling Basin (Dutch Offshore) and related exploration potential. *Netherlands Journal of Geosciences*, 85(3), 221-238.
- Ahlich, N., Noack, V., Hübscher, C., Seidel, E., Warwel, A., & Kley, J., 2022. Impact of Late Cretaceous inversion and Cenozoic extension on salt structure growth in the Baltic sector of the North German Basin. *Basin Research*, 34(1), 220-250.
- Andsbjerg, J., & Dybkjær, K., 2003. Sequence stratigraphy of the Jurassic of the Danish Central Graben. *Geological Survey of Denmark and Greenland (GEUS) Bulletin*, 1, 265-300.
- Arfai, J., Jähne, F., Lutz, R., Franke, D., Gaedicke, C. & Kley, J., 2014. Late Palaeozoic to Early Cenozoic geological evolution of the northwestern German North Sea (Entenschnabel): New results and insights. *Netherlands Journal of Geosciences* 93(4): 147-174.
- Arfai, J., & Lutz, R., 2017. 3D basin and petroleum system modelling of the NW German North Sea (Entenschnabel). In *Geological Society, London, Petroleum Geology Conference series (Vol. 8, pp. PGC8-35)*. Geological Society of London.
- Bachmann, G.H. & Grosse, S., 1989. Struktur und Entstehung der Norddeutschen Beckens – Geologische und geophysikalische Interpretation einer verbesserten Bouger-Schwerekarte. *Veröffentlichungen Niedersächsische Akademie der Geowissenschaften* 2: 24-47.
- Bachmann, G.H. & Hoffmann, N., 1997. Development of the Rotliegend Basin in Northern Germany. *Geologisches Jahrbuch D (103)*: 9-31.
- Bachmann, G.H., Geluk, M.C. et al., 2010. Triassic. In: Doornenbal, J.C. & Stevensen, A.G. (eds.) *Petroleum Geological Atlas of the Southern Permian Basin Area*. European Association of Geoscientists and Engineers (EAGE), Houten, The Netherlands, 149–173.
- Bouroulllec, R., Verreussel, R. M. C. H., Geel, C. R., De Bruin, G., Zijp, M. H. A. A., Körösi, D., Munsterman, D. K., Janssen, N. M. M. & Kerstholt-Boegehold, S. J., 2018. Tectonostratigraphy of a rift basin affected by salt tectonics: synrift Middle Jurassic–Lower Cretaceous Dutch Central Graben, Terschelling Basin and neighbouring platforms, Dutch offshore. *Geological Society, London, Special Publications*, 469(1), 269-303.
- Cartwright, J. A., 1987. Transverse structural zones in continental rifts—an example from the Danish Sector of the North Sea. In: *Conference on petroleum geology of North West Europe*. 3, 441-452.
- Cartwright, J., 1991. The kinematic evolution of the Coffee Soil Fault. *Geological Society, London, Special Publications*, 56(1), 29-40.
- Clausen, O.R., Nielsen, S.B., Egholm, D.L., Goleadowski, B., 2012. Cenozoic structures in the eastern North Sea Basin a case for salt tectonics. *Tectonophysics* 514e517, 156e167.
- Damtoft, K., Andersen, C., Thomsen, E., 1987. Prospectivity and hydrocarbon plays of the Danish central trough. In: Brooks, J., Glennie, K. (eds.), *Petroleum Geology of North West Europe*. Graham & Trotman, London, pp. 403–417.

- de Jager, J., 2003. Inverted basins in the Netherlands, similarities and differences. *Netherlands Journal of Geosciences*, 92, 355-366
- de Jager, J. 2007. Geological development. In: Wong, T.E., Batjes, D.A.J. & de Jager, J. (eds.) *Geology of the Netherlands*. Royal Netherlands Academy of Arts and Sciences, Amsterdam, 5-26.
- de Jager, J., & Geluk, M. C., 2007. Petroleum Geology. In: Wong, T.E., Batjes, D.A.J. & de Jager, J. (eds.) *Geology of the Netherlands*. Royal Netherlands Academy of Arts and Sciences, Amsterdam, 241-264.
- Doornenbal, H., den Dulk, M., Thöle, H., Jähne-Klingberg, F., Britze, P. & Jakobsen, F., 2021a: Deliverable 3.7 – A harmonized cross-border velocity model. GEOERA 3DGEO-EU; 3D Geomodeling for Europe; project number GeoE.171.005., Report, 33 p.
- Doornenbal, H., den Dulk, M., Thöle, H., Jähne-Klingberg, F., Britze, P. & Jakobsen F., 2021b: Deliverable 3.9 – Final report incl. lessons learned; GEOERA 3DGEO-EU; 3D Geomodeling for Europe; project number GeoE.171.005. Report, p.25.
- Duffy, O. B., Gawthorpe, R. L., Docherty, M., & Brocklehurst, S. H., 2013. Mobile evaporite controls on the structural style and evolution of rift basins: Danish Central Graben, North Sea. *Basin Research*, 25(3), 310-330.
- Geluk, M.C. 2007. Triassic. In: Wong, T.E., Batjes, D.A.J. & de Jager, J. (eds.) *Geology of the Netherlands*. Royal Netherlands Academy of Arts and Sciences, Amsterdam, 85-106.
- Geluk, M.C., Paar, W.A. & Fokker, P.A., 2007 – Salt. *Geology of the Netherlands*, 283-294
- Grad, M., & Polkowski, M., 2016. Seismic basement in Poland. *International Journal of Earth Sciences*, 105(4), 1199-1214.
- Grassmann, S., Cramer, B., Delisle, G., Messner, J., & Winsemann, J., 2005. Geological history and petroleum system of the Mittelplate oil field, Northern Germany. *International Journal of Earth Sciences*, 94(5), 979-989.
- Graversen, O., 2006. The Jurassic-Cretaceous North Sea Rift Dome and Associated Basin Evolution. American Association of Petroleum Geologists Annual Convention, Calgary, Alberta, June 19-22, 2005.
- Herngreen, G.F.W., & Wong, T.E., 2007. Cretaceous. In: Wong, T.E., Batjes, D.A.J. & de Jager, J. (eds.): *Geology of the Netherlands*. Royal Netherlands Academy of Arts and Sciences (Amsterdam): 127-150.
- Huuse, M., & Clausen, O.R., 2001. Morphology and origin of major Cenozoic sequence boundaries in the eastern North Sea Basin: top Eocene, near-top Oligocene and the mid-Miocene unconformity. *Basin Research* 13(1): 17-41.
- Ineson, J. R., Bojesen-Koefoed, J. A., Dybkjær, K., & Nielsen, L. H., 2003. Volgian–Ryazanian ‘hot shales’ of the Bo Member (Farsund Formation) in the Danish Central Graben, North Sea: stratigraphy, facies and geochemistry. *Geological Survey of Denmark and Greenland (GEUS) Bulletin*, 1, 403-436.
- Jackson, M. P., & Hudec, M. R. 2017. *Salt tectonics: Principles and practice*. Cambridge University Press.

- Jackson, M.P.A., & Talbot, C.J., 1986. External shapes, strain rates and dynamics of salt structures. *Geological Society of America Bulletin* 97: 305-323.
- Jähne-Klingberg, F., Bense, F. & Warsitzka, M., 2018. A comparison of the kinematics and structural evolution of major Mesozoic rifts of the southeastern North Sea and Northern Germany. 80th EAGE Conference & Exhibition 2018, 11 – 14 June 2018, Copenhagen, Denmark. Extended abstract.
- Jakobsen, F., Britze, P., Thöle, H., Jähne-Klingberg, F., Doornenbal, H., Bouroullec, R. & Verreussel, R., 2020a. Lithostratigraphic / chronostratigraphic correlation profiles through the study area. 3D Geomodeling for Europe Report GeoE.171.005
- Jakobsen, F., Britze, P., Thöle, H., Jähne-Klingberg, F., Doornenbal, H. & Vis, G.-J., 2020b. Harmonized stratigraphic chart for the North Sea area NL-DE-DK. 3D Geomodeling for Europe Report GeoE.171.005
- Kley, J., & Voigt, T., 2008. Late Cretaceous intraplate thrusting in central Europe: Effect of Africa-Iberia-Europe convergence, not Alpine collision. *Geology*, 36(11), 839-842.
- Kley, J., Franzke, H. J., Jähne, F., Krawczyk, C., Lohr, T., Reicherter, K., Scheck-Wenderoth, M., Sippel, J., Tanner, D., & Van Gent, H., 2008. Strain and stress. In: Littke, R., Bayer, U., Gajewski, D. & Nelskamp, S. (eds.). *Dynamics of complex intracontinental basins: the central European Basin system* (pp. 97-124). Berlin, Heidelberg, Germany: Springer-Verlag.
- Lott, G. K., Wong, T. E., Dussar, M., Andsbjerg, J., Mönnig, E., Feldman-Olszewska, A., & Verreussel, R. M. C. H., 2010. Jurassic. In: Doornenbal, J.C. & Stevenson, A.G. (eds.): *Petroleum Geological Atlas of the Southern Permian Basin Area*. EAGE Publications b.v. (Houten): 175-193.
- Lyngsie, S. B., & Thybo, H., 2007. A new tectonic model for the Laurentia– Avalonia– Baltica sutures in the North Sea: A case study along MONA LISA profile 3. *Tectonophysics*, 429(3-4), 201-227.
- Maystrenko, Y., Bayer, U., Brink, H. J., & Littke, R., 2008. The Central European basin system—an overview. In: Littke, R., Bayer, U., Gajewski, D. & Nelskamp, S. (eds.). *Dynamics of complex intracontinental basins: the Central European Basin System* (pp. 16-34). Berlin, Heidelberg, Germany: Springer-Verlag.
- Maystrenko, Y. P., Bayer, U., & Scheck-Wenderoth, M., 2013. Salt as a 3D element in structural modeling – Example from the Central European Basin System. *Tectonophysics*, 591, 62–82.
- Mazur, S., Scheck-Wenderoth, M. & Krzywiec, P., 2005. Different modes of Late Cretaceous-Early Tertiary inversion in the North German and Polish basins. *International Journal of Earth Sciences*, 94, 782-798.
- Michelsen, O., Nielsen, L. H., Johannessen, P. N., Andsbjerg, J., & Surlyk, F., 2003. Jurassic lithostratigraphy and stratigraphic development onshore and offshore Denmark. *Geological Survey of Denmark and Greenland (GEUS) Bulletin*, 1, 145-216.
- Møller, J. J., & Rasmussen, E. S., 2003. Middle Jurassic–Early Cretaceous rifting of the Danish Central Graben. *Geological Survey of Denmark and Greenland (GEUS) Bulletin*, 1, 247-264.

- Müller, S., Arfai, J., Jaehne-Klingberg, F., Bense, F., & Weniger, P., 2020. Source rocks of the German Central Graben. *Marine and Petroleum Geology*, 113, 104-120.
- Narkiewicz, M., Maksym, A., Malinowski, M., Grad, M., Guterch, A., Petecki, Z., & Jankowski, L., 2015. Transcurrent nature of the Teisseyre–Tornquist Zone in Central Europe: results of the POLCRUST-01 deep reflection seismic profile. *International Journal of Earth Sciences*, 104(3), 775-796.
- Nottvedt, A., Gabrielsen, R. H., & Steel, R. J., 1995. Tectonostratigraphy and sedimentary architecture of rift basins, with reference to the northern North Sea. *Marine and Petroleum Geology*, 12(8), 881-901.
- Penge, J., Munns, J.W., Taylor, B. & Windle, T.M.F., 1999. Rift-raft tectonics: examples of gravitational tectonics from the Zechstein basins of northwestern Europe. In: Fleet, A.J. & Boldy, S.A.R. (eds.) *Petroleum Geology of Northwest Europe. Proceedings of the 5th Conference*. Geological Society, London, *Petroleum Geology Conference Series*, 5, 201–213.
- Peryt, T.M., Geluk, M.C., Mathiesen, A., Paul, J. & Smith, K., 2010. Zechstein. In: Doornenbal, J.C. & Stevenson, A.G. (eds.): *Petroleum Geological Atlas of the Southern Permian Basin Area*. EAGE Publications b.v. (Houten): 123-147.
- Petersen, H.I., Hertle, M. & Sulsbrück, H., 2017. Upper Jurassic–lowermost Cretaceous marine shale source rocks (Farsund Formation), North Sea: kerogen composition and quality and the adverse effect of oil-based mud contamination on organic geochemical analyses. *Int. J. Coal Geol.* 173, 26–39.
- Petersen, H.I. & Hertle, M., 2018. A review of the coaly source rocks and generated petroleum systems in the Danish North Sea: an underexplored Middle Jurassic petroleum system? *J. Pet. Geol.* 41 (2), 135–154.
- Petersen, H.I., Andsbjerg, J., Bojesen-Koefoed, J.A. & Nytoft, H.P., 2000. Coal-generated oil: source rock evaluation and petroleum geochemistry of the Lulita oilfield, Danish North Sea. *J. Pet. Geol.* 23 (1), 55–90.
- Pharaoh, T.C., Dusa, M., Geluk, M.C., Kockel, F., Krawczyk, C.M., Krzywiec, P., Scheck-Wenderoth, M., Thybo, H., Vejrbæk, O.V. & Van Wees, J.D., 2010. Tectonic evolution. In: Doornenbal, J.C. and Stevenson, A.G. (eds.): *Permian Basin Area*. EAGE Publications b.v. (Houten): 25-57.
- Pletsch, T., Appel, J., Botor, D., Clayton, C.J., Duin, E.J.T., Faber, E., Górecki, W., Kombrink, H., Kosakowski, P., Kuper, G., Kus, J., Lutz, R., Mathiesen, A., Ostertag-Henning, C., Papiernek, B. & Van Bergen, F., 2010. Petroleum generation and migration. In: Doornenbal, J.C. and Stevenson, A.G. (eds.): *Petroleum Geological Atlas of the Southern Permian Basin Area*. EAGE Publications b.v. (Houten): 225-253.
- Ponsaing, L., Bojesen-Koefoed, J. A., Thomsen, E., & Stemmerik, L., 2018. Temporal organic facies variations of Upper Jurassic-lowermost Cretaceous source rocks in the Danish Central Graben, North Sea. *International Journal of Coal Geology*, 195, 217-237.
- Rasmussen, E.S., 2009. Neogene inversion of the Central Graben and Ringkøbing- Fyn High, Denmark. *Tectonophysics* 465: 84-97.

- Rommelts, G., 1995. Fault-related salt tectonics in the southern North Sea, the Netherlands. In: Jackson, M.P.A., Roberts, D.G., Snelson, S. (eds.), *Salt Tectonics: a Global Perspective*, AAPG Memoir. 65, pp. 261-272.
- Scheck-Wenderoth, M., Maystrenko, Y., Hübscher, C., Hansen, M., & Mazur, S., 2008. Dynamics of salt basins. In: Littke, R., Bayer, U., Gajewski, D. & Nelskamp, S. (eds.), *Dynamics of complex intracontinental basins, the Central European Basin System* (pp. 17-34). Berlin, Heidelberg, Germany: Springer-Verlag.
- Sippel, J., 2009. The paleostress history of the Central European Basin system (Doctoral dissertation, Deutsches GeoForschungsZentrum GFZ Potsdam).
- Smit, J., van Wees, J. D., & Cloetingh, S., 2016. The Thor suture zone: From subduction to intraplate basin setting. *Geology*, 44(9), 707-710.
- Stemmerik, L., Ineson, J. R., & Mitchell, J. G., 2000. Stratigraphy of the Rotliegend Group in the Danish part of the northern Permian Basin, North Sea. *Journal of the Geological Society*, 157(6), 1127-1136.
- Stewart, S.A., 2007. Salt tectonics in the North Sea Basin: a structural style template for seismic interpreters. In: Ries, A.C., Butler, R.W.H. & Graham, R.H. (eds.) *Deformation of the Continental Crust: The Legacy of Mike Coward*. Geological Society, London, Special Publications, 272, 361-396.
- Stewart, S.A. & Clark, J.A. 1999. Impact of salt on the structure of the Central North Sea hydrocarbon fairways. In: Fleet, A.J. & Boldy, S.A.R. (eds.) *Petroleum Geology of Northwest Europe*. Proceedings of the 5th Conference. Geological Society, London, Petroleum Geology Conference Series, 5, 179-200.
- Stollhofen, H., Bachmann, G. H., Barnasch, J., Bayer, U., Beutler, G., Franz, M., Kästner, M., Legler, B., Mutterlose, J. & Radies, D., 2008. Upper Rotliegend to early cretaceous basin development. In: Littke, R., Bayer, U., Gajewski, D. & Nelskamp, S. (eds.), *Dynamics of complex intracontinental basins: The Central European Basin System* (pp. 181-207). Berlin, Heidelberg, Germany: Springer-Verlag.
- Taylor, J.C.M., 1998. Upper Permian - Zechstein. In: Glennie, K.W. (ed.): *Petroleum Geology of the North Sea: Basic Concepts and Recent Advances*. Blackwell (Oxford): 174-212.
- ten Veen, J.H., van Gessel, S. & den Dulk, M., 2012. Thin-and thick-skinned salt tectonics – Examples from the Dutch North Sea. *Netherlands Journal of Geosciences* 91-4: 447-464.
- Thöle, H., Jähne-Klingberg, F., Doornenbal, H., den Dulk, M., Britze, P. & Jakobsen F., 2021: Deliverable 3.8 – Harmonized depth models and structural framework of the NL-GER-DK North Sea. Report, p.77; GEOERA 3DGEO-EU; 3D Geomodeling for Europe; project number GeoE.171.005.
- Underhill, J.R. & Partington, M.A., 1993. Jurassic thermal doming and deflation in the North Sea: Implications of the sequence stratigraphic evidence. In: Parker, J.R. (ed.): *Petroleum Geology of Northwest Europe: Proceedings of the 4th conference: The Geological Society (London)*. Petroleum Geology Conference series 4: 337-345.

6. Jurassic to Lower Cretaceous tectonostratigraphy of the German Central Graben, southern North Sea

- van Adrichem Boogaert, H.A. & Kouwe, W.F.P., 1993. Stratigraphic nomenclature of The Netherlands; revision and update by RGD and NOGEPa, Section G, Upper Jurassic and Lower Cretaceous. Mededelingen Rijks Geologische Dienst, 50, 1-80.
- van der Molen, A.S., Dudok, H.W. & Wong, T.E., 2005. The influence of tectonic regime on chalk deposition: examples of the sedimentary development and 3D stratigraphy of the chalk Group in the Netherlands offshore area. *Basin Research*, 17, 63–81.
- van Winden, M., de Jager, J., Jaarsma, B., & Bouroullec, R., 2018. New insights into salt tectonics in the northern Dutch offshore: a framework for hydrocarbon exploration. Geological Society, London, Special Publications, 469(1), 99-117.
- Vejbæk, O.V. & Andersen, C., 1987. Cretaceous-early Tertiary inversion tectonism in the Danish Central Trough. In: Ziegler, P.A. (ed.): *Compressional intra-plate deformations in the Alpine Foreland*. *Tectonophysics* 137: 221-238.
- Vendeville, B.C. 2002. A new interpretation of Trusheim's classic model of salt diapir growth. *Transactions of the Gulf Coast Association of Geological Societies*, 52, 943.
- Verreussel, R. M. C. H., Bouroullec, R., Munsterman, D. K., Dybkjær, K., Geel, C. R., Houben, A. J. P., Johannessen, P. N. & Kerstholt-Boegehold, S. J., 2018. Stepwise basin evolution of the Middle Jurassic–Early Cretaceous rift phase in the Central Graben area of Denmark, Germany and The Netherlands. Geological Society, London, Special Publications, 469(1), 305-340.
- Walter, R., (ed.), 2007. *Geologie von Mitteleuropa*. Schweizerbart'sche Verlagsbuchhandlung, (Stuttgart) 7: 511 pp.
- Warsitzka, M., Kley, J., Jähne-Klingberg, F., & Kukowski, N., 2016. Dynamics of prolonged salt movement in the Glückstadt Graben (NW Germany) driven by tectonic and sedimentary processes. *International Journal of Earth Sciences*, 106(1), 131-155.
- Warsitzka, M., Jähne-Klingberg, F., Kley, J. & Kukowski, N., 2018. The timing of salt structure growth in the Southern Permian Basin (Central Europe) and implications for basin dynamics. *Basin Research*, 31(2), 337-360.
- Wong D. A., 2007. Jurassic. In: Wong, T.E., Batjes, D.A.J. & de Jager, J. (eds.): *Geology of the Netherlands*. Royal Netherlands Academy of Arts and Sciences (Amsterdam): 107-125.
- Wride, V. C., 1995. Structural features and structural styles from the Five Countries Area of the North Sea Central Graben. *First Break*, 13(10).
- Ziegler, P.A., 1990. *Geological Atlas of Western and Central Europe*, 2nd edn. Shell Internationale Petroleum Maatschappij B.V.; Geological Society Publishing House (Bath): 239.
- Ziegler, P.A., 1992. North Sea rift system. *Tectonophysics* 208(1-3): 55-75

7. Synthesis and conclusions

7.1. Amplitude anomalies and their relation to shallow gas accumulations

Amplitude anomalies in reflection seismic data were identified in the German Central Graben that indicate natural gas occurrences. The potential shallow gas accumulations share several common characteristics with shallow gas fields offshore The Netherlands. The shallow gas accumulations appear on reflection seismic data as stacked high amplitude anomalies (bright spots) with a typical peak-over-trough pattern, mostly in combination with one or more other amplitude anomalies that serve as direct hydrocarbon indicators (Fig. 21). These other anomalies are velocity push-downs, seismic attenuation, flat spots, and gas chimneys. Other common characteristics are the location above Zechstein salt domes in unconsolidated Cenozoic sediments (Fig. 16 and Fig. 17). The shallow gas accumulations are clearly related to salt structures within the Dutch and German Central Graben area. The gas is trapped in anticlinal structures, while faults and fractures above salt domes potentially provide migration pathways for hydrocarbons. The close relationship of salt structures with gas seepage and shallow gas accumulations is known in the Dutch North Sea (Hovland and Judd, 1988; Schroot et al., 2005; ten Veen et al., 2013). The origin of the amplitude anomalies from natural gas was verified by documenting gas leakage above the related salt structures (Fig. 30). Gas flares were detected and identified in the water column above the presumed shallow gas accumulations with a ship-based multibeam echosounder. The concentrations of dissolved methane in the sea water above these salt structures was considerably to slightly increased in contrast to sea water unrelated to amplitude anomalies. Additionally, echosounder profiles showed enhanced reflections with high amplitudes and acoustic signal blanking below above the shallow gas accumulations, further indicating the presence of gaseous hydrocarbons. High amplitude anomalies can be gas-induced as well as the consequence of a change in lithology. The common occurrence of different amplitude anomalies that are indicative of hydrocarbons on reflection seismic data, the analogue characteristics to known shallow gas fields offshore The Netherlands, and the hydroacoustic and geochemical evidence of gaseous hydrocarbons in the water column above salt domes all together strongly suggests a hydrocarbon origin of the amplitude anomalies. The question of the origin of the gas, though, is not yet resolved. Available literature for shallow gas accumulations in the southern Central Graben, especially its Dutch sector, provides arguments for either a microbial, a thermogenic, or also a mixed origin (e.g., Schroot et al., 2005; ten Veen et al., 2013; Verweij et al., 2018). We presume, that most of the shallow gas is microbial in origin, but there are indications of a thermogenic contribution. These indications include amplitude anomalies that may be connected to gas migration from deeper sources (e.g., gas chimneys), the geographic restriction of the amplitude anomalies on areas with Mesozoic sediments, and proven thermogenic contributions to Dutch shallow gas fields.

7.2. Impact of the tectonostratigraphic evolution on the petroleum systems of the Southern Central Graben

7.2.1. Pre-rift (Altena Group)

The potential for generating hydrocarbons of six Uppermost Triassic to Lowermost Cretaceous formations was investigated. Additionally, the tectonostratigraphic evolution from the Lower Jurassic to the Lower Cretaceous of the German Central Graben was reconstructed. The investigated pre-rift horizons of the Rhaetian Sleen Formation and the Lower Jurassic Aalburg formations reached the gas window and probably generated hydrocarbons (Fig. 42). Their potential for conventional hydrocarbon accumulations is restricted but they may have contributed to shallow gas accumulations in the area. Mapping on reflection seismic data of the Lower Jurassic Posidonia Shale Formation showed that it is only present in small areas in the south and south-east of the German Central Graben (Fig. 40). The Posidonia Shale in the German Central Graben is in part currently in the maturity window for oil generation and may produce hydrocarbons according to the results of the petroleum system modeling. However, the absence of the Posidonia in the rest of the German Central Graben and potentially in parts of the southern Danish Central Graben is not fully explained by the Mid Jurassic erosion. The pillar maps (Fig. 53) and the erosional outlines of the subsidence maps (Fig. 51 and Fig. 52) show that large areas of the German Central Graben without the Posidonia Shale Formation were probably not affected by erosion. This is the case for the John Graben area, where the seismic reflection pattern of the Lower Jurassic shows no sign for neither the presence of the Posidonia Shale nor for erosional truncation. Explanations for the absence of the Posidonia Shale Formation are, e.g., that there is a hiatus of non-deposition or erosion of these deposits that is not resolved by the reflection seismic data used for interpretation, or that the thickness of the Posidonia Shale is reduced in the area to such an extent that is not resolved in seismic reflection patterns. Due to the restricted and unclear presence of the Posidonia Shale Formation, its contribution to shallow gas accumulations in the German part of the graben is probably only minor.

7.2.2. TMS-1

The results from the petroleum system modeling of the Central Graben Subgroup (Lower, Middle, and Upper Graben formations) within the German Central Graben show that the coal bearing interval is in the maturity window for gas generation for the deeper parts and in the window for oil generation in the shallower parts of the German Central Graben (Fig. 41). They have the potential to have contributed to shallow gas accumulations in the area. The permeable terrestrial and coastal sediments around the coal layers may have supported hydrocarbon migration. The sediments are the lower part of TMS-1 and represent the initial phase of rifting and the subsequent transgression. The distribution of potential Middle to Upper Jurassic reservoir and source rocks of TMS-1 is mostly limited to the axis of the graben and associated sub-basins because subsidence is mostly driven by rift tectonics (Fig. 51). The terrestrial sediments of the subgroup are important for the petroleum system of the southern Central graben both as reservoir and source rocks. Accumulations of oil and gas were discovered in sandstones of the Middle to Upper Jurassic Lower Graben, Middle Graben, Upper Graben and Friese Front formations (Wong, 2007). E.g., the F03-FB field contains gas and condensate accumulated in sandstones

of the Lower, Middle and Upper Graben formations (Lott et al., 2010). The F03-FB field is sourced by the Lower Jurassic Posidonia Shale Formation that is mature for gas generation in large parts of the Dutch Central Graben (Lott et al., 2010). In the central and northern North Sea, middle Jurassic coals are regarded as prolific source rocks for hydrocarbons (Isaksen et al., 2002; Mouritzen et al., 2018; Petersen et al., 2018). In the Danish Central Graben, the Bryne and Lulu formations contain coals, coaly shales and carbonaceous shales that are primarily gas-prone but are also able to produce liquid hydrocarbons and are currently mature for hydrocarbon generation (Petersen and Hertle, 2018). Oil, condensate, and gas accumulations that are sourced by Middle Jurassic coaly source rocks were discovered in the Søgne Basin, the northernmost part of the Danish Central Graben and in the western and southern Danish Central Graben, of which the fields in the Søgne basin have been proven to be commercial (Petersen and Hertle, 2018). In the upper part of TMS-1 of the Danish Central Graben, oil-prone source rock intervals of marine mudstones are found in the lower part of the Lola Formations, which may locally contribute to hydrocarbon accumulations (Pletsch et al., 2010). Due to the ongoing transgression, the marine mudstones of the Lola Formation or the lower Kimmeridge Clay Formation are more widespread than the previous terrestrial sediments.

7.2.3. TMS-2

TMS-2 is characterized by the onset of sedimentation within adjacent basins outside the Central Graben axis, e.g., the Terschelling Basin. The sedimentation of the marine mud of the Kimmeridge Clay Formation in the Dutch and German part of the Central Graben or the upper Lola Formation and the lower part of the Farsund Formation in the Danish Central Graben continued from TMS-1 to TMS-2. Within these formations, the ratio of marine organic matter to terrestrial organic matter as well as the organic content itself increases roughly from the base to the top (Petersen et al., 2017). There are more oil prone and more gas prone intervals, depending on an anoxic or slightly more oxic depositional environment and the amount of terrestrial input (Petersen et al., 2017). However, no hydrocarbon accumulations are known that are charged solely from these intervals, but they may have contributed to accumulations that are credited to the Bo Member of the Farsund Formation at their top. The petroleum system modeling of the Kimmeridge Clay Formation indicates that the top of the formation is early mature to oil generation, while its base is mature for gas generation in deeper parts of the basin (Fig. 41). Depending on the kerogen type and organic amount, liquid or gaseous hydrocarbons may have been generated, albeit probably in no commercial amounts. However, gas from these intervals may have contributed to shallow gas accumulations in the area. The deposition of TMS-2 is particularly affected by the division of the structural development of the Dutch part of the graben and the German / Danish part of the graben by the Johannes fault and the MCGTZ. The subsidence rate and thickness of TMS-2 is considerably increased in the northern Dutch Central Graben, probably due to ongoing fault activity in combination with significant salt redistribution (Fig. 51). This decoupled development of the Dutch Central Graben may have contributed to favorable conditions regarding depth and timing for the present-day hydrocarbon accumulations in the area.

7.2.4. TMS-3

During the deposition of TMS-3, fault activity decreased while salt withdrawal and salt tectonics increased. Decreasing rates of subsidence and ceasing of fault activity indicates an early post-rift stage (Andsbjerg and Dybkjaer, 2003). This development led to a shift of the sedimentary depocenters away from the main bounding faults to the flanks of the ascending salt domes (Fig. 52). Also, sedimentation affected not only the main graben axis and adjacent basin, like TMS-2, but also reached the adjacent plateaus such as the Schillgrund Plateau. Other characteristics of TMS-3 are the widespread sand deposition in the Dutch Central Graben and widespread basin anoxia. The Scruff Greensand Formation in the northern Dutch Central Graben and the adjacent German Central Graben consists of fine-grained sandstones that were deposited in topographic depressions on downfaulted graben margins (Herngreen and Wong, 1989). The sandstone serves as a reservoir rock, e.g., for the F03-FA gas field in the northern Dutch Central Graben (Abbink et al., 2006). The widespread basin anoxia due to restricted basin circulation led to the deposition of organic rich, kerogen-type II hemipelagic mudstones. These mudstones are, if mature, an excellent source rock for oil. In the German Central Graben, though, the Clay Deep Member is immature (Fig. 41). Offshore The Netherlands, they are called Clay Deep Member and offshore Norway Mandal Formation. As the Bo Member of the Farsund Formation, they are the most prolific one of the Danish Central Graben (Ineson et al., 2003). These “Hot Shales” (due to their high gamma-ray signal) completely supersede the sandstones of the Scruff Greensand Formation and their initiation coincides with the first activities of the Late Kimmerian II pulse (Wong, 2007). Equivalent rocks form under the name “Kimmeridge Clay” the most prolific source rocks for oil in the central and northern North Sea (Evans et al., 2003). The salt tectonics that gained momentum in this tectonostratigraphic period had a tremendous influence on the petroleum system of the southern Central Graben. Most of the hydrocarbon field in the Dutch and Danish Central Graben feature structural 4-way dip closure traps related to salt tectonics (Pletsch et al., 2010). The relationship between salt tectonics and structural traps applies also to the shallow gas fields and accumulations in the northern Dutch and German Central Graben.

7.2.5. TMS-4 until the present

TMS-4 describes the phase of basin evolution, when rifting ceased and a regional transgression affected the region (Verreussel et al., 2018; Fig. 52). The area became subject to thermal subsidence and a depositional environment with a more even sediment distribution (Wong, 2007). Ongoing transgression resulted in the deposition of shallow marine bioclastic carbonates of the Chalk Group (Herngreen and Wong, 2007; de Jager, 2007). These bioclastic limestones are the most important reservoir rocks of the Danish Central Graben, where most of the currently proven reserves are trapped (Pletsch et al., 2010). They are characterized by high porosities and low permeabilities (Jakobsen et al., 2005). The hydrocarbons are trapped in anticlinal structures

due to later compression or above salt diapirs, along the flanks of salt diapirs, or in chalk-internal stratigraphic traps (Vejbaek et al., 2010). In the Late Cretaceous, the tectonic regime changed from extensional to compressional due to the Alpine orogeny. The new stress regime reactivated normal faults as reverse faults and inverted the southern Central Graben (Herngreen and Wong, 2007). It also significantly affected the local petroleum systems. In strongly inverted areas of the graben, like the southern Dutch Central Graben, source rocks like the Posidonia Shale Formation were uplifted out of the temperature interval of the maturity window for oil generation until the present day (de Jager & Geluk, 2007). Rapid sedimentation in the Cenozoic led to the preservation of organic matter in Miocene to Pleistocene clay and poorly consolidated mudstones and resulted in microbial gas generation from the Early Pleistocene until today (Verweij et al., 2018). The microbial natural gas migrated laterally along permeable layers and vertically along crestal faults above salt domes into anticlinal structures created by salt diapirism that served as traps. There, it potentially mixed with thermogenic gas from Rhaetian to Early Cretaceous source rocks that migrated upwards along tectonically or diapirism-induced faults, fractures, or disturbed sediments at the flanks of salt domes, closing the cycle from Cenozoic shallow gas accumulations to the Mesozoic rift system.

References

- Abbink, O. A., Mijnlief, H. F., Munsterman, D. K. & Verreussel, R. M. C. H., 2006. New stratigraphic insights in the 'Late Jurassic' of the southern Central North Sea Graben and Terschelling Basin (Dutch Offshore) and related exploration potential. *Netherlands Journal of Geosciences*, 85(3), 221-238.
- Andsbjerg, J. & Dybkjær, K., 2003. Sequence stratigraphy of the Jurassic of the Danish central graben. In: Surlyk, F., Ineson, J.R. (eds.), *The Jurassic of Denmark and Greenland*. Geological Survey of Denmark and Greenland Bulletin, vol. 1. pp. 265–300.
- de Jager, J. 2007. Geological development. In: Wong, T.E., Batjes, D.A.J. & de Jager, J. (eds.) *Geology of the Netherlands*. Royal Netherlands Academy of Arts and Sciences, Amsterdam, 5–26.
- de Jager, J. & Geluk, M. C., 2007. Petroleum Geology. In: Wong, T.E., Batjes, D.A.J. & de Jager, J. (eds.) *Geology of the Netherlands*. Royal Netherlands Academy of Arts and Sciences, Amsterdam, 241–264.
- Evans, D., Graham, C., Armour, A. & Bathurst, P. (eds.), 2003. *The Millennium Atlas: petroleum geology of the central and northern North Sea*. The Geological Society of London, London.
- Herngreen, G.F.W. & Wong, Th.E., 1989. Revision of the Late Jurassic stratigraphy of the Dutch Central North Sea Graben. *Geologie en Mijnbouw* 68: 73–105.
- Herngreen, G.F.W. & Wong, T.E., 2007. Cretaceous. In: Wong, T.E., Batjes, D.A.J. & de Jager, J. (eds.): *Geology of the Netherlands*. Royal Netherlands Academy of Arts and Sciences (Amsterdam): 127-150.
- Hovland, M. & Judd, A. G., 1988. *Seabed Pockmarks and Seepages*. London: Graham and Trotman.
- Ineson, J.R., Bojesen-Koefoed, J.A., Dybkjær, K. & Nielsen, L.H., 2003. Volgian–ryazanian 'hot shales' of the Bo member (Farsund Formation) in the Danish central graben, North Sea: stratigraphy, facies and geochemistry. In: Surlyk, F., Ineson, J.R. (eds.), *The Jurassic of Denmark and Greenland*, vol. 1. Geological Survey of Denmark and Greenland Bulletin, pp. 403–436.
- Jackson, M. P., & Hudec, M. R. 2017. *Salt tectonics: Principles and practice*. Cambridge University Press.
- Isaksen, G.H., Patience, R., Van Graas, G. & Jenssen, A.I., 2002. Hydrocarbon system analysis in a rift basin with mixed marine and nonmarine source rocks: the South Viking Graben, North Sea. *AAPG Bull.* 86 (4), 557–592.
- Jakobsen, F., Ineson, J.R., Kristensen, L., Nytoft, H.P. & Stemmerik, L., 2005. The Valdemar Field, Danish Central Graben: field compartmentalization and regional prospectivity of the Lower Cretaceous chalk play. In: Doré, A.G. and Vining, B.A. (eds.): *Petroleum Geology: North-West Europe and Global Perspectives – Proceedings of the 6th Petroleum Geology Conference*. The Geological Society (London): 177-186.

- Lott, G. K., Wong, T. E., Dugar, M., Andsbjerg, J., Mönnig, E., Feldman-Olszewska, A., & Verreussel, R. M. C. H., 2010. Jurassic. In: Doornenbal, J.C. & Stevenson, A.G. (eds.): Petroleum Geological Atlas of the Southern Permian Basin Area. EAGE Publications b.v. (Houten): 175-193.
- Mouritzen, C., Farris, M.A., Morton, A. & Matthews, S., 2018. Integrated Triassic stratigraphy of the greater Culzean area, UK central North Sea. *Pet. Geosci.* 24 (2), 197–207.
- Petersen, H.I. & Hertle, M., 2018. A review of the coaly source rocks and generated petroleum systems in the Danish North Sea: an underexplored Middle Jurassic petroleum system? *J. Pet. Geol.* 41 (2), 135–154.
- Petersen, H.I., Hertle, M. & Sulsbrück, H., 2017. Upper Jurassic–lowermost Cretaceous marine shale source rocks (Farsund Formation), North Sea: kerogen composition and quality and the adverse effect of oil-based mud contamination on organic geochemical analyses. *Int. J. Coal Geol.* 173, 26–39.
- Petersen, H.I., Hertle, M. & Mauritzen, E., 2018. The Middle Jurassic coaly-sourced petroleum system in the Danish North Sea – an overlooked exploration target? In: 80th EAGE Conference and Exhibition, 11-14 June 2018, Copenhagen, Denmark. Extended Abstract.
- Pletsch, T., Appel, J., Botor, D., Clayton, C.J., Duin, E.J.T., Faber, E., Górecki, W., Kombrink, H., Kosakowski, P., Kuper, G., Kus, J., Lutz, R., Mathiesen, A., Ostertag-Henning, C., Papiernek, B. & Van Bergen, F., 2010. Petroleum generation and migration. In: Doornenbal, J.C. and Stevenson, A.G. (eds.): Petroleum Geological Atlas of the Southern Permian Basin Area. EAGE Publications b.v. (Houten): pp. 225-253.
- Schroot, B.M., Klaver, G.T. & Schüttenhelm, R.T., 2005. Surface and subsurface expressions of gas seepage to the seabed—examples from the Southern North Sea. *Mar. Petrol. Geol.* 22 (4), 499–515.
- ten Veen, J., Verweij, H., Donders, T., Geel, K., de Bruin, G., Munsterman, D., Verreussel, R., Daza Cajigal, V., Harding, R. & Cremer, H., 2013. Anatomy of the Cenozoic Eridanos Delta Hydrocarbon System. TNO Report TNO 2013 R10060. TNO Utrecht, The Netherlands.
- Vejbæk, O.V., Andersen, C., Dugar, M., Hengreen, G.F.W., Krabbe, H., Leszczyński, K., Lott, G.K., Mutterlose, J. & Van der Molen, A.S., 2010. Cretaceous. In: Doornenbal, J.C. and Stevenson, A.G. (eds.): Petroleum Geological Atlas of the Southern Permian Basin Area. EAGE Publications b.v. (Houten): 195-209.
- Verreussel, R. M. C. H., Bouroullec, R., Munsterman, D. K., Dybkjær, K., Geel, C. R., Houben, A. J. P., Johannessen, P. N. & Kerstholt-Boegehold, S. J., 2018. Stepwise basin evolution of the Middle Jurassic–Early Cretaceous rift phase in the Central Graben area of Denmark, Germany and The Netherlands. *Geological Society, London, Special Publications*, 469(1), 305-340.
- Verweij, J.M., Nelskamp, S.N., ten Veen, J.H., de Bruin, G., Geel, K. & Donders, T.H., 2018. Generation, migration, entrapment and leakage of microbial gas in the Dutch part of the Southern North Sea Delta. *Mar. Pet. Geol.* 97, 493–516.

Wong D. A., 2007. Jurassic. In: Wong, T.E., Batjes, D.A.J. & de Jager, J. (eds.): *Geology of the Netherlands*. Royal Netherlands Academy of Arts and Sciences (Amsterdam): 107-125.

8. Outlook

This thesis aimed to advance the understanding of the stratigraphic and tectonic evolution, as well as of the petroleum systems of the German Central Graben. Nevertheless, when some questions were answered, new ones appeared. There is still plenty of research to do to fully understand the (German) Central Graben and its petroleum systems. Here, I want to give some suggestions for future work.

For a better understanding of the evolution of the salt structures and sub-basins, I recommend a backstripping study and reconstruction of the graben. The reconstruction of 2D sections, or even in 3D, in combination with 1-D backstripping of significant locations will increase our knowledge on basin evolution and subsidence patterns. As encouragement, I refer to the research of Warsitzka et al. (2016) on the Glückstadt Graben.

The salt tectonics and diapirism in the German Central Graben and adjacent areas are a further important topic. The complex history of extensional and compressional tectonics, loading and unloading, faulting, and the various sub-basins will make it an interesting field of work. There is still a lot that we do not know about their evolution, driving forces and structural styles, mechanisms of diapirism, and much more. Here, I refer to van Winden et al. (2018) as an exemplary work.

I also recommend a detailed seismic facies analysis of the Mesozoic rocks (chapter 5 and chapter 6). As described before, there is a change in the source rock facies in some of the formations, e.g., the Posidonia Shale Formation, the Kimmeridge Clay Formation, and the “Hot Shales” that may be reflected on seismic data. A more accurate distinction between the different lithologies of the Middle Jurassic Central Graben Subgroup may be possible. Also, yet unmapped Upper Jurassic sand accumulations, similar to the Scruff Greensand Formation or the Noordvaarder Member of the Kimmeridge Clay Formation may be discovered this way. This would have a potential impact regarding hydrocarbon accumulations, gas storage, or carbon capture and storage (CCS).

The role, impact, and evolution of the important transfer zones, e.g., the MCGTZ deserves further investigation. During the work for this thesis, the significance of the MCGTZ became clear, however, we do not know much about this important fault zone yet. I firmly recommend doing research on its evolution, and impact on tectonic and stratigraphy of the area. Here, I recommend Wride (1995) as literature.

If I had a wish and unlimited resources, I would drill a well from the seafloor through a shallow gas accumulation in the German Central Graben and through the suspected source rocks and make a geochemical analysis of the complete interval to answer the question of the origin of the shallow gas. If I had a second wish, I would also confirm the presence or non-presence of the Posidonia Shale Formation with a well in the German part of the graben.

References

van Winden, M., de Jager, J., Jaarsma, B. & Bouroullec, R., 2018. New insights into salt tectonics in the northern Dutch offshore: a framework for hydrocarbon exploration. Geological Society, London, Special Publications, 469(1), 99-117.

Warsitzka, M., Kley, J., Jähne-Klingberg, F. & Kukowski, N., 2016. Dynamics of prolonged salt movement in the Glückstadt Graben (NW Germany) driven by tectonic and sedimentary processes. International Journal of Earth Sciences, 106(1), 131-155.

Wride, V. C., 1995. Structural features and structural styles from the Five Countries Area of the North Sea Central Graben. First Break, 13(10).

Curriculum vitae

Personal details

Name	Simon Maximilian Müller
Date of birth	15 August 1985
Place of birth	Weißenburg i. Bay.
Nationality	German

Work experience

04/2020 - today	Geoscientist at the Federal Company for Radioactive Waste Disposal (BGE = Bundesgesellschaft für Endlagerung), Peine, Germany
01/2015 – 12/2019	Geoscientific research associate within the project “Subsurface Potentials for Storage and Economic Use in the North German Basin” (TUNB = Tieferer Untergrund Norddeutsches Becken) at the Federal Institute for Geosciences and Natural Resources (BGR = Bundesanstalt für Geowissenschaften und Rohstoffe), Hannover, Germany.
09/2014 – 12/2014	Structural geologist at PVG GmbH, Gelsenkirchen, Germany
03/2014/ - 05/2014	Mud-Logger at SST Consult, Aachen, Germany

Education

09/2016 - today	Doctoral candidate at the Gottfried Wilhelm Leibniz University Hannover, Germany
04/2011 - 09/2013	Master of Science (M. Sc.) in Applied Geosciences at RWTH University, Aachen, Germany; specialization: Energy and Mineral Resources (EMR); Thesis: “ <i>Permeability measurements with sorbing and inert gases as a function of effective stress on coal samples from the Surat Basin, Queensland, Australia</i> ”
04/2011 - 09/2013	Bachelor of Science (B. Sc.) in Applied Geosciences at RWTH University, Aachen, Germany; Thesis: “ <i>Organic geochemical and petrological studies on organic matter-rich carbonates from Tarfaya Basin, Morocco</i> ”
06/2005	University-entrance diploma (Abitur), Werner-von-Siemens Gymnasium, Weißenburg i. Bay., Germany

Danksagung

Ich danke...

- ... meiner Betreuerin Frau Prof. Dr. Jutta Winsemann und meinem Betreuer Herrn Hon.-Prof. Dr. Christoph Gaedicke für ihren fachlichen Input und ihren Rat bei inhaltlichen und methodischen Fragen, aber auch für Ihre große Geduld und Empathie, Ihre Hilfsbereitschaft und, wenn nötig, Ihren notwendigen Druck, um diese Arbeit auch zu beenden.
- ... meinen mittlerweile ehemaligen Kollegen bei der BGR, namentlich Herrn Dr. Dieter Franke, Herrn Dr. Lutz Reinhardt und Herrn Dr. Rüdiger Lutz, dafür, dass sie für Rat immer zur Verfügung standen, sie sich die Mühe machten, meine Manuskripte zu lesen, zu korrigieren und mit ihren fundierten Anmerkungen zu versehen, und einfach dafür, dass ihre Tür immer offenstand.
- ... meinem ehemaligen Kollegen Stefan Kluger dafür, dass er immer da war, wenn es technische Probleme gab und er immer eine Lösung hatte.
- ... meinem ehemaligen Kollegen Herrn Dr. Philipp Weniger für seinen Rat, wenn es geochemisch wurde.
- ... meiner ehemaligen Kollegin Frau Dr. Katrin Schwalenberg dafür, dass sie mir die wissenschaftliche Ausfahrt auf dem Forschungsschiff Heincke ermöglicht hat.
- ... meinem Kollegen Herrn Dr. Jashar Arfai dafür, dass ich mit ihm fünf Jahre das Büro teilen durfte, für seinen fachlichen Input, und vor allem für seine nie erschöpfende Hilfsbereitschaft.
- ... meinen Freunden und ehemaligen Kollegen Frau Dr. Heidrun Stück und Herrn Dr. Frithjof Bense einerseits dafür, dass ich mich fachlich immer auf sie verlassen konnte, aber vor allem für ihre Freundschaft, ihre selbstlose und stets verfügbare Hilfsbereitschaft, und dafür, dass sie immer da waren, wenn es auch abseits von Beruf und Promotion nötig war.
- ... meinem Freund und ehemaligen Kollegen Fabian Jähne-Klingberg, Wissenschaftler mit Leib und Seele, für sein unermüdliches Engagement und dafür, dass er seinen Sachverstand und sein scheinbar grenzenloses geologisches Wissen bereitwillig geteilt hat. Ohne sein kompromissloses Augenmerk auf Qualität gäbe es die Arbeit in dieser Form nicht.
- ... meinen Eltern Gabriela und Walter Müller, sowie meinen Schwiegereltern Barbara und Lothar Thiel für ihre beständige und vielfältige, unschätzbar wertvolle Unterstützung.
- ... meiner Frau Franziska, für Ihre grenzenlose Unterstützung, für Ihre unendliche Geduld und – man muss auch sagen- Leidenschaft. Während der Arbeit an der Dissertation sind wir mehrfach umgezogen, haben Arbeitgeber gewechselt, einen Dackel adoptiert,

haben geheiratet und eine Familie gegründet. Du warst immer meine Konstante an meiner Seite, mein größter Ansporn, ohne dich hätte ich es nicht geschafft, wahrscheinlich nicht einmal begonnen.

... meinem Sohn Felix Leopold, der mich wohl in gleichem Maße behindert wie angespornt hat, die Dissertation fertigzustellen.

... meiner alten Dackeldame Tilda, für ihre stille Liebe, die Ruhe und Gemütlichkeit, die sie in meinen Feierabend gebracht hat, und dafür, dass sie mich mit ihrer Dickköpfigkeit immer zum Lachen gebracht hat.

List of publications

Müller, S., Reinhardt, L., Franke, D., Gaedicke, C., & Winsemann, J., 2018. Shallow gas accumulations in the German North Sea. *Marine and Petroleum Geology*, 91, 139-151. doi: 10.1016/j.marpetgeo.2017.12.016.

Müller, S., Arfai, J., Jähne-Klingberg, F., Bense, F., & Weniger, P., 2020. Source rocks of the German Central Graben. *Marine and Petroleum Geology*, 113, 104-120. doi: 10.1016/j.marpetgeo.2019.104120.

Römer M., Blumenberg M., Heeschen K., Schloemer S., Müller H., **Müller S.**, Hilgenfeldt C., Barckhausen U., & Schwalenberg K., 2021. Seafloor Methane Seepage Related to Salt Diapirism in the Northwestern Part of the German North Sea. *Frontiers in Earth Science*, 9:556329. doi: 10.3389/feart.2021.556329.

Müller, S., Jähne-Klingberg, F., Thöle, H., Jakobsen, F., Bense, F., Winsemann, J., Gaedicke, C., *in review*. Jurassic to Lower Cretaceous tectonostratigraphy of the German Central Graben, southern North Sea. Submitted to *Netherlands Journal of Geosciences*.